UNIVERSITÉ LAVAL

Design of novel well-defined organorhenium heterogeneous catalyst for unsaturated fatty acid derivatives self-metathesis

Thèse

Abdelnasser Abidli

Doctorat en sols et environnement
Philosophiae Doctor (Ph.D.)

Québec, Canada

Résumé

La formation des liaisons C-C est parmi les cibles les plus élevés de la science et de la technologie de la catalyse. Dans ce cadre, la réaction de métathèse catalytique a gagné une importance considérable en raison de l'efficacité du processus de transformation. Par conséquent, un grand progrès a été réalisé dans ce domaine avec le développement de plusieurs catalyseurs homogènes et hétérogènes, ainsi que les différentes approches de métathèse. Cette formule a permis une conception plus facile et plus durable de diverses stratégies de synthèse dans différents domaines, y compris la synthèse organique, la science des polymères, *etc.* Cependant, le développement des catalyseurs de métathèse robustes pour les applications à grande échelle est encore une tâche difficile.

Tenant compte de cela, les résultats de recherche présentés dans cette thèse de doctorat se concentrent sur la synthèse d'un nouveau catalyseur hétérogène de métathèse. Par conséquent, le méthyltrioxorhénium (MTO) a été supporté sur différents matériaux à base d'alumine. La performance des catalyseurs synthétisés a été étudié par l'auto-métathèse de l'oléate de méthyle, choisi comme substrat modèle; volumineux et fonctionnalisé, afin d'évaluer la tolérance des espèces actives aux groupements fonctionnels, ainsi que d'évaluer sa diffusion à l'intérieur des canaux mésoporeux. Tout d'abord, des supports très organisés à base alumine mésoporeux organisée modifiée avec le chlorure de zinc ($ZnCl_2$-AMO) ont été préparés avec succès grâce à un procédé sol-gel puis une imprégnation post-synthèse. Le MTO supporté sur ces supports catalytiques est très actif pour l'auto-métathèse de l'oléate de méthyle, avec des vitesses de réaction plus élevées et une meilleure sélectivité par rapport aux catalyseurs à base d'alumine classiques. Cette amélioration est attribuée à des meilleurs phénomènes de transfert de masse à l'intérieur du réseau mésoporeux organisé. Ensuite, nous avons développé une voie de synthèse efficace en une seule étape pour la préparation des matériaux $ZnCl_2$-AMO. Cette approche a permis l'accès à des supports $ZnCl_2$-AMO très ordonnés avec de meilleurs rendements de synthèse ainsi que de meilleures propriétés physiques et de surface. En outre, ces fonctionnalités améliorées ont permis aux catalyseurs à base de MTO supportés sur ces matériaux préparés en une seule étape de manifester une meilleure performance catalytique par rapport à celle de $ZnCl_2$-AMO préparé par le processus en plusieurs étapes. Toutefois, des études spectroscopiques

ont révélé la formation d'espèces actives semblables sur la surface pour tous les supports catalytiques préparées. Ces caractérisations nous ont guidés pour étudier et proposer un mécanisme complet pour les voies de formation des produits de métathèse, ainsi que le cycle catalytique de métathèse, démontrant l'effet d'encombrement stérique sur l'interface de catalyseurs qui contrôle la sélectivité de la réaction.

La synthèse des catalyseurs de métathèse MTO/$ZnCl_2$-AMO nous a permis d'effectuer efficacement les transformations de métathèse utilisant des matières premières renouvelables (par exemple des acides gras estérifiés provenant des huiles végétales), offrant un accès à une variété de monomères fonctionnalisés, qui pourraient éventuellement être utilisés pour d'autres transformations telles que la synthèse des bio-polymères à valeur ajoutée à base (par exemple, les bioplastiques, biosurfactants)

Abstract

Sustainable C-C bond forming reactions have been among the highest target of catalysis science and technology. In this scope, metathesis reaction has been gaining enormous attention due to the efficiency of the transformation process. Therefore, a great progress has been made in this area by developing several homogeneous and heterogeneous catalysts as well as distinct metathesis reaction approaches. This allows an easier and more sustainable design for various synthesis strategies in different fields including organic synthesis, polymer science, *etc.* However, the development of robust metathesis catalysts for large scale applications is still a challenging task.

Taking this into account, this research presented in this doctoral dissertation is focusing on the synthesis of new heterogeneous metathesis catalysts. Therefore, methyltrioxorhenium (MTO) was supported on various alumina-based materials. The synthesized catalysts' performance was studied though methyl oleate self-metathesis, chosen as a model bulky functionalized substrate, in order to evaluate the active species tolerance to functional groups as well as to evaluate its diffusion inside the mesoporous channels. First, highly organized $ZnCl_2$-modified OMA supports were successfully prepared through a sol-gel method followed by a post-synthesis modification *via* wet-impregnation process. MTO supported on these catalytic supports were found o be highly active for methyl oleate self-metathesis, displaying higher reaction rate and products selectivity compared to the conventional wormhole-like alumina-based catalysts. This improvement is ascribed to enhanced mass transfer phenomena inside the organized mesoporous network. Afterwards, we have developed efficient one-pot synthesis route $ZnCl_2$-modified OMA supports. Interestingly, this approaches allowed access to numerous highly ordered $ZnCl_2$-modified OMA supports with better synthesis yields and improved textural and surface properties. Moreover, these enhanced features allowed the MTO-based catalyst supported on these one-step prepared materials to exhibit higher metathesis reaction performance compared to $ZnCl_2$-modified OMA supports prepared *via* the two-steps processes. However, spectroscopic investigations revealed the formation of similar surface active species for all the prepared catalytic supports. These characterizations guided us to study and propose a comprehensive mechanism of metathesis products formation pathways as well as the

metathesis catalytic cycle, demonstrating the steric hindrance effect on the catalysts interface that governed the reaction selectivity.

The synthesis of the 3 wt.% MTO/$ZnCl_2$-OMA catalysts allowed us to efficiently perform metathesis reaction using renewable feedstock (*e.g.* fatty acid esters derived from vegetable oils), offering access to a variety of functionalized monomers which could be used for further transformations such as the synthesis of value-added bio-based polymers (*e.g.* bioplastics, biosurfactants)

Table of Contents

List of Tables

List of Figures

List of Schemes

List of Abbreviations

AMO	*Alumine Mésoporeux Organisée/Ordonnée.*
ATR-FTIR	Attenuated Total Reflection- Fourier Transform Infrared spectroscopy
BET	Brunauer-Emmett-Teller method
BE	Binding Energy (eV)
BJH	Barrett-Joyner-Halenda method
Bu	Butoxide
D_P	Average Pore Diameter (Barrett-Joyner-Halenda method)
DRX	*Diffraction des Rayons X*
EDX	Energy Dispersive X-ray spectrometry
ADESF	*Analyse Dispersive en Énergie par Spectrométrie de Fluorescence*
EISA	Evaporation-Induced Self-Assembly
FID	Flame Ionization Detector
FTIR	Fourier Transform Infrared spectroscopy
GC	Gas Chromatography
GC-MS	Gas Chromatography-Mass Spectroscopy
ICP	Inductively Coupled Plasma */spectrométrie par torche à plasma*
ICP-OES	Inductively Coupled Plasma-Optical Emission Spectrometry
IL	Ionic Liquids
IRTF	*Spectroscopie Infrarouge à Transformée de Fourier*
IUPAC	International Union of Pure and Applied Chemistry
MAS NMR	Magic-Angle Spinning Nuclear Magnetic Resonance
MEB	*Microscopie Électronique à Balayage*
meso	mesoporous
MET	*Microscopie Électronique à Transmission*
MS	Mass Spectroscopy
MTO	Methyltrioxorhenium
MW	Microwaves
ND	Not determined
OMA	Organized/Ordered Mesoporous Alumina
OP, op	One-Pot

PAS	Propagating Active Species
Pr	Propoxide
RMN	*Résonnance Magnétique Nucléaire*
SAXS	Small-Angle X-Ray Scattering
S_{BET}	Specific Surface Area (Brunauer-Emmett-Teller method)
SEM	Scanning Electron Microscopy
SPX	*Spectrométrie de Photoélectrons induits par rayons X*
TEM	Transmission Electron Microscopy
st	Two-steps
V_P	Total pore volume (Barrett-Joyner-Halenda method)
WAXRD	Wide-Angle X-Ray Diffraction
XPS	X-ray Photoelectron Spectroscopy
XRD	X-Ray diffraction

You can never solve a problem on the level on which it was created.

The whole of science is nothing more than a refinement of everyday thinking.

To raise new questions, new possibilities, to regard old problems from a new angle, requires creative imagination and marks real advance in science.

The value of a college education is not the learning of many facts but the training of the mind to think

Albert Einstein

I dedicate this dissertation to my beloved parents and my wonderful family...

Also, to Professor Chewki Ziani-Cherif who inspired me to pursue doctoral studies...

Acknowledgements

Foremost, I would like to express my sincere gratitude to my mentor and advisor Professor *Antoine Karam* for his guidance, encouragement, continuous support, enthusiasm and immense knowledge that helped me to succeed my Ph.D. studies.

I am also grateful to Prof. *Khaled Belkacemi* for his first mentorship (2013-2015), the N_2 adsorption-desorption analysis and for providing his laboratory facility at Laval University where the materials/catalysts synthesis and the metathesis reaction experiments were conducted. I could not have done this without his financial support and commitment. He gave me a wonderful opportunity for self-improvement.

I would like to thank Professor *Josée Fortin* for the improvement of the present thesis particularly during the initial assessment. I also want to show my sincere gratitude to my thesis committee Professor *Antoine Karam,* Professor *Josée Fortin,* Professor *Murielle Subirade* and Professor *Alfred Jaouich* for giving their valuable time, efforts and expertise to review my work and consider my thesis, as well as for providing me with insightful and constructive comments during the thesis submission and evaluation, which motivated me to widen my research from various perspectives.

I wish to express my sincere thanks to *Alain Adnot, Pierre Audet, Prof. Safia Hamoudi, Ronan Corcuff, André Ferland, Alain Brousseau, François Paquet-Mercier* and *Richard Janvier* for their technical assistance in various analysis; XPS, MAS NMR, XRD, GC-MS, SEM-EDX, ICP-OES, FTIR and TEM, respectively.

In my daily work I have been blessed with friendly and cheerful scientists. I would like to thank the rest of the research group, my colleagues *Zeineb BenRejeb, Ourida Aissaoui, Dr. Cherif Larabi, Dr. Lilya Boudriche* and *Dr. K. T. Venkateswara Rao* for their support, advices, encouragements and their kind friendship. In many ways I have learned much from them. A special thanks to all my dear friends *Ayyoub, Aniss, Atef, Majid, Leila, Olfa, Ourida* and *Tiha.*

I wish to thank all professors as well as all research and administrative staff for everything i have learned and for all their precious help during my Ph.D. studies in Université Laval.

I will take this opportunity to express gratitude to the Natural Sciences and Engineering Research Council of Canada (NSERC) and Canadian Foundation for Innovation (CFI) who provided funds for this research project. Also, special gratitude to the Faculty of Agriculture and Food Sciences (FSAA) and the Department of Soil Sciences and Agri-Food Engineering for their financial support during my Ph.D. studies.

Last but not the least, I would like to thank my family for their unconditional love and support.

Many thanks to all of you

Preface

This Ph.D. thesis is composed of seven chapters, three of them are written in the form of scientific papers where the candidate (A. Abidli) is the principle author. Two articles are published and the third one is submitted for publication (under review) at the time of the thesis submission. In these works, the candidate designed and performed all of the experiments. The characterizations data were taken by the respective specialists who are acknowledged. The candidate collected and analyzed all data. With the exception of the first article where Prof. Khaled Belkacemi contributed to the revision of the manuscript with the candidate, all manuscripts were written and revised by the candidate (A. Abidli).

The present thesis is structured as follow; first an introduction on the research background and motivations (Chapter 1), then a detailed state-of-the-art literature review (Chapter 2). Afterwards we present our founded research hypothesis and set the projects objectives (Chapter 3). Subsequently, the three articles are presented in various chapters (Chapters 4 to 6). Finally, we present the conclusions and our future outlook (Chapter 7).

Chapter 4 reports the synthesis of hexagonally well-ordered mesoporous alumina materials modified with $ZnCl_2$ (post-synthesis; two-steps). These materials were used as catalytic supports for MTO, and then these catalysts were successfully evaluated for their performance in methyl oleate self-metathesis reaction. Higher reaction rate, conversion and selectivity towards desired products was achieved compared to MTO-based catalysts supported on conventional wormhole-like mesoporous alumina. The corresponding results were published as *"Synthesis, characterization and insights into stable and well organized hexagonal mesoporous zinc-doped alumina as promising metathesis catalysts carrier",* authored by A. Abidli, S. Hamoudi and K. Belkacemi, *Dalton Transactions*, **2015**, 44 (21), p. 9823-9838.

Chapter 5 reports the synthesis of hexagonally well-ordered mesoporous alumina materials modified with $ZnCl_2$ prepared *via* the newly developed one-pot process. Detailed comparison between the materials synthesis process (one-pot *vs*. two-steps syntheses) as well full characterizations and catalytic performance are described. The MTO-based catalysts supported on the one-pot prepared supports showed enhanced methyl oleate self-

metathesis activity due to the enhanced features of the one-pot synthesized materials. Higher methyl oleate conversion was reached as well as better reaction selectivity towards desired metathesis reaction products compared the MTO-based catalysts supported on two-steps prepared supports. The corresponding results were published as "*One-pot direct synthesis route to self-assembled highly ordered Zn-decorated mesoporous aluminium oxide toward efficient and sustainable metathesis heterogeneous catalyst design",* authored by A. Abidli, *RSC Advances*, **2015**, 5 (112), p. 92743-92756.

Unlike previous chapters (4 and 5), which focused on the synthesis and the characterization of the catalytic supports as well as the evaluation for methyl oleate self-metathesis, in Chapter 6 we focus on the characterization and the study of the catalysts prepared using organized mesoporous alumina synthesized *via* tow-steps and one-pot processes. The surface active species and metathesis reaction products were fully identified and investigated. These investigations allowed us the study of the mechanistic pathways for methyl oleate self-metathesis products formation as well as the catalytic cycle. The corresponding results will be submitted as "*Well-defined organorhenium-based selective heterogeneous catalyst supported on stable ordered mesoporous $ZnCl_2$-Al_2O_3: metathesis activity, surface active sites and mechanistic pathway"* authored by A. Abidli.

Avant-propos

Cette thèse de doctorat se compose de huit chapitres, trois d'entre eux sont rédigés sous forme d'articles scientifiques où le candidat (A. Abidli) est l'auteur principal. Deux articles sont publiés et le troisième est soumis pour publication au moment de la présentation de la thèse. Dans ces travaux, le candidat a conçu et réalisé toutes les expériences. Les données sur les caractérisations ont été prises par des spécialistes qui sont remerciés. Le candidat a collecté et analysé toutes les données. À l'exception du premier article où le Pr. Khaled Belkacemi a contribué à la révision du manuscrit avec le candidat, tous les manuscrits ont été rédigés et révisés par le candidat (A. Abidli).

La présente thèse est structurée comme suit; d'abord une introduction sur le contexte scientifique et les motivations du projet (chapitre 1), puis une revue détaillé de la littérature (chapitre 2). Ensuite, nous présentons nos hypothèses de recherche et nous définissons les objectifs des projets (chapitre 3). Par la suite, les trois articles sont présentés dans divers chapitres (4 à 6). Enfin, nous présentons les conclusions et les futures perspectives (chapitre 7).

Chapitre 4 rapporte la synthèse des matériaux d'alumines mésoporeuses hexagonales très ordonnées modifiée avec du chlorure de zinc (post-synthèse; deux étapes). Ces matériaux ont été utilisés comme supports catalytiques pour le méthyltrioxorhénium (MTO), puis ces catalyseurs ont été évalués avec succès pour leur performance dans la réaction d'auto-métathèse de l'oléate de méthyle. Un taux de réaction supérieur, une conversion plus élevée et une meilleure sélectivité vers les produits souhaités sont atteint avec ces catalyseurs par rapport aux catalyseurs de MTO à base d'alumine mésoporeuse conventionnelle désordonnée. Les résultats correspondants ont été publiés en tant que *"Synthesis, characterization and insights into stable and well organized hexagonal mesoporous zinc-doped alumina as promising metathesis catalysts carrier",* par A. Abidli, S. Hamoudi and K. Belkacemi, *Dalton Transactions*, **2015**, 44 (21), p. 9823-9838.

Chapitre 5 rapporte la synthèse des matériaux d'alumines mésoporeuses hexagonales très ordonnées modifiée avec du chlorure de zinc préparés par un procédé en une seule étape nouvellement mis au point. Une comparaison détaillée entre les processus de synthèse des

matériaux (synthèse en une seule étape et synthèse en deux étapes), ainsi que des caractérisations complètes et l'évaluation de la performance catalytique sont décrits. Les catalyseurs MTO supportés sur les supports préparés en une seule étape ont montré une activité catalytique améliorée pour l'auto-métathèse de l'oléate de méthyle à cause des propriétés améliorées des matériaux synthétisés en une seule étape. Une conversion supérieure de l'oléate de méthyle a été atteinte, ainsi qu'une meilleure sélectivité de la réaction vers les produits de métathèse souhaités par rapport aux catalyseurs MTO supportés sur les supports préparés en deux étapes. Les résultats correspondants ont été publiés en tant que "*One-pot direct synthesis route to self-assembled highly ordered Zn-decorated mesoporous aluminium oxide toward efficient and sustainable metathesis heterogeneous catalyst design",* par A. Abidli, *RSC Advances*, **2015**, 5 (112), p. 92743-92756.

Contrairement aux chapitres précédents (4 et 5), qui portent sur la synthèse et la caractérisation des supports catalytiques ainsi que leur évaluation pour l'auto-métathèse de l'oléate de méthyle, au chapitre 6, nous nous concentrons sur la caractérisation et l'étude des catalyseurs préparés en utilisant matériaux d'alumines mésoporeuses hexagonales très ordonnées synthétisés par des processus en deux étapes et aussi en une seule étape. Les espèces actives de surface et des produits de métathèse ont été identifiés et étudiés. Ces données nous ont permis l'étude des voies mécanistiques qui conduisent à la formation des produits de l'auto-métathèse de l'oléate de méthyle ainsi que le cycle catalytique. Les résultats correspondants seront soumis en tant que "*Well-defined organorhenium-based selective heterogeneous catalyst supported on stable ordered mesoporous $ZnCl_2$-Al_2O_3: metathesis activity, surface active sites and mechanistic pathway"* par A. Abidli.

Chapter 1: Introduction

In this chapter, the role of catalysis and green chemistry in developing efficient tools for environment protection and resolving issues related to the pollutions phenomena are discussed. In this scope, the green metathesis routes and catalysis is evoked when dealing with biomass and wastes valorization (*e.g.* unsaturated fatty acids) are also discussed.

General introduction and background

Pollution is one of various phenomena affecting earth life conditions; environmentally and economically. This phenomenon is a result of many factors. In fact, the exhaustive use of fossil energy is the major one. Meanwhile, many studies were lunched to build up green alternatives to become less dependent on fossil resources in the long term [1]. This transition has to be designed economically, ecologically and being socially acceptable. On this basis, we have to significantly reduce the consumption of fossil resources in order to manage as long as possible with the existing stocks. In the meantime, we have to find appropriate substitutes to this risky strategy [2]. This unsustainable situation is rising the awareness level, leading and forcing to think and debate about diversification strategy in the energy supply, to create new strategies to face these growing challenges including depletion of fossil fuel reserves, the significant fuel price rise, climate changes, global warming [3, 4] and other environmental concerns [5]. Therefore, renewable energy was set as an ambitious alternative, exploring its benefits and taking advantage of several resources such as wind, biomass, tidal energy, geo-thermal, biofuels, small-scale hydro and wave-generated power [6], solar energy [7], *etc.* These resources are abundant, inexhaustible and environmentally friendly reserves. Moreover, renewable raw materials [8, 9] including wood, plant oils, plant fibers, sugars, starch, cellulose, wool and pelt, are used for both energy production and material applications, *e.g.* for fuels, textile fibers, construction materials, paper, lubricants, plastics, drugs, *etc.*

Recently, much more attention has been given to the use of biomass and renewables to produce value-added products. In this area, catalysis plays a majors role by offering numerous tools for the conversion of these raw materials [10-16]. More interestingly, some of the industrial by-products which sometimes are considered as harmful and hazardous wastes, can not only be eliminated through catalytic processes, but also valorized into highly desired compounds. Catalysis is one of the green chemistry aspects. Up-to-date research efforts are focusing on making catalysis greener by designing catalysts and catalytic reactions to be more environmentally friendly by generating less wastes (by-products), using less hazardous chemicals, reducing energy consumption, *etc.* Thus, these

green catalysts and catalytic processes can be used effectively for biomass conversion and wastes valorization [17, 18].

In this field, several catalytic routes have been advantageously explored for the conversion of these raw materials, including hydrogenation [19], deoxygenation [20], hydrodeoxygenation [21], oxidation [22], esterification [23], *etc.* Metathesis reaction has been one of these efficient catalytic strategies towards biomass valorization [24, 25], especially with catalysts bearing well-defined organometallic surface species [26, 27]. Among all the catalytic systems, solid catalysts meet all the requirements for efficient catalytic processes for biomass conversions at their interface [28]. Thus, current research efforts are highly focused on the design of new robust solid catalysts with higher performance and stability as well as low cost-production. Porous catalysts are considered as the largest class of catalysts developed in this scope. They are structurally favorable for biomass mass transfer and conversion [29], while particular attention is paid to mesoporous solid catalysts [30]. As a result, the field of supported porous metal oxide catalysts has been gathering enormous attention for their suitable applications in metathesis reaction [31, 32].

Currently, organorhenium oxides-based catalysts are one of the most efficient heterogeneous metathesis catalysts [33], which attract enormous attention in catalysis. Particularly, MTO-based catalysts are among the latest generations in this family and the most explored metathesis catalysts [34-36]. However, up-to-date issues related to the catalysts selectivity and performance (conversion and reaction rate) are still challenging tasks. In addition, several issues remain unresolved when dealing with the existing catalytic supports used for this metathesis system.

Chapter 2: Review of literature

2.1. Green catalysis toward clean industry and environment protection

2.1.1. Catalysis in industry

Along with other chemical transformations, catalysis science and technologies are widely used at the industrial scale since the first industrial catalytic application in 1746 by John Roebuck and Samuel Gardner who developed the *lead chamber* process for the manufacture of sulfuric acid [37, 38]. Catalysis is highly beneficial by reducing the time and the cost of value-added products fabrication, as well as enabling shorter synthetic methods minimizing the overall carbon-footprint of chemical manufacturing. In addition, catalytic conversions reduce by-products formation while increasing the yields and selectivity compared to the traditional stoichiometric, non-selective reactions which have high energy consumption and high waste production [39, 40]. Thus, catalyst offers an alternative, energetically favorable mechanism to the non-catalytic reaction. Indicating that, catalysis plays an important role in industry [41, 42], offering answers to both economical and environmental problems in different fields including pharmaceuticals, chemicals, agrochemicals, electronics, materials and polymers, as well as petroleum and energy, producing high value-added products (*e.g.* plastics, drugs, food additives, cosmetics and more). Currently, over 90 % of industrial processes include at least one catalytic step involving heterogeneous and/or homogeneous catalysts, while this is increasing steadily [43, 44]. Thus, the research for robust catalysts has been one of the highest priorities in the chemical industry enabling economical and environmentally-sound manufacturing processes.

Pharmaceutical industry is one of the most important sectors that appeal for catalysis, reducing enormously the cost of drugs. The manufacturing of pharmaceutical ingredients is known for its high dropout rates during development, long time processes and extreme caution regarding the products purity and stability. In this particular sector, there is a high demand on enantioselective catalysts prepared with designed chiral ligands to control the

selectivity of bioactive compounds production in enantiomerically enriched form in which enantiomeric purity can be critical [45, 46]. However, pharmaceutical industry is one of the industrial sectors that generates the largest portion of waste [39]. A wide range of industrial catalytic processes have been developed including catalytic coupling reactions (C-C bond formation), carbonylation, hydrocyanation, hydroformylation, oxidation, polymerization, hydrogenation and olefin metathesis [40, 47].

In the petrochemical industry, for instance, catalytic cracking has been performed traditionally at higher temperatures and pressure without catalyst. However, the presence of catalysts (*e.g.* zeolite) [48] allowed these transformations to perform efficiently at lower temperatures and pressure. Similarly, other petrochemical transformations were developed using industrial catalysts such as isomerization including chlorinated alumina doped with platinum or sulfated zirconia (SZ) [49], as well as reforming process over Pt/Al_2O_3 catalysts [50]. The use of catalysts at the industrial scale allowed expensive products to be more available and accessible by lowering their manufacturing cost, as well as leading to further discovery of new classes of compounds. Table 1 summarizes the most common industrially established catalytic transformations.

Table 1: Largest processes based on heterogeneous catalysis [44].

Reaction	**Catalyst**
Catalytic cracking of crude oil	Zeolites
Hydrotreating of crude oil	Co-Mo, Ni-Mo, Ni-W (sulfidic form)
Reforming of naphtha (to gasoline)	Pt, Pt-Re, Pt-Ir
Alkylation	H_2SO_4, HF, solid acids
Polymerization of ethylene, propylene	Cr, $TiCl_x/MgCl_2$
Epoxidation of ethylene to ethylene oxide	Ag
Vinyl chloride synthesis (ethylene + Cl_2)	Cu (as chloride)
Steam reforming of methane to CO + H_2	Ni
Water-gas shift reaction	Fe (oxide), Cu-ZnO
Methanation	Ni
Ammonia synthesis	Fe
Ammonia oxidation to NO and HNO_3	Pt-Rh
Acrylonitrile synthesis from propylene and ammonia	Bi-Mo, Fe-Sb (oxides)
Hydrogenation of vegetable oils	Ni
Sulfuric acid synthesis	V (oxide)
Oxidation of CO & hydrocarbons (car exhaust)	Pt, Pd
Reduction of NO_x (in exhaust)	Rh, vanadium oxide

World class recognition of scientific progress in catalysis field is a great indicator of the importance of this area of chemistry. Between 1901 and 2012, the Nobel Foundation recognized achievements related to chemical and enzymatic catalysis at least 15 times. Among these laureates, in 2001, William S. Knowles, Ryoji Noyori (hydrogenation) and K. Barry Sharpless (oxidation) were awarded the Nobel Prize for the development of catalytic asymmetric synthesis [51-54]. Also, Yves Chauvin, Robert H. Grubbs and Richard R. Schrock were awarded the 2005 Nobel Prize for developing metathesis reaction and making breakthroughs in discovering transition-metal catalysts [55-57]. More recently, Richard F. Heck, Ei-ichi Negishi, and Akira Suzuki shared the Nobel Prize in 2010, for the development of palladium-catalyzed cross-coupling in organic synthesis [58-60].

2.1.2. Chemical industry and environmental issues

Industrial mass production of chemicals is one of the large environmental dilemmas of modern society. Despite the great progress made in catalysis and the advantages offered to resolve economical and environmental issues, chemical industry is, unfortunately, one of the most important pollution sources. It affects air, water and soil, thus damaging human and animal health as well as plant life. For instance, nitrogen dioxide (NO_2), sulfur dioxide (SO_2), carbon monoxide (CO), carbon dioxide (CO_2), methane (CH_4) and chlorofluorocarbons (CFCs) are the major share of toxic and harmful atmospheric pollutants gases (Figure 1a). These gases are generated from the chemical industrial and manufacturing activities, as well as fossil fuels burning (*e.g.* energy supply, transportation, industry, see Figure 1b) leading to harmful consequences such as acid rain. Moreover, due to these greenhouse gases emissions into the air, global warming has been increasing at a steady pace as a serious outcome of this chemical pollution.

In addition to agricultural (*e.g.* pesticide residues) and domestic wastes, industrial wastes are the most important factor that contributes to water pollution. Hazardous substances such as heavy metals (*e.g.* Cd, Hg), inorganic pollutants (*e.g.* HCl), and organic pollutants such dioxin are released in water as a by-products of high-temperature processes (*e.g.* incomplete combustion, pesticide production, *etc.*). Dioxin is classified with the persistent organic pollutants (POPs) substances that are highly resistant to environmental degradation. This situation is very alarming, thus urgent solutions should be explored towards the

reduction of the amount of pollution (generation and management) while preserving the desired economical growth and industrial evolution.

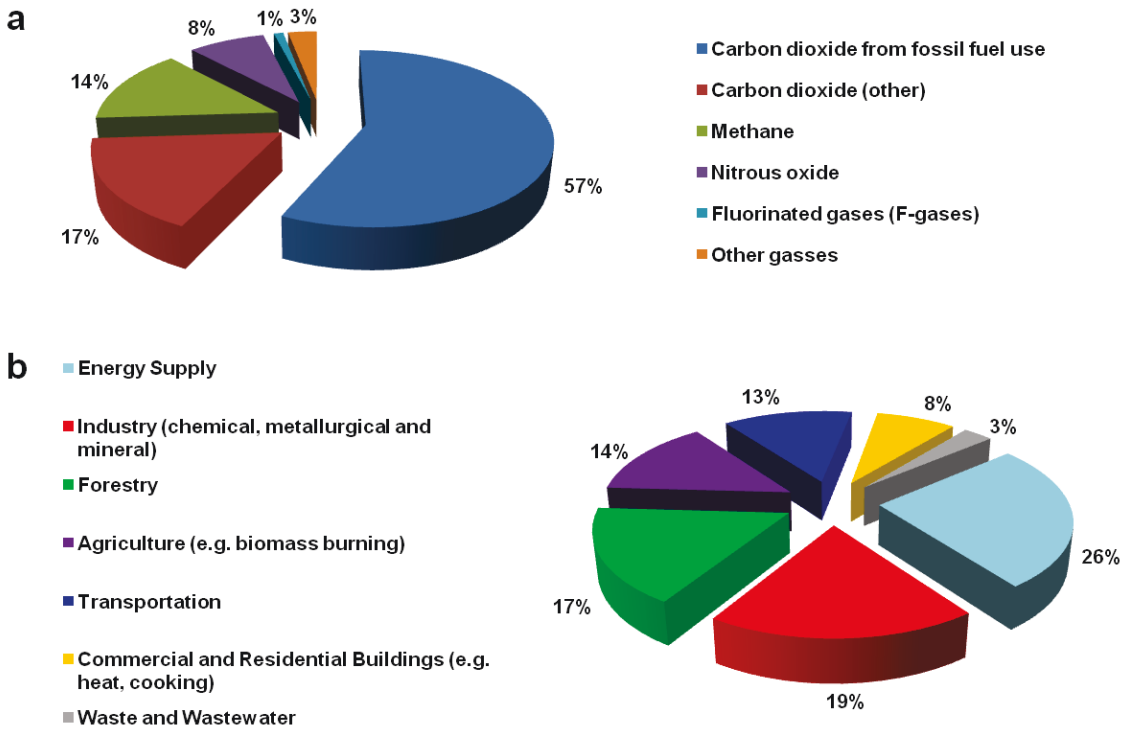

Figure 1. Distribution of global greenhouse gas emissions (a) by gas and (b) by source [61].

2.1.3. Green chemistry leading to green catalysis

This alarming situation and the increased threat to life on earth have been stimulating numerous initiatives to resolve these issues. Thus, efforts have been focused on improving the vital chemical industry sector, especially in the last twenty years, with more ecofriendly considerations in order to reduce the amount of toxic and hazardous substances generated from this industry. On the other hand, efforts are also focused on using less hazardous substances in manufacturing processes. Since the introduction of the "green chemistry" concept in 1990 and the publication of the 12 principles of green chemistry in 1998 (Figure 2) as well as the increasing regulatory requirements and advanced industrial technology, huge investments have been made in order to design more clean and sustainable catalysis [62]. The use of catalysts to perform chemical transformations is one of the green chemistry

principles. However, further combination of other green aspects using catalysts created the *so-called* "green catalysis" [63]. Thus, many research groups around the globe have been focusing on the elaboration of safer and cost-effective catalytic processes. Moreover, cleaner catalytic transformations are investigated avoiding the use of toxic and hazardous reagents and solvents.

Figure 2. Green chemistry 12 principles [62].

A quick survey of these green aspects is presented as follow:

(i) Selective and atom efficient transformations: Usually, catalytic transformations are highly selective, minimizing the production of wastes or undesirable by-products which are often difficult to eliminate, and present a high environmental impact. However, some

multistep synthesis of complex compounds generate enormous waste tonnage, which is considered as the biggest drawback in fine chemicals and pharmaceuticals industries for instance.

(ii) Green solvents: Modern catalytic synthesis strategies are often based on free-solvent reactions [64]. However, sometimes solvents are needed, thus several catalytic transformations can be performed using green solvents (Figure 3a) such as: water, ionic liquids, and biomass-derived organic solvents such as ethyl lactate, 2-methyltetrahydrofuran and γ-valerolactone, supercritical carbon dioxide, fluorous solvents and high boiling point alcohols like poly(ethylene glycol) [65-70], *etc.*

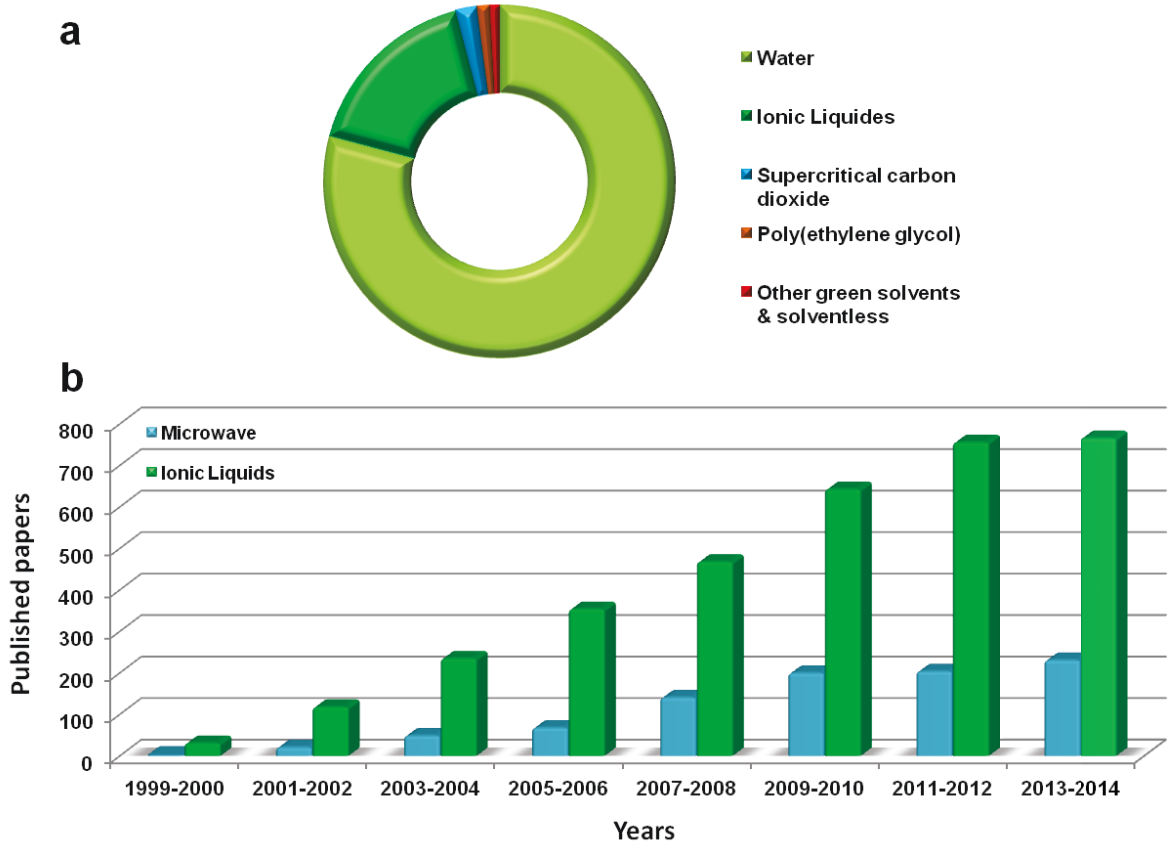

Figure 3. (a) Proportion of published articles describing catalyzed reactions in green solvents, source: Web of Science, period 1999-2014. (b) Evolution of using microwave heating and ionic liquids for catalyzed reactions, source: Web of Science.

Thus, such solvents are often required to stabilize catalytic species or the avoid catalysts deactivation upon complexation that often occurs when using conventional solvents especially in homogeneous catalysis. Furthermore, using these green solvents render the catalytic process safer and easy to handle due to their low toxicity and high chemical and thermal stabilities, as well their high diffusivity and miscibility [71]. Furthermore, these solvents are recyclable owing to their easy separation and extraction [71]. While heterogeneous catalysis (biphasic catalysis) avoids the use of enormous amounts of solvent usually required for phase separation and products purification, these solvents are promising candidates as truly green industrial solvents [72].
Increasing attention has been paid to green chemistry aspects. For instance, Figure 3b shows a constantly increasing use of microwave heating and ionic liquids in catalysis.

(iii) Energy efficiency: The ideal catalytic transformations are those performed under ambient temperature and pressure conditions. However, if needed, energy consumption should be as efficient as possible. Thus, microwave heating is one of these methodologies based on alternative energy sources offering a rapid and direct heating of reaction substrates and catalysts. Microwave heating may even enhance the transformations selectivity when overcoming activation energy barriers at different elementary catalytic steps without giving enough time for by-products to form [73]. Moreover, using microwave irradiation could offer more safety features compared to conventional heating when accidents (*e.g.* fire, explosion) may occur due to long exposure to heating sources and overheating phenomenon. Solar energy is also considered as one of the most sustainable alternative energy sources which has been advantageously applied in catalysis (*e.g.* photocatalysis) [74].

(iv) Cost-effective catalysis: Catalyzed reactions usually have fast kinetics which reduces the time and the cost of manufacturing processes and enhances the productivity of catalytic transformation. In addition, the recyclability of the catalysts renders the process more effective. Moreover, catalysis reduces the use of solvents and reagents compared to stoichiometric reactions, which is beneficial for the chemical industry. Advantageously, the

catalytic transformations also reduce the cost related to the use of protecting groups in non-catalyzed reactions by offering protecting group-free selective catalyzed pathways.

Since its establishment, green catalysis aspects have continued to gain interest [75]. A clear sign of this was provided by the citation for the 2005 Nobel Prize in Chemistry awarded to Chauvin, Grubbs, and Schrock, and according to the Swedish Academy of Sciences olefin metathesis reaction is “a great step forward for green chemistry”.

2.1.4. Catalysis in service of environment protection

In addition to the use of catalysts with their green features including less hazardous solvents use and less wastes (by-products) generation, catalysis also offers many solutions to several environmental issues in various forms and pathways (Figure 4).

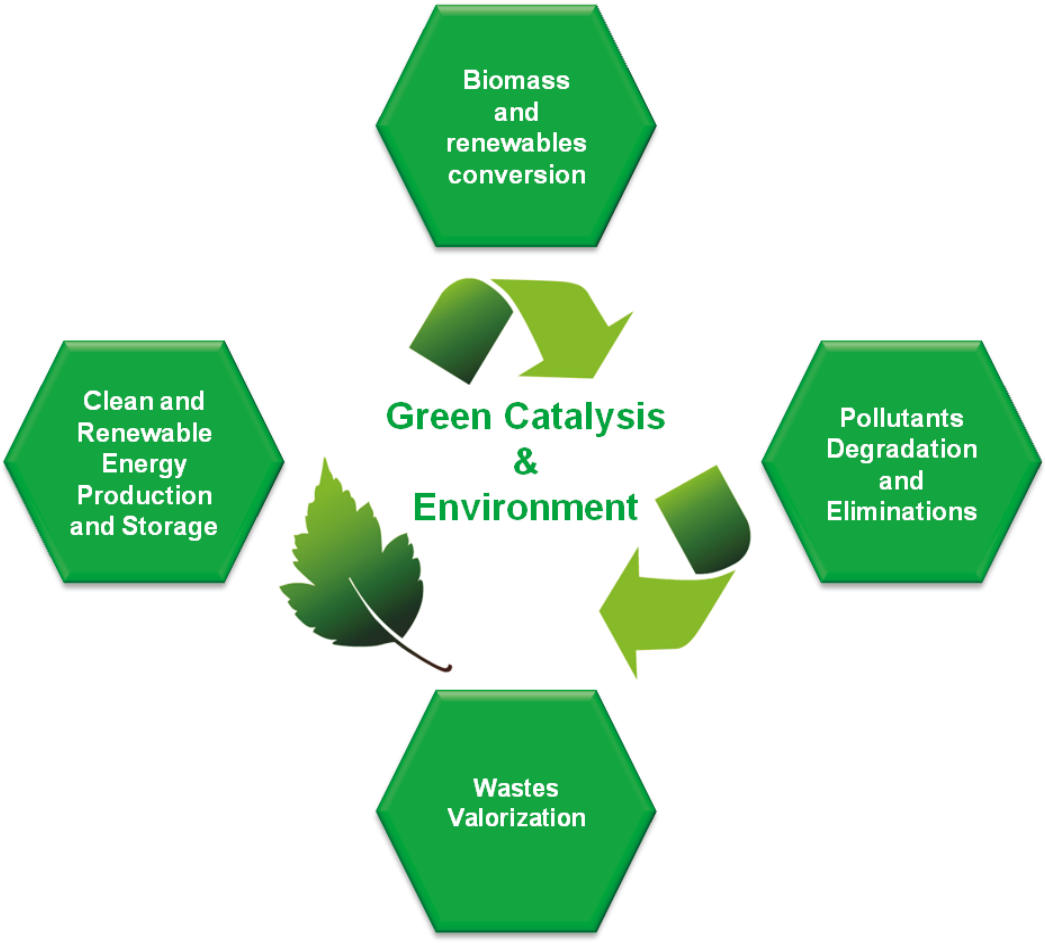

Figure 4. Various green catalytic tools for environment protection.

Catalytic applications take advantage of biomass, and renewables availability and low cost for the production of value-added products mostly with excellent biodegradability. Catalysis not only consumes efficiently clean energy, but also is a suitable alternative for both production and storage of clean and renewable energy. Furthermore, catalysis has a direct impact on environment protection, not only for the elimination and degradation of wastes and pollutants, but also in helping their recycling and valorization into value-added products.

(i) Biomass and renewables conversion and biodegradability: Many feedstocks for the production of value-added compounds are based on petroleum, which is not a renewable resource. This situation is encouraging many research groups to explore new alternatives to ensure the sustainability (environmentally, economically and socially) and long-term productivity for future generations. This interest has increased significantly in the last two decades as the necessity for a renewable source of carbon has become more evident [12, 76]. Therefore, catalysis was and still is among the powerful tools that is helping to overcome this issue by offering several pathways for the conversion of cheap, functionalized and readily available biomass and renewable feedstock into high value-added platforms. These renewable feedstock supplies helped greatly to advance the modern chemical industry, especially supplies that do not compete with our food production. Table 2 summarizes some selected catalytic conversions of various biomass and renewables into value-added products including:

(a) Carbohydrates: monosaccharides (glucose, fructose, arabinose and galactose), disaccharide (*e.g.* lactose, cellobiose), polysaccharides (*e.g.* cellulose) and derivatives [77-80].
(b) Furanic compounds: furfural, 5-hydroxymethylfurfural (HMF), isosorbide [81, 82].
(c) Biomass-derived carboxylic acids: arabinonic, glutamic, itaconic, lactic, levulinic and succinic acid [83, 84].
(d) Fatty compounds: edible fats and oils (C=C bonds, carboxylic group and fatty nitriles) [20, 85-87].
(e) Wood and extractives derivatives: terpenes, phenolic compounds (*e.g.* creosol) [88, 89].
(f) Glycerol [90, 91], *etc.*

Table 2: List of selected catalytic transformations of biomass and renewables into value-added products from recent literature

Renewable feedstock	Catalytic conversions
(a) Carbohydrates: monosaccharides (glucose, fructose, arabinose and galactose), disaccharide (*e.g.* lactose, cellobiose), polysaccharides (*e.g.* cellulose) and derivatives	▪ Hydrogenation of glucose to sorbitol [92, 93] ▪ Deoxygenation of glucose to 2-deoxysorbitol [92] ▪ Dehydration of glucose to 5-hydroxymethylfurfural [94, 95] ▪ Isomerization of D-glucose into D-fructose [96] ▪ Dehydration of fructose to 5-hydroxymethylfurfural [97] ▪ Oxidation of arabinose to arabinonic acid [98] ▪ Oxidation of D-galactose to galactonic acid [99] ▪ Oxidation of lactose to lactobionic acid [100] ▪ Hydrogenation of lactose into lactitol [101] ▪ Oxidative depolymerization of starch, xylans, potato flesh and wheat flour to polyhydroxycarboxylic acids [102] ▪ Degradation of cellobiose into glucose [103] ▪ Hydrolysis of cellobiose and cellulose to glucose and total reducing sugars [104, 105] ▪ Hydrolysis and hydrogenation of cellobiose and cellulose into sorbitol [106, 107] ▪ Oxidation of cellobiose to gluconic acid [108, 109] ▪ Bio-mimetic artificial catalytic degradation of polysaccharide [103]
(b) Furanic compounds: furfural, 5-hydroxymethylfurfural (HMF), isosorbide	▪ Hydrogenation of 5-hydroxymethyl-2-furaldehyde (HMF) to 2,5 bis(hydroxymethyl)tetrahydrofuran [110] ▪ Oxidation of 5-hydroxymethyl-2-furfural into 2,5-diformylfuran [111, 112] or furan-2,5-dicarboxylic acid [113] ▪ Deoxygenation of furfural to 2-methylfuran [114] ▪ Hydrogenation/rearrangement of furfural into cyclopentanone [115, 116] or cyclopentanol [116] ▪ Hydrogenation/ hydrogenolysis of furfural into 1,5-pentanediol [117] ▪ Hydrogenation of furfural to furfuryl alcohol [82, 118] ▪ Oxidative esterification of furfural into methyl furoate [119] ▪ Epimerization of isosorbide into isoidide [120] ▪ Transamination of isosorbide [121]
(c) Biomass-derived carboxylic acids: arabinonic, glutamic, itaconic, lactic, levulinic and succinic acid	▪ Hydrogenation of arabinonic acid to arabitol [10] ▪ Hydrogenation of glutamic acid to pyroglutaminol or to prolinol [122] ▪ Decarboxylation of itaconic acid into methacrylic acid [123] ▪ Esterification of itaconic acid into itaconate esters [124] ▪ Enantioselective hydrogenation of itaconic acid [125] ▪ Decarbonylation of lactic acid into acetaldehyde [126] ▪ Hydrogenation of lactic acid to 1,2-propanediol [127] ▪ Dehydration of lactic acid into acrylic acid [128] ▪ Esterification of lactic acid into n-butyl lactate [129] ▪ Hydrogenation of levulinic acid to γ-valerolactone [130] and 2-methyltetrahydrofuran [131] ▪ Esterification of levulinic acid into ethyl levulinate [132] ▪ Biocatalyzed esterification of succinic acid into dioctyl esters [133] ▪ Hydrogenation of succinic acid to tetrahydrofuran (THF) [134], 1,4-butanediol [135], and γ-butyrolactone [136] ▪ Catalytic wet air oxidation of succinic acid [137]

(d) Fatty compounds: edible fats and oils (C=C bonds, carboxylic group and fatty nitriles)	▪ Deoxygenation of fatty acids [138] ▪ Epoxidation of fatty acids and esters [139] ▪ Oxidative cleavage of unsaturated fatty acid [140] ▪ Metathesis of unsaturated fatty acid [141] ▪ Esterification and of fatty acid [142] ▪ Transesterification of fatty acid esters [143, 144] ▪ Hydrodeoxygenation of fatty acids [145] ▪ Hydrothermal catalytic cracking of fatty acids [146] ▪ Hydrogenation of unsaturated fatty acid (C=C) [147] ▪ Hydrogenation of fatty acids and esters into fatty alcohols [148-150] ▪ Hydrogenation of fatty nitriles to fatty amines [151] ▪ Isomerization of fatty acids [152] ▪ Amidation of fatty acids [153] ▪ Steam reforming of fatty acids [154]
(e) Wood and extractives derivatives: terpenes, phenolic compounds (*e.g.* creosol)	▪ Metathesis of *β*-pinene [155] and (-)-*α*-pinene [156] ▪ Polymerization of *α*-pinene [157] ▪ Oxidation of isolongifolene into isolongifolen-9-one [158] ▪ Stereoselective hydrogenation of (-)-*α*-pinene, *cis*-verbanone [159], citronellol and menthol [160] ▪ Hydroxylation of *α*-ionone and *β*-ionone to their corresponding mono-hydroxylated derivatives [161] ▪ Oxidative dehydrogenation α-terpinene to conjugated di-olefin [162] ▪ Epoxidation of *α*-pinene, 5-vinyl-2-norbornene [162] and hydroxy-containing unsaturated terpenes (*α*-terpineol, terpinen-4-ol, menth-1-en-9-ol, menth-1-ene, limonene and *α*-terpinylacetate) [163] ▪ Selective isomerization of 3-carene to 2-carene [164] ▪ Hydroformylation of (+)-*R*-limonene and (−)-*R*-carvone [165] ▪ Hydrodeoxygenation of lignin-derived phenolic compounds into alkanes [166, 167] ▪ Aerobic oxidation of lignin-derived phenolic compounds [168] ▪ Catalytic deoxygenation of phenolic compounds [169] ▪ Steam reforming of guaiacol [170] ▪ Condensation of creosol with short-chain aldehydes into bisphenols [171]
(f) Glycerol	▪ Esterification of glycerol into glyceryl diacetate and triacetate [172, 173] ▪ Condensation of glycerol with acetone into solketal [174] ▪ Dehydration of glycerol into acrolein [175] ▪ Catalytic glycerol reforming [176] ▪ Oxydehydration of glycerol into acrylic acid [177] ▪ Hydrogenolysis of glycerol into 1,2-propanediol [178] ▪ Oxidation of glycerol into glyceric acid [179] ▪ Carbonylation of glycerol with urea into glycerol carbonate [180, 181]

(ii) Pollutants degradation: One of the direct routes of catalysis implication in environment protection is the elimination of persistent biological, organic and inorganic hazardous substances found in water, air, soil, through catalytic degradation. In this scope enormous attention was focused on the development of sustainable routes both to prepare effective catalysts and to develop new efficient strategies for pollutants selective remediation. However, heterogeneous photocatalysis holds the major share of these

catalysts and catalytic processes [182], and this field has significantly exploded in the past decade [183, 184]. Interestingly, these processes use efficiently the light irradiation energy (UV or visible), even if some catalysts were revealed to be active also while in the dark [185].

Nowadays, the waste streams from chemical industry are strictly controlled and treated before being released in the environment. Herein, we are listing some of the recent examples of catalytic application for air, water and soil contaminants eliminations:

(a) Air:

- Photocatalytic degradation of NO_x gases through oxidation of NO and NO_2 toxic gases [186-188]
- Photocatalytic oxidation of NO and carbon particulate matter are air pollutants emitted by diesel engines to CO_2 and N_2 [189]
- Catalytic oxidation for the elimination of volatile organic compounds (VOCs) including formaldehyde [190], toluene [191], benzene [192], xylenes [193], *etc.*

(b) Water:

- Elimination of the methyl blue from wastewater by advanced oxidation process [194]
- Photocatalytic degradation of pesticides found in citrus processing industry wastewater (thiabendazole, imazalil and acetamiprid) [195]
- Degradation of high concentration azo-dye wastewater [196]
- Elimination of halogenated organic compounds [197], particularly the degradation of wastewater chlorinated compounds (*e.g. p*-chloroaniline) [198], 2,4-dichlorophenoxyacetic [199], pentachlorophenol [200], 1,2-dichloroethane [201], as well as 1,2-dichlorobenzene [202] and trichloroethylene [201], *etc.*

(c) Soil and solid wastes:

- Oxidative degradation of nitrophenols contaminate the soil into nontoxic carbon and nitrogen minerals [203]
- Photocatalysts for the degradation of Rhodamine B [204]

(iii) Wastes valorization: In addition to elimination and degradation, wastes treatment can allow access to several chemical platforms and value-added compounds. Thus, green catalysis can serve as efficient tool to protect our resources. Such process is essential for delivering a sustainable development and a long term growth. The conversion of these contaminants can be performed selectively in a mixture or after separation. Several renewables among those stated in the Table 2 above can be generated as industrial by-

products, and then they can be converted into value-added products as illustrated by the examples reported above (Table 2). A variety of these valorized products are used directly as cheap raw materials. Among these products we find mainly lactose from dairy industry [205], glucose from rice straw waste [206], silica from rice husk generated from industrial production of rice [207], high density polyethylene from plastic industry [208], and free fatty acids from animal fat residues in wastewater [209].

(iv) Clean and renewable energy use, production and storage: In addition to the environmental consequence of using fossil feedstock (oil, natural gasses, coal, *etc.*), the dependence on these energy sources is a highly risky strategy for long term sustainable economy. Therefore, alternative energy sources (*e.g.* wind, nuclear, hydroelectric power, *etc.*) are highly desired to build up a better future on earth. In addition to the efficient use of clean energy of different forms in catalysis (*e.g.* solar energy and microwave), green catalysis can also serve to produce and store clean and renewable energy especially hydrogen and biofuels (*e.g.* bioalcohols, bioethers, syngas, biogas, *etc.*). Several examples are reported in the literature including the catalytic capture of CO_2 and its conversion into synthetic natural gas (CH_4) [210], the production of clean and renewable hydrogen energy through catalytic water splitting by using solar energy [211], catalytic electrochemical hydrogen evolution reaction [212], and the electrocatalytic reduction of carbon dioxide and monoxide to produce liquid fuel (ethanol) [213], as well as numerous catalytic processes for biofuel production such as biomass hydrodeoxygenation [214], esterification [215], transesterification [216], hydrogenation [217], *etc.* Similarly, several strategies were developed for the storage of clean energy such as ambient temperature catalytic dehydrogenation to produce hydrogen from viable hydrogen storage medium (*e.g.* formic acid) [218], methane, hydrogen, and acetylene storage in metal-organic frameworks [219] as well as electrocatalyst for higher-capacity rechargeable lithium batteries [220], *etc.*

2.1.5. Green and sustainable catalysts design

Along with the development of green catalytic transformations, ingeniously a remarkable progress has been also made toward green preparation of catalysts themselves. Therefore, as illustrated in Figure 5, variety of approaches have been developed for the green design and synthesis of catalysts, including; the design of magnetically recoverable catalysts,

nanocatalysis, biocatalysis (enzymatic), heterogenized homogeneous catalysts, bio-based catalysts synthesis (using bio-base precursors and templates) as well as the use of green tools for the synthesis of catalysts (*e.g.* ionic liquids, microwaves, *etc.*)

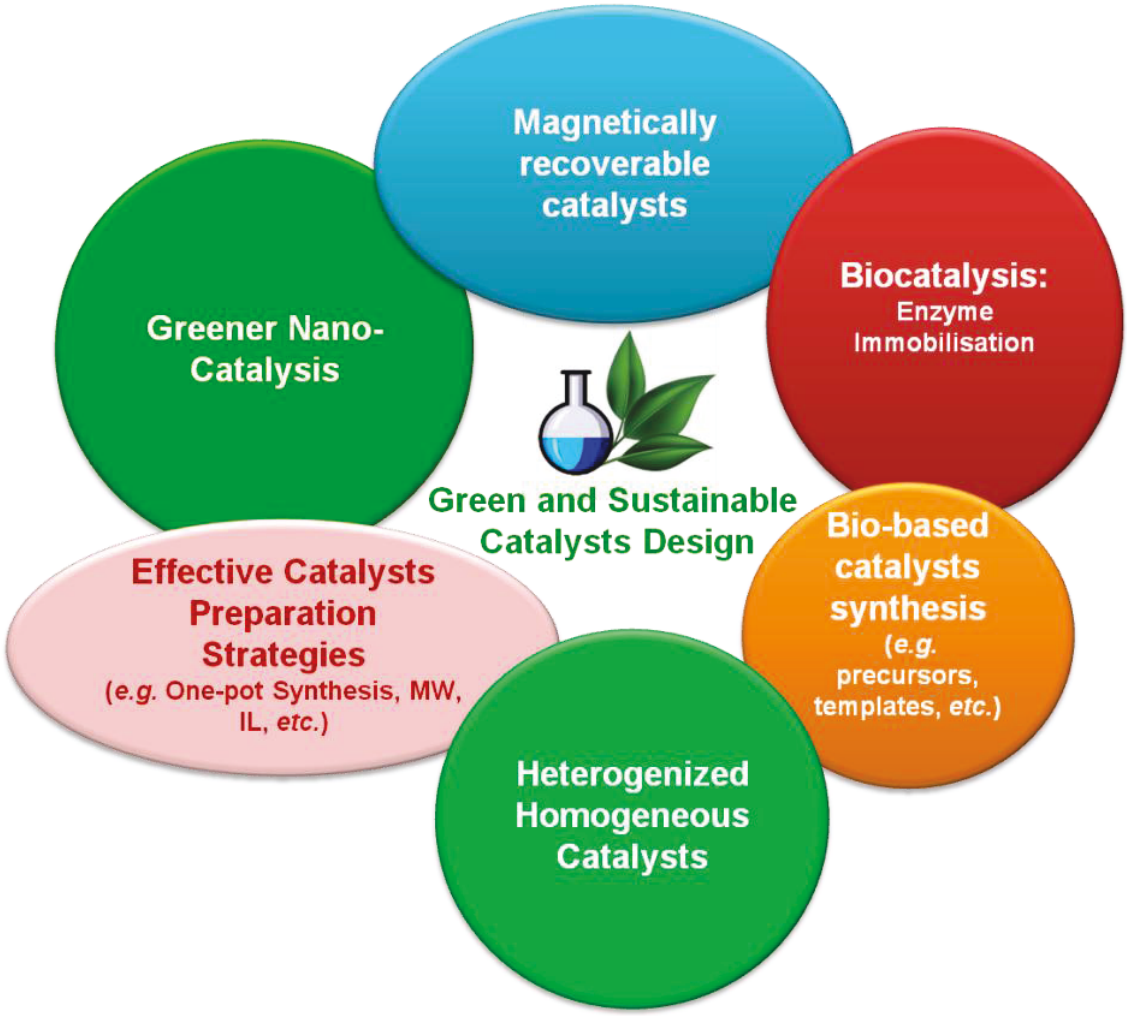

Figure 5. Different approaches towards the design of green and sustainable catalysts. MW: microwaves; IL: ionic liquids.

(i) Magnetically recoverable catalysts: This methodology is considered as a powerful tool in heterogeneous catalysis enhancing the sustainability of several catalytic processes, especially those using expensive catalysts which can be easily retrievable using this technique. Thus, purification and separation processes are made even more efficient, resolving issues related to waste generation and management. The preparation techniques of these catalysts are currently undergoing rapid development. However, these catalysts are

usually based on magnetic metal nanoparticles, magnetic alloys or metal oxides (*e.g.* Fe_3O_4) as well as polymer-derived and porous structures-immobilized magnetic materials (*e.g.* magnetic nanoparticle conjugated mesoporous nanocatalyst Fe_3O_4@SBA-15) [221, 222], with different magnetic properties. However, iron nanoparticles constitutes the major share of these materials allowing access to hybrid structures incorporating other catalytically active metals either in decorated or core shell type entities (Figure 6a).

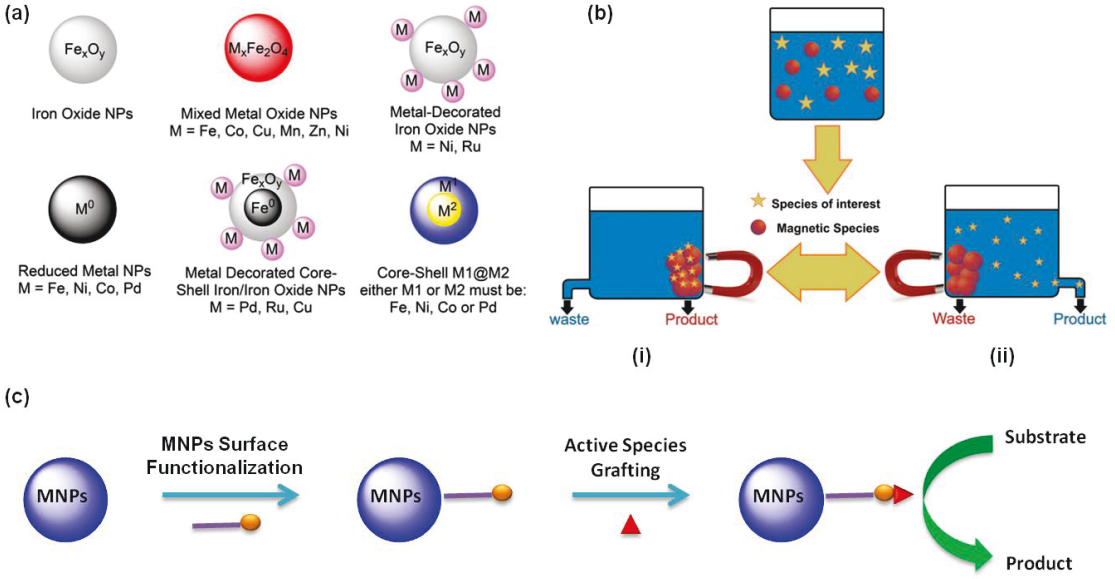

Figure 6. (a) Strategies for the design of catalytic bare magnetic nanoparticles (Reproduced from Ref. [223] with permission from The Royal Society of Chemistry). (b) Examples of the use of magnetic separation (Reproduced from Ref. [224] with permission from The Royal Society of Chemistry). (c) Traditional methodology for the incorporation of catalytically active species onto functionalized magnetic nanoparticles.

These catalysts are usually affordable, less toxic and stable under harsh conditions [223-226]. This elegant strategy is offering a special pseudo-homogenous phase that can be simply separated using an external magnet avoiding laborious centrifugation and/or filtration processes, while preserving the catalytic features of the recovered materials usually without loss of activity [225]. Magnetic separation is performed either to capture the targeted species (*e.g.* catalyst preparation, see Figure 6bi) or to isolate the final product (*e.g.* performing reaction, see Figure 6bii) [224]. The design of these catalysts is often

based on surface modification of magnetic nanoparticles with active catalytic species (Figure 6c) [227]. These magnetic nanoparticles are solid supports having small size and high surface area enabling excellent loading and high catalytic activity [225]. These catalysts have been showing excellent performances for a wide range of catalytic transformations [228].

(ii) Green nanocatalysts: Recently, nanocatalysis is gathering expanded attention, mainly because it bridges homogeneous catalysis performing catalytic processes at a single metal site from reactants to products, and heterogeneous catalysis through the use of insoluble microscopic powders [229]. The nanoscale features of these catalysts benefit widely from the increased surface-to-volume ratio and the accessibility of active surface sites, especially for surface-dependent catalysis [229]. These catalysts are highly stable and efficient for environmental perspectives such as degradation of organic pollutants over heterogeneous Fenton catalysts through the generation of hydroxyl radicals from hydrogen peroxide [230] and for the generation and storage of clean energy (*e.g.* hydrogen) [231]. These fascinating features and applications make catalysis greener [229, 232].

(iii) Biocatalysis: Enzymatic catalysis is gaining an increased popularity as the most powerful biotechnological tool in the chemical industry due to its remarkable efficiency and selectivity. Enzymes are considered as green catalysts due to their biodegradability and their inexpensive production which is usually performed *via* fermentation of renewable feedstock [39]. However, regeneration and recovery of enzymes is often troublesome. Thus, in order to offer more cost-effective and greener catalytic processes, several enzymes (*e.g.* lipase) have been successfully immobilized on solid catalytic supports (*e.g.* porous materials) and membranes enabling excellent activity, stability and recycling, thus improving the process economics (Scheme 1) [233-237]. Moreover, enhanced performance is often observed with immobilized enzymes compared to their free counterparts, due to their favourable interactions with the support as well as their protection and preservation of the enzyme properties under drastic conditions (improved stability) [238]. These biocatalysts are widely used for biorenewables production through biomass breakdown [239, 240], in functional cosmetics synthesis [241], and carbon dioxide capture applications

[242]. This field is enjoying a tremendous growth, while numerous biocatalysts have been successfully commercialized as a step forward to large-scale applications and automation with industrial biocatalysts with high products quality and lower environmental footprint replacing traditional conversions through chemicals [242-244].

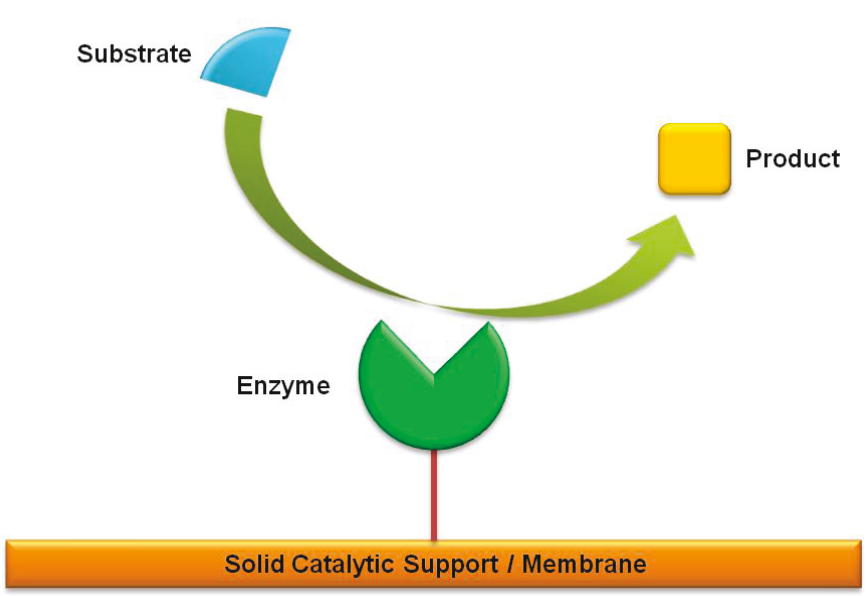

Scheme 1. Illustration of enzyme immobilization on solid catalytic supports or membranes as highly active biocatalysts.

(iv) Effective catalysts preparation: In addition to developing green tools for performing more sustainable catalytic conversion, considerable efforts have been also focused on sustainable preparation of the catalyst itself using green conditions such as:

- **Microwave-assisted catalysts synthesis:** Microwave heating is offering various benefits enhancing catalytic transformations [245]. Similarly, microwave technology was also successfully applied for the synthesis of catalysts and catalytic materials (*e.g.* nanomaterials, mesoporous materials, *etc.*). Using microwave heating is offering great improvements when used for either liquid-phase synthesis (*e.g.* hydrothermal synthesis), solid-state synthesis or even for calcination and thermal treatment processes (*e.g.* carbothermal reductions, chemical vapor deposition, *etc.*) [246]. Not surprisingly, microwave-assisted synthesis with controllable thermal activation was found faster,

simpler and more economical than conventional convective heating methods. Moreover, these synthesis processes are achieved with significant energy savings enabling easy scalability, thus overcoming a major drawback usually encountered in chemistry of materials [247-249]. Furthermore, microwave heating allows a great control over the materials morphological and textural properties [250]. These materials features can be tailored upon variation of synthesis conditions (*e.g.* precursors, reaction medium, *etc.*) which could have distinct microwave absorption abilities [251]. It was reported that the fast heating rates when using microwaves enhances the dispersion of supported catalysts [252], and the uniformity of pore network in porous materials [246, 253]. Also, it generates phase, morphology and size-controlled uniform particles by promoting homogeneous molecular nucleation and growth as well as rapid crystallization rates compared to conventional heating [254-259], often leading to materials with large external surface areas [256]. These interesting features offered by microwave heating method, usually leads to more active and stable catalysts and catalytic materials [260].

- **Ionic liquids for catalysts preparation; formation, stabilization and recyclability of catalysts:** Besides being one of the most effective reaction media due to several parameters (solid-like nonvolatility properties, unique mobility with great and useful surface area, high stability, and easy recyclability), ionic liquids are also used as dual solvent-catalysts [261, 262]. Ionic liquids can be used as a highly efficient Brønsted acid catalysts for various transformations (*e.g.* esterification [263], Mannich [264], oxidative desulfurization reactions [265], *etc.*) often without any additional catalysts [266], especially when using ionic liquids bearing superacid functionalities [261]. These catalysts showed impressive performance and recyclability within distinct catalytic systems (homogeneous, heterogeneous and biphasic catalysis) [267]. Similarly, several homogeneous catalysts have been effectively tagged on ionic liquids showing excellent catalytic activity and efficient recyclability and reuse [268, 269]. Furthermore, ionic liquids have been successfully used to promote the formation and stabilization of catalysts and catalytic materials as useful catalyst support (*e.g.* for metal nanoparticles) [267, 270]. ionic liquids can serve as catalysts support for homogeneous, heterogeneous and biocatalysts**.** However, they can also be covalently bonded to functionalized solid

catalysts (*e.g.* metal oxides, polymers, *etc.*) [271-273]. Interestingly, ionic liquids-immobilized/functionalized catalysts were reported the undergo a synergetic effect that promotes their catalytic activity [271]. The extraction of reaction products is more efficient in the presence of ionic layer due to the immiscibility of ionic liquids with many organic solvents simplifying the work-up procedure. It is thus more easy and practical to recover and recycle the catalyst found in this ionic layer [262], avoiding problems related to catalysts leaching. Moreover, recently, an emerging trend consists on combining ionic liquids and magnetic nanoparticles advantages, through the preparation of magnetically supported ionic liquid-based recoverable catalysts with a fascinating performance and recyclability because it could easily be recovered by separation using an external magnet [274-277]. However, ionic liquids could be also used for the synthesis of catalytic materials either as solvent [278, 279], template [280-283], or even as reactant/precursor [284-286].

(v) Heterogenized homogeneous catalysts:

Due to the remarkable activity and interesting modulation abilities of homogeneous catalysts, enormous efforts have been focused recently on developing practical strategies for their recycling and regeneration towards cost-effective applications. In similar fashion to enzymes immobilization, the heterogenization of homogeneous catalysts has been also showing remarkable results upon their grafting on a variety of functionalized solid catalytic supports [287]. This strategy is widely used for the synthesis of immobilized asymmetric stereoselective catalyst [288, 289]. Numerous papers have been reported describing successful heterogenization of molecular catalysts in solid supports [267]. Usually, immobilization strategies are based on covalent bonding through highly reactive ligands and/or functionalized solid surface [287, 290, 291]. However, these homogeneous metal complex catalysts can also be immobilized *via* ion pair formation (electrostatic interactions) or entrapment [292]. Micro-encapsulation in polymer films is also an effective strategy to immobilize homogeneous catalysts [290]. These immobilization strategies do not only promote the regeneration of the catalysts but also enhance the catalysts stability and the activity with a uniform distribution on the support surface. These catalysts exhibit higher catalytic efficiency and robustness than their homogeneous analogues without

significant loss of catalytic activity after recycling and reuse several times [293, 294]. Furthermore, the immobilization process can help to transform an inactive homogeneous system into an efficient catalyst due to the pseudo-dilution effect, with reduced formation of aggregates in the supported system that usually take place in the homogeneous counterpart system. Furthermore, as described above, IL can also serve as an efficient support for homogeneous catalyst immobilization.

(vi) Catalysts biosynthesis:

Despite the conversion of biomass renewable resources and wastes into value-added products through catalytic transformations, these resources are also used for the preparation of catalysts and catalytic materials in various forms. These inexpensive available compounds can be used as precursors for the synthesis of functional materials, for instance, glucose as carbon source for the synthesis of metal carbides [295]. and other carbon-based materials [296]. Silica and carbon-derived materials can be economically prepared from rice husk pyrolysis char, agar extracts, cellulose, 2-furaldehyde and plant material wastes as precursors; these prepared silica and carbon-derived materials are successfully used as adsorbents and catalysts [297-301]. The ideal synthesis of porous and nano-shaped materials is through template-free strategies [302]. However, when templates are required we should appeal for cheap and available compounds. Thus, in addition to their use as precursors, inexpensive compounds from biomass renewable resources and wastes are also used as templates for the synthesis, growth and formation of various nanostructured materials (*e.g.* SnO_2, Fe_3O_4, TiO_2, Al_2O_3) [303-306]. However, these compounds can also be used both as precursors and templates [307, 308]. More interestingly, even the residues of used catalysts can be reused to prepare a new catalyst. For instance, the dissolved metals (*e.g.* V, W, *etc.*) in leaching solution can be separated and involved in another catalyst preparation process for more cost-effective and environmentally friendly synthesis [309].

(vii) Nanomaterials, nanoparticles and metal-based catalysts toxicity and environmental risks:

No doubt that nanomaterials and related catalysts provided various solutions and breakthroughs towards the advancement and enhancement of various transformations. However, the ultimate success of many nanotechnologies will depend on our ability to understand and manage nanomaterial health risks [310]. Therefore, awareness of nanomaterials' toxicity should be raised among scientists and manufacturers handling them. In this scope and recently, limited research are conducted in this area and few reports have been published dealing with the "nanotoxicology" aspects [311-313], while, more attention should be paid to this serious issue in order to establish a greener nanotechnology. The small size of nanoparticles allows them to penetrate easy into various environments even inside cells (human, animal and plants). Therefore, the main threat of these compounds is their contribution in increasing the proportion of nanometer-sized particles in the environment and expanding the variety of chemical compositions [311]. The exposure to this kind of conditions (*e.g.* air pollution) may lead to serious consequences such as lung damage (*e.g.* inhaled nanoparticles), respiratory and cardiovascular diseases, as well as various cancers due to non-inhalation routes of nanoparticles (*e.g.* dermal and medical injectables) [311, 312, 314]. Moreover, the penetration of nanomaterial into living cells can cause tissue inflammation as well as major abnormal biochemical cellular function or cell death [311, 312, 314]. On the other side, some of the nanoparticles are relatively benign to biological systems. This beneficial feature is allowing the use of nanomaterials for therapeutical aims, such as cell tracking, drug delivery agents and biomedical devices [315-317].

Eventually, multidisciplinary efforts should be made in order to manage the use and application of these nanomaterials towards technological and industrial development, while limiting their impact on environment and health. The fundamental understanding and identification of nanoparticles-related toxins creation and exposure mechanisms and pathways, as well as their biochemical interactions within organisms can greatly help to reduce human exposure to toxic nanomaterials [311]. It is also, crucially important that novel nanomaterials must be biologically characterized for their health hazards to ensure

risk-free use [318], for instance the development of specific or general *in vitro* screening assays [319].

On the other hand, catalysts' degradation and particularly catalysts-related metal residues could be harmful. Therefore, limiting this phenomena and is a challenging task to ensure that the concentrations of heavy metals leachate (*e.g.* Cd, Co, Ni, Cu, Au, Cr, *etc.*) should be low compared with the environmental standards. These components can bind to, and interfere with the functioning of vital cellular components, causing serious diseases.

Currently, methods that are used for metal species immobilization on catalytic support are often based on covalent interactions, these methods are considered as highly efficient grafting strategies. Nevertheless, studies showed that, for instance, pH is a major controlling factor in metal leachability of metal-based catalysts [320]. Therefore, comprehensive analytical characterizations of the catalysts' residue in the isolated compounds should be performed, especially when elaborating either a pilot plant or scale-up production catalytic systems. Similar characterizations should also be conducted on wastes (*e.g.* by-products) generated by these processes, to allow acceptable landfill disposal of the leach residues. Like final product/by-products toxicity evaluation and treatment, thousands of tons per year of spent catalysts generated by industry (food, chemical, petroleum, petrochemical, *etc.*), which contain significant amount of metals [321], should be similarly neutralized.

Nowadays, depending on the nature of these metals and their environments (*e.g.* water, soil, *etc.*), numerous technologies are employed to re-mediate toxic heavy metals such as extraction (*e.g.* volatization), isolation, physical separation (mechanical), immobilization, chelating agents, oxidation/reduction, *etc.* Nonetheless, regardless of their heavy metal nature some of these metals are essential, in small quantities, for human health. Furthermore, metals encapsulation was found to be an efficient strategy to reduce heavy metals concentrations and toxicity. *In vitro* biopersistence studies showed that carbon nanotubes-encapsulated (non-bioavailable) metal particles in catalysts persists in a stable and biologically unavailable form, suggesting that simple removal of bioavailable (free) metal is a promising strategy for reducing these catalysts' health risks [322]. Similarly,

encapsulation using clay was found to lead to formation of a matrix around the heavy metals to prevent leaching [323].

2.2. Harmful plastic wastes and bioplastic production

2.2.1. Plastic wastes elimination and catalysis

Among all pollution source, solid wastes are the most threatening due to the enormous amount generated by the industry. Plastic packaging waste is currently a major share of solid wastes, increasing environmental concerns because it likely ends up in landfill sites and may take thousands of years to be eliminated [324]. Nearly all these wastes are non-biodegradable and their complex composition hampers their recycling or their reuse especially [325].

Efforts have been made in order to establish efficient routes for plastic waste management. However, current options are generally limited to recycling and landfill disposal. Moreover, incineration is also widely used for this purpose. However, practically, in some cases, this method has serious consequences such as the generation of hazardous emissions of potentially carcinogenic compounds as well as poisonous gases [208]. Interestingly, several heterogeneous catalytic applications (*e.g.* depolymerization) are found very useful and effective for the degradation of plastic wastes, in addition to their valorization into value-added products [208], fuels and chemicals [326].

2.2.2. Bioplastics as a suitable alternative to conventional polymers

In the early 1980s, bio-based plastics were introduced as nonpetroleum-based polymers decreasing the environmental and economical problems derived from production, use, and disposal of petroleum-based plastics [327]. Bioplastics are ecofriendly plastics with lower environmental impact. Some of these plastics are ideally biodegradable which can be degraded to carbon dioxide and water by the action of naturally occurring microorganisms [328]. In the past two decades, bioplastics gathered a wide attention for their highly potential material-like properties, low production costs, and their friendly non polluting degradation [329], biodisintegration in the environment [330], as well as the environmentally and non costly regeneration process [331]. Bioplastics can be produced by modification of naturally occurring polymers. However, these polymers are mainly

prepared starting from monomers units. Bio-based feedstock monomers production for the synthesis of thermoplastics can be divided into three main categories; (i) *via* thermoforming processes, (ii) catalytic conversion or (iii) fermentation using microorganisms [332]. These monomers are combined to prepare conventional polymers or followed by a polymerization step. Bio-based polymers can displace current petroleum-based polymers in the market. Nowadays, many bio-based polymers are commercially available; *e.g.* polyethylene furandicarboxylate from corn-based fructose, poly-β-hydroxybutyrate [332], polyhydroxyalkanoate [333, 334], starch [335], polylactic acid and bio-based polyethylene [336]. Interestingly, most bio-based polymers, particularly polyhydroxyalanoate, polylactic acid and polybutylene succinate demonstrate biodegradability, something most petroleum-based polymers lack.

2.2.3. Bioplastics application spectrum

The production of bio-based polymers at industrial large-scale enhanced the availably of these unique materials for several applications. Bio-based plastics are used in many manufacturing process offering a wide range of biodegradable, low toxic and environmentally friendly products as illustrated in Figure 7.

Figure 7. Application of bioplastic products in diverse fields

However, these bio-polymers are widely used for agricultural applications, considering the direct relationship of agricultural products with human health (*e.g.* food packaging) because of the interesting features of such polymers (*e.g.* low toxicity). Thus, various products have been made including shopping bags, kitchen utensils, food packaging bio-based plastic bottles and food bags. These polymers also are currently used for medical applications [327] (*e.g.* biomedical devices and tools, drugs packaging, *etc.*), automobile industry [337] (*e.g.* tires and other automobile parts and devices), electronic devices like cell phone parts [338] and other household equipments.

2.2.4. Development, challenges and future of bioplastics

Biopolymers are not fossil fuel-dependent which helps to preserve fossil feedstock reserve and reduces anthropogenic greenhouse gas emissions, having a lower impact than conventional polymers. This is highly beneficial against eutrophication, carcinogens, and ozone layer depletion. They also contribute to increase the security of raw material supply through the transition from fossil feedstock to sustainable bio-based renewable and low-cost feedstock [336, 339]. Despite all these advantages and beneficial features, bioplastic industry is still facing challenges, like inferior mechanical properties and processability. These drawbacks limit their potential use in some high-volume markets like automotive, but their biodegradability can make them a valuable choice in markets such as biomedical and agriculture.

With no doubts, this class of polymers is the future toward ecofriendly use and elimination of solid wastes. These bio-based polymers are highly interesting due to their green and cost-effective life cycle, their biodegradability and recyclability features. Thus, these polymers are expected to widen their application field, especially with high expectations due to several factors such as:

- Secured feedstock: raw materials availability
- Regulations: meets and respects international environment and heath standards
- Performance: progressive improvement of thermal and physical properties
- Growing market: exploded and significant demand in the target markets

2.3. Recent advances in olefin metathesis

Biopolymers synthesis is essentially based on the accessibility of the starting materials (monomers units). In this scope, as one of the commonly used methods, catalytic conversion of renewable substrates are widely varied offering access to simple and functionalized monomers that can be used as building blocks to prepare such bio-based polymers. Therefore, efforts have been focused on exploring efficient catalytic routes for this purpose. Metathesis reaction is one of these efficient routes providing rapid and direct access to such interesting monomers.

2.3.1. Olefin metathesis and landmark catalysts

Metathesis reaction is one of the most powerful tools in synthetic chemistry [55-57, 340]. Metathesis reaction was originally discovered by Anderson and Merckling in 1955 [341], then confirmed by Banks and Bailey [342] more than fifty years ago. Later, it was mechanistically established by Chauvin and Hérisson [343]. Metathesis reaction is defined as a transalkylidenation reaction involving substituents rearrangement of molecules containing C=C bonds resulting in exchange of alkylidene fragments. This double bond substituents exchange occurs through scission of the later and the regeneration of a newly redistributed double bond as illustrated in Scheme 2 [343]. The discovery and development of metathesis reaction gained an enormous impact in chemistry. Therefore, Yves Chauvin, Robert H. Grubbs and Richard R. Schrock were jointly awarded the 2005 Nobel Prize in Chemistry [55-57]. Since then, the development of sustainable, efficient, stable, and selective catalysts is a continuous research challenge as well as the increased attention toward the use of metathesis reaction in synthetic chemistry (Figure 8).

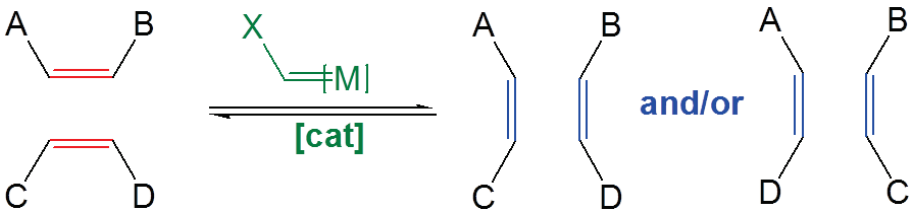

Scheme 2. The general proposed metathesis pathway by Hérisson and Chauvin. Ref. [57, 343]

First, the metathesis reaction was observed with alkenes, and then it was expanded to alkynes [344-346] and alkanes [347-349]. Meanwhile, a variety of transition-metal complexes involving W, Mo, Re, and Ru have been proved to be efficient catalysts for metathesis reaction. Olefin metathesis gathered a big industrial interest as a powerful tool for C-C double bond formation, which was highly advantageous enabling rapid, mild and cleaner conditions as well as low cost for manufacturing process of pharmaceutical products, fine chemicals, pesticides and polymers [350, 351]. Phillips Petroleum [352] using WO_3/SiO_2 and Shell's Higher Olefins Process (SHOP) [353] using MoO_3/Al_2O_3 are the most well-known industrial processes for metathesis reaction proceeding until nowadays.

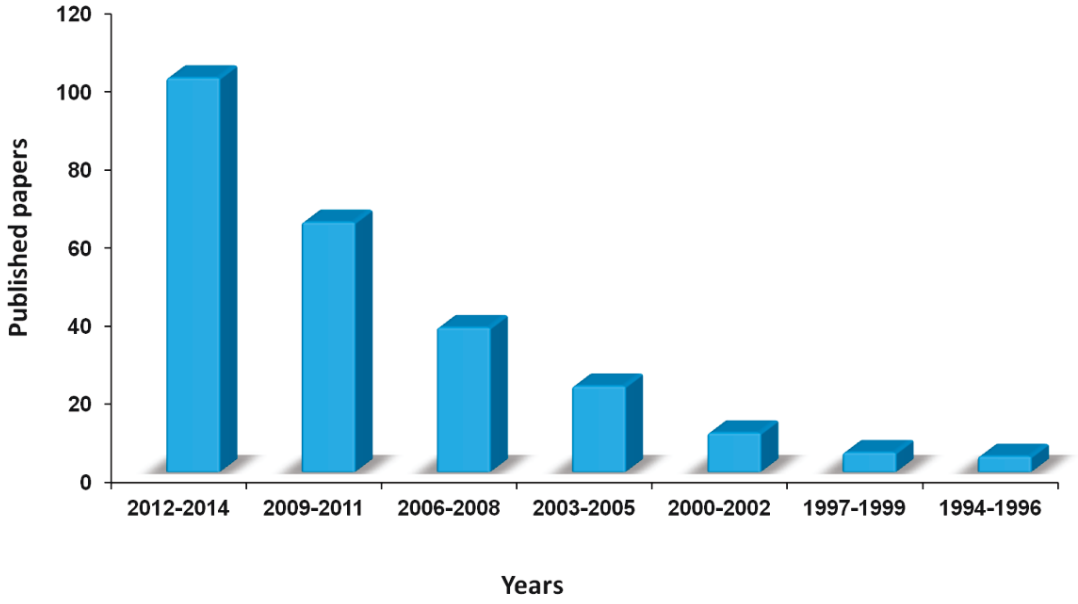

Figure 8. Evolution of published papers reporting the synthesis of metathesis catalysts and/or the use of metathesis reaction in synthetic chemistry, source: Web of Science, period 1994-2014.

2.3.2. Homogeneous *vs.* heterogeneous metathesis catalysts: advantages and progress

Besides metathesis catalysts, in general, heterogeneous and homogeneous catalysis have widely emerged in different industrial fields. However, industrially heterogeneous catalysts are the leaders; nearly 85% of all industrial catalytic processes are based on heterogeneous

catalysts [43], *e.g.* petroleum refining cracking process over Pt/Re on alumina, zeolite [354], methanol synthesis over $Cu/ZnO/Al_2O_3$ [355] and styrene production over mesoporous alumina supported iron oxide catalyst [356]. Heterogeneous catalyst active sites engineering and modification are widely enhanced by the development and the improvement of the spectroscopic analysis methods, which was and still is a topic of high interest since the introduction of the catalytically active site concept by Taylor ninety years ago [357].

On the other hand, costly homogenous catalysts are mainly used in small-scale laboratory synthesis, particularly when selectivity is critical and product-catalyst separation problems can be easily solved. Homogeneous catalytic systems are generally far more selective for a single product, more active, and more easily studied from chemical and mechanistic aspects. Moreover, they are kinetically easy to determine due to the simplicity of the catalytic system and the obvious interaction with substrates (*e.g.* olefins for metathesis), as well as the clear pathway for active sites and intermediate species formation. In addition, homogeneous catalysts are easily modified for optimizing selectivity, thus ligands steric and electronic properties are broadly tailored for that purpose. Nevertheless, these homogeneous systems are more susceptible to poisoning and they are far more sensitive to permanent deactivation due to their low stability, especially towards thermal conditions, which make their decomposition very fast. In general, homogeneous catalysts deactivation takes many forms including accidental contact air or moisture; lability of metal−ligand bonds or ligands degradation; inhibition by the solvents, by deposition of bulk metal; by reaction products accumulation or substrate functionalities [358]. Moreover, stable catalytic intermediates are often formed during the reaction; such undesired complex doesn't offer any catalytic activity which alters the catalytic cycle, decreasing the catalyst activity and reducing its life cycle. Furthermore, since these catalysts operate in single-phase media, their separation from products/reactants is often extremely difficult, if not impossible to achieve, while catalysts poisoning sometimes results in inorganic salts formation which are highly toxic and hazardous to dispose of.

In contrast, heterogeneous catalysts are insoluble solids found in a different phase from substrates, solvents and products, which makes the catalyst active interface site less

exposed to poisoning conditions. The biphasic media allows easy separation of substrates/products, rapid solvents extraction and easy recovery and recycling of the solid catalyst without exhausting costly experimental workup. Thus, highly pure products are easily isolated with no or minimized catalyst (*e.g.* metals) trace in the final products. Moreover, some heterogeneous catalysts are even more selective than their homogeneous counterparts. However, the presence of numerous kinds of active sites on the catalyst surface as well as the low concentration of desired active sites alters the heterogeneous systems selectivity and activity.

Heterogeneous systems tolerate a wide range of temperatures and pressures, which makes their use and storage safer compared to the homogeneous systems. However, heterogeneous catalyst deactivation is not excluded especially with supported catalyst on porous materials including chemical, thermal, and mechanical deactivation phenomena, through several mechanism such as poisoning, fouling, thermal degradation and sintering, vapor formation, vapor-solid and solid-solid reactions, coking as well as attrition/crushing [359]. However, poisoning due to strong chemisorption of species (*e.g.* reactants, products, or impurities) on catalytic sites which block sites for catalytic reaction, is the most commonly encountered [359].

In many cases, kinetic and mechanistic analyses of homogeneous heterogeneous systems performance have contributed to provide insights on the reasons behind catalysts deactivation, which paved the way for further studies to avoid such catalyst design and reaction conditions. The development of sustainable catalysts could be established through a combination of the advantages of homogeneous and heterogeneous catalysis, *e.g.* heterogenizing homogeneous catalysts by grafting transition-metal inorganic/organometallic complex catalysts on high surface area mesoporous solid supports through covalent or ionic bonding [360-363], these support are considered as a highly effective rigid ligands. Other attractive combined catalytic systems have been developed; *e.g.* thermomorphic soluble fluorous biphase catalysts,[364] functionalized room-temperature ionic liquids [365], supercritical fluids extraction for catalyst regeneration/activation [366, 367] and “ship-in-a-bottle” trapped catalysts [368].

For metathesis reaction, the most active homogeneous catalysts developed are transition metals-based alkylidene complexes. Grubbs, Hoveyda-Grubbs, Schrock catalysts (Scheme 3) are the most successful among them and they are commercially available [55-57, 340, 369]. These homogeneous catalysts are very active and selective, and they are also compatible with a wide range of functional groups [370].

However, these homogeneous catalysts are expensive and often non-reusable. Thus, it is a priority to develop recyclable heterogeneous catalysts. Typical heterogeneous catalysts for metathesis are based on supported transition metal complexes, sometimes in presence of co-catalysts or promoters usually using silica or alumina-based supports. Thus several supported metathesis catalysts have been developed including supported metal oxides such as rhenium (ReO_x/Al_2O_3, ReO_x/SiO_2-Al_2O_3), molybdenum (MoO_x/SiO_2, MoO_x/Al_2O_3, MoO_x/SiO_2-Al_2O_3) and tungsten-based catalysts (WO_x/SiO_2 and WO_x/SiO_2-Al_2O_3) [31], generating distinct mono-oxo, dioxo, trioxo and oligomeric mono-oxo surface species (Scheme 4).

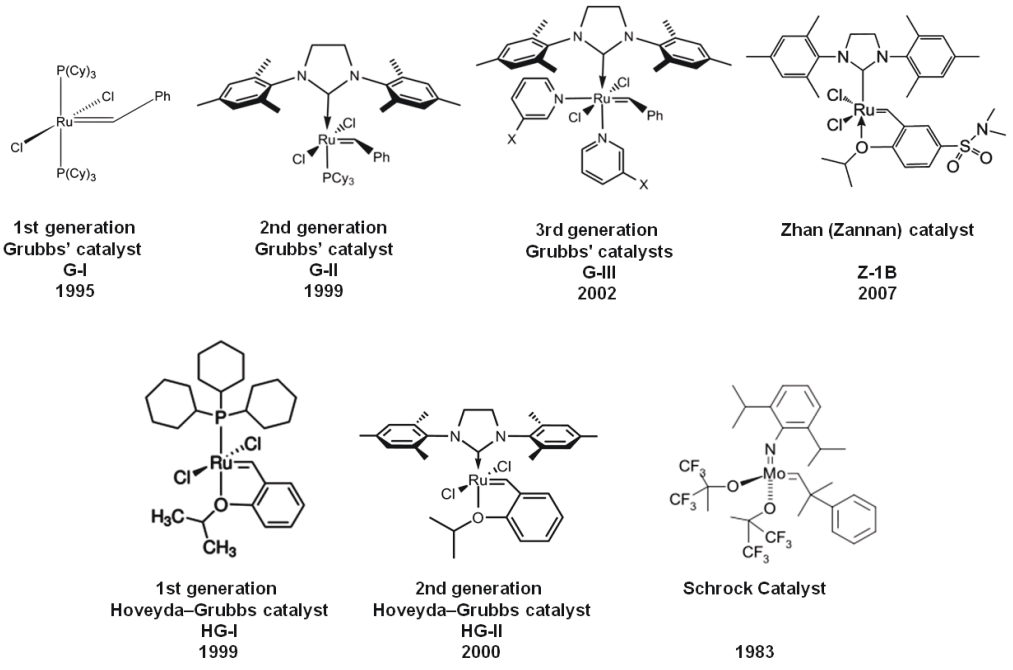

Scheme 3. Well-known commercial homogeneous metathesis catalysts

Regardless of the progress made in heterogeneous metathesis catalysts development, there is still unresolved issues related to fundamental aspects which are still not fully understood [31], such as surface reaction intermediates identification, the molecular structures and oxidation states of the catalytic active sites, as well as the reaction mechanisms and active species regeneration.

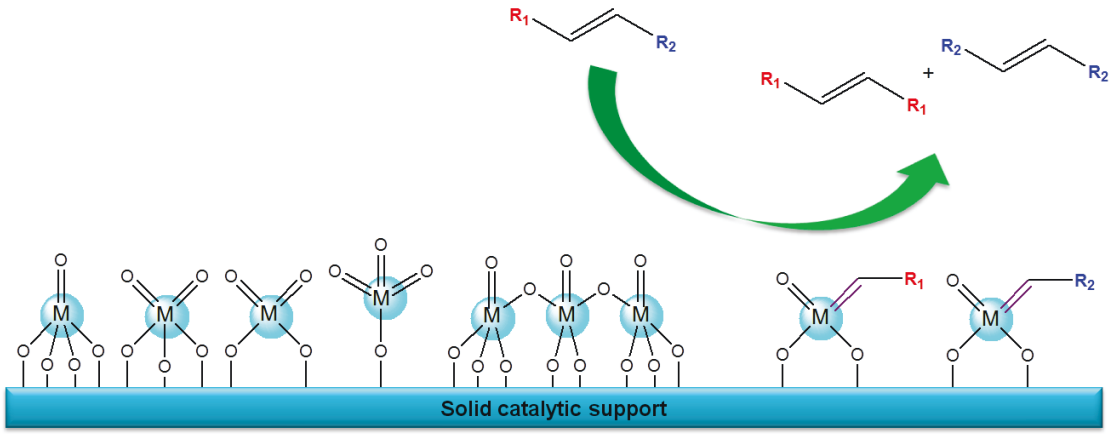

Scheme 4. Traditional heterogeneous metathesis catalysts (M: Re, Mo, W).

2.3.3. Re_2O_7/Al_2O_3 catalytic system and related catalysts

Organometallic oxides are key compounds in chemistry, easily accessible and have displayed a surprisingly broad range of catalytic activities [371-374]. They have been widely studied and incorporated for their catalytic activity [375, 376]. More particularly, several organometallic oxides-based catalytic systems were extensively studied for their metathesis activity, and were successfully developed with an excellent performance.

In addition to molybdenum [377] and tungsten oxide [378], rhenium oxides also exhibit interesting metathesis activity [379]; *e.g.* Re_2O_7 supported on different oxide (TiO_2, Al_2O_3, SiO_2) or mixed oxide (SiO_2–Al_2O_3). Re_2O_7/Al_2O_3 is one of the most used and studied catalytic systems for metathesis reaction. This catalyst was introduced for the first time by Verkuijlen *et al.* [380] using Me_4Sn as co-catalyst. Afterwards, co-catalysts of general formula SnR_4 emerged [381, 382]. Low-rhenium-loading Re_2O_7/SiO_2-Al_2O_3-SnR_4 or -PbR_4 (R = alkyl) catalysts proved to be highly active for bulky functionalized olefins metathesis due to their high Brønsted acidity [383-385]. SiO_2-Al_2O_3 support showed higher activities

than alumina alone [384]. In agreement with these results, Re_2O_7/SiO_2-Al_2O_3-R_4Sn showed higher conversions compared to Re_2O_7/Al_2O_3-R_4Sn [386]. Re_2O_7-based catalyst activity towards metathesis is attributed to ReO_4^- reactivity. FTIR analysis showed that ReO_4^- ions interact with basic surface OH groups only, while other interactions with neutral and acidic OH groups were detected at higher Re_2O_7 loadings, and more acidic phosphorus-bonded OH groups reacted with ReO_4^- ions at low Re_2O_7 loadings [387]. The Re_2O_7/Al_2O_3 catalytic system stability was greatly affected at higher temperatures. In contrast, alkyltin compounds led to a large increase in activity at lower loadings [386]. Re_2O_7/Al_2O_3 are not stable due to the few interactions (linkage) of the ReO_4^- ions with the hydroxyl groups on the alumina support surface [386]. This catalytic system remains inactive after only the first cycle, where it can be regenerated and partially activated with additional co-catalyst amount and further thermal treatment under oxygen flow [388, 389].

Addition of MoO_3, V_2O_5, or WO_3 oxides as metathesis reaction promoters to the Re_2O_7/Al_2O_3-R_4Sn and Re_2O_7/SiO_2-Al_2O_3-R_4Sn systems proved to be beneficial to enhance the metathesis reaction rate,[385, 390] while, addition of 6% B_2O_3 was shown to be efficient to increase the metathesis reaction activity of alumina and alumina-silica supported Re_2O_7 [391]. Re_2O_7/SiO_2-Al_2O_3 and $Re_2O_7/B_2O_3/SiO_2$-Al_2O_3 catalytic systems were proven to be very active for metathesis reaction of bulky functionalized substrates (*e.g.* fatty acid esters) without using any tin-based co-catalyst. Furthermore, germanium and silicon were used as promoters, *e.g.* R_4Ge, R_4Si, R_3GeH, R_3SiH (R= Me, Et, Bu) achieving good conversions with reasonable selectivity [392]. Recently, Re_2O_7/Al_2O_3 catalyst was investigated without the addition of any co-catalyst; furthermore, the metathesis reaction was performed under continuous supercritical CO_2 flow as a carrier to deliver reactants and remove products over the heterogeneous catalytic bed of Re-oxide supported on γ-Al_2O_3, showing a high metathesis reaction activity for simple non bulky functionalized olefins, but the catalyst was completely deactivated within 100-150 min [393]. Other Re_2O_7-based related species were reported for their metathesis reaction activity; ReO_3-based complex was also isolated as an active catalyst for metathesis reaction, which is obtained from Re_2O_7 and several organic-inorganic precursors [394]. The catalytic system $Re(CO)_5Cl/C_2H_5AlCl_2$ showed also an interesting metathesis reaction activity [395].

2.3.4. MTO-based catalyst

As pointed-out above, the most widely used heterogeneous catalysts for metathesis reaction of bulky functionalized olefins were Re_2O_7 supported on alumina and silica-alumina materials [389, 396]. However these catalysts are often susceptible to deactivation and require the use of toxic tin-based promoters and additives such as Bu_4Sn to increase the catalyst reactivity. The presence of tin also hinders the catalyst regeneration due to the deposed SnO_2 species on the catalyst surface, formed during each recycling process, which reacts with the active Re oxide and poison the catalyst [388]. Thus, owing to these limitations of Re_2O_7-based heterogeneous catalysts, the need for alternative approaches without using toxic molecules arises.

2.3.4.1. Organorhenium-based catalysts

The development of new organorhenium catalysts and the investigation of their activity is still underway; *e.g.* (pentamethylcyclopentadienyl) trioxorhenium (VII) **2** [373], (cyclopentadienyl) trioxorhenium (VII) **3** [397] and phenyl trioxorhenium (VII) **4** [373] were also reported as potential catalytic systems (Scheme 5).

Methyltrioxorhenium (VII) **1** (MTO) (Scheme 5) has been synthesized from Re_2O_7, as described in the pioneering work of Beattie *et al.* [398-400] MTO **1** is highly active not only for olefin metathesis reaction [35], but also for Diels-Alder cycloaddition, aromatic oxidation, olefin epoxidation, Baeyer-Villiger oxidation [373], dehydration, amination, and disproportionation of alcohols [401]. MTO exhibits excellent activities for metathesis reactions [34], due to its steric accessibility with a low coordination number and small ligands, a strong metal-carbon bond, as well as a pronounced Lewis acidity at the Re(VII) metal center. Moreover, in addition to the stability in air and with acids, MTO is characterized by a high thermal stability which is maintained even far above its melting point (m.p. 106°C). MTO is also soluble in all organic solvents and water without decomposition [36, 402].

On the other hand, (Cyclopentadienyl)trioxorhenium(VII) $CpReO_3$ **3** suffers greatly from the lability of the Cp-Re bond under oxidative conditions and in the presence of electron donor ligands or donor solvents leading to instable adducts [397]. Similarly, other trioxorhenium-based compounds such as (Pentamethyl cyclopentadienyl)

trioxorhenium(VII) **2**, (pentaethyl cyclopentadienyl) trioxorhenium (VII) **2'**, phenyltrioxorhenium (VII) **4** suffer from ligands steric hindrance under catalytic conditions [403], while compound **4** suffers also from the low stability of the phenyltrioxorhenium(VII) catalytic system [373], which decomposes even at room temperature [404]. Ethylrhenium trioxide **5** and isobutylrhenium trioxide **6** (Scheme 5) are prepared from dirhenium heptaoxide [404]. Ethylrhenium trioxide **5** is an air- and moisture-stable liquid; it is highly stable at room temperature, even in the absence of coordinating solvents. Ethylrhenium trioxide decomposition occurs slowly at 60 °C. Surprisingly, deactivation *via* β-hydrogen elimination is excluded with ethylrhenium trioxide which prevent its decomposition [404]. Isobutylrhenium trioxide **6** is also characterized by its thermal stability, which decompose at higher temperatures (120 °C) compared to ethylrhenium trioxide [404].

Besides organorhenium oxides, Chabanas *et al.* [405] reported the synthesis of a novel Re-based complex [Re(≡CBu-*t*)(=CH Bu-*t*)(CH_2Bu-*t*)$_2$] **7** supported on silica as a highly active well-defined metathesis heterogeneous catalyst for simple acyclic olefins (Scheme 5).

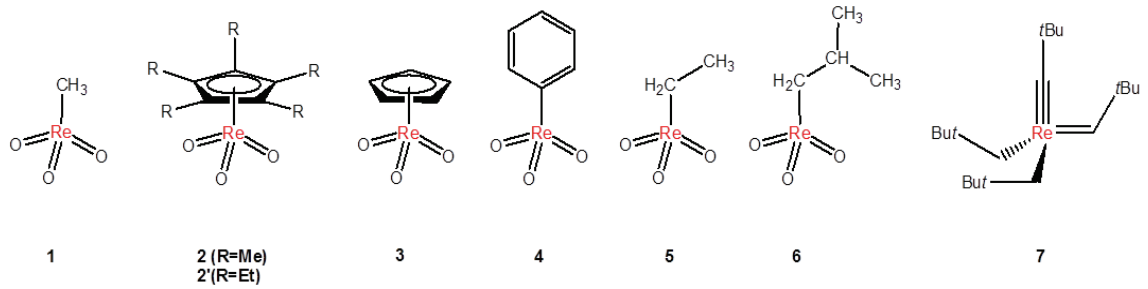

Scheme 5. Synthesized organorhenium oxide (1-6) and the tBu-based Re precursor (7)

2.3.4.2. Adsorbed methyltrioxorhenium (MTO) and metathesis reaction activity

Several assessments were established through the studies of the nature of the interactions between Re_2O_7 and the support in the catalytic systems [386, 387, 406, 407]. Similarly, MTO chemisorption on different inorganic oxides having different acid-base surface properties has also been studied. The results showed that when MTO was supported on silica SiO_2 (weak Brønsted acid sites) and titania TiO_2 (only Lewis acid sites) no activity was detected, while low activity was observed when supported on magnesia

MgO (no acid sites). However, niobia Nb_2O_5 supported-MTO showed a high metathesis reaction activity [408], demonstrating the correlation of Lewis/Brønsted acidity with metathesis reaction activity. Similar conclusions were drawn when studying other supports like Al_2O_3-SiO_2 [409]. Afterwards, several supports were proved to be efficient for MTO heterogenizing such as: Al_2O_3, MoO_3, CoO and different mixed oxides; Al_2O_3/MoO_3, Al_2O_3/CoO, Al_2O_3/CoO/MoO_3 and CoO/MoO_3 [410]. Moreover, zeolite was reported to be a suitable host to encapsulate MTO, and the encapsulated MTO has been proved to be highly effective for metathesis reaction [411]. MTO itself doesn't present any metathesis reaction activity when used alone in liquid phase; however the use of soluble Lewis acids such as $AlCl_3$, or $AlCl_3/Me_4Sn$ showed a good metathesis reaction activity of MTO in solution [36, 399].

Rhenium-alkyl complex are the origin of metathesis active intermediate species formation on the surface, where metallocarbene is resulting from the methyl substituent on the rhenium center of the MTO molecule [408, 412]. MTO supported on alumina showed a higher catalytic activity toward metathesis reaction compared to Re_2O_7/Al_2O_3, because the MTO-based catalyst already has the carbenic active species. The μ-methylene between Re and Al_S in [$Al_SCH_2ReO_3$] are generated through MTO interaction with the surface Lewis acidic sites of alumina. The formation of these propagating carbenic species was evidenced by solid-state NMR, IR, and by extended X-ray absorption fine structure spectroscopy (EXAFS) characterizations [413-417]. It has been also reported that [CH_3ReO_3] can tautomerize to [H_2C=$Re(O)_2OH$] photochemically under the influence of UV light (Scheme 6) [418-421]. On the other hand, the post formation of these species with Re_2O_7-based catalyst required an alkylation agent (*e.g.* tin-based additives) through an *in situ* generation which is hampered with bulky functionalized olefins (*e.g.* fatty acid esters) [413].

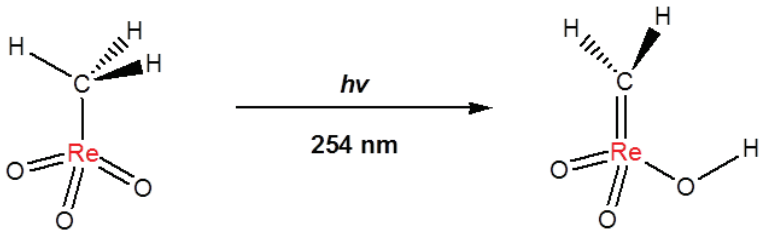

Scheme 6. Photo-induced tautomerization of MTO. Ref. [418-421]

Several studies investigating the chemisorbed CH_3ReO_3 (MTO) on alumina, reported that in addition to the maintained Re-C bond when MTO reacts with the Lewis acidic sites (surface aluminum atoms), other species are generated; majorly oxo ligand which can be coordinated with Lewis acidic Al sites, and minor formation of the μ^2-CH_2 species coordinated to the Lewis acidic Al sites after C-H bond splitting, thus OH group is formed on the support surface, as well as the carbenic active species (Scheme 7a) [416, 422-424].

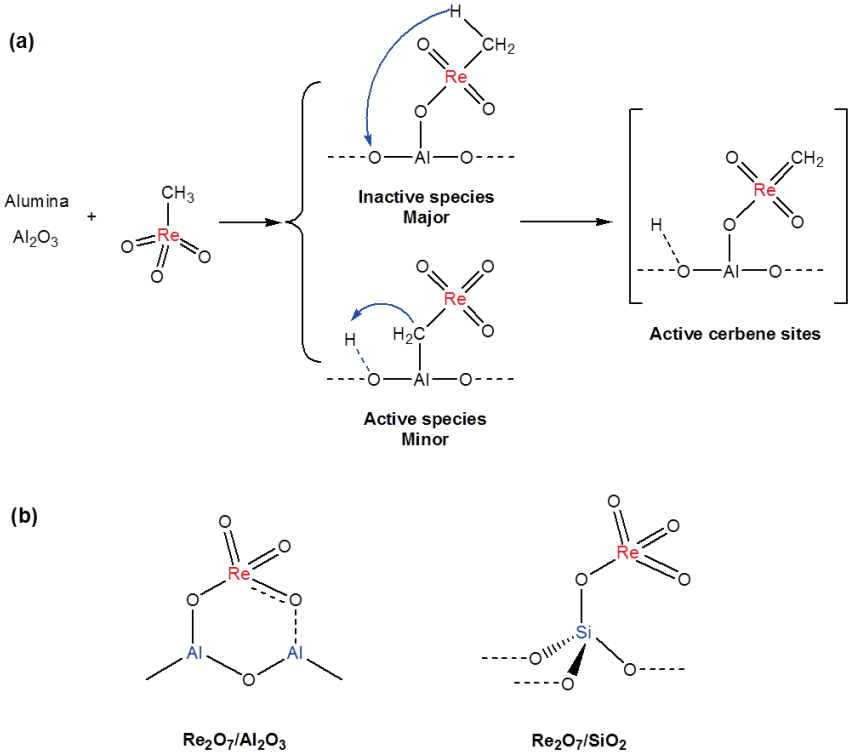

Scheme 7. (a) The major and the minor proposed surface species generated upon interaction of MTO on alumina and the resulting carbene sites; (b) The proposed generated Re-based species on alumina and silica surface with Re_2O_7.Ref. [413]

Similar oxo interactions were reported for the Re-based species generation when Re_2O_7 is supported on alumina or silica, then further alkylation with alkylation agents or carbon chain of the subjected olefins (Scheme 7b). Major species can also be obtained from the interaction of one of the adjacent bridging oxygens (AlOSi) on the surface with the Re center when supported on amorphous silica-alumina [425].

Generally the mechanistic pathway proposed for alkene metathesis reaction, particularly in the presence of Re-based catalyst includes the following four steps; first the coordination of the alkene with the Re center, then [2 + 2]-cycloaddition, the resulting metallacyclobutane can adopt both plausible structures; in trigonal bipyramid or square-based pyramid geometries (Scheme 8a). After that, reversely cycloreversion ring-opening occurs through a retro-[2 + 2]-cycloaddition and finally de-coordination of Re-based complex releasing the desired metathesis reaction products [424, 426, 427].

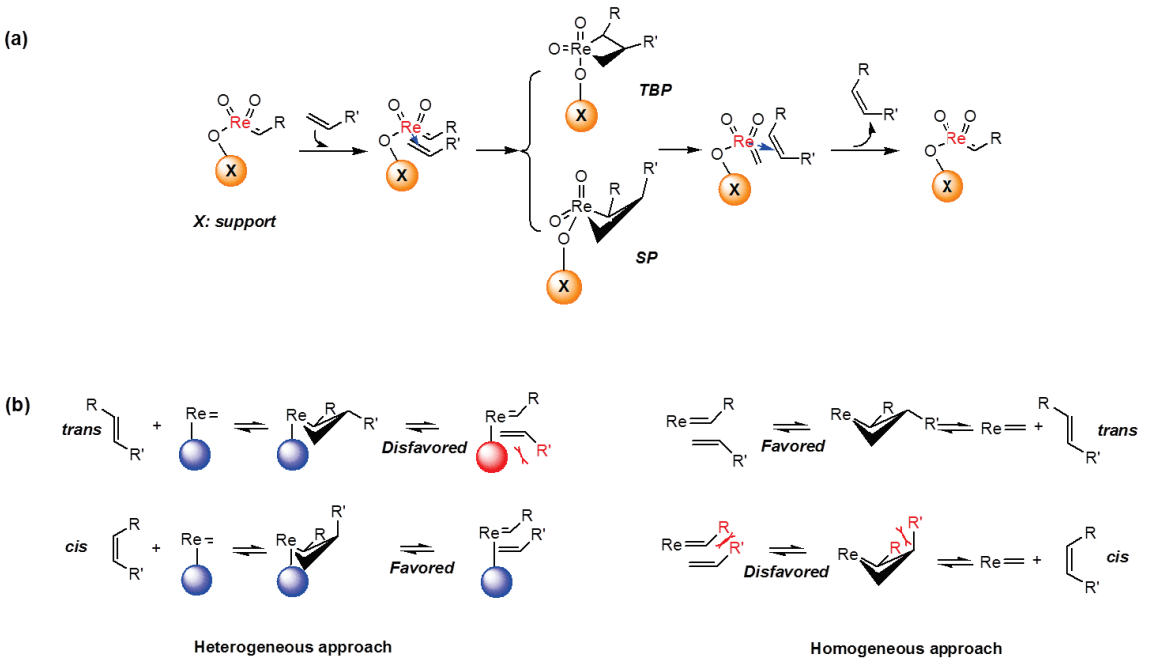

Scheme 8. (a) Proposed mechanistic pathway for alkene metathesis reaction in the presence of the MTO-based catalysts; (b) metathesis reaction sterioselectivity governed by [1, 2] interactions for both homogeneous and heterogeneous approach. TBP: Trigonal bipyramid; SP: square-based pyramid. Ref. [413, 428, 429]

Noteworthy, that as foreseen with pentacoordinated complexes, the interconversion between TBP and SP geometries is highly probable [424, 426, 427] (Scheme 8a). When MTO is grafted on solid supports, the support matrix is playing the role of bulky rigid ligand causing [1, 2] interactions with a great steric hindrance, therefore the reverse

metathesis reaction selectivity is observed compared to the homogeneous approach in order to minimize the [1, 2] interactions (Scheme 8b) [413].

Furthermore, MTO-based catalysts have been proved to be highly active with many bulky functionalized olefins without the use of toxic promoters.[36, 408, 412, 414] Mandelli *et al.* [391] reported a successful methyl oleate self-metathesis over MTO/SiO_2-$A1_2O_3$ reaching good conversions of 66%. Salameh *et al.* [413] reported that MTO supported on Al_2O_3 is also efficient catalyst for bulky functionalized olefin metathesis reaction (*e.g.* ethyl oleate). Thus, after numerous optimizations and the use of a series of catalytic supports for the heterogeneous MTO-based catalyst, alumina was found to be the most suitable support. The alumina support exhibits better catalytic performance than several other materials including; niobia, titania, alumino-silicate, *etc.* Recently, a successful methyl oleate self-metathesis over MTO supported on $ZnCl_2$-modified wormhole-like mesoporous alumina exhibiting higher metathesis reaction activity comparing to unmodified alumina supports was reported [430, 431], reaching higher methyl oleate conversion (up to 91%, 52% of desired metathesis reaction products selectivity). Using the same catalytic system (MTO/$ZnCl_2$-Al_2O_3), a successful selective triolein self-metathesis a bulky triglyceride ester was also recently reported [432].

2.3.5. Green olefin metathesis

Olefin metathesis is “a great step forward for green chemistry” and for a sustainable technology and industry [433], where two carbon-carbon double bond attached-substituents are exchanged producing new molecules while atom economy concept is really established. In addition, catalytic metathesis reaction process in its basis respects fully the remaining green chemistry principles including preventing wastes, generating degradable and less hazardous substances with less side products, in a safe process using safer chemicals and renewable feedstock if possible under mild conditions at ambient temperature and pressure with an efficient energy consumption [434].

2.3.5.1. Microwave-assisted metathesis reaction

Since the first application of microwave technology in organic synthesis in 1986 [435, 436], enormous attention was gained in this field as one of the green chemistry aspects. Several papers have been reported demonstrating that microwave heating is highly

beneficial for catalyzed metathesis reaction over conventional heating not only by a fast heating reducing dramatically the reaction time, but also enhancing the metathesis reaction rate, the catalyst stability which increase its life time, especially for thermally sensitive catalysts by eliminating the wall effect [437, 438]. The microwave heating is an eco-compatible approach due to the efficient energy consumption as well as direct and effective heat transfer to the substrates.

2.3.5.2. Metathesis reaction in ionic liquids media

In a green perspective, many papers recently described metathesis reaction in ecofriendly green solvents, particularly in aqueous media [439]. However, this cannot be successfully generalized due to the insolubility of some homogeneous catalysts in water and also the higher sensitivity of other homogeneous/heterogeneous catalysts to moisture. Therefore, a great attention was focused on using ionic liquids as green metathesis reaction solvents [440, 441]. Ionic liquids are liquid salts having low melting points, called also ionic fluids. The gained interest was as a result of their remarkable properties [442]; ionic liquids are highly stable allowing a safe storage even for a long period without decomposition, they allow a safer synthesis having no vapor pressure which resolves greatly the issues related to volatile organic solvents, possessing good thermal stability which is beneficial when high reaction temperature is required. Moreover, due to their high polarity, ionic liquids absorb effectively microwave energy *via* an ionic conduction mechanism [443-447], which makes their combination with microwave heating highly potential for enhancing many synthetic applications [448-451]. Also, ionic liquids dissolve a wide range of organic, inorganic and organometallic compounds and gases (H_2, CO, O_2 and supercritical CO_2). This property can easily be tuned using different cations and counteranions in the synthesis of ionic liquids. In addition, ionic liquids are beneficial for catalytic applications using metal complexes, enzymes and organic substrates with excellent performances, avoiding any coordination of these active species with ionic liquids that may decrease their reactivity. Several metathesis reaction applications were successfully carried out in ionic liquids media [452-457]. Furthermore, many homogeneous catalysts were efficiently immobilized on ionic liquids [262, 458-462]. Thurier *et al.* [463] reported a ruthenium-based catalyzed methyl oleate self-metathesis in ionic liquid media using [bmim][OTf], [bmim][NTf_2] and [bdmim][NTf_2] ionic liquids.

2.4. Application of catalytic metathesis reaction in oleochemistry

2.4.1. Oleochemicals as starting materials

The use of biomass as renewable starting materials for energy production, chemicals and materials manufacturing is a big step towards a sustainable development [464]. Plants oils are offering many alternatives for renewable energy [465, 466]. Vegetable oils represent nearly 80% of the global oil and fat production, while 20% only are from animal origin [467]. Oils and fats, mainly fatty acids and glycerides are the most abundant renewable starting materials [468-472], receiving a high attention in all fields of chemical industry. These starting materials can be readily used through various chemical conversions and catalytic transformations, becoming among the most interesting basic oleochemicals [471, 473], due to the carboxy groups and the C-C double bonds functionalities. Several fatty acids are widely available [467], such as oleic [474], linoleic [475], linolenic [476], erucic [477], ricinoleic [478], petroselinic [479], calendic [480], α-eleostearic [481], santalbic [482] and vernolic [483] acids from sunflower, soybean, linseed, rape seed, castor oil, *Coriandrum sativum*, *Calendula officinalis*, tung oil, *Santalum album* (*Linn*.) and *Vernonia galamensis,* respectively.

Polymer production is highly benefiting from naturally occurring oleochemicals resources [484], *e.g.* thermoplastic polyesters and polyurethanes were prepared from vegetable oils [485]. The synthesis of polymer precursors through catalytic transformations of natural oils is one of the interesting applications [486], and particularly, the synthesis of long-chain building blocks for polymers production [487]. For instance, oleic acid and undecylenic acid derivatives were efficiently used for the synthesis of several new semi-crystalline polyurethanes [488], while polyester precursors were produced using low value oleic and linoleic acids residues contained in a paper industry wastes [489].

2.4.2. Catalytic metathesis reaction for oleochemicals conversion

As mentioned above, renewable feedstock is the main supply for bioplastics synthesis, thus several bioresources were used for the synthesis of bio-polymers including proteins [490], starch and cellulose [491], as well as the valorization of fatty acid waste [492]. Therefore, oleochemicals are providing access to functionalized monomers which are gathering enormous attention. Catalysis is among several tools used for the valorization of such

compounds through different transformations (Figure 9) including esterification [493], hydrogenation [87], isomerization [494], epoxidation [88], *etc.*

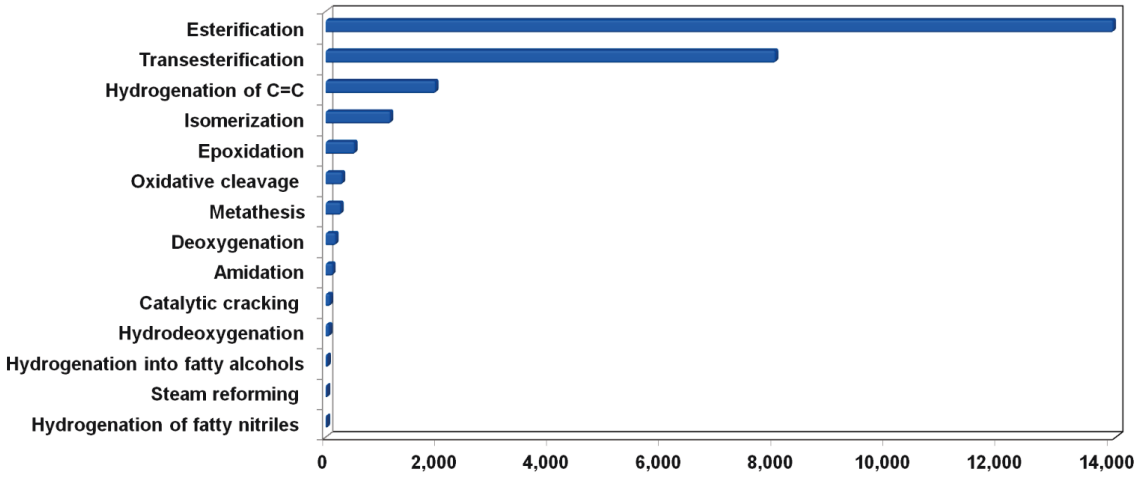

Figure 9. Proportion of all published articles (including 2015) reporting various catalytic transformations of fatty acid and derivatives, source: Web of Science.

Metathesis reaction is one of the efficient rapid transformations that offer direct access to industrially important building blocks from oleochemicals in one reaction step [495]. Metathesis reaction of fats and oils is a clean and atom efficient catalytic reaction with no by-product formation [465]. It is one of the most interesting fatty acid esters transformation, due to the subjected C-C double bond found in the unsaturated fatty acids backbones, which undergo C=C substituents rearrangement resulting in exchange of alkylidene fragments, using various catalysts developed for metathesis reaction of bulky functionalized olefins.

Many catalytic systems were reported for this purpose. However, most of these systems are hardly sustainable, due to several parameters including: recycling difficulties especially with homogeneous systems, low tolerance for functional groups, by-products generation, low stability and decomposition, high temperature activation, as well as the need for hazardous and toxic co-catalyst. These and more drawbacks will be discussed in details in the following sections. In our project, we are developing a robust heterogeneous catalyst to perform fatty acids derivatives metathesis reaction for bioplastic production, expecting to offer answers for the addressed issues faced with the available catalysts.

2.4.3. Evolution of functionalized unsaturated fatty acid-derivatives metathesis reaction

Many papers were published reporting on fatty acid esters metathesis reaction [496-499]. In the early 1970s, Van Dam *et al*. [500, 501] reported in their pioneering work a successful metathesis reaction of several long-chain unsaturated fatty acid esters substrates including; methyl oleate, methyl elaidate, methyl erucate, methyl undecenate, methyl linoleate and methyl linolenate over the tungsten hexachloride tetramethyltin (WCl_6/Me_4Sn) homogeneous catalyst. Table 3 summarizes some selected remarkable examples and the related catalytic systems. Several studies demonstrated a satisfactory metathesis reaction activity, while it has been proven that unsaturated fatty esters should be carrying at least one methylene group between the carboxylic group and the subjected C-C double bond to be able to undergo catalytic metathesis reaction [389].

Table 3: Selected fatty acid esters metathesis applications and the related catalytic systems

Fatty acids derivatives metathesis	**Catalytic systems/conditions**	**References**
Methyl oleate self-metathesis and cross-metathesis with E-3-hexene	Re_2O_7/Al_2O_3 and R_4Sn (co-catalyst) with R: CH_3, C_2H_5, C_4H_9, C_6H_{11}, C_8H_{17}, *i*-C_3H_7), or LiR_4, $Me_3Al_2Cl_3$	Bosma *et al*. [389] Boelhouwer and Mol. [502]
Methyl oleate self-metathesis	WCl_6/Me_4Sn	Verkuijlen *et al*. [503]
Ethenolysis methyl linoleate	WCl_6/Me_4Sn in chlorobenzene at 30°C for 24h	Faujan *et al*. [504]
9-Decenyl acetate cross-metathesis with 1-butene	$(CO)_5W$:$CPh(OCH_3)$-$SnCl_4$-$SiCl_4$, for 2-4 h, at 80-100 °C, in chlorobenzene or hexane	Banasiak. [505]
Ethyl oleate self-metathesis	$W(OAr)_2Cl_4$ and R_4M (R = Me, *n*-Bu; M = Sn, Pb)	Quignard *et al*. [506, 507]
Methyl oleate self-metathesis	$W(CH$-*t*-$Bu)(N$-2,6-C_6H_3-*i*-$Pr_2)[OCMe(CF_3)_2]_2$ for 2-3 h at 25 °C	Schaverien *et al*. [508]
Methyl oleate self-metathesis	Low-rhenium-loading catalysts Re_2O_7/Al_2O_3-SnR_4 (R = Me, Et, or Bu) and MoO_3, V_2O_5, or WO_3, at RT for 90 min.	Xiaoding *et al*. [385, 390]
Methyl oleate self-metathesis	Low-rhenium-loading catalysts Re_2O_7/SiO_2-Al_2O_3 and R_4Sn or R_4Pb, (R = alkyl), at RT for 2h.	Xiaoding and Mol. [383]
Methyl oleate self-metathesis	Low-loading Re_2O_7/Al_2O_3-B_2O_3 with R_4M, (M = Sn or Pb, R = alkyl) catalysts	Xiaoding *et al*. [384]

A wide range of fatty acids and their derivatives were successfully subjected for metathesis reaction. For instance, methyl 10-undecenoate obtained from castor oil *via* pyrolysis was

investigated for self- and cross-metathesis reactions over ruthenium based metathesis catalysts [509]; methyl ricinoleate was also subjected to cross-metathesis with methyl acrylate with both Hoveyda-Grubbs' (HG) and Zannan catalysts [510]. Similarly, methyl soyate was deeply investigated through metathesis reaction catalyzed by ruthenium Grubbs' second generation catalyst [511]. Moreover, soy acids, soy methyl esters, rapeseed acids, tall acids and linseed acids were subjected to metathesis reaction over Grubbs' catalyst under solvent-free conditions [512]. Furthermore, crude oil mixtures were treated under metathesis reaction conditions, *e.g.* crude palm oil ethenolysis in the presence of WCl_6/Me_4Sn [513]; single- and multiple-component sunflower oil fatty acid ester systems (palmitate, stearate , oleate , linoleate , arachidate and behenate) in the presence of the 3wt% Re_2O_7/SiO_2-Al_2O_3//Bu_4Sn heterogeneous catalyst [514], and recently, self-metathesis of the unsaturated non-edible oil methyl esters of tobacco in the presence of Grubbs' second generation catalyst [515].

Several catalytic systems were hampered by olefins bearing functional groups due to the ability of these functionalities to interfere in different metathesis reaction stages. This resulted in a competition with the targeted olefin C=C double bond through complexation with the metal center or interaction with the co-catalyst, leading to poisoning of active catalytic species. In addition, polar groups (alcohols, acids, peroxides) could affect the active intermediate metallacyclobutane species, leading to their decomposition *via* a reductive elimination [496]. Moreover, by-products can be obtained with the WCl_6/Me_4Sn catalyst which can also undergo transesterification reaction when traces of alcohols are present in the reaction media, like in the case of palm oil crude mixture for instance [516, 517]. Other heterogeneous supported catalytic systems were reported for metathesis reaction of fatty acids derivatives, like $Mo(CO)_6/Al_2O_3$. This later is highly active at 50 °C, while higher temperatures are required to achieve good catalytic activity with several other systems such as; WO_3/Al_2O_3 (350 °C), WO_3/SiO_2 (400 °C), $MoO_3.CoO/AI_2O_3$ (150 °C) [518], which is a major drawback. Noteworthy, several bromo- and choloro-alokoxy complexes $W(OAr)_2Cl_4$ (OAr = $OC_6H_3Me_2$-2,6, $OC_6H_2Me_3$-2,4,6, $OC_6H_3Ph_2$-2,6, $OC_6H_3Br_2$-2,6, $OC_6H_3C_{12}$-2,6, or $OC_6H_3F_2$-2,6), with MR_4 (M = Sn, Pb; R = Me, n-Bu) as co-catalysts exhibit good activity with several functionalized cyclic and acyclic olefins [506, 507]. $RuCl_2(PPh)_3$ and $RhCl(PPh)_3$ were also reported as efficient metathesis

catalysts, and they showed a low tolerance for functional groups. However, particular ligands and experimental conditions were required to improve their stability and functional groups tolerance, such as activation by oxygen [519-521].

2.4.4. Methyl oleate metathesis reaction

Methyl oleate is one of the most interesting fatty acid esters that have been widely studied in catalysis trough various transformations including hydroformylation [522], oxidative cleavage [523], alkoxycarbonylation [524], *etc*. Methyl oleate was extensively used as a model molecule for metathesis reaction of bulky functionalized olefins. Herein we are reviewing a series of catalytic systems previously developed for methyl oleate metathesis reaction, for both self-metathesis (Table 4) and cross-metathesis (Table 5), mostly ethenolysis.

In some cases, methyl oleate cross-metathesis with several alkenes afforded the thermodynamic self-metathesis products *via* a side reaction in addition to the kinetic cross-metathesis products, like those reported for methyl oleate ethenolysis catalyzed by different N-heterocyclic carbene-based ruthenium catalysts [525].

Methyl oleate self-metathesis was widely investigated in the presence of homogeneous Grubbs' catalyst [526-530], and other homogeneous ruthenium-based catalysts [463, 531-535]. Other catalytic systems like $K_2[ReCl_6]$ /SiO_2.Al_2O_3 or $[ReCl_x(OR)_y]_n$/SiO_2.Al_2O_3were successfully developed with a high metathesis reaction activity even with bulky functionalized olefins such methyl oleate [536]. However, further activations were always required for those catalysts. For instance, thermal activation of these catalysts under nitrogen is one of the major drawbacks, due to the high temperatures required for activation up to 300-360 °C [536]. Catalytic promoters also were required with different indenylidene type Ru catalysts, it has been reported that tetrafluoro-1,4-benzoquinone is a beneficial additive to achieve high conversion and selectivity for both methyl oleate self-metathesis and cross-metathesis with (Z)-2-butene-1,4-diol diacetate [537].

Table 4: Catalytic systems used for methyl oleate self-metathesis

Catalytic system	References
2 wt.% Re_2O_7/7.5 wt.% B_2O_3/SiO_2-Al_2O_3 + Bu_4Sn (co-catalyst)	Rodella *et al*. [538]
3% $Re_2O7/SiO_2.Al_2O_3$ + Et_4Sn (co-catalyst)	Sibeijn and Mol [539].
0.43-6.0 wt.% silica-supported Hoveyda-Grubbs (HG) complex catalysts (HG/SiO_2)	Zelin *et al*. [540]
WCl_6-Me_4Sn	Verkuijlen *et al*. [503]
WCl_6-Me_4Sn or Re_2O_7/Al_2O_3-Me_4Sn	Kohashi and Foglia [389, 500, 541, 542].
W(CH-*t*-Bu)(N-2,6-C_6H_3-*i*-Pr_2)[$OCMe(CF_3)_2$]$_2$ for 2-3 h at 25 °C	Schaverien *et al*. [508]
Low-rhenium-loading catalysts Re_2O_7/Al_2O_3- R_4Sn (R = Me, Et, or Bu) and MoO_3, V_2O_5, or WO_3 at RT for 90 min.	Xiaoding *et al*. [385, 390]
Low-rhenium-loading catalysts $Re_2O_7/SiO_2.Al_2O_3$ and R_4Sn or R_4Pb, (R = alkyl), at RT for 2h.	Xiaoding and Mol [383].
Boron added Low-loading $Re_2O_7/Al_2O_3.B_2O_3$ + R_4M, (M = Sn or Pb, R = alkyl) catalysts	Xiaoding *et al*. [384] Rodella and Buffon [538, 543].
$K_2[ReCl_6]$ /$SiO_2.Al_2O_3$ or $[ReCl_x(OR)_y]_n/SiO_2$-Al_2O_3	Brégeault *et al*. [536]
Laser-photoreduced supported MoO_3/SiO_2 and $MoO_3/SiO_2.Al_2O_3$ catalysts, activated at 500 °C under oxygen flow	Mol [544].
Phoban-indenylidene ruthenium complex [$(PhobC_v)_2Cl_2Ru=C_{15}H_{10}$]	Forman *et al*. [545]
2 wt.% Re_2O_7 supported on SiO_2-Al_2O_3 or B_2O_3/SiO_2-Al_2O_3 with R_4Ge, R_4Si, R_3GeH or R_3SiH (R= Me, Et, Bu) as promoters	Buffon *et al*. [392]
$RuCl_3$ or $RuBr_3$ hydrate, a phosphine, and an alkyne	Nubel and Hunt [546].
RuX_3 hydrate, PCy_3, and 2-butyne-1,4-diol diacetate (BDD) catalyst (X: Cl or Br)	
Re alkylidene complex supported on silica [(=SiO)Re(CH_2tBu)(=CHtBu)(≡CtBu)]	Chabanas *et al*. [547]
Silica supported Ru complexes with the H_2ITap ligand (1,3-bis(2',6'-dimethyl-4'dimethyl aminophenyl)-4,5-dihydroimidazol-2-ylidene)	Cabrera *et al*. [548]
Magnetic nanoparticles-supported second generation Hoveyda-Grubbs' (HG-II) catalyst, loading of 0.28 mmol ruthenium/g (magnetic support)	Yinghuai *et al*. [549]
Biphasic liquid-liquid supported Grubbs' and Grubbs-Hoveyda (HG) catalyst; ionic Ru–alkylidenes [Ru[$(4\text{-}CO_2)(1\text{-}CH_3)Py^+$)]$_2$($IMesH_2$)(=CH-2-(2-PrO)-$C_6H_4$)][$OTf^-$]$_2$ and [RuCl[$(4\text{-}CO_2)(1\text{-}CH_3)Py^+$)]($IMesH_2$)(=CH-2-(2-PrO)-$C_6H_4$)][$OTf^-$]; ($IMesH_2$: 1,3-dimesitylimidazolin-2-ylidene, Py: pyridine, OTf^-: triflate), also using monolith-supported ionic liquids	Autenrieth *et al*. [550, 551]
BMIM·NTf_2 and OMIM·NTf_2 ionic liquid-tagged ruthenium-based catalyst with continuous super critical CO_2 flow as a carrier	Duque *et al*. [552]
Phosphine and pyridine linked mesoporous molecular sieves (SBA-15 and MCM-41) immobilized Grubbs' catalysts	Bek *et al*. [553]
Hoveyda-Grubbs (HG) immobilized on mesoporous molecular Sieves (SBA-15 and MCM-41)	Balcar *et al*. [554]
A series of indenylidene type Ru catalysts	Kajetanowicz *et al*. [537]

Table 5: Catalytic systems used for methyl oleate cross-metathesis

Catalytic system	Olefins	References
Ruthenium-based Grubbs' second-generation catalysts	Ethyl acrylate	Abbas and Slugovc [555].
Grubbs' 1st generation catalyst	*cis*-2-butene-1,4-diyl diacetate	Behr and Gomes [556]. Burdett *et al*. [527]
Re_2O_7/Al_2O_3 and R_4Sn (co-catalyst) with R: CH_3, C_2H_5, C_4H_9, C_6H_{11}, C_8H_{17}, *i*-C_3H_7), or LiR_4, $Me_3Al_2Cl_3$	*E*-3-hexene	Bosma *et al*. [389] Boelhouwer and Mol [502].
18% Re_2O_7/Al_2O_3 + Bu_4Sn (co-catalyst)	Ethene	Sibeijn and Mol [557].
N-heterocyclic carbene-based ruthenium catalysts	Ethene	Schrodi el al. [525]
First generation Hoveyda catalyst	Ethene	Miao *et al*. [558]
Magnetic nanoparticles supported second generation Hoveyda- Grubbs (HG) catalyst, loading of 0.28 mmol ruthenium/g (magnetic support)	Methyl acrylate	Yinghuai *et al*. [549]
Ruthenium-based homogeneous catalysts	Ethyl acrylate	Abbas and Slugovc [555].
Grubbs' catalysts homogeneous catalysts	Ethene, propene, butane or octane	Nickel *et al*. [529]
Ruthenium-based homogeneous catalysts	Ethene	Kadyrov *et al*. [531]
N-heterocyclic carbene (NHC) ruthenium-based homogeneous metathesis catalysts	Ethene	Thomas *et al*. [559]
Cyclic (alkyl)(amino)carbenes (CAACs) ruthenium-based homogeneous metathesis catalysts	Ethene	Anderson *et al*. [560]
BMIM·NTf_2 and OMIM·NTf_2 ionic liquid-tagged ruthenium-based catalyst with continuous super critical CO_2 flow as a carrier.	Dimethyl maleate	Duque *et al*. [552]
Imido alkylidene monoaryloxide-pyrrolide (MAP) molybdenum complexes	Ethene	Marinescu *et al*. [561]
Ruthenium-benzylidene olefin metathesis homogeneous catalysts	2-Butene	Patel *et al*. [534]
Ruthenium-based homogeneous catalyst in a microfluidic designed dual-phase	Ethene	Park *et al*. [562]
Hoveyda-Grubbs' Catalyst 2nd generation (HG-II), Grubbs' catalyst 1st generation and 2nd generation ruthenium-based homogeneous metathesis catalysts.	Methyl acrylate	Rybak and Meier [563].
A series of indenylidene type Ru catalysts	(*Z*)-2-butene-1,4-diol diacetate	Kajetanowicz *et al*. [537]
Ruthenium-based homogeneous catalysts	*trans*-stilbene, styrene, methyl cinnamate and hexen-3-ol	Doll. [564]
Silica-ionic liquid-tagged Grubbs' first generation catalyst	Ethene	Aydos *et al*. [565]

As discussed in the upper section, most of the developed homogeneous and heterogeneous catalyst presents major and critical drawbacks. As a result, many papers were reported describing methyl oleate metathesis over supported active homogeneous catalysts attempting to combine both homogeneous and heterogeneous catalysts advantages. For

instance, metathesis reaction over silica-supported Hoveyda-Grubbs' (HG) complex (HG/SiO_2). This catalyst remains active even after being supported, while further amounts of HG complex were added in reaction mixture at different stage which represents a major drawback. Moreover, unfortunately the supported catalyst (HG/SiO_2) has been significantly deactivated after recycling [540].

Noteworthy that, Pillai *et al.* [430, 431] recently reported an efficient methyl oleate self-metathesis over MTO-based catalysts (Scheme 9). In this study the authors established a new design of MTO-based catalyst and investigated its performance and improvements (rate, conversion and selectivity) for methyl oleate self-metathesis. In our study, starting material (methyl oleate) for metathesis reaction is prepared from oleic acid. It is worth to highlight that oleic acid is the main constituent in used vegetable oils and waste cooking oils [566], and is also a by-products in the industrial extraction of oleaginous plants [567].

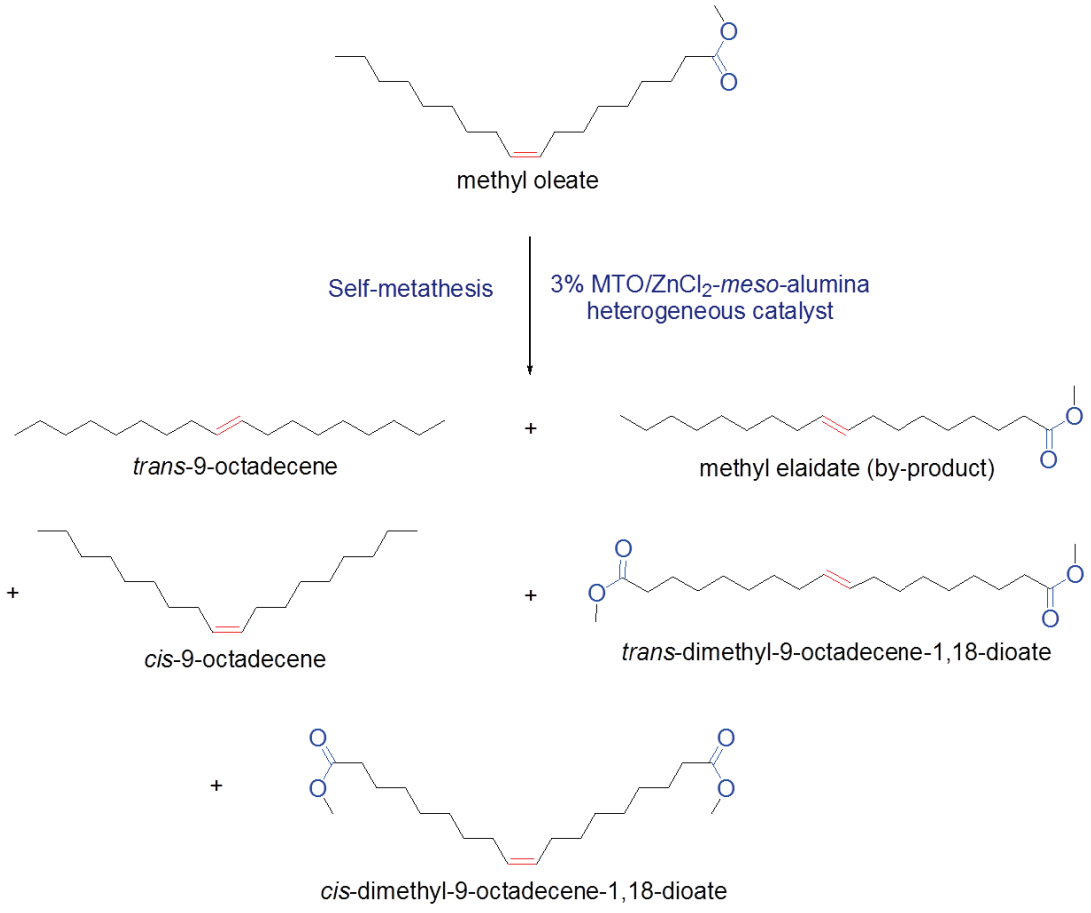

Scheme 9. Methyl oleate self-metathesis over MTO-based catalyst

Through this metathesis reaction process, these renewable feedstock will be converted to value-added chemicals (functionalized monomers for bioplastic production), thus lowering their synthesis process by using such low-cost starting material. On the other hand, we are contributing in waste valorization and reducing these environmentally hazardous disposals, resolving a serious issue related to their management. It is important to mention that oleic acid is found at considerable amounts in industrial wastewater [568, 569].

2.5. Organized mesoporous materials: well-ordered hexagonal mesoporous alumina, synthesis, application and opportunities

2.5.1. Ordered materials in heterogeneous catalysis

Ordered materials attracted an enormous attention of many research groups focusing on the enhancement of several heterogeneous catalysts activities and selectivity. This was carried out by the improvement of the surface organization and porous network uniformity of these materials [570-576]. These textural aspects offered advantageous alternatives towards desired shape-selective catalysis which are governed by mass transfer phenomena. These phenomena can be tuned by controlling the porosity and the surface homogeneity [577]. Moreover, this key point is more critical when selectivity is an issue, dealing with bulky functionalized molecules that undergo both intra- and inter-molecular reactions. Despite the increasing progress that has been achieved since the first synthesis of hexagonally ordered mesoporous silica [578-580], the synthesis of ordered materials for catalytic applications still remains as a hot research topic. Indeed, various organized mesoporous siliceous and non-siliceous materials were targeted, among them; cubic MCM-41 and MCM-48 [581], SBA-15 [580] and KIT-6 [582], in addition to ordered mesoporous carbon (CMK-1 and CMK-3) [583, 584], niobia [585, 586], titania [586], zirconia [586], tantalum oxide[587] and other several non-siliceous interesting ordered mesoporous metal oxides [588] and hybrid materials [589].

2.5.2. Wormhole-like alumina *vs.* well-ordered hexagonal mesoporous alumina

Mesoporous molecular sieves based catalysts are now widely used for olefin metathesis [590]. Among these mesoporous materials, alumina exhibited great performances. For instance, alumina structure is more complicated than silica for example. Aluminum atoms

are present in different coordination state (from 3 to 6). Generally they are either in a tetrahedral (25%) or an octahedral (75%) geometry, which is the origin of the variety in the Lewis acid sites strengths. In addition to the aluminum surface sites, surface hydroxyl groups also exist [424]. Recently, Pillai *et al.* [430, 431] reported an efficient methyl oleate self-metathesis over MTO supported on $ZnCl_2$-modified mesoporous alumina, using an amorphous conventional alumina with a wormhole-like structure. This catalyst support was found to be a suitable carrier for metathesis reaction activity. However, there is still a room for further improvement of the MTO-based catalyst performance. Thus, an enhanced catalyst design is required. Several papers described the beneficial role of the organized mesoporous alumina support over conventional (disordered) alumina in the presence of Re_2O_7 for simple olefin metathesis [591-593]. This enhancement of the activity was attributed mainly the higher BET surface area, while the selectivity was attributed to the uniform and regular pore size distribution and total pore volumes throughout the material.

Few reports are found describing the preparation of ordered mesoporous alumina using distinct aluminum precursors and templating agents, as well as different conditions for thermal treatment to get the final material. Table 6 summarizes all the procedures reported previously for the preparation of ordered mesoporous alumina. Ordered mesoporous alumina (OMA) has been one of the challenging non-siliceous organized materials to synthesize [594, 595]. Niesz *et al* .[596] reported a Pluronic P123-templated sol-gel synthesis of OMA where the synthesis was performed at 40 °C affording high BET surface and narrow pore size distribution. Liu *et al.* [597] reported a nanocasting synthesis templated by mesoporous CMK-3 carbon. A Pluronic F127-templated synthesis of OMA was also reported by Yuan *et al.* [598] Recently, Wu *et al.* [599] reported an efficient OMA synthesis using inexpensive aluminum nitrate at 30 °C. OMA with relatively large mesopores have been obtained using a swelling agent in a Pluronic P123-templated synthesis. Along with high surface area and pore size, as well as uniform mesoporous network, great efforts have also been focused on achieving thermally and hydrothermally stable crystalline framework walls of OMA [573, 597, 598]. Moreover this feature can help the material to maintain large surface area even after thermal treatment at high temperatures [600].

Table 6: Previously reported procedures for the preparation of ordered mesoporous alumina materials

Aluminum Precursor	Templating agent	Calcination conditions[a]	BET[b] (m^2/g)	P_V[c] ($cm^3\ g^{-1}$)	D_{BJH}[d] (nm)	References
Aluminum *sec*-butoxide	Lauric acid	703/0.5/1.5 (N_2/Air)	710	0.41	1.9	Vaudry *et al*. [601]
Aluminum *sec*-butoxide	Stearic acid	420/5/6 (Air)	488	0.53	3.4	Cejka *et al*. [602]
Aluminum isopropoxide	Pluronic P123	400/1/4 (Air)	520	0.82	4.9	Huang *et al*. [600]
Aluminum *sec*-butoxide	Pluronic PE 9400 or 10400	450/1/6 (Air)	400	0.63	3.5	Balcar *et al*. [592]
Aluminum tri-tert-butoxide	Pluronic P123	400/1.5/4 (O2)	410	0.80	6.7	Niesz *et al*. [596]
Aluminum isopropoxide	Pluronic P123	400/1/4 (Air)	530	0.59	6.3	Cai *et al.* [603]
Aluminum nitrate nonahydrate	Pluronic P123	400/1/4 (Air)	307	0.45	11.1	Cai *et al*. [603]
Aluminum isopropoxide	Pluronic P123	600/0.4/3 (O2)	259	0.54	5.8	Dacquin *et al*. [604]
Aluminum isopropoxide	Pluronic F127	400/1/4 (Air)	480	0.68	9.8	Yuan *et al*. [598]
Aluminum isopropoxide	Pluronic F127	400/1/4 (Air)	338	0.39	6.9	Grant *et al*. [605]
Aluminum isopropoxide	Pluronic F127	550/1/5 (Air)	252	0.56	9.2	Wang *et al.* [606]
Aluminum isopropoxide	Pluronic P123	500/1/4 (Air)	344	0.50	5.0	Wu *et al.* [599]
Aluminum isopropoxide	Pluronic P123	700/1/4 (Air)	292	0.62	9.06	Morris *et al*. [607]
Aluminum isopropoxide	Pluronic P123	550/1/4 (Air)	300	0.40	3.5	Li *et al*. [608]
Aluminum *sec*-butoxide	Stearic acid	410/0.5/2 (N_2) 420/0.5/9 (Air)	758	0.68	3.7	Cejka *et al*. [609]
Aluminum isopropoxide	Pluronic P123	700/1/4 (Air)	307	0.75	9.5	Yuan *et al*. [610]
Aluminum isopropoxide	Pluronic P123	400/1/4 (Air)	351	0.94	10.0	Jaroniec and Fulvio [611]
Aluminum nitrate nonahydrate	Functionalized mesoporous carbon (FMC)	600/1/5 (N_2)	332	0.84	8.0	Wu *et al*. [612]
Aluminum nitrate nonahydrate	ordered mesoporous carbon CMK-3	450/2/4 550/2/3	396	0.46	4.6	Liu *et al*. [613]

[a]Expressed as calcination temperature (°C)/temperature ramp (°C/min)/calcinations time (h).[b]BET surface area, [c]pore volume, and [d]pore size distribution

In order to establish a versatile and cost-effective preparation of OMA materials, many approaches have been investigated. These studies revealed the importance of many key-control factors in order to overcome limitations over ordered mesoporous network formation. Therefore, the effect of inorganic precursors-template ratio was investigated [577]. Furthermore, many process parameters were deeply investigated and among them, the complexation effect of anions and hydro-carboxylic acid and organic-inorganic interface protectors and template-assistants during aging process [600, 614-616], synthetic routes [617], swelling agents and co-solvents,[618] salt-like effect of water and acid concentration [619], the pH of the synthesis medium and nature of pH adjustor [605], as well as the calcination temperature [610].

2.5.3. Organized mesoporous alumina modification

It has been demonstrated recently that $ZnCl_2$-modified wormhole-like mesoporous alumina exhibited higher metathesis reaction activity as compared to alumina supports [430-432]. Similarly, the targeted organized mesoporous alumina needs to be modified using $ZnCl_2$. The particular acidic properties of the alumina surface attributed to Lewis-acid aluminum species and Brønsted-acid hydroxyl groups, promoted significantly the incorporation of several metals and other metal oxides on alumina. Frequently, OMA modification and synthesis under high thermal conditions led to partial or complete loss of the mesoporous hexagonal arrangement [607]. Therefore, doping metals and metal oxides on OMA and preserving the well-ordered 2D-hexagonal mesostructure is a challenging procedure. In this perspective, various elements were supported on OMA and simultaneously maintaining the organized structure. For instance, Ni, Mg, Fe, Cr, Cu, Ce, La, Y, Ca and Sn were successfully supported on OMA [603, 607]. Si-, Ce-, and Zr-doped OMA [620], Ce-Zr-Co-doped OMA [621, 622], Cu/Ce-OMA [623], La-doped OMA [624] and noble metals-doped OMA (Pt, Ag and Pd) [625] were also prepared. Similarly, OMA-supported metal oxides such as; MgO, CaO, TiO_2, and Cr_2O_3 [607] and ordered titania-alumina mixed oxides [626] were also obtained. In addition, to prevent OMA collapse, the metal-modified OMA were obtained with uniform metal dispersion. These materials presented high catalytic activities for various reactions including carbon dioxide reforming of methane [627], hydrogen production [628], CO oxidation [625], thiophene hydrodesulfurization [629] and methanol dehydration [630]. Metathesis reaction could be one of these applications that can benefit

from the ordered mesostructure network of alumina and modified-alumina, especially when *trans*- or *cis*-selectivity is critical and highly desired.

2.5.4. $ZnCl_2$ incorporation on alumina, surface acidity and metathesis reaction activity

Oikawa *et al*. [631] demonstrated in their pioneering work that the aluminum Lewis acidic sites are more involved in MTO/Al_2O_3 catalyst activation than the Brønsted hydroxyl acidic sites. These findings led to many attempts towards the enhancement of surface Lewis acidity. Several metallic precursors were investigated for their acidity, *e.g.* Ga, Mg, Mn, and Zn-based halides, and the overall results showed greater improvements with Zn-based promoters [430]. Furthermore, many zinc-based promoters were tested for this purpose; *e.g.* $ZnCl_2$, $ZnBr_2$, and $Zn(NO_3)_2$ [631] as well as ZnI_2 [631], and the highest activity was observed with the chlorine-based zinc precursor ($ZnCl_2$) for methyl oleate [430] and methyl 10-undecenoate metathesis reaction [631]. This could be explained by the highest chlorine electronegativity; Cl (3.16) > Br (2.96) > I (2.66) which leads to the lower polarizability of the Zn-Cl bond easing its insertion on the alumina surface matrix *via* interaction with surface hydroxyl groups. This phenomena is supported by the XPS data proving the presence of Zn-Cl and mostly the Cl-Zn-Cl species after incorporation, which are coordinated to basic terminal hydroxyl groups of alumina [430] that are bonded to tetrahedral and octahedral Al sites. In alumina surface, terminal hydroxyl groups are highly mobile [632] and more reactive [633], thus they will be neutralized completely after $ZnCl_2$ incorporation as indicated in ^{1}H MAS NMR [430, 431, 634] and IR [634] spectra. However, coordination of zinc atoms with acidic bridging hydroxyl groups is not completely excluded. XPS results are in agreement with elemental analysis of $ZnCl_2$-modified alumina with different Al/Zn ratio, where Cl/Zn molar ratios lower than 2 were observed [634]. In contrast with $ZnCl_2$ modified zeolite [635-637], it is important to point out that alumina surface is carrying different types of hydroxyl groups according to the attribution of Knözinger and Ratnasamy [638]. The most probable species are Al-O-Zn-Cl [431] with HCl elimination due to a minor neutralized amount of bridging hydroxyl groups [634] (Scheme 10), also O-Al-Zn-Cl species may be present on the surface (Scheme 10). Besides that, EXAFS spectrum showed the presence of tetrahedral Zn species [634] which could be attributed to O$ZnCl_2$Al bonding. Further investigation of pH changing through

$ZnCl_2$ incorporation revealed an unexpected transfer of Cl from Zn to Al atom [634]. Moreover, alumina surface acidity depends upon the temperature of the thermal treatment [408], therefore the number of both Lewis and Brønsted acid sites is lower at high temperatures. The enhancement of metathesis reaction rate may be due also to MTO interaction with grafted Cl forming Re-Cl bond [634] (Scheme 10).

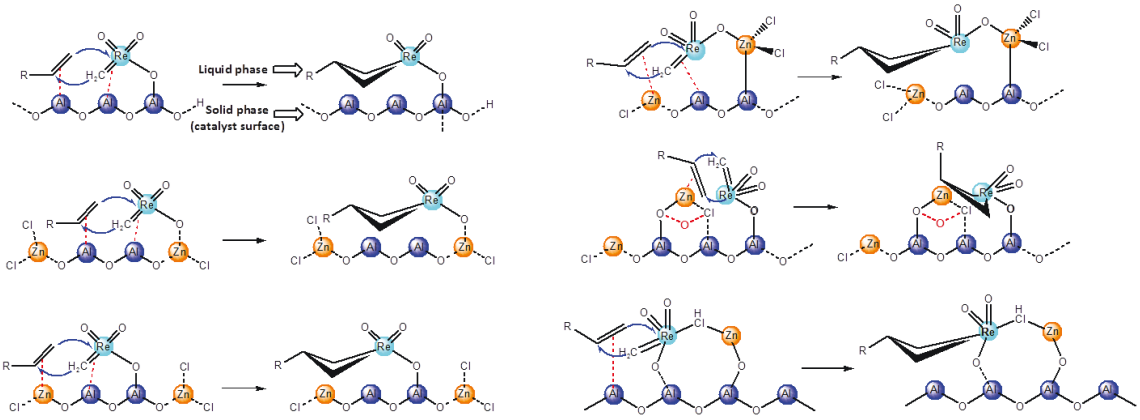

Scheme 10. Proposed mechanistic participation of the adsorbed zinc atoms in metathesis reaction pathway.

In our study, we deeply investigate the optimization of the synthesis of well-organized hexagonal $ZnCl_2$-modified alumina. The effects of aluminum precursor and interfacial protectors (CA: carboxylic acids) on mesophase formation are investigated using simple carboxylic acids to prepare a series of ordered modified-alumina. A comprehensive mechanism of mesopores formation using carboxylic acids will be proposed. Thus, the catalytic activity for methyl oleate self-metathesis using MTO supported on these well-ordered Zn-modified Al_2O_3 will be investigated for the first time on this material and a complete comparison with wormhole-like alumina will be made and discussed.

2.6. One-pot materials preparation: synthesis of functionalized mesoporous catalytic materials

As mentioned above, in our study, the functionalization of the prepared organized mesoporous alumina is required to enhance the Lewis acidity of the support which was found to improve the catalytic performance of the MTO-based catalyst [430]. However, the

results obtained for this two-steps procedure (*i.e.* preparation then functionalization) revealed a major drawback of this strategy; a decreased specific surface area was observed after functionalization which is due to the effect of the pore filling and the second calcination process. This is a considerable issue, knowing that in heterogeneous catalysis it is widely established that the catalytic performance is usually proportional to the specific surface area [639-642], affecting mainly the chemisorption rate of substrates and active intermediates [643], as well as the loading and dispersion of supported active species [644]. Therefore, an urgent solution is required to overcome these issues.

2.6.1. One-pot and multicomponents synthesis: from organic synthesis to materials chemistry

One-pot and multicomponents synthesis were found to be highly efficient, particularly in organic synthesis, enabling fascinating simultaneous or cascade transformations in a very impressive order. These synthesis fashions were greatly enhanced through studying and controlling parallel and competitive reactions. In organic synthesis, these reactions were proven to exhibit a remarkable selectivity upon varying substrates substituents (*i.e.* electrophile type and/or nucleophile strength), reaction media and other experimental conditions which offer an outstanding control over the reactivity of the reaction mixture constituents. In addition to avoiding laborious and complex synthesis process, these strategies are considered as green alternatives to conventional synthesis [645-647], allowing fast synthesis without the need to isolate intermediates (extraction and purification) while reducing the amount of generated hazardous by-products and the use of harmful solvents as well as reducing the energy consumption for the overall synthesis (*e.g.* heating source, stirring, *etc.*). Furthermore, these methodologies can dramatically reduce the costs of starting materials and the use of manpower, offering access to value-added products often with challenging structural diversity and complexity trough simple process [648]. These features make these green strategies an important element in the synthetic chemist's toolbox for the design of environmentally-benign and sustainable chemical processes.

Similarly, this green technology can be transferred to the chemistry of materials; the preparation of functionalized materials often requires laborious multistep synthesis

procedures, including multiple filtration, evaporation and calcination processes. Therefore, these conventional strategies are usually required for better control over the final materials shape, size and other properties, as well as to ensure to synthesis reproducibility. However, these protocols clearly present many drawbacks such as time consuming synthesis, lower production yields, and inefficient energy consumption. All these disadvantages may hinder the scalability of these materials synthesis and delay exploring further possible catalytic applications. Synthesis of modified catalyst supports are among the materials suffering from these laborious strategies, for instance, as mentioned above, $ZnCl_2$-modified mesoporous alumina. Conventionally, these modified catalysts supports require at least two preparation steps, first the support synthesis and second the modification of the support either by doping or functionalizing the surface sites.

The ideal desired synthetic strategy consists on gathering all the preparation steps in a single one. Therefore, during the last twenty-five years, functionalized and composite materials one-pot synthetic fashion has emerged (*e.g.* Ag@TiO_2 synthesis) [649]. During the last ten years, this methodology gathered a constant increasing attention. Interestingly, similar modified and composite materials were obtained with enhanced yields and properties using single-step synthesis instead of multistep procedures (*e.g.* graphene-CdS [650], AgI/BiOI [651], Zn-doped SnO_2 [652], Au@TiO_2, Au@ZrO_2, Ag@TiO_2, and Ag@ZrO_2 [653], Ag@AgCl [654], Au@PtCu [655], Au/N-TiO_2 [656], *etc.*). This methodology offers numerous features including shortening the synthesis time, improving the products yields and reducing the work out related to each step. In addition, great energy economy is offered by eliminating multiple thermal treatments especially when higher temperatures are required (hydrothermal synthesis, calcination steps, *etc.*). Furthermore, the consumption of large amount of reagents, solvents and synthetic gases is minimized. Overall, these features allow establishing a cost-effective production of useful functional materials and easing their reproducibility and scalability. Despite all these advantages, one-pot synthesis is often difficult to control and deeper investigations are usually required to help predicting the pathway of the formed materials. This is mainly due to the complexity of molecular interactions and behaviors of the introduced compounds in the same reaction mixture which can trigger several simultaneous mechanistic pathways.

2.6.2. Mesoporous alumina synthesis and challenges

Among several functionalized supports, modified mesoporous alumina exhibited high catalytic activity for metathesis reaction as it was recently reported for methyl oleate and triolein self-metathesis [430-432]. Moreover, several metal halides MX_y (M = Ca, Mg, Ga, Zn, Mn; X = Cl, Br, and I; y = 2 or 3) and zinc nitrate $Zn(NO_3)_2$ were screened as promoters for the alumina support [430, 631]. However, $ZnCl_2$ exhibited the best catalytic performance as promoter for the MTO-based catalyst [430]. More recently, a successful synthesis and $ZnCl_2$ incorporation on hexagonal well-ordered mesoporous alumina (OMA, *p6mm* symmetry) with a uniform cylindrical porous network was reported [657]. This well-organized support was found to be an effective alternative to the conventional wormhole-like mesoporous alumina support. Thus, faster kinetics and enhanced conversion and selectivity were reached, mainly due to improved diffusion and mass transfer phenomena through the well structured mesoporous channels of the OMA support [657].

However, the synthesis of this catalyst support is usually performed *via* a two steps process. First, mesoporous alumina is prepared *via* a long sol-gel reaction (up to 20 h), then the solid product is filtered, washed, dried and finally calcined at 400 °C [430-432]. Consequently, in a second step the synthesized mesoporous alumina is modified using $ZnCl_2$ at room temperature. The mixture is allowed to dry after 24 h and then calcined again at 400 °C [430-432]. Afterwards, an enhanced synthesis of this catalyst support *via* a rapid and simple synthesis of organized mesoporous alumina (OMA) was reported [657, 658]. This, improvement brought us a step closer to more efficient synthesis. However, despite the progress made, this two steps synthesis is laborious and affects the physicochemical properties of the final materials as explained above. The double calcination process causes further dehydroxylation of the support and alters the surface area and the porosity of the prepared materials. In addition, small amount were obtained with a significant loss in the synthesis yield through the two steps synthesis steps. Therefore, several attempts to optimize the synthesis process were performed.

In this study, the design of an efficient one-pot synthesis of well organized $ZnCl_2$-modified OMA is attempted, by combining of the two steps in a single one to access to well-organized materials with better features. The mesoporous network formation could be

achieved *via* an evaporation self-induced assembly sol gel process. The targeted materials will be thoroughly characterized and compared with their counterparts prepared *via* the two steps process. In addition to the possible enhanced physicochemical features of the one-pot synthesized materials, these materials will be tested for their catalytic activities in order to evaluate the benefits of these materials over those prepared *via* two-steps process. In this scope, MTO will be supported on the prepared well ordered zinc-doped mesoporous alumina. Self-metathesis reaction test will be performed using methyl oleate as model bulky functionalized olefinic substrate to produce value-added compounds from renewable biomass source and low cost raw materials. Similarly, the catalytic test result of the one-pot synthesized catalysts will be compared to those obtained using the two-steps prepared support.

The expected improvements could be explained by the improvement of the mechanistic pathways of metathesis reaction. Since the Re atom center is impregnated on alumina surface through covalent oxo bonding with the aluminum Lewis acidic sites on the surface, the $ZnCl_2$ incorporation on alumina increases the surface Lewis acidity by increasing the number of Lewis acidic sites. Thus, more loaded MTO molecules are coordinated (activated) which increase the metathesis reaction rate. In addition, zinc atoms may play a major role for metallic assistance in olefin drawing near the MTO carbenic active sites in alumina surface, this phenomenon is not excluded with aluminum atom centers (see Scheme 10). All this features including MTO loading, surface Lewis acid sites concentration are proportional to the specific surface area of the alumina support. Thus, the possible enhancement of the specific surface area through the on-pot process compared to the conventional procedure is expected to offer improved metathesis reaction activity.

4.6.3. Applications and opportunities in materials chemistry and catalysis

It is worth to mention that this rapid and simple process is greatly advantageous. The $ZnCl_2$-modified alumina (and zeolite) is an interesting catalytic support showing excellent activities for other application besides metathesis reaction such as methyl chloride synthesis from methanol and hydrochloric acid [637, 659]. $ZnCl_2$ impregnated on alumina and alumina-silica exhibits a remarkable performance for the catalytic alkylation of benzene with diethyl ether, ethyl and isopropyl alcohols [660-663]. Furthermore, metal halides and

particularly $ZnCl_2$ supported on mesoporous materials are very active for other applications. For instance, mesoporous carbon nitride ($ZnCl_2$/mp-C_3N_4) and doped graphitic carbon nitride (Zn-g-C_3N_4) demonstrated high performances in the catalytic cycloaddition of CO_2 with propylene oxide to propylene carbonate [664], and transesterification of ethylene carbonate with methanol to dimethyl carbonate [665], respectively. Thus, the development of a reproducible well-designed strategy for the synthesis of such materials *via* a one-pot process will pave the way to generalize this methodology for the synthesis of other functionalized materials that are conventionally prepared through laborious multistep processes, especially doped or modified mesoporous materials that are widely used in catalysis, toward establishing efficient design of highly potential and sustainable heterogeneous catalysts. The efficiency of this rapid and low cost strategy could create new opportunities for large-scale synthesis of such important functional materials.

Chapter 3:

Research hypothesis and project objectives

3.1. Hypotheses

3.1.1. Scope of the study

In homogeneous catalytic systems, all metal centers contribute in the reaction mechanism, while heterogeneous catalytic pathways only involve the exposed atoms on external surface or inside the pores. These atoms are responsible for the interactions with substrate molecules on the solid-liquid catalysts' interface. The development of new generation of sustainable heterogeneous catalysts can be achieved through designing a catalytic system with well-defined and accessible surface active sites, which will lead to improved catalytic performance and allows establishing a clearer structure-activity relationship. This rational design may offer to numerous issues related to the catalyst activity and selectivity.

Among catalytic transformations, olefin metathesis is highly dependent on the availability of the surface active sites. It is worth to mention that metal-based alkylidene surface sites interacts with the olefin's C=C bond leading to substituents rearrangement, where the double bond substituents are exchanged *via* olefin's C=C bond scission and the regeneration of a newly redistributed double bond (metathesis reaction products).

Like other heterogeneous systems, metathesis catalysts (*e.g.* MTO-based catalysts) are facing similar activity-selectivity issues. In view of the reported literature, enhancing the reaction rate, conversion and selectivity of MTO-based catalysts are still challenging tasks. Therefore, the focus of this study is to design efficient MTO-based catalysts for the valorization of industrial vegetable wastes (unsaturated fatty acids). First, our approach consist on developing a green, reproducible and optimized strategy for the synthesis of highly organized mesoporous alumina and modified organized alumina (through two-steps and one-pot process) as suitable supports for MTO-based catalysts. This new catalyst design is aiming to improve the metathesis reaction rate, activity and selectivity of the MTO-based catalysts compared to the wormhole-like alumina-based catalyst (Pillai *et al.*

Appl. Catal., A, 2013, 455, 155-163, and *Fuel*, 2013, 110, 32-39) allowing much more efficient use of surface area. The OMA-based catalyst design may offer an enhanced metathesis reaction rate with improved mass transfer phenomena through well-arranged cylindrical pore channels with a uniform steric hindrance, as well as lowering the substrate/products residence time. Then based on shape-selective catalysis criteria using OMA support interconnected mesoporous network, this catalyst design is aiming to enhance the selectivity of methyl oleate self-metathesis towards desired metathesis reaction products (9-octadecene and dimethyl-9-octadecene-1,18-dioate) and reduce the production of unwanted metathesis reaction products (methyl elaidate). The functional group (*e.g.* carboxylic acid and ester groups) tolerance of these catalysts, make them suitable candidates for this application. Also, it may enhance the linkage between the MTO and the support which prevents desorption of the incorporated MTO molecules.

Moreover, we aim to develop a new method for the synthesis of this $ZnCl_2$-modified OMA supports through a one-pot process as a green chemistry approach, thus reducing the amount of hazardous chemicals used, energy consumption (*e.g.* stirring for synthesis, evaporation and calcination, *etc.*) as well as the preparation time and cost. Moreover, the materials prepared *via* one-pot approach are expected to have better textural properties (*i.e.* larger BET specific surface area and total pore volume) mainly due to reduced pore filling with $ZnCl_2$ and calcination affects on the textural properties. In addition, avoiding an additional calcination step will prevent further dehydroxylation of the alumina supports surface, which will enhance the $ZnCl_2$ incorporation as well as the MTO impregnation. These features will offer the new catalysts better performance compared to the supports prepared through the two-steps process. Overall, the design of well-defined MTO-based catalyst with improved surface sites accessibility and distribution will facilitate the study of the structure-activity relationship including mechanistic pathway of the methyl-oleate self metathesis reaction products formation as well as the catalytic cycle.

In addition to the ecofriendly aspect of this catalyst design, this MTO-based catalyst will be used for unsaturated fatty acids (industrial wastes) valorization into highly desired chemical platforms and industrially important compounds. Methyl oleate self-metathesis products can be used as functionalized monomers for bio-based polymers production, especially, in

view of the current increasing attention around these biodegradable polymers towards reducing the environmental impact of the hazardous solid wastes generated from plastic disposal. In this scope, we propose the following hypothesis in order to overcome these issues by designing a new well-defined robust metathesis catalyst.

3.1.2. Hypotheses of the study

First hypothesis: Using $ZnCl_2$-modified well-ordered hexagonal mesoporous alumina ($ZnCl_2$-OMA) as catalytic supports for MTO improves the methyl oleate self- metathesis reaction rate, conversion and selectivity compared to wormhole-like alumina structure.

Second hypothesis: Rapid and cost-effective one-pot synthesis of $ZnCl_2$-modified OMA supports for MTO-based catalyst offers enhanced supports' features which will offer improved catalytic performance compared to the two-steps prepared $ZnCl_2$-modified OMA supports.

Third hypothesis: Experimental characterizations of metathesis reaction products and catalyst active sites lead to well-predicted structure-activity relationship including mechanistic pathway of the methyl-oleate self metathesis products formation as well as the catalytic cycle.

3.2. Objectives

3.2.1. General objective

The main objective of this research project is to design a new metathesis reaction catalytic system based on MTO-based catalyst, aiming for enhanced metathesis reaction rate, conversion and selectivity, through a green approach. Its activity will be evaluated for methyl oleate self-metathesis to produce symmetrical monomers towards the production of biopolymers.

3.2.2. Specific objectives

In order to verify the formulated research hypotheses, the following objectives were set:

- ✓ Design and optimize the synthesis procedure of organized mesoporous alumina (OMA) by screening several precursors and starting materials, and verifying the procedure's reproducibility
- ✓ Proceed to the spectroscopic investigation of the materials growth and formation mechanism
- ✓ Perform the preparation of $ZnCl_2$-modified OMA supports in a one-step process
- ✓ Evaluate the organized structure stability upon incorporation of $ZnCl_2$ for both approaches (two-steps and one-pot synthesis)
- ✓ Evaluate both synthesized $ZnCl_2$-modified OMA supports as catalytic supports of MTO-based catalysts for methyl oleate self-metathesis as a model bulky functionalized molecule
- ✓ Propose a complete and detailed mechanism for the formation of each methyl oleate self-metathesis product as well as the complete catalytic cycle involved
- ✓ Establish a comparative study between the performance of wormhole-like alumina-based catalysts and both prepared OMA-based catalysts, as well as Grubbs 2nd generation catalyst, including the kinetic profiles (reaction rate), conversion, and selectivity towards desired metathesis reaction products
- ✓ Characterize and study the textural and surface properties of the designed materials and catalysts in order to establish a structure-performance relationship (*e.g.* metathesis reaction products formation pathways, catalytic cycle, *etc.*)

This new generation of heterogeneous catalysts will be used to produce functionalized symmetrical building blocks (metathesis reaction products) starting from renewable feedstock (vegetable oils), for the production of bio-based polymers (*e.g.* bioplastics, biosurfactants, *etc.*) of high performance, either by polymerization/functionalization of these monomers or by attaching them to readily available synthetic or natural polymers.

Chapter 4:

Synthesis, characterization and insights into stable and well organized hexagonal mesoporous zinc-doped alumina as promising metathesis catalysts carrier

Abdelnasser Abidli, Safia Hamoudi and Khaled Belkacemi

Department of Soil Sciences and Agri-Food Engineering, Laval University. G1V 0A6, Quebec City, Quebec, Canada

Published in *Dalton Trans.,* **2015**, 44, 9823-9838.

Résumé

Une série d'alumines mésoporeuses hexagonales très ordonnées et d'alumines mésoporeuses modifiées avec du zinc ont été synthétisé par un procédé sol-gel au moyen d'un processus d'auto-assemblage induit par évaporation, utilisant du Pluronic F127 comme agent structurant non ionique et plusieurs précurseurs d'aluminium. Le processus a été réalisé par l'intermédiaire de plusieurs acides carboxyliques avec l'acide chlorhydrique dans l'éthanol comme solvant. L'imprégnation réussie de $ZnCl_2$ a été réalisée tout en maintenant la structure ordonnée de l'alumine. Les propriétés de surface et de porosité des matériaux synthétisés ont été étudiées. La physisorption d'azote a révélé une surface spécifique BET de 394 m^2 g^{-1} et un volume des pores d'environ 0,55 cm^3 g^{-1}. Les analyses DRX (diffraction des rayons X) aux petits angles ont montré la structure hexagonale bien organisée, même après l'incorporation de chlorure de zinc. L'arrangement organisé de la structure a été confirmé par microscopie électronique à transmission (MET). La composition Zn / Al des matériaux obtenus a été confirmée par analyse ADESF (Analyse Dispersive en Énergie par Spectrométrie de Fluorescence) et SPX (spectrométrie de photoélectrons induits par rayons X), et la quantité de zinc incorporée a été analysée par ICP (spectrométrie par torche à plasma). La modification de surface suite à l'imprégnation de chlorure de zinc a été analysée par SPX, RMN (résonnance magnétique nucléaire) en état solide (^1H et ^{27}Al) et IRTF (spectroscopie infrarouge à transformée de Fourier). Les effets des conditions de synthèse et le mécanisme de formation de la mésostructure ont été explorés. L'activité catalytique de plusieurs catalyseurs à base de méthyltrioxorhénium (MTO) supportés sur des matériaux d'alumines mésoporeuses hexagonales a été testée pour l'auto-métathèse de l'oléate de méthyle. Les résultats ont montré une amélioration de la cinétique de métathèse en utilisant l'alumine hexagonale par rapport à l'alumine conventionnelle. Ce comportement pourrait être attribué au transfert de masse amélioré à l'intérieur de l'alumine mésoporeuse hexagonale. Ces matériaux ont été préparés avec une taille des pores et une structure convenable, ce qui les rend des candidats appropriés pour d'autre applications comme supports catalytiques pour la métathèse d'oléfines fonctionnalisées plus encombrants et même d'autres transformations catalytiques, en raison de leur acidité de Lewis et leurs réseaux poreux uniformes qui conduisent a des sélectivité et des phénomènes de transfert de masse améliorés.

Abstract

A series of highly ordered hexagonal mesoporous alumina and $ZnCl_2$-modified OMA samples are synthesized *via* a sol-gel method through an evaporation-induced self-assembly (EISA) process using Pluronic F127 as nonionic templating agent and several aluminum precursors. The process was mediated using several carboxylic acids along with hydrochloric acid in ethanol. Successful impregnation of $ZnCl_2$ was achieved while maintaining the ordered structure. The surface and poral properties of the materials were investigated. N_2-physisorption analysis revealed a BET surface area of 394 $m^2\ g^{-1}$ and a pore volume around 0.55 $cm^3\ g^{-1}$. Moreover, small-angle XRD diffraction patterns highlighted the well-organized hexagonal structure even upon the incorporation of $ZnCl_2$. The organized-structure arrangement was further confirmed by transmission electron microscopy (TEM) analysis. The Zn/Al composition of the final materials was confirmed by EDX and XPS analysis, and the zinc amount incorporated was analyzed by ICP. Furthermore, the surface modification *via* $ZnCl_2$ impregnation was analyzed by XPS, ^{1}H and ^{27}Al MAS-NMR and FTIR spectroscopic techniques. In addition, the effects of synthesis conditions and the mechanism of the mesostructure formation were explored. The catalytic activity of several MTO-based catalyst supported on these hexagonal mesoporous alumina materials was tested for methyl oleate self-metathesis. The results showed improved kinetics using hexagonal alumina in comparison to those using wormhole-like alumina counterparts. This behavior could be attributed to better mass transfer features of hexagonal mesoporous alumina. The prepared materials with desirable pore size and structure are suitable candidates as catalyst supports for metathesis reaction of bulky functionalized olefins and other catalytic transformations due to their enhanced Lewis acidity and more uniform pore networks favoring enhanced and selective mass transfer phenomena.

Keywords: 2D hexagonal ordered mesoporous alumina; sol-gel preparation; evaporation-induced self-assembly; p6mm symmetry; metathesis reaction

4.1. Introduction

Ordered materials attracted an enormous attention of many research groups focusing on the enhancement of several heterogeneous catalysts activities and selectivity. This was carried out by the improvement of the surface organization and porous network uniformity of these materials [570-576]. These textural aspects offered advantageous alternatives towards desired shape-selective catalysis which are governed by mass transfer phenomena. These phenomena can be tuned by controlling the porosity and the surface homogeneity [577]. Moreover, this key point is more critical when selectivity is an issue, dealing with bulky functionalized molecules that undergo both intra- and inter-molecular reactions. Despite the increasing progress that has been achieved since the first synthesis of hexagonally ordered mesoporous silica [578-580], the synthesis of ordered materials for catalytic applications still remains as a hot research topic. Indeed, various organized mesoporous siliceous and non-siliceous materials were targeted, among them; cubic MCM-41 and MCM-48 [581], SBA-15 [580] and KIT-6 [582], in addition to ordered mesoporous carbon (CMK-1 and CMK-3) [583, 584], niobia [585, 586], titania [586], zirconia [586], tantalum oxide [587] and other several non-siliceous interesting ordered mesoporous metal oxides [588] and hybrid materials [589].

Ordered mesoporous alumina (OMA) has been one of the challenging non-siliceous organized materials to synthesize [594, 595]. Niesz *et al.* [596] reported a Pluronic P123-templated sol-gel synthesis of OMA where the synthesis was performed at 40 °C affording high BET surface and narrow pore size distribution. Liu *et al.* [597] reported a nanocasting synthesis templated by mesoporous CMK-3 carbon. A Pluronic F127-templated synthesis of OMA was also reported by Yuan *et al.* [598]. Recently, Wu *et al.* [599] reported an efficient OMA synthesis using inexpensive aluminum nitrate at 30 °C. OMA with relatively large mesopores have been obtained using a swelling agent in a Pluronic P123-templated synthesis. Along with high surface area and pore size and uniform mesoporous network, great efforts have been also focused on achieving thermally and hydrothermally stable crystalline framework walls of OMA. [573, 597, 598] Moreover this feature can help the

material to maintain large surface area even after thermal treatment at high temperatures [600].

In order to establish a versatile and cost-effective preparation of OMA materials, many approaches have been investigated. These studies revealed the importance of many key-control factors in order to overcome limitations over ordered mesoporous network formation. Therefore, the effect of inorganic precursors-template ratio was investigated [577]. Furthermore, many process parameters were deeply investigated among them, the complexation effect of anions and hydro-carboxylic acid and organic-inorganic interface protectors and template-assistants during aging process [600, 614-616], synthetic routes [617], swelling agents and co-solvents,[618] salt-like effect of water and acid concentration [619], the pH of the synthesis medium and nature of pH adjustor [605], as well as the calcination temperature [610].

The particular acidic properties of the alumina surface attributed to Lewis-acid aluminum species and Brønsted-acid hydroxyl groups, promoted significantly the incorporation of several metals and other metal oxides on alumina. Frequently, OMA modification and synthesis under high thermal conditions led to partial or complete loss of the mesoporous hexagonal arrangement [607]. Therefore, doping metals and metal oxides on OMA and preserving the well-ordered 2D-hexagonal mesostructure is a challenging procedure. In this perspective, various elements were supported on OMA and simultaneously maintaining the organized structure. For instance, Ni, Mg, Fe, Cr, Cu, Ce, La, Y, Ca and Sn were successfully supported on OMA [603, 607]. Si-, Ce-, and Zr-doped OMA [620], Ce–Zr-Co-doped OMA [621, 622], Cu/Ce-OMA [623], La-doped OMA [624] and noble metals-doped OMA (Pt, Ag and Pd) [625] were also prepared. Similarly, OMA-supported metal oxides such as; MgO, CaO, TiO_2, and Cr_2O_3 [607] and ordered titania-alumina mixed oxides [626] were also obtained. In addition, to prevent OMA collapse, the metal-modified OMA were obtained with uniform metal dispersion. These materials presented high catalytic activities for various reactions including carbon dioxide reforming of methane [627], hydrogen production [628], CO oxidation [625], thiophene hydrodesulfurization [629] and methanol dehydration [630].

Catalytic metathesis reaction could be one of these applications that can benefit from the ordered mesostructure network of alumina and modified-alumina, especially when *trans*- or *cis*-selectivity is critical and highly desired.

Actually, metathesis reaction is an efficient transformation offering direct access to industrially important products from oleochemicals in one reaction step. Metathesis reaction of fats and oils is a clean catalytic and atom efficient reaction with no by-product formation [465]. It is a transalkylidenation reaction involving substituents rearrangement of molecules containing C=C bonds resulting in exchange of alkylidene fragments.

A number of catalysts have been developed for metathesis reaction of bulky functionalized olefins. The most active homogeneous catalysts developed are transition metals-based alkylidene complexes. Grubbs, Hoveyda-Grubbs, Schrock catalysts are the most successful among them and they are commercially available [340]. These homogeneous catalysts are active and compatible with a wide range of functional groups. However, they are expensive and often non-reusable. Typical heterogeneous catalysts for metathesis reaction are based on transition metal complexes in presence of co-catalysts or promoters. Traditional catalytic systems consist of metal chlorides, oxides and oxychlorides, often based on Mo, W, and Re and less commonly based on Os, Ir and Ti with co- catalysts which are generally Lewis acids or organometallic compounds of non-transition metals like Al and Sn [396].

Methyl oletate was used as a model molecule for the studies on metathesis reaction of bulky functionalized olefins contained in vegetable. The most widely used heterogeneous catalysts for methyl oleate self-metathesis were Re_2O_7 supported on alumina and silica-alumina materials [389, 396]. However these catalysts require the use of toxic tin-based promoters and additives such as Bu_4Sn to increase the catalyst reactivity. The presence of tin also hinders the catalyst regeneration due to the deposed SnO_2 species on the catalyst surface, formed during each recycling process which reacts with the active Re oxide [388].

Owing to the above limitations of Re_2O_7-based heterogeneous catalysts, the need for alternative approaches without using toxic molecules arises. MTO was found to be an active organorhenium complex for metathesis reaction without the use of toxic promoter [408, 412]. We have demonstrated recently that $ZnCl_2$-modified wormhole-like mesoporous alumina exhibited higher metathesis reaction activity comparing to alumina supports [430-432]. Furthermore, we hypothesized that a well structurally organized alumina would be more suitable, expecting to improve the catalyst performance for the bulky functionalized olefin metathesis reaction.

In the present work, we report the synthesis of well-organized hexagonal $ZnCl_2$-modified alumina. The effects of aluminum precursor and interfacial protectors (CA: carboxylic acids) on mesophase formation were investigated using simple carboxylic acids to prepare a series of ordered modified-alumina. A comprehensive mechanism of mesopores formation using carboxylic acids is proposed. The catalytic activity for methyl oleate self-metathesis using MTO supported on these well-ordered Zn-modified Al_2O_3 was investigated for the first time on this material and comparison with wormhole-like alumina is also discussed. Particularly, methyl oleate conversion as well as formation of desired (9-octadecene and dimethyl-9-octadecene-1,18-dioate) and undesired metathesis reaction products (methyl elaidate).

4.2. Experimental section

4.2.1. Chemicals and reagents

Pluronic F127 ($EO_{106}PO_{70}EO_{106}$, MW = 12 600), aluminum isopropoxide $Al(OPr^i)_3$ (≥98.0%), aluminum-tri-*sec*-butoxide $Al(OBu^s)_3$ (97.0%), citric acid (≥99.5%), L-(+)-tartaric acid (≥99.5 %), fumaric acid (≥99.5 %), oxalic acid (>99.0%), maleic acid (≥99.0%), acetic acid (≥99.7%), zinc chloride ($ZnCl_2$, 99.9%), oleic acid (≥99.0%) and BF_3·MeOH (14% in methanol) were purchased from Sigma-Aldrich Canada (Oakville, ON, Canada). Aluminum tri-*tert*-butoxide $Al(OBu^t)_3$ (97.0%) was purchased from VWR International (Mississauga, ON, Canada). Aluminum nitrate nonahydrate $Al(NO_3)_3$•$9H_2O$ (99.9%), hydrochloric acid (HCl, 36.5-38 wt%) and malonic acid (≥99.0%) were purchased from Acros Organics (Morris Plains, NJ,

USA). Cyclohexane (99.9%), hexane (99.0%), and ethanol (99.9%) were purchased from Fisher Scientific (Ottawa, Ontario, Canada). Methyl oleate was prepared by etherification of oleic acid with BF_3·MeOH. All reagents were used as received without further purification. High purity commercial standards (methyl oleate, methyl elaidate and 9-octadecene) were purchased from Sigma-Aldrich Canada (Oakville, ON, Canada). All gases used were provided by Praxair at a purity of at least 99.995%.

4.2.2. Alumina and modified-alumina synthesis

4.2.2.1. Synthesis of well-ordered hexagonal mesoporous alumina (*meso*-Al_2O_3)

Highly ordered hexagonal mesoporous alumina (Al_2O_3-*meso*) materials were synthesized through an extended sol-gel process associated with nonionic block copolymer as a directing agent, in a similar procedure described by Yuan *et al.* [610] Their synthesis was screened under different conditions (carboxylic acid, aluminum precursor and calcination temperature). Typically, Pluronic F127 (2.17 g) was dissolved in anhydrous ethanol (20 mL) under stirring at room temperature. Then, the investigated carboxylic acid (2.6 mmol) was added. The pH of the solution was adjusted below 2 by adding hydrochloric acid (1.0-1.5 mL), giving a clear solution. The investigated aluminum-precursor (10 mmol) was subsequently added under vigorous stirring. The mixture was then covered with polyethylene film, and left under stirring at room temperature for 5 h. The solvent was removed slowly in a drying oven at 60 °C and aged for 48h. The obtained solid was heated from room temperature to 400 °C with a slow ramping rate (1 °C/min), and calcined for 4 h in air. The obtained Al_2O_3–*meso* material was calcined further at higher temperatures (up to 1100 °C) at ramping rate of 10 °C/min for 1 h in air (2 h for 600-700 °C).

4.2.2.2. Modification of ordered alumina with $ZnCl_2$

The modification of ordered alumina with $ZnCl_2$ was carried out using the procedure reported in our previous works [430-432]. In a typical synthesis, *meso*-Al_2O_3 (2.0 g) was suspended in ethanol (20 mL) under stirring at room temperature. $ZnCl_2$ (334 mg, 2.45 mmol) was dissolved in ethanol (10 mL) by applying a 30 s vortex mixing. The addition of $ZnCl_2$ solution to *meso*-Al_2O_3 suspension was carried out drop wise

under stirring. The mixture was kept under stirring at room temperature for 24 h in air, allowing a complete evaporation of ethanol. The obtained dried sample was heated from room temperature to 400 °C with a ramping rate of 2 °C/min, and then calcined for 4 h in air, providing $ZnCl_2$-modified Al_2O_3–*meso* with optimized Al:Zn molar ratio of 8:1 as reported in our previous works [430-432].

4.2.3. Catalyst synthesis, catalytic activity evaluation and GC analysis of the reaction products

In a typical synthesis, prior to reaction (before adding MTO), the prepared $ZnCl_2$-modified OMA support was first grounded into a fine powder using a mortar and pestle for smaller catalysts particle size. Then, it was loaded into a borosilicate glass cell and heated in an electrical furnace for 2 h at 540 °C (10°C/min heating ramp), under inert argon atmosphere. Afterwards, the system was cooled down to the reaction temperature (45°C) under the same Ar flow. For MTO impregnation, 200 mg of $ZnCl_2$-modified OMA supports were suspended in hexane (1 mL) in a 10 mL reactor under N_2 purge. The reactor was then capped with a septum, and sealed with parafilm. Subsequently, 6.2 mg of MTO were dissolved in hexane (1 mL) using a vortex mixer, then the prepared MTO solution was added to the above modified-alumina suspension under vigorous stirring, and kept under slow nitrogen flow for 15 min. Finally, the N_2 flow was increased allowing complete solvent evaporation, offering the MTO/$ZnCl_2$-OMA catalyst with an optimal loading of 3 wt.%.

The synthesized catalysts were tested for methyl oleate self-metathesis in hexane under controlled dry atmosphere at 45 °C for 3h. During 90 min of methyl oleate self-metathesis reaction, aliquots were taken at different time intervals. The reaction was monitored by GC analysis using dodecane as internal standard. The metathesis reaction products were identified and quantified using commercially available highly pure external standards and GC-MS analysis as reported in our previous works [430-432]. This identification allowed us to quantify the resulting desired (9-octadecene and dimethyl-9-octadecene-1,18-dioate), undesired metathesis reaction products (methyl elaidate), as well as the remained non-converted staring materials (methyl oleate).

Methyl oleate self-metathesis reaction conversion (Conv.), yields, desired metathesis reaction product yield (DMP) and selectivity (*S*) were calculated based on the following formulas:

$$\text{Conv.}\,(\%) = \frac{[\text{moles of initial methyl oleate}] - [\text{moles of methyl oleate final}]}{[\text{moles of methyl oleate initial}]}\ x\ 100$$

$$\text{Yield i}(\%) = \frac{[\text{moles of obtained product i}]}{[\text{moles of initial methyl oleate}] - [\text{moles of methyl oleate final}]}\ x\ 100$$

$$\text{DMP}\ (\%) = \text{Yield of } 9-\text{octadecene} + \text{Yield of dimethyl} - 9 - \text{octadecene} - 1{,}18 - \text{dioate}$$

$$S = \frac{\text{Yield of desired metathesis reaction products}}{\text{Yield of the undesired metathesis reaction product}}$$

4.2.4. Characterization of the materials and the surface sites

The prepared alumina and $ZnCl_2$-modified alumina materials were characterized using Powder X-ray diffraction (XRD) and N_2 physisorption. Also transmission electron microscopy (TEM), scanning electron microscopy (SEM) and Energy-dispersive X-ray (EDX) spectroscopy measurements were performed. The synthesized materials were also characterized using X-ray photoelectron spectroscopy (XPS), inductively coupled plasma optical emission spectroscopy (ICP-OES), ^{1}H and ^{27}Al magic angle spinning nuclear magnetic resonance (MAS NMR) techniques, as well as Fourier transform infrared (FTIR) spectroscopy.

4.2.4.1. Powder X-ray diffraction (XRD) measurements

The crystal structures and purity of the calcined samples were analyzed by XRD using a an Ultima III Rigaku monochromatic diffractometer (Model D/MAX-2200, with CuKα radiation source (λ=1.54059 Å) operated at a voltage of 40 kV and a current of 44 mA. Small angle XRD measurements were performed over the 2θ angle range of 0.6-6° at a scanning rate of 0.5°/min. The different crystal phases

were identified by wide angle XRD measurements. The patterns were collected from 10° to 80° at a speed of 5.0°/min.

4.2.4.2. Brunauer–Emmett–Teller (BET) surface area measurements

The textural properties (specific surface area, total pore volume and pore size distribution) and surface analysis of calcined samples were performed by nitrogen adsorption/desorption isotherms. The samples were initially out-gassed under vacuum (10^{-4} Torr) at 250-300 °C during 12 h. Then, the multipoint BET surface area measurement was carried out using a volumetric adsorption analyzer (Model Autosorb-1, Quantachrome Instruments, Boyton Beach, FL) at liquid nitrogen temperature -196 °C (77 K). The specific surface area was evaluated using the Brunauer–Emmett–Teller (BET) method. Total pore volume was estimated from the amount adsorbed at the relative pressure P/P_0 = 0.990 single point. Pore size distribution curves were calculated using the desorption branch of the N_2-adsorption/desorption isotherms and the Barrett-Joyner-Halenda (BJH) method as reported in the literature for this type of materials [666-668].

4.2.4.3. Transmission electron microscopy (TEM) studies

The pore size and morphology were examined by transmission electron microscopy (TEM). The micrographs were taken from a JEM-1230 electron microscope (JEOL, Japan) equipped with a lanthanum hexaboride (LaB_6) thermionic emission source, operated at an acceleration voltage up to 80 kV, using Gatan dual-view multiscan camera. For TEM observations, the powdered samples were dispersed in methanol and sonicated for 10 min. A drop of the obtained suspension (5 μL) was then placed uniformly onto a Formvar film coated nickel grid (200 meshes) and it was allowed to dry in air at room temperature before analysis.

4.2.4.4. Microstructural characterizations SEM/EDX

The microstructure, morphology and elemental composition of the synthesized materials were determined using scanning electron microscopy (SEM) along with energy dispersive X-ray spectrometry (EDX). Before analysis, powdered samples were dispersed on a copper grid (300 mesh) coated with a Lacey amorphous carbon

film. The samples were deposited by cathodic sputtering in vacuum chambers (100 mTorr), using an Au/Pd thin film to make the surface electrically conductive for better sensitivity and higher imaging resolution. The characterization was carried out on a JEOL model JSM-840A scanning electron microscope equipped with an energy-dispersive X-ray (EDX) spectrometer operating at an accelerating voltage of 15 kV using secondary electron mode at high vacuum (10^{-6} Torr). EDX spectra of the particles were collected using a single-point quantitative analysis taken from several random areas of the sample. SEM images were acquired using OrionTM software at different magnifications (X 350-3000). The EDX signals were obtained by focusing a high energy electron beam on the particles and accumulating the spectra within an acquisition time of 60 s using Spirit^{TM} Bruker AXS Microanalysis software. Average atomic ratio of the present elements was calculated from several EDX spectra at different points of the prepared sample.

4.2.4.5. Inductively coupled plasma optical emission spectrometry (ICP-OES) analysis

The actual Al/Zn atomic ratio and the Re loading in the prepared catalyst supports was determined by ICP-OES using a Perkin-Elmer Optima 4300DV ICP-emission spectrometer with radial plasma viewing. For analysis, 10 mg of sample were digested with 5 mL of *aqua regia* (nitro-hydrochloric acid) solution. After 24 h, the solution was filled up to 50 mL with deionized water for sample dilution to perform ICP experiments. Measurements from emission spectra for the dissolved species were conducted using calibration curves of a series of Al, Zn and Re standard solutions. The experimental ICP metal composition values were compared to the expected Al/Zn atomic ratio for each sample.

4.2.4.6. X-ray photoelectron spectroscopy (XPS) measurements

Identification of material surface species and their oxidation/coordination states was achieved by means of XPS analysis. XPS spectra were recorded on an AXIS ULTRA from Kratos Analytical (Manchester, UK) equipped with a double X-ray source for non-monochromatic Al-Mg (Kα) X-ray irradiation, a monochromatic Al (Kα) X-ray irradiation source (1486.6 eV), and an electrostatic analyzer of large

radius. The base pressure in the UHV XPS chamber was bellow 5 x 10^{-10} Torr. All spectra were acquired with the Al monochromatic source at room temperature operated at 300 W. The working pressure in the analyzing chamber was less than 10^{-7} Torr. The survey spectrum used to determine the elementary apparent composition was recorded with pass analyzer energy of 160 eV and an energy step of 1 eV, using lenses in the hybrid mode, which maximizes sensitivity [669, 670]. The detailed spectra were obtained with pass energy of 20 or 40 eV, and an energy step of 50 or 100 meV. The charge neutralizer was used for charge compensation of the non-conducting samples. The binding energies were corrected for charge shifts, with the use of the C1*s* set at 285 eV peak as internal reference [671]. The uncertainty in the reported binding energy (BE) values is ±0.1 eV. The survey spectra were recorded in the binding energy range 0–1150 eV, and detailed spectra were recorded for O1s, Zn2*p*, Zn Auger L2M45 M45, Cl2*p* and Al2*p*. Curve fitting and deconvolution were performed using mixed Gaussian/Lorentzian line shapes after a Shirley-type background removal by using the CasaXPS 2.3.15 software [672].

4.2.4.7. ^{1}H -MAS NMR measurements

Catalyst framework was investigated by solid-state NMR spectroscopy. ^{1}H-MAS NMR spectra were recorded on a Bruker AVANCE 300 (Bruker BioSpin Ltd.) wide bore NMR spectrometer equipped with superconducting magnet of 7.1 Tesla using a conventional 4mm-broadband resonance magic angle spinning MAS probehead at operating Larmor frequencies of 300.1 MHz. The dehydrated samples were quickly packed into a 4 mm-zirconia (ZrO_2) rotor, and then the spectra were acquired at room temperature at a typical spinning rate of 10 kHz at the magic angle. Single pulse excitation^{1}H-NMR experiments were performed for Al_2O_3-*meso* and the $ZnCl_2$-modified Al_2O_3-*meso* using a 90° pulse length of 2.25 μs, an acquisition time of 30 ms, and a recycle delay between scans of 60 s. Eight scans were collected for each ^{1}H-MAS-NMR spectrum. All the corresponding chemical shift values were referenced to tetramethylsilane (TMS) signal (0.0 ppm in a spinning rotor).

4.2.4.8. ^{27}Al-MAS NMR investigations

The form, coordination state and environment of aluminum, as well as the surface and intrinsic Lewis acidic site concentrations were studied by means of ^{27}Al solid-state magic-angle spinning (MAS) NMR spectroscopy measurements. The experiments were conducted on a Bruker Avance 300 (7.1 T) instrument. ^{27}Al-MAS-NMR spectra were obtained using a high-speed broadband MAS-probe with an outer diameter of 4 mm, and rotated around the Magic Angle at a rate of 10 kHz controlled within ±2 Hz using a Bruker MAS-controller, with an acquisition time of 15.4 ms. The system was operated at a resonance frequency of 78.1 MHz for ^{27}Al nuclei. All spectra were obtained at room temperature. For the 1D- spectrum measurements, a short single excitation $\pi/10$ pulse of 0.6 μs was applied. The small flip angle of the ^{27}Al pulse was advantageously used to improve signal intensity quantification of the quadrupole nucleus [673]. The relaxation time was set at 250 ms, and 2000 scans were recorded. The ^{27}Al-NMR ppm scale was referenced to $Al(NO_3)_3 \bullet 9H_2O$ by adjusting the signal to 0 ppm [674].

4.2.4.9. Fourier transform infrared (FTIR) spectroscopy studies

FTIR investigations of the mesophase formation pathway were carried out in a Nicolet Magna 850 FTIR spectrometer (Thermo Fisher Scientific Inc.) equipped with a liquid nitrogen-cooled MCT detector in absorbance mode under static conditions. Before analysis, the samples were degassed under vacuum (10^{-4} Torr) at 250 °C overnight. FTIR spectra were recorded at room temperature in the mid-IR spectral range; 400-4000 cm^{-1} region at 4 cm^{-1} resolution accumulating 128 scans. ATR-FTIR data acquisition and manipulation were performed with Omnic™ software (v. 6.1) and presented as absorbance. Spectra were obtained using a 45° trough-style sample holder with a zinc selenide (ZnSe) internal reflection element (56 mm×10 mm×3 mm) (PIKE Technologies, Inc) yielding nine internal reflections, while deconvolution of the IR spectra was carried out using the ORIGIN software (OriginLab Corporation, Northampton, MA).

4.3. Results and discussion

4.3.1. Material characterizations

Physisorption analysis and material physical properties

Aluminum-tri-*sec*-butoxide was used as aluminum precursor for the synthesis of conventional wormhole-like alumina as reported in our previous work [430-432]. Therefore, different hexagonal OMA materials were prepared using the same precursor in the presence of several, inexpensive mono-, di- and tri-carboxylic acids. Table 7 shows the physical properties of these materials.

Table 7: Physical properties of the prepared hexagonally OMA and $ZnCl_2$-modified OMA obtained by means of nitrogen adsorption–desorption isotherms.

Alumina	Acid	Aluminum precursor	S_{BET}[a] (m^2/g)	V_P[b] (cm^3/g)	D_P[c] (nm)	$ZnCl_2$-Modified Al_2O_3[d]	S_{BET}[a] (m^2/g)	V_P[b] (cm^3/g)	D_P[c] (nm)
Al_2O_3-1	Citric	$Al(OBu^s)_3$	362	0.46	3.4	$ZnCl_2$-Al_2O_3-1	316	0.44	3.8
Al_2O_3-2	Tartaric	$Al(OBu^s)_3$	394	0.49	3.8	$ZnCl_2$-Al_2O_3-2	154	0.26	3.8
Al_2O_3-3	Fumaric	$Al(OBu^s)_3$	313	0.43	3.9	$ZnCl_2$-Al_2O_3-3	214	0.31	3.8
Al_2O_3-4	Oxalic	$Al(OBu^s)_3$	317	0.39	3.8	$ZnCl_2$-Al_2O_3-4	ND[e]	ND	ND
Al_2O_3-5	Maleic	$Al(OBu^s)_3$	319	0.31	3.4	$ZnCl_2$-Al_2O_3-5	ND	ND	ND
Al_2O_3-6	Malonic	$Al(OBu^s)_3$	298	0.29	3.4	$ZnCl_2$-Al_2O_3-6	ND	ND	ND
Al_2O_3-7	Acetic	$Al(OBu^s)_3$	378	0.55	3.8 and 4.9	$ZnCl_2$-Al_2O_3-7	ND	ND	ND
Al_2O_3-8	Citric	$Al(OBu^t)_3$	300	0.53	5.5	$ZnCl_2$-Al_2O_3-8	239	0.41	4.9
Al_2O_3-9	Tartaric	$Al(OBu^t)_3$	324	0.59	5.6	$ZnCl_2$-Al_2O_3-9	257	0.44	5.6
Al_2O_3-10	Citric	$Al(OPr^i)_3$	321	0.24	4.9	$ZnCl_2$-Al_2O_3-10	241	0.38	3.8 and 4.9
Al_2O_3-11	Tartaric	$Al(OPr^i)_3$	289	0.46	5.6	$ZnCl_2$-Al_2O_3-11	190	0.39	5.7
Al_2O_3-12	Citric	$Al(NO_3)_3$•$9H_2O$	337	0.30	3.8	$ZnCl_2$-Al_2O_3-12	139	0.40	3.8 and 6.5
Al_2O_3-13	Tartaric	$Al(NO_3)_3$•$9H_2O$	293	0.58	3.8	$ZnCl_2$-Al_2O_3-13	222	0.46	3.8

aBET specific surface area (m2/g); bBJH pore volume (cm3/g) determined at P/P0 = 0.997; cBJH average pore diameter (nm); dAl:Zn atomic ratio of 8:1 determined by ICP-OES analysis; eND: Not determined.

Figure 10 shows the nitrogen adsorption-desorption isotherms of hexagonal OMA synthesized using different carboxylic acids. All isotherms are IV-type and exhibit H1-type hysteresis loops.

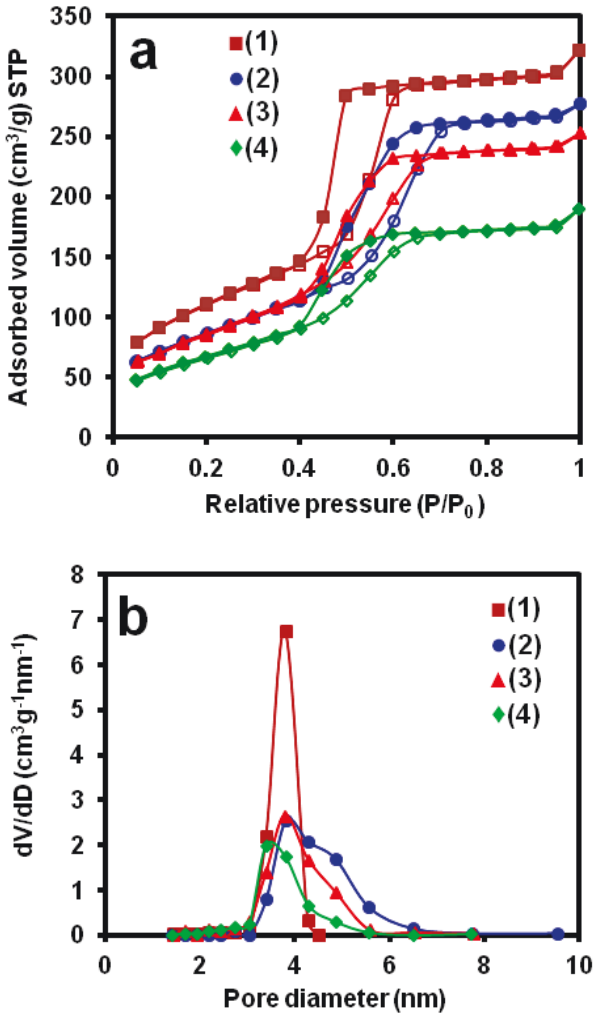

Figure 10. (a) Nitrogen adsorption–desorption isotherms and (b) pore size distributions of the prepared OMA samples: (1: Al_2O_3-2) Al_2O_3-tartaric, (2: Al_2O_3-3) Al_2O_3-fumaric, (3: Al_2O_3-4) Al_2O_3-oxalic and (4: Al_2O_3-5) Al_2O_3-maeilc acid, synthesized using $Al(OBu^s)_3$ and calcined at 400 °C.

These isotherms display well-known patterns of organized mesoporous network containing cylindrical channels. Moderate to relatively large BET surface area (up to 394 m^2/g), pore volume (up to 0.55 cm^3/g) and uniform narrow pore distribution with average pore size of 3.4-4.9 nm were obtained (Table 7).

A slight difference was observed with the investigated carboxylic acids (see also Figure 24 in the Supporting Information) which could be attributed to their similar coordination

abilities with Al centers *via* monodentate or bridging bidentate modes during the mesophase formation process [675]. Moreover, similar BET surface area and pore volume were obtained using different aluminum precursors (See Table 7) showing also typical type-IV curves with H1-hysterisis (Figure 11) characteristic for mesoporous solids [676].

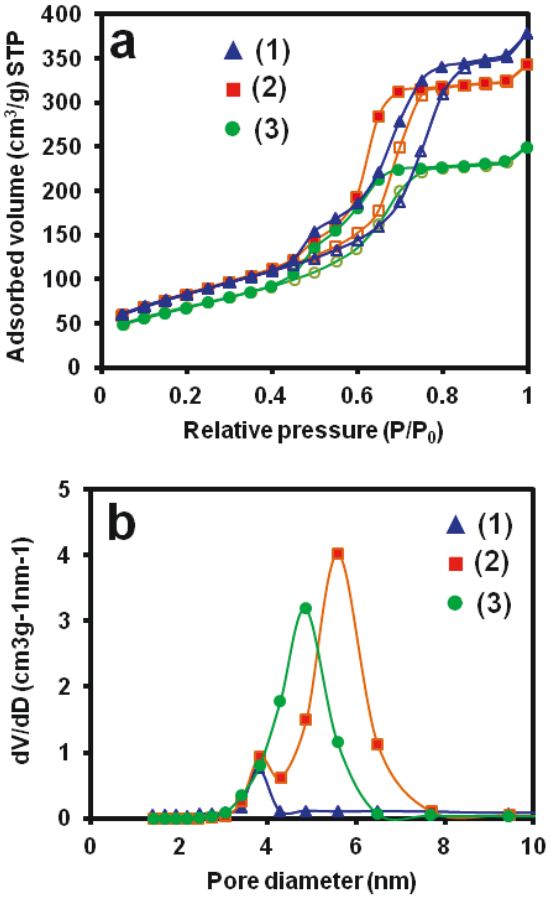

Figure 11. (a) Nitrogen adsorption–desorption isotherms and (b) BJH pore size distributions curves of the prepared OMA samples using tartaric acid with different aluminum precursors: (1: Al_2O_3-13) Al_2O_3-$Al(NO_3)_3$•$9H_2O$, (2: Al_2O_3-9) Al_2O_3-$Al(OBu^t)_3$ and (3: Al_2O_3-11) Al_2O_3- $Al(OPr^i)_3$. All samples were calcined at 400 °C.

However, the OMA prepared with $Al(OBu^t)_3$ and $Al(OPr^i)_3$ afforded larger pore diameters up to 5.6 and 5.7 nm, respectively. The slight difference observed using distinct aluminum precursors may be attributed to the different organic-inorganic interfaces obtained during the templating pathway, allowing distinct chelation between Al atoms, carboxylic acids and

Pluronic F127 moiety [677]. It could be also due to different density charge levels at these interfaces, allowing the self-assembly process in ethanol prior to the hydrolysis [678]. These pathways are governed by Van der Waals interactions, covalent and hydrogen bonding [586].

BET analysis of the $ZnCl_2$-modified OMA supports showed a decreased BET surface area while pore volume and pore distributions are retained even upon pores filling by $ZnCl_2$ (Table 7). Therefore, it is suggested that this drop in BET surface is mainly due to additional calcination step (4 h at 400 °C) in comparison to the original OMA. Moreover, similar shifts were observed using other aluminum precursors (Table 7; see also Figure 25 in the Supporting Information).

XRD analysis

Hexagonally mesostructured materials were successfully obtained as shown from small-angle XRD results in Figure 12a.

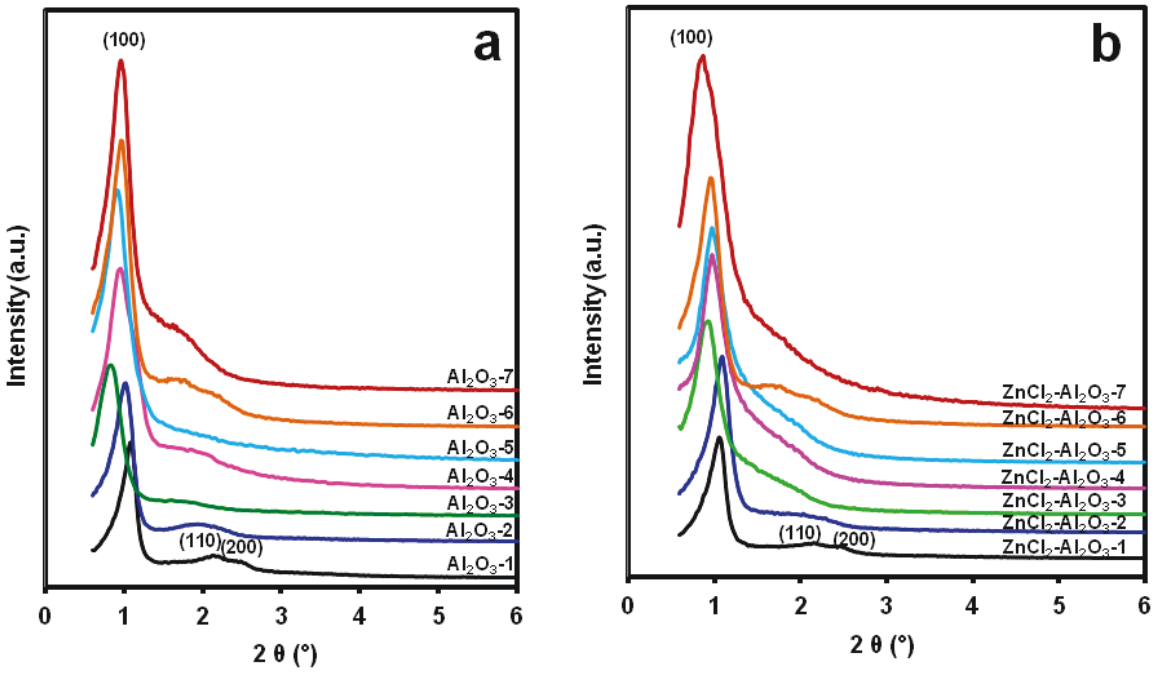

Figure 12. Small-angle powder X-ray diffraction patterns for the prepared (a) ordered mesoporous alumina and (b) the $ZnCl_2$-modified ordered mesoporous alumina synthesized using $Al(OBu^s)_3$ and calcined at 400 °C.

The samples calcined at 400 °C exhibited three diffraction peaks (100, 110 and 200) at around 2θ = 1.0, 2.0 and 2.3°, respectively. This confirms the hexagonal mesostructure, which can be attributed to the *p6mm* space group [596, 598]. The formation of well-organized mesoporous network is confirmed by the high signal-to-noise ratio in small angle XRD patterns with narrow width at half-maximum of the (100) diffraction peak.

$ZnCl_2$ incorporation did not result in any ordered mesostructure collapse, as shown in Figure 12b indicating similar patterns to those obtained with OMA materials.

Small angle XRD patterns of $ZnCl_2$-modified OMA, prepared using other aluminum precursors exhibited similar diffraction peaks (Figure 13). However, the main diffraction peak at around 1.0° was slightly shifted to lower angles for the sample prepared with $Al(OPr^i)_3$ indicating the presence of relatively larger pore size [679]. This suggestion confirms the results of BET analysis.

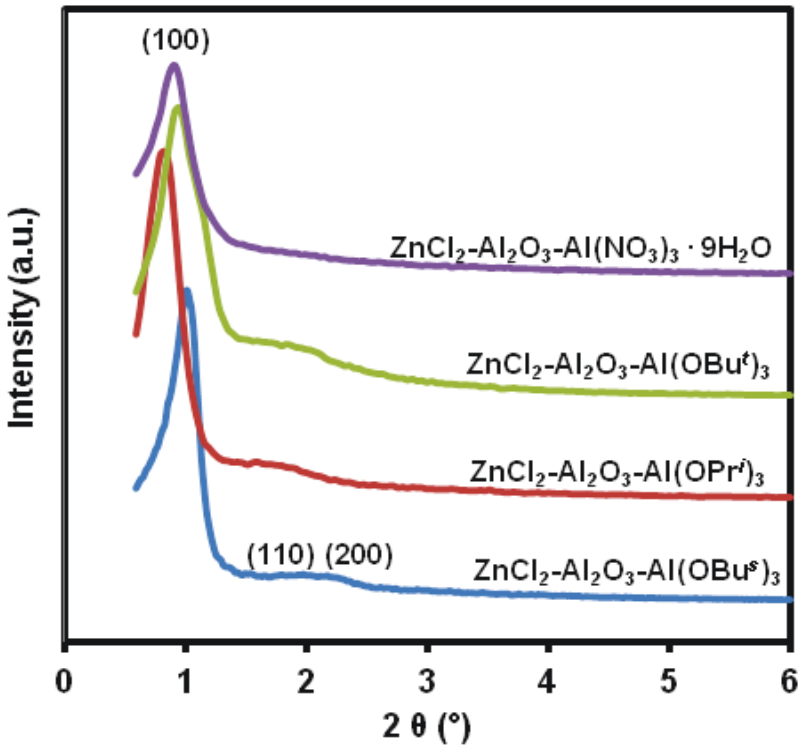

Figure 13. Small-angle powder X-ray diffraction patterns for the prepared $ZnCl_2$-modified OMA calcined at 400 °C using tartaric acid with different aluminum precursors.

Wide-angle XRD (WAXRD) patterns displayed in Figure 14 reveals the absence of any crystalline Al_2O_3 phase in the sample treated at 400 °C, suggesting that only amorphous network is formed. Moreover, further annealing at higher temperatures (800 °C) found to be sufficient to crystallize amorphous Al_2O_3 into the γ-Al_2O_3 phase as confirmed by wide-angle XRD patterns showing well-resolved diffraction peaks (111, 220, 311, 222, 400, 511 and 440) at around 2θ = 20, 34, 37, 39, 47, 62 and 77° . These peaks are assigned to the presence of γ- Al_2O_3 reflections (JCPDS Card, 10-0425). The presence of single γ-Al_2O_3 phase was observed with all the screened aluminum precursors. Surprisingly, this γ-Al_2O_3 phase remains stable even at elevated temperature up to 1000 °C, demonstrating the high thermal stability of these materials. However, under higher thermal treatment (1100 °C) conversion of γ-Al_2O_3 phase into α-Al_2O_3 phase (JCPDS Card, 11-0661) was observed.

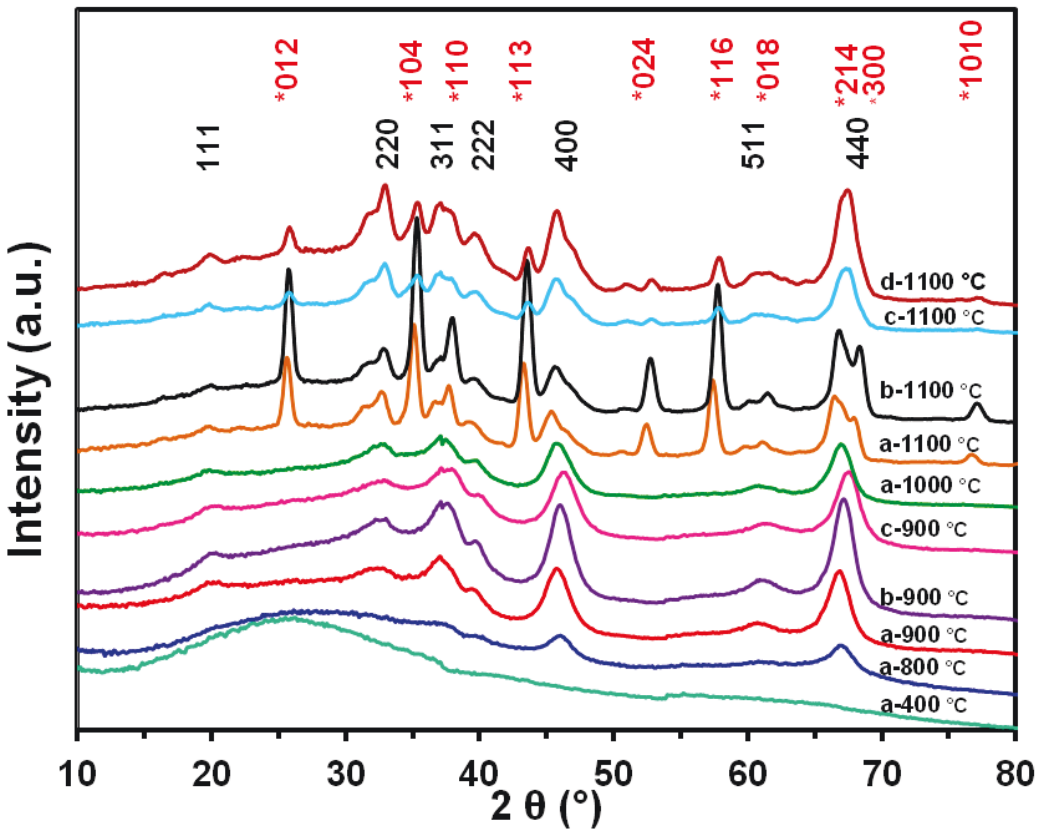

Figure 14. Wide-angle XRD patterns of OMA samples calcined at different temperatures, prepared using citric acid with different aluminum precursors: (a: Al_2O_3-1) $Al(OBu^s)_3$, (b: Al_2O_3-8) $Al(OBu^t)_3$ and (c: Al_2O_3-10) $Al(OPr^i)_3$. Both γ-Al_2O_3 and α-Al_2O_3* phase diffraction peaks are indexed.

TEM analysis

In agreement with XRD measurements, the TEM images confirm that highly organized self-assembly process was achieved using the different carboxylic acids (Figure 15), revealing the hexagonal mesostructure and showing clearly the ordered mesoporous network aligned along [110] direction and arranged along [001] direction.

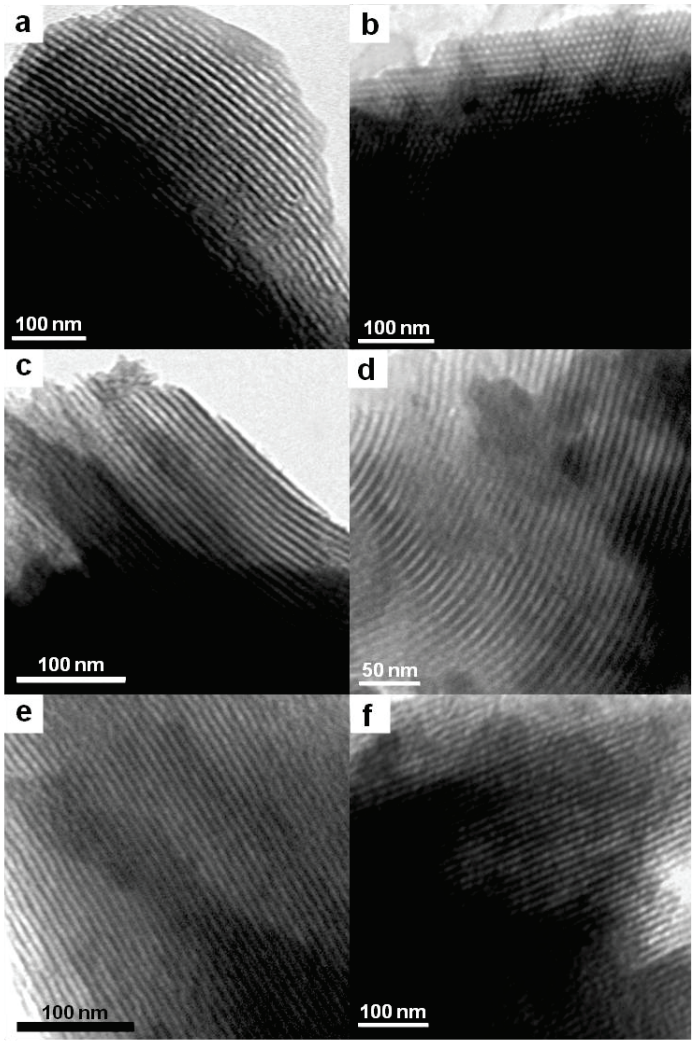

Figure 15. TEM images of the synthesized ordered mesoporous alumina materials using $Al(OBu^s)_3$ with different carboxylic acids; (a: Al_2O_3-1) citric, (c: Al_2O_3-3) fumaric, (d: Al_2O_3-6) malonic, (e: Al_2O_3-2) tartaric and (f: Al_2O_3-4) oxalic acid, viewed along [001] orientation and (b: Al_2O_3-5) maleic acid, viewed along [110] orientation.

Similar observations were portrayed in $ZnCl_2$-modified OMA samples (see Figures 26 and 27 in the Supporting Information) in accordance with XRD results, confirming thus the maintained organized structure even after $ZnCl_2$ incorporation. It is worth to observe that the mean pore sizes as evaluated by TEM analysis are in the vicinity of 3 to 6 nm, confirming the mean pore sizes determined with BET analysis.

SEM analysis

The SEM images displayed in Figure 16a highlight the microstructure of the non-uniform plate-shaped particles of the obtained OMA after template removal and crystal growth. The use of different carboxylic acids and several aluminum precursors did not result in any significant difference in the microstructure of the prepared OMA (Figures 28 and 29 in the Supporting Information).

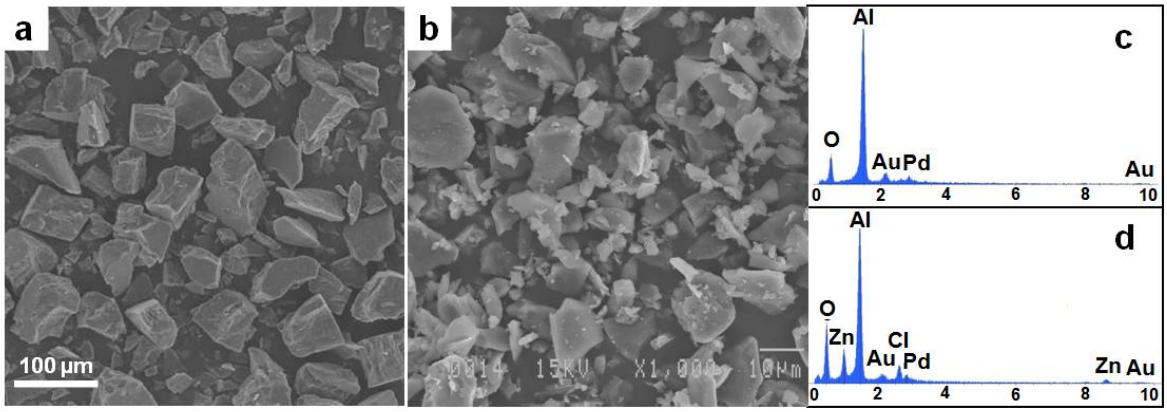

Figure 16. Representative SEM images obtained for (a: Al_2O_3-4) OMA and (b: $ZnCl_2$-Al_2O_3-4) $ZnCl_2$-modified OMA supports' microparticles prepared using oxalic acid with $Al(OBu^s)_3$. Energy dispersive X-ray (EDX) spectra of (c) OMA and (d) $ZnCl_2$-modified OMA supports samples prepared using oxalic acid-$Al(OBu^s)_3$

The SEM images display also the presence of microparticles which can be attributed to irregular aggregation of many nanoscale single crystals under thermal treatment. Moreover the microstructure observed with OMA was slightly modified after $ZnCl_2$ incorporation as depicted in Figure 16b (see also Figure 28 in the Supporting Information). The impregnation process allowed the formation of relatively smaller and less regular particle morphology and size. This can be observed in Figure 16b which shows medium-sized

particles around 8-15 µm. It is believed that the presence of such smaller microparticles could be due to mechano-chemical dislocation effect during the $ZnCl_2$ incorporation process. The EDX spectrum of OMA sample displayed in Figure 16c exhibits only a strong signal for O and Al elements highlighting the evidence for mesoporous Al_2O_3 formation. Whilst, Au/Pd and C were also detected deriving from Au/Pd thin film used to enhance the sample surface electrical conductivity for better improved detection purpose and from the carbon film used for samples deposition, respectively.

EDX analysis of $ZnCl_2$-modified Al_2O_3 samples depicted in Figure 16d shows also the presence of O and Al elements belonging to Al_2O_3 material. In addition, it shows the presence of both Zn and Cl elements owing to the impregnation of $ZnCl_2$ into to Al_2O_3 materials.

XPS analysis

The XPS measurements of OMA samples confirmed the presence of only Al and O elements as depicted in the survey spectrum (Figure 30a in the Supporting Information) with the desired alumina stoichiometry having an Al:O atoms ratio close to 2:3. Al2*p* spectrum displayed in Figure 17a shows a strong signal at 74.3 eV binding energy, which is assigned to the Al element from the anhydrous amorphous alumina phase.[680] Moreover, all Al species (IV, V and VI) contribute to form the Al2*p* peak [681]. The deconvolution of O1*s* XPS spectrum of OMA samples reveals the presence of three different oxygen species on the bulk alumina (Figure 17b). The hidden signals were detected at 530.9, 532.1 and 533.1 eV, which are assigned to bulk oxygen from Al_2O_3 crystal matrix (Al-O-Al), the surface hydroxyl groups (Al-O-H) and the strongly adsorbed H_2O molecules, respectively [680]. The presence of such moisture traces could be the reason behind the slight shift in the Al_2O_3 stoichiometry.

Figure 17d depicts the spectrum of Al2*p* peak of $ZnCl_2$-modified OMA supports at 74.7 eV. In comparison to the peak obtained for OMA material, the Al2*p* binding energy increased from 74.3 to 74.7 eV. This small shift could be attributed to the Al environment changes, especially surface hydroxyl groups that are modified with $ZnCl_2$ [680]. However, this non-significant shift implies that all Al species on both OMA and $ZnCl_2$-modified

OMA supports exhibit the same Lewis acidic properties.

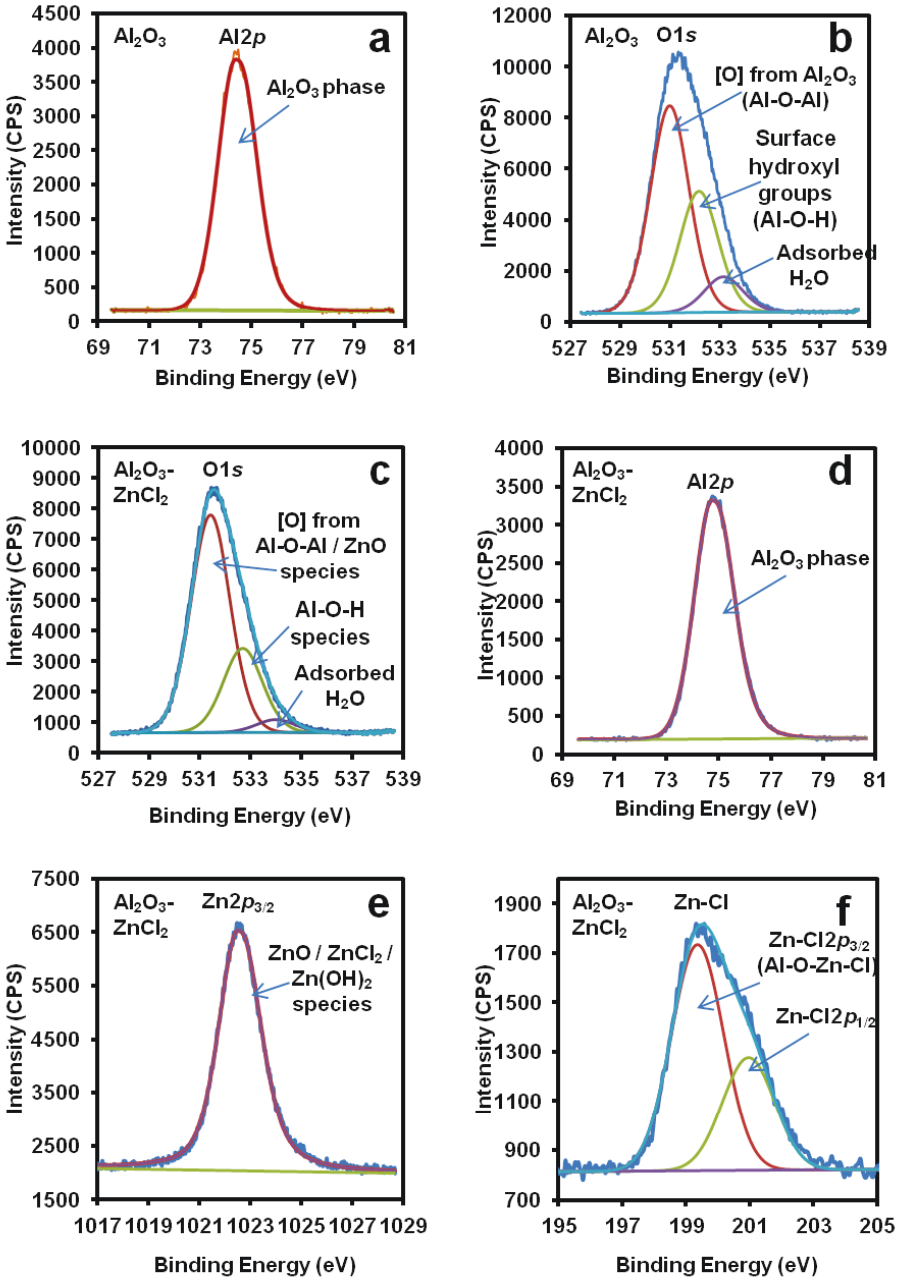

Figure 17. XPS spectra of (a) Al 2*p* and (b) O 1*s* of the prepared OMA and (c) O 1*s* and (d) Al 2*p* (e) Zn 2$p_{3/2}$ and (f) Cl 2$p_{3/2}$ and Cl 2$p_{1/2}$ of the $ZnCl_2$-modified OMA.

On the other hand, similar O1*s* XPS spectrum was obtained for $ZnCl_2$-modified OMA supports samples (Figure 17c) without a significant shift, whilst lower intensities were observed for Al-O-H and H_2O signals. The estimated ratio of oxygen intensity in Al-O-Al

over the oxygen in Al-O-H increased from ~ 2 (hexagonal mesoporous alumina) to ~ 3 ($ZnCl_2$-modified OMA). This may be due to the formation of Zn-O bonding as a consequence of $ZnCl_2$ interactions with Al-O-H species.

Therefore, the occurrence of these species decreased after $ZnCl_2$ treatment of OMA. It is worth to note that was also suggested to be assigned to the formation of ZnO species resulted from the interaction of Zn with surface hydroxyl [682]. The H_2O low intensity signal is simply attributed to the second thermal treatment which helped to remove significant amount of moisture compared to bulk OMA.

The XPS analysis of $ZnCl_2$-modified OMA supports revealed the presence of Zn and Cl elements in addition to Al and O (Figure 30b in the Supporting Information). The expected nominal Al:Zn ratio of 8:1 is confirmed by ICP-OES analysis. However, the atomic element calculations resulted in Zn/Cl stoichiometry around 1.6 to 1.8. This statement could indicate that further to $ZnCl_2$, other Zn-Cl species are dispersed on the OMA surface as pointed out previously by Pillai *et al.* [430, 431]

Regarding the zinc element, Zn2$p_{3/2}$ XPS spectra displayed a unique signal at 1022.5 eV (Figure 17e). However, it is difficult to distinguish between different Zn^{2+} species since the presence of Zn^{2+} signal at this binding energy could be attributed to ZnO species (1022.5 eV)[683], $ZnCl_2$ (1022.5 ±0.2 eV)[684] or $Zn(OH)_2$ (1022.6 eV) [685]. Nonetheless, it could be hardly assigned to a spinel $ZnAl_2O_4$ phase (1022.0 eV) [682]. Therefore, the chlorine XPS spectra are necessary to confirm the nature of the related Zn^{2+} species. XPS spectrum of chlorine ions displayed in Figure 17f exhibits two signals at 199.3 and 200.9 eV for Cl2$p_{3/2}$ and Cl2$p_{1/2}$, respectively after peak deconvolution process. These signals are assigned to Cl bonded to Zn. The Zn-Cl species were also confirmed as Zn-Cl2$p_{3/2}$ with binding energy of 199.1 ± 0.2-0.9 and Zn-Cl2$p_{1/2}$ with a binding energy of 200.6 ± 0.2-1.462 eV. Moreover, the Zn-Cl2$p_{3/2}$ is suggested to be bonded to the alumina surface *via* OH groups as Al-O-Zn-Cl [686]. The calculated low Zn/Cl stoichiometry compared to the incorporated $ZnCl_2$ could be attributed to a partial removal of chlorine from the support surface upon $ZnCl_2$ decomposition under thermal treatment (400 °C) as reported recently by Schmidt *et al.* [637]

^{1}H and ^{27}Al –MAS-NMR Analyses

To confirm the presence of Zn-O-Al bond, ^{1}H-MAS-NMR analysis was conducted investigating the possible interaction of $ZnCl_2$ with the surface hydroxyl groups and the possible types of Zn/Cl species which can be obtained upon alumina modification. Recently, it was suggested that the incorporation of $ZnCl_2$ to alumina may lead to the formation of mixed Zn/O/Cl species, but the possible presence of bulk $ZnCl_2$ or elemental zinc is completely eliminated [637].

First of all, the ^{1}H-MAS-NMR was conducted on OMA only and the results are depicted in Figure 18a which exhibit two main peaks observed at 1.7 and 3.8 ppm.

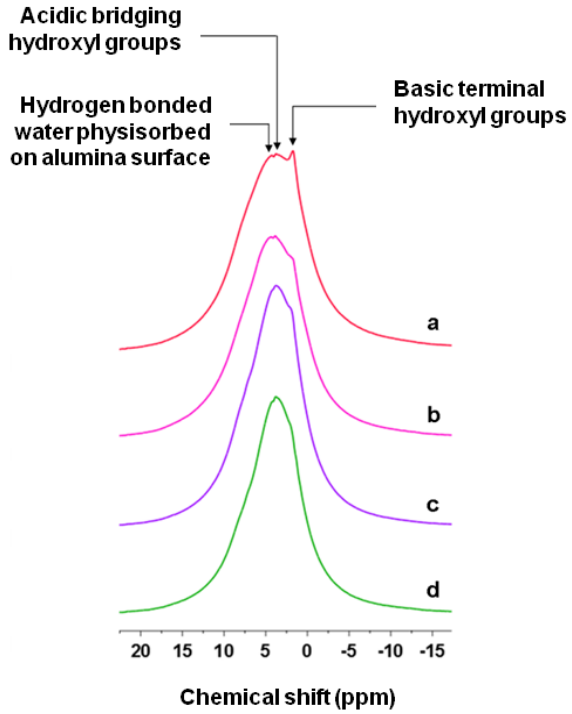

Figure 18. ^{1}H-MAS-NMR spectra of (a: Al_2O_3-4) OMA prepared with oxalic acid-$Al(OBu^{s})_3$. $ZnCl_2$-modified alumina prepared with (b: $ZnCl_2$-Al_2O_3-4) oxalic acid-$Al(OBu^{s})_3$, (c: $ZnCl_2$-Al_2O_3-9) tartaric acid-$Al(OBu^{t})_3$ and (d: $ZnCl_2$-Al_2O_3-10) citric acid-$Al(OPr^{i})_3$. All samples were calcined at 400 °C.

These peaks can be assigned to the basic terminal hydroxyl groups and the acidic bridging hydroxyl groups of intermediate strength, respectively as it was previously reported by

Decanio *et al.* [687]. In contrast, strong acidic and basic hydroxyl groups were detected using wormhole-like alumina as reported in our previous work [430, 431], as well as in other published results [634]. An additional peak was also observed at 4.3 ppm for OMA sample, which is assigned to hydrogen bonded water physisorbed on alumina surface [687, 688].

Afterwards, the $ZnCl_2$-modified OMA supports were analyzed and the results are reported in Figures 18b-18d. As depicted in these figures, the ^{1}H-MAS-NMR spectra reveal the elimination of the peak at 1.7 ppm. These observations suggest that the basic terminal hydroxyl groups are neutralized upon $ZnCl_2$ addition. It is believed that $ZnCl_2$ is bonded to the alumina surface *via* this type of hydroxyl groups forming various Al-O-Zn-Cl species; this was confirmed by combining the ^{1}H-MAS-NMR results with those obtained by XPS analysis. This neutralization leads to a drop in Brønsted acidity, and as a result an enhanced Lewis acidity of the catalyst support is obtained. The peak attributed to hydrogen bonded water physisorbed on alumina was observed also with $ZnCl_2$-modified alumina (Figure 18b). This peak was eliminated in other samples (Figures 18c-18d) which may be due to water trace removal *via* the second calcination process upon alumina modification.

Distinct shapes of the main signal were observed along with variation of carboxylic acid and aluminum precursors used for OMA and $ZnCl_2$-modified OMA supports synthesis. Decanio *et al.* [687] suggested that this signal broadening can be attributed to the strong ^{1}H-^{1}H dipolar interactions of the neighboring hydroxyl groups or physisorbed H_2O molecules. These ^{1}H-MAS-NMR results are supported by the DRIFT analysis reported previously by Tovar *et al.* [634] and in our previous work [430, 431] describing the disappearance of the terminal hydroxyl signals and decrease in bridging hydroxyl signals in the modified-wormhole-like alumina samples spectra in comparison to the initially analyzed wormhole-like alumina.

Figure 19 shows the ^{27}Al-MAS-NMR spectra of as-prepared dried OMA and OMA calcined at 400 °C as well as $ZnCl_2$-modified OMA. Several carboxylic acids and aluminum precursors were screened for the preparation of these materials.

The ^{27}Al-MAS- NMR spectra of the non-calcined (dried) samples exhibit a single peak

centered at around δ = 0 ppm which can be assigned to the octahedral Al-symmetry [685]. This was ascribed to the AlOOH intermediate phase [689]. The spectra of calcined materials exhibit tree major signals at around δ = 5, 35 and 62 ppm compared to the as-prepared OMA, which are assigned to six-, five- and four-coordinated aluminum centers (Al^{3+}), respectively [690].

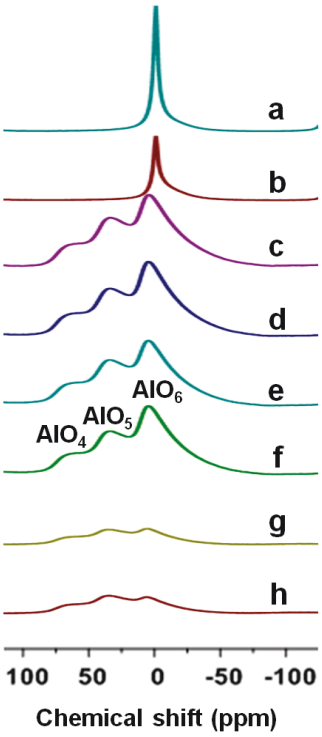

Figure 19. ^{27}Al-MAS-NMR spectra of as-made OMA prepared using (a) citric acid-$Al(OPr^i)_3$ and (b) citric acid-$Al(OBu^t)_3$, and calcined OMA samples prepared using (c: $ZnCl_2$-Al_2O_3-10) citric acid-$Al(OPr^i)_3$, (d: $ZnCl_2$-Al_2O_3-8) citric acid-$Al(OBu^t)_3$, (e: $ZnCl_2$-Al_2O_3-11) tartaric acid-$Al(OPr^i)_3$, (f: $ZnCl_2$-Al_2O_3-9) tartaric acid-$Al(OBu^t)_3$, (g: $ZnCl_2$-Al_2O_3-4) oxalic acid-$Al(OBu^s)_3$ and (h: $ZnCl_2$-Al_2O_3-2) tartaric acid-$Al(OBu^s)_3$. All samples were calcined at 400 °C.

This was attributed to the enhanced dehydration and dehydroxylation upon calcination process [666]. All these peaks appear for both calcined and $ZnCl_2$-modified OMA. However, compared to as-synthesized dried samples, calcined samples exhibit two new signals with high intensity for peaks at δ = 35 (AlO_5) and 62.0 ppm (AlO_4) and lower intensity for the peak at 5.6 ppm (AlO_6).

The origin of the observed conversion of octahedral Al-symmetry to pentahedral and tetrahedral ones could be due to the partial substitution of oxygen ions by hydroxyl groups in octahedral Al-centers during the template removal [691, 692]. Furthermore, the spectra of calcined OMA samples exhibit a relatively strong signal for Al penta-coordinated indicating higher content of AlO_5 centers. Fu *et al.* [693] related this phenomenon to the oxygen deficiency and distorted Al-O inside the alumina framework, as well as the substantial defects induced by relatively large surface area of the mesoporous networks [694, 695]. No significant difference on the distribution environment of Al centers was observed when using distinct aluminum precursors.

On the other hand, performing the synthesis in the presence of different carboxylic acids did not affect the Al coordination distribution for all OMA samples. In the case of $ZnCl_2$-modified OMA, regardless of the Al precursor used, and for the samples using tartaric acid, the AlO_5 and AlO_6 distributions were conserved after $ZnCl_2$ incorporation (Figure 20).

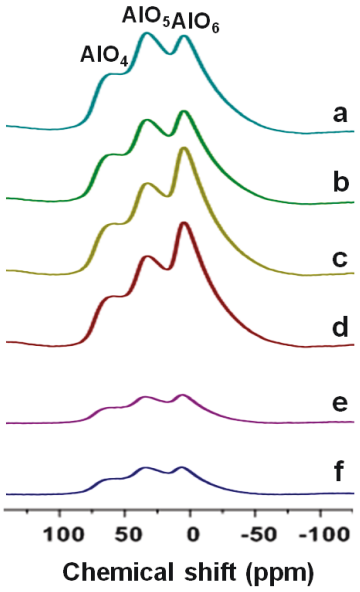

Figure 20. ^{27}Al-MAS-NMR spectra of $ZnCl_2$-modified alumina synthesized using (a: $ZnCl_2$-Al_2O_3-10) citric acid-Al(OPr^i)$_3$, (b: $ZnCl_2$-Al_2O_3-8) citric acid-Al(OBu^t)$_3$, (c: $ZnCl_2$-Al_2O_3-11) tartaric acid-Al(OPr^i)$_3$, (d: $ZnCl_2$-Al_2O_3-9) tartaric acid-Al(OBu^t)$_3$, (e: $ZnCl_2$-Al_2O_3-4) oxalic acid-Al(OBu^s)$_3$ and (f: $ZnCl_2$-Al_2O_3-2) tartaric acid-Al(OBu^s)$_3$. All samples were calcined at 400 °C.

However, lower signal of AlO_6 was observed when citric acid was used. Surprisingly, this distribution was not observed with the corresponding unmodified OMA. It is believed that the tri-carboxylic acid (citric) led to higher amount of AlO_6 on OMA surface compared to the one prepared using the di-carboxylic acid (tartaric). This can be ascribed to the relative difference in the complexation ability of these acids with the Al precursors and bonding to the template before calcination process. It is then suggested that the difference on the exposed amount of AlO_6 can only be observed after $ZnCl_2$ incorporation upon interaction of Zn atoms preferably with AlO_6 coordination sites. Moreover, such selective doping was previously reported when Cu-doped Al_2O_3 was investigated showing high Cu atoms preference towards AlO_5 sites [693]. Therefore, the synthesized Al_2O_3 materials with high penta-coordinated aluminum distribution centers are highly desirable for heterogeneous catalysis [693].

4.3.2. Mechanism of OMA and $ZnCl_2$-modified OMA supports formation

In order to simplify the mechanistic pathway for the mesophase formation and based on well-established mechanisms and theories [578, 579, 598, 695, 696], we propose herein a comprehensive mechanism for OMA synthesis and $ZnCl_2$ incorporation as schematically illustrated in Figure 21.

In this mechanism, it is shown that the uniform aggregation of liquid-crystal phase of surfactant micelles is the main factor to be controlled in order to obtain such organized mesostructure. This agglomeration is obtained after a self-assembly process mediated by complexation effect of carboxylic acids with Al cations, as well as the nonionic surfactant (F127) *via* Van der Waals forces and hydrogen bonding [598].

Therefore, carboxylic acids are used as interfacial protectors to prevent chlorine ions from complexation with Al atoms. Cl^- anions can coordinate strongly with Al species leading the organized assemblies to collapse during the evaporation process [598]. Finally, the templating agent (Pluronic F127; organics) is removed upon calcination under 400 °C, providing the hexagonally structured mesoporous network.

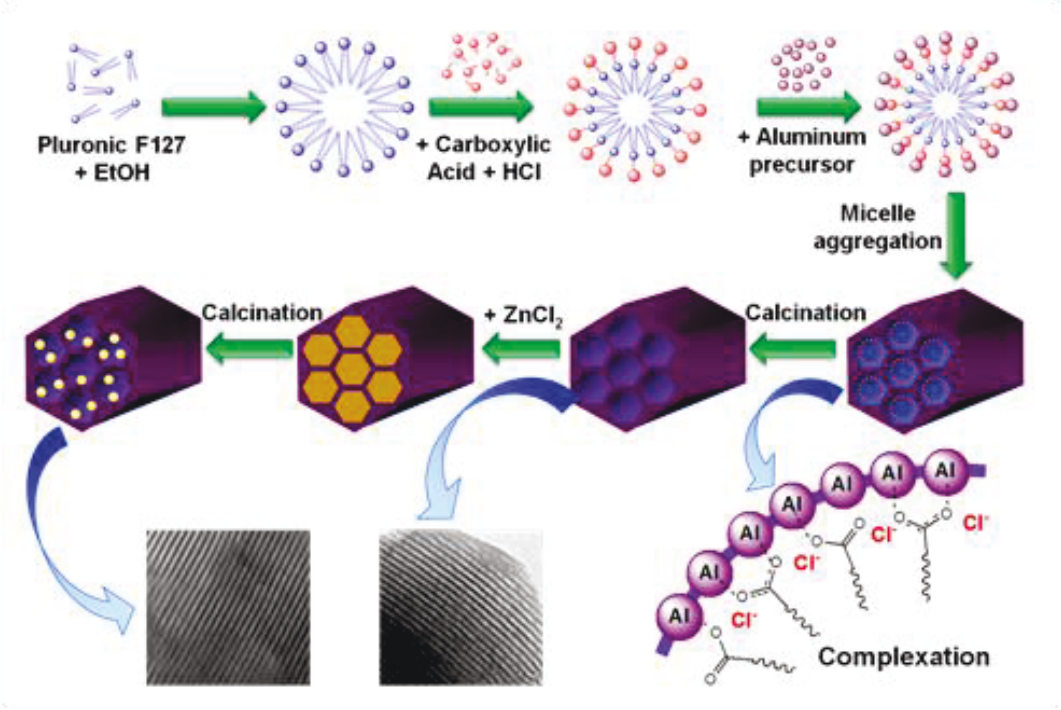

Figure 21. Proposed mechanistic scheme for the formation of organized mesoporous alumina and $ZnCl_2$-modified OMA.

ATR-FTIR analysis

ATR-FTIR measurements were conducted to verify and support the proposed mechanism involving the carboxylic acid-mediated mesophase formation and its interaction with aluminum metal centers. Figure 22 shows the ATR-FTIR spectra of both pure carboxylic acids and as-prepared alumina samples synthesized using different carboxylic acids and aluminum precursors. Pure citric and tartaric acid samples exhibit well-resolved signals at around 1728 and 1709 cm^{-1}, respectively.

These bands are assigned to the carbonyl stretching vibration υ (C=O) of the free carboxylic acids. Moreover, for both acids, their spectra exhibit a second band at around 1677 and 1686 cm^{-1}, respectively. This band can be assigned to the H-bonded carbonyl stretching vibration υ (C=O) of the free carboxylic acids. Also, symmetric stretching vibrations υ_s (COO^-) for free citric and tartaric acid are detected at around 1416 and 1443 cm^{-1}, respectively [697].

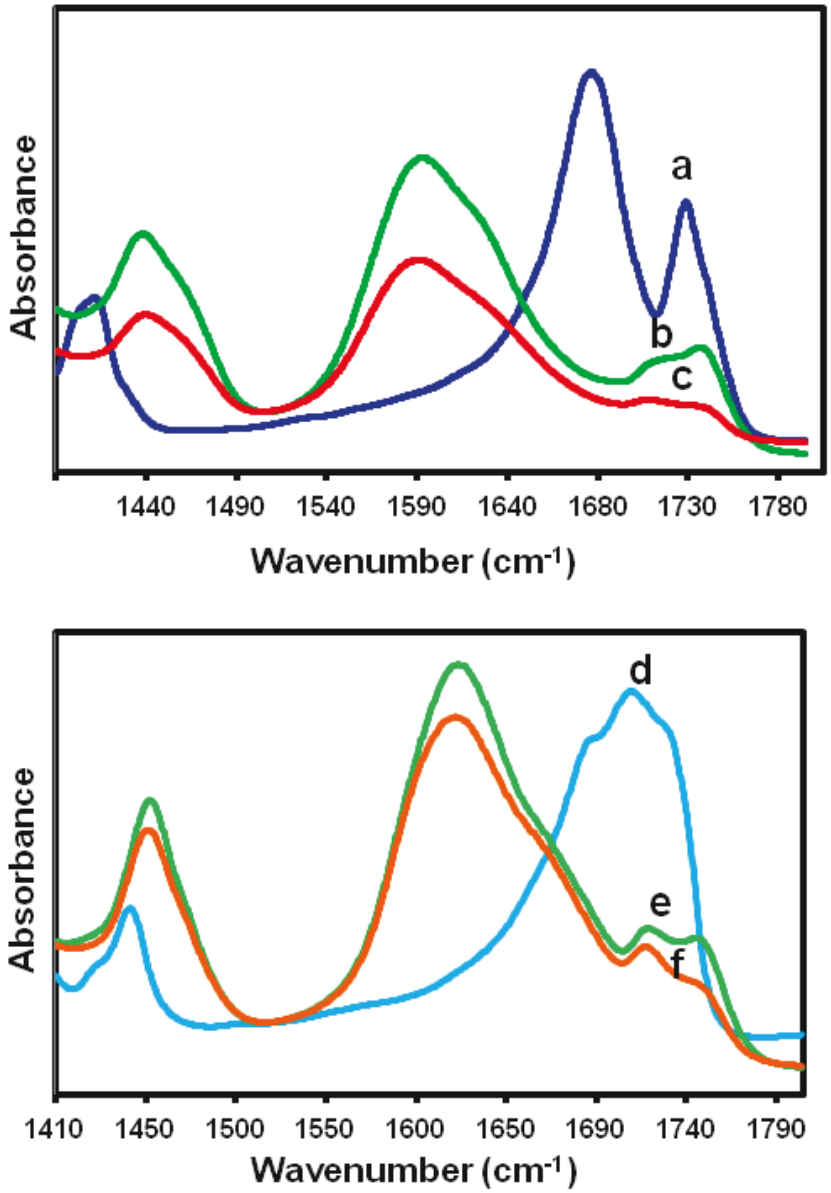

Figure 22. ATR-FTIR absorbance spectra of (a) citric and (d) tartaric acid samples, and the as-prepared alumina samples synthesized using (b) citric acid-Al(OBu^t)$_3$, (c) citric acid-Al(OPr^i)$_3$, (e) tartaric acid-Al(OBu^t)$_3$ and (f) tartaric acid-Al(OPr^i)$_3$.

In the case of the as-synthesized alumina samples, they exhibit two new signals in addition to those observed for free citric acid, while the signal at around 1720-1740 cm^{-1} decreases, indicating the neutralization of citrate ions by Al atoms [598] . The newly appeared signals are assigned to the aluminum-coordinated citrate and tartrate groups: the increased signals at around 1438 and 1450 cm^{-1} are assigned υ (C=O) due to the monodentate coordination

of citrate and tartrate groups to aluminum centers, respectively [698]. In addition, the spectra exhibit well-resolved bands at around 1590 and 1618 cm^{-1}, which are assigned to the asymmetric stretching vibrations υ_a (COO^-) complexed to Al atoms [697]. These results demonstrate the evidence of carboxylic acid-Al coordination pathway leading to the mesophase formation and growth. These interactions are not tightly dependent on the nature of the carboxylic acid or the aluminum precursor.

4.3.3. Catalytic activity for methyl oleate self-metathesis over heterogeneous MTO-based catalysts supported on organized mesoporous alumina

In order to evaluate the performance of the synthesized hexagonal mesoporous alumina materials as catalytic supports, some of the formulated MTO-based catalysts supported on these materials have been tested for their catalytic activity conducted on methyl oleate self-metathesis (See Scheme 11). The obtained results were also compared to those acquired using MTO-based catalysts supported on wormhole-like mesoporous alumina for the same reaction under identical reaction conditions (45 °C, 90 min of reaction time) as optimized previously by Pillai *et al.* [430, 431] These results are summarized in Table 8.

As already reported by Pillai *et al.* [430, 431], methyl oleate self-metathesis with the MTO/$ZnCl_2$-Al_2O_3-*meso* catalyst gave the primary metathesis reaction products 9-octadecene and dimethyl-9-octadecene-1,18-dioate in both *cis* and *trans* isomers. Methyl elaidate, which is the *trans*-isomer of methyl oleate, is also formed during the reaction. This product was obtained from the non-productive or degenerate metathesis reaction as previously described [414, 430, 431]. It is worth to observe that when 3 wt% MTO supported on mesoporous alumina, unmodified with $ZnCl_2$ was used as catalyst [430, 431], only weak methyl oleate conversion of 2.4% was reached after 3 h of reaction, testifying the poor catalyst performance: The yield of total metathesis reaction products was 2.4% where only 43% of this yield is ascribed to the desired metathesis reaction products (**1**, **2**, **4** and **5)**. The selectivity towards the desired products (9-octadecene and dimethyl-9-octadecene-1,18-dioate) is in the vicinity of ~ 42%. The same catalyst modified with $ZnCl_2$ markedly boosted the conversion up to ~ 87% after the same reaction time where the total metathesis reaction product yield attained 86.7% with 52% attributed to the desired

metathesis reaction products. This catalyst yielded also ~ 34% of methyl elaidate (undesired product) as reported in our previous work [430, 431].

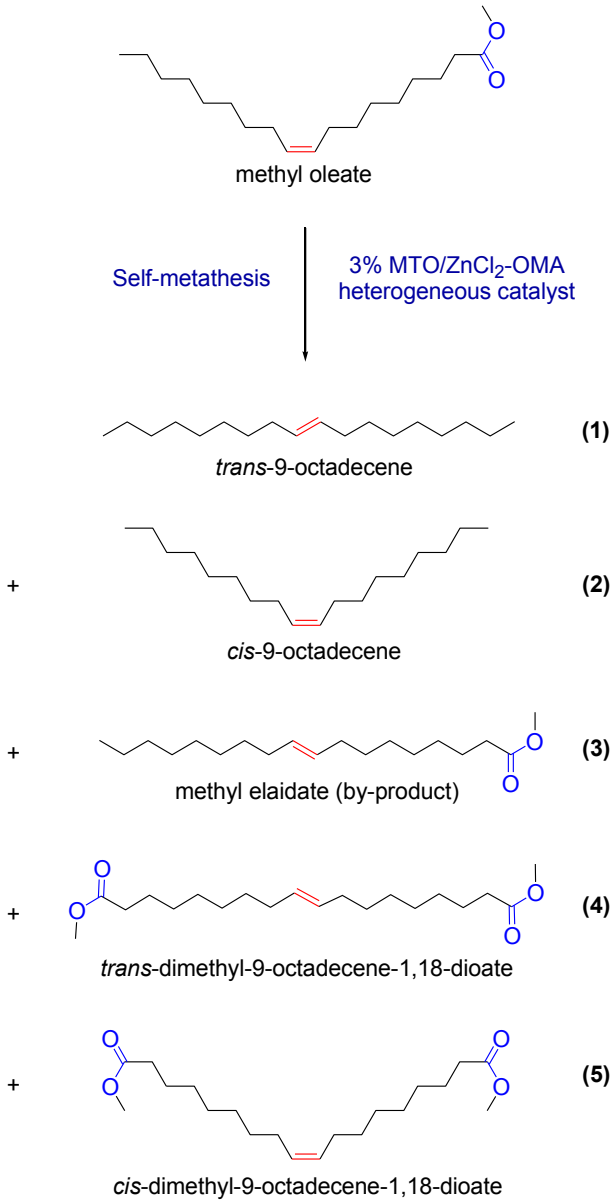

Scheme 11. Reaction pathway of methyl oleate self-metathesis.

The MTO-based catalysts supported on some hexagonal alumina such as Al_2O_3-2 and -11 (Cata #2 and Cata #3, respectively) exhibited somewhat similar activity compared to the MTO-based catalyst supported on wormhole-like alumina. They reached comparable

conversion. It is interesting to note that almost all these $ZnCl_2$-modified OMA supports when they were tested as catalyst supports for methyl oleate self-metathesis, displayed almost similar conversion around 87 to 88% at identical reactions conditions. These catalysts were fairly more selective towards desired metathesis reaction products. Their yield of desired products was slightly higher. This was reflected in somewhat lowering the non-productive metathesis reaction product (methyl elaidate), indicating thus, a better selectivity towards the formation of the desired products. This statement is verified also in the next section treating the kinetics of the reaction.

Table 8: Catalytic activity for methyl oleate self-metathesis over heterogeneous MTO-based catalysts supported on organized or wormhole-like mesoporous alumina.

Catalyst[d]	**1**[a]	**2**[a]	**3**[a]	**4**[a]	**5**[a]	**Conv**[b]	**DMP**[c]	**References**
Cata #1 ($ZnCl_2$-Al_2O_3-1): $Al(OBu^s)_3$ + citric	15.5	14.3	35.0	9.1	4.3	78.2	43.2	This work
Cata #2 ($ZnCl_2$-Al_2O_3-2): $Al(OBu^s)_3$ + tartaric	29.3	8.5	32.9	12.9	4.6	88.2	55.3	This work
Cata #3 ($ZnCl_2$-Al_2O_3-11): $Al(OPr^i)_3$ + tartaric	31.8	8.9	30.2	14.1	2.4	87.4	57.2	This work
Cata #4 ($Al(OBu^s)_3$)	24.4	8.3	34.3	16.2	3.6	86.7	52.4	Pillai *et al.* [430, 431]
Cata #5 ($Al(OBu^s)_3$)	0.2	0.3	1.4	0.2	0.3	2.4	1.0	Pillai *et al.* [430, 431]

[a]The numbers appearing for the metathesis reaction products 1, 2, and 3 (Scheme 13) are expressed in terms of individual product yield ($yield_i$).
[b]Conv.: conversion.
[c]DMP: desired metathesis reaction products.
[d]The investigated catalysts were 3 wt% MTO/$ZnCl_2$-Alumina-1, Alumina-2 and Alumina-11 in the case of **Cata #1**, **Cata #2** and **Cata #3**, respectively. **Cata #4** consisted of 3 wt% MTO on $ZnCl_2$-modified disordered wormhole-like mesoporous alumina, while **Cata #5** was 3 wt% MTO on disordered wormhole-like mesoporous alumina only, reported by Pillai *et al.* [430, 431].

4.3.4. Kinetic profiles of methyl oleate self-metathesis over MTO-based catalysts supported on $ZnCl_2$-modified OMA

The activity and the products distribution yields of methyl oleate self-metathesis over MTO-based catalysts as shown in Table 8 were reached after 90 min of reaction. This long reaction time is considered sufficient to reach the chemical and thermodynamic reaction equilibria of methyl oleate self-metathesis. However, it is possible that this time would be finally shorter than can really appear in order to achieve such equilibria. In fact, for similar reaction conditions, this equilibrium time is dependent on how quick is the reaction for a given catalyst. This cannot be confirmed if a kinetic study is not carried out. For that

purpose, methyl oleate self-metathesis is kinetically evaluated at the investigated temperature of 45 ^{o}C as depicted in Figure 23. It is clearly shown that the metathesis reaction equilibrium was reached early far from 90 min of reaction for MTO-based catalysts supported on both types of $ZnCl_2$-modified OMA where high methyl oleate conversions were obtained.

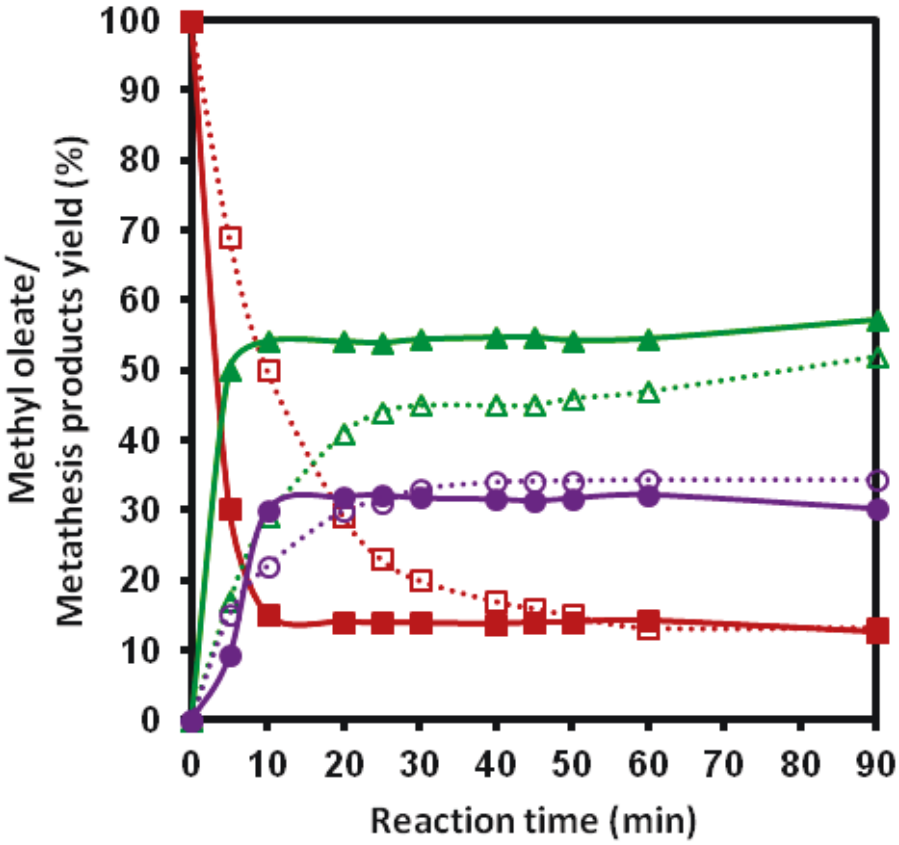

Figure 23. Time-course profiles of methyl oleate self-metathesis over 3 wt% MTO/$ZnCl_2$-Al_2O_3 catalysts using highly ordered hexagonal and wormhole-like mesoporous Al_2O_3. Symbols: For ordered hexagonal Al_2O_3: ■ Methyl oleate; ▲ Desired metathesis reaction products; ● Methyl elaidate. For wormhole-like Al_2O_3: □ Methyl oleate; Δ Desired metathesis reaction products; ○ Methyl elaidate.

At the beginning of these equilibria, the yield of desired metathesis reaction products attained 54% and 47% after 60 min of reaction when the catalysts were supported on

hexagonal and wormhole-like mesoporous alumina, respectively. Moreover, with hexagonal alumina, the MTO-based catalyst seemed to be more selective towards desired metathesis reaction products where only 30% of methyl elaidate, a non-productive metathesis reaction product, was generated. Nevertheless, the time where the reaction begins to reach its equilibrium (onset equilibrium time) is much smaller (~10 min) when hexagonal alumina was used in comparison to wormhole-like structured alumina (30 to 40 min), indicating a huge activity of the MTO-based catalyst supported on hexagonally structured alumina which kinetically outperformed the MTO-based catalyst supported on wormhole-like structured alumina. Consequently, the new catalyst is more selective towards the desired products. Indeed, the products **1**, **2**, **4**, and **5** were formed *via* productive metathesis reaction pathway, whereas the product **3** was formed *via* non-productive metathesis reaction pathway which is a parallel unwanted side reaction. Frequently, the selectivity (*S*) can be defined as the yield of desired products over the yield of all undesired products. Then for the self-metathesis reaction, *S* can be evaluated by:

$$S = \frac{\text{Yield of desired metathesis reaction products } (\mathbf{1}, \mathbf{2}, \mathbf{4} \text{ and } \mathbf{5})}{\text{Yield of the undesired metathesis reaction product } (\mathbf{3})}$$

Table 9 summarizes this selectivity for both MTO-based catalysts using hexagonal and wormhole-like mesoporous aluminas.

Therefore, it is evident that the MTO-based catalyst using hexagonal mesoporous alumina is more selective towards the desired metathesis reaction products than that using wormhole-like alumina.

Even if the activity levels reached with both types of mesoporous alumina materials were quite similar, the kinetics was drastically improved with hexagonal mesoporous alumina compared to wormhole like alumina. In our opinion this could be attributed to the difference in the porous network structure of both alumina materials which greatly influenced the mass transfer phenomena, adsorption/desorption kinetics of the reactant (methyl oleate) as well as the desorption of the reaction products. In other words, in the

case of wormhole-like structure, the reactant will take much more time to adsorb and react on the catalytic sites as well as the products to desorb from the catalyst pores.

Table 9: Selectivity towards the desired metathesis reaction products for the heterogeneous MTO-based catalysts supported on hexagonal or wormhole-like mesoporous aluminas.

Catalysts	***S***
Cata #1 ($ZnCl_2$-Al_2O_3-1): $Al(OBu^s)_3$ + citric	1.234
Cata #2 ($ZnCl_2$-Al_2O_3-2): $Al(OBu^s)_3$ + tartaric	1.681
Cata #3 ($ZnCl_2$-Al_2O_3-11): $Al(OPr^i)_3$ + tartaric	1.894
Cata #4: $Al(OBu^s)_3$	1.531
Cata #5: $Al(OBu^s)_3$	0.714

This is due to the irregular and interconnected porous network characterizing a wormhole-like framework structure, in comparison to the more regular hexagonal pores obtained with highly organized mesoporous alumina where the reactant and products diffusion inside the porous network, in addition to reactant adsorption on the catalyst sites and desorption of the products from the catalyst could be much easier and faster. The kinetics could be tightly dependent on the textural mesoporosity available for transporting substrates to the surface catalytic active sites. This suggestion corroborates that reported by Pauly *et al.* [699] when they studied the effect the textural mesoporosity and the catalytic activity of mesoporous molecular sieves with wormhole framework structures.

4.4. Conclusions

A successful preparation of hexagonal well-ordered mesoporous alumina and $ZnCl_2$-modified alumina in a simple, versatile, and reproducible process was carried out by a bottom-up approach through an evaporation-induced self-assembly technique, using Pluronic F127 and different carboxylic acids and aluminum precursors. The synthesis allowed the formation of well-organized mesoporous alumina materials with moderate to relatively large BET surface areas and pore volumes, as well as uniform mesoporous networks. In order to generalize the synthesis methodology developed, we decided to use different starting materials (aluminum precursors and carboxylic acids). The use of various aluminum precursors was mainly motivated by the cost of the starting materials in order to establish a cost-effective process, for instance, the inorganic salt $Al(NO_3)_3 \bullet 9H_2O$ is

cheaper. However, we used others precursors with various alkoxy chains in order to study their complexation behavior during the self-assembly process, as shown in the formation mechanism (Figure 21). The complexation ability of carboxylic acids with Al centers is the key factor, leading to a successful well-ordered assembly process. On the other hand, the use of different carboxylic acids as interfacial protectors was essentially motivated by their different structure and functionalities (mono-, di- and tri-acids). These functionalities were proved to be a key factor during the self-assembly process (Figure 21). $ZnCl_2$ enhanced greatly the Lewis acidity of the supports, while mainly Al–O–Zn–Cl species are formed on the surface as illustrated with XPS and MAS NMR analyses. Theses ordered materials are potential candidates as catalyst supports for selective heterogeneous catalytic reactions, such as metathesis reaction of bulky functionalized fatty molecules. The hexagonal aluminas exhibited faster kinetics than those obtained with the wormhole-like alumina counterparts. This behavior could be attributed to better mass transfer features of hexagonal mesoporous aluminas. These findings and the synthesis reported herein are key points to elaborate a promising strategy for the synthesis and functionalization of various novel metal-doped organized supports. Moreover, they can pave the way to explore opportunities for the large-scale production of a wide range of these interesting organized modified-mesoporous materials as catalyst supports.

Acknowledgements

The authors gratefully acknowledge the Natural Sciences and Engineering Research Council of Canada (NSERC) and Canadian Foundation for Innovation (CFI) who provided funds for this research. Alain Adnot, Pierre Audet and Richard Janvier are acknowledged for XPS characterization, MAS NMR analysis and TEM measurements, respectively. The authors thank Dr K. T. Venkateswara Rao for his technical advice and for his kind suggestions during the early stages of this project.

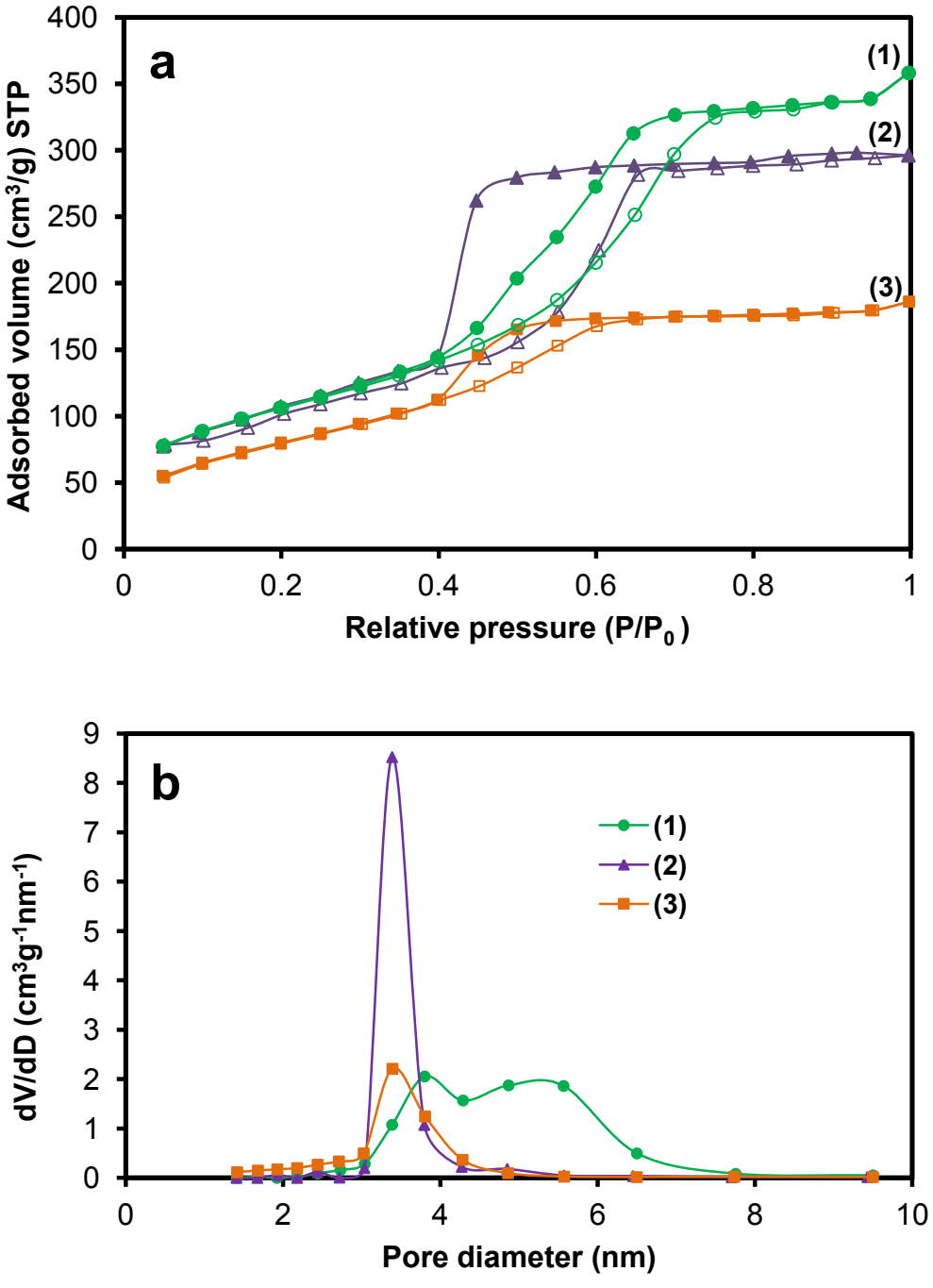

Figure 24. (a) Nitrogen adsorption–desorption isotherms and (b) BJH pore size distributions curves of the prepared OMA samples using $Al(OBu^s)_3$: (1: Al_2O_3-7) Al_2O_3-acetic, (2: Al_2O_3-1) Al_2O_3-citric, (3: Al_2O_3-6) Al_2O_3-malonic.

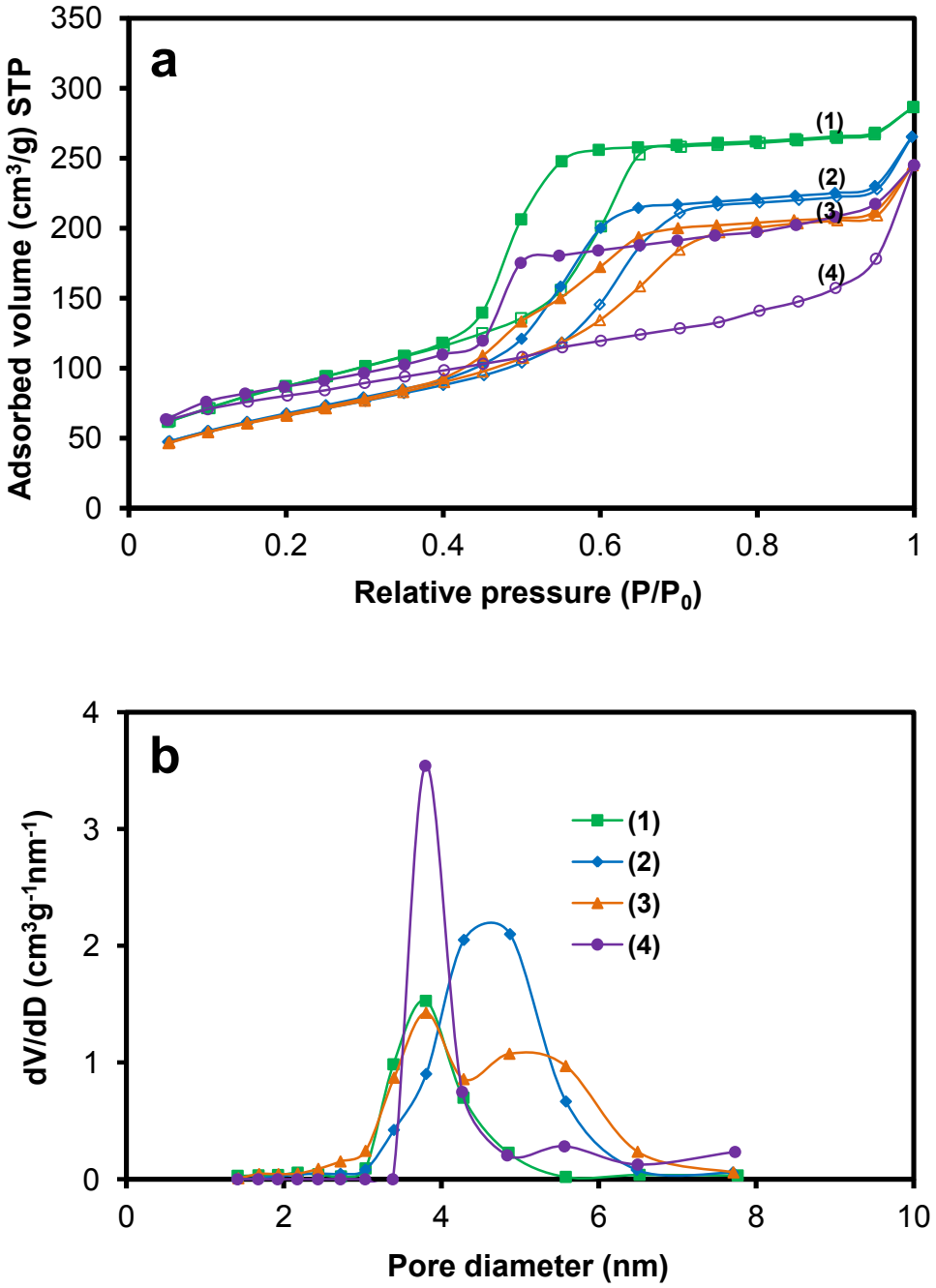

Figure 25. (a) Nitrogen adsorption–desorption isotherms and (b) BJH pore size distributions curves of the prepared $ZnCl_2$-modified OMA samples using citric acid with different aluminum precursors: (1) $ZnCl_2$-Al_2O_3-$Al(OBu^s)_3$, (2) $ZnCl_2$-Al_2O_3-$Al(OBu^t)_3$, (3) $ZnCl_2$-Al_2O_3- $Al(OPr^i)_3$ and (4) $ZnCl_2$-Al_2O_3-$Al(NO_3)_3 \cdot 9H_2O$. All samples were calcined at 400 °C.

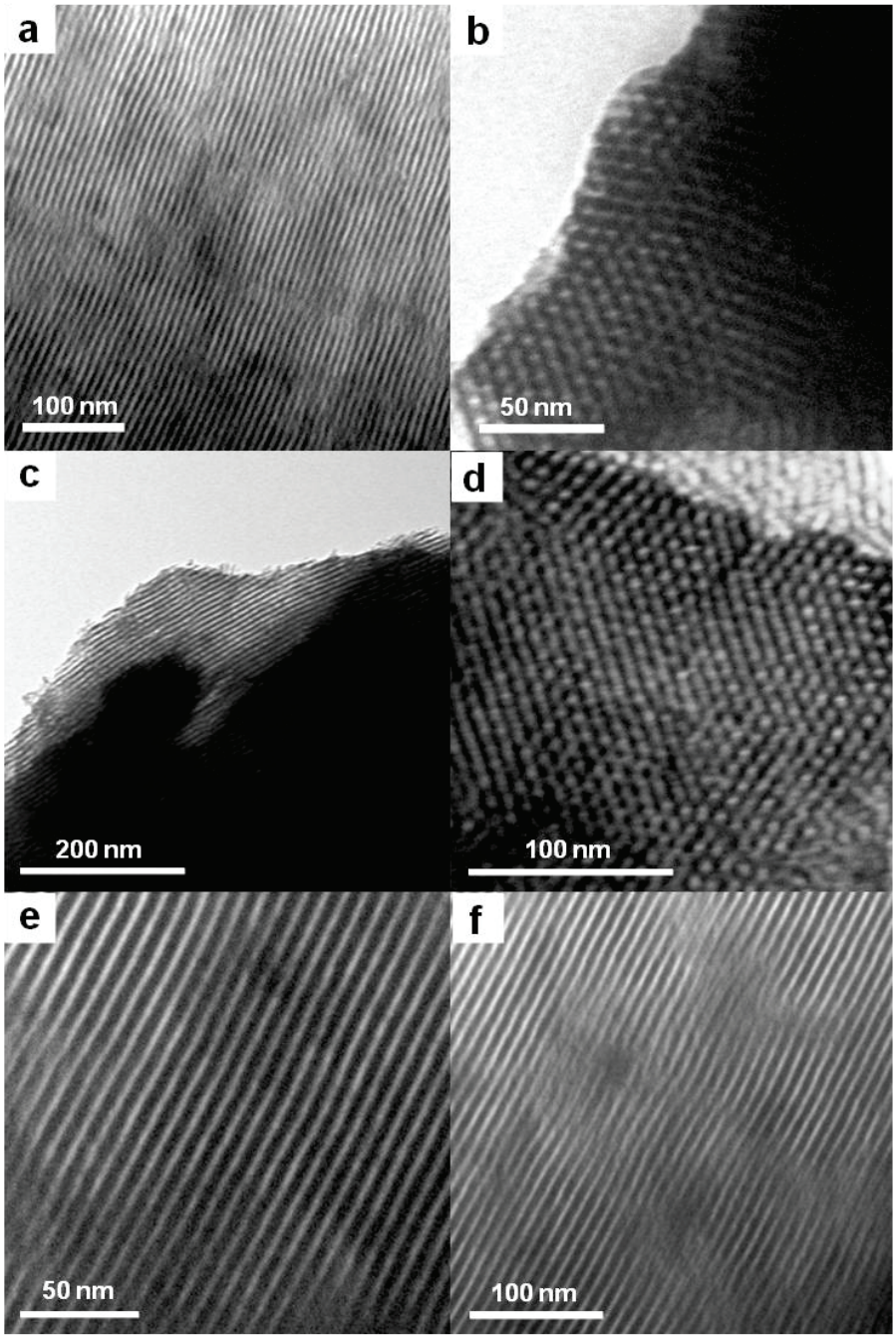

Figure 26. TEM microphages of the prepared $ZnCl_2$-modified OMA supports with different carboxylic acids using $Al(OBu^s)_3$; (a: $ZnCl_2$-Al_2O_3-1) citric, (c: $ZnCl_2$-Al_2O_3-4) oxalic, (e: $ZnCl_2$-Al_2O_3-2) tartaric and (f: $ZnCl_2$-Al_2O_3-3) fumaric viewed along [001] orientation and (b: $ZnCl_2$-Al_2O_3-5) maleic and (d: $ZnCl_2$-Al_2O_3-6) malonic viewed along[110] orientation.

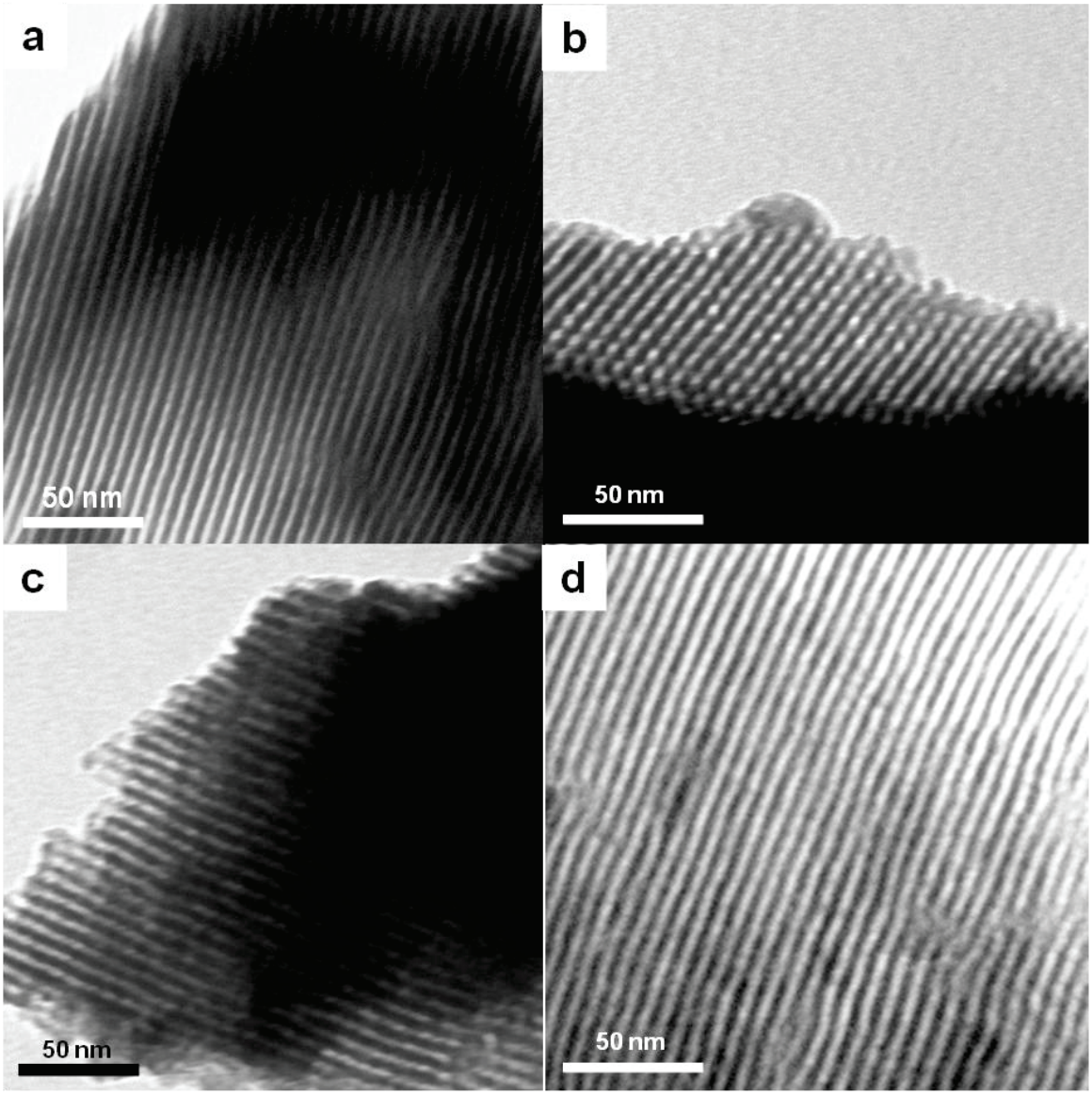

Figure 27. TEM microphages of the prepared $ZnCl_2$-modified OMA supports using tartaric acid with different aluminum precursors; with (a: $ZnCl_2$-Al_2O_3-11) aluminum isopropoxide, (c: $ZnCl_2$-Al_2O_3-13) aluminum nitrate nonahydrate and (d: $ZnCl_2$-Al_2O_3-2) aluminum-tri-sec-butoxide viewed along [001] orientation, and (b: $ZnCl_2$-Al_2O_3-9) aluminum tri-*tert*-butoxide viewed along [110] orientation.

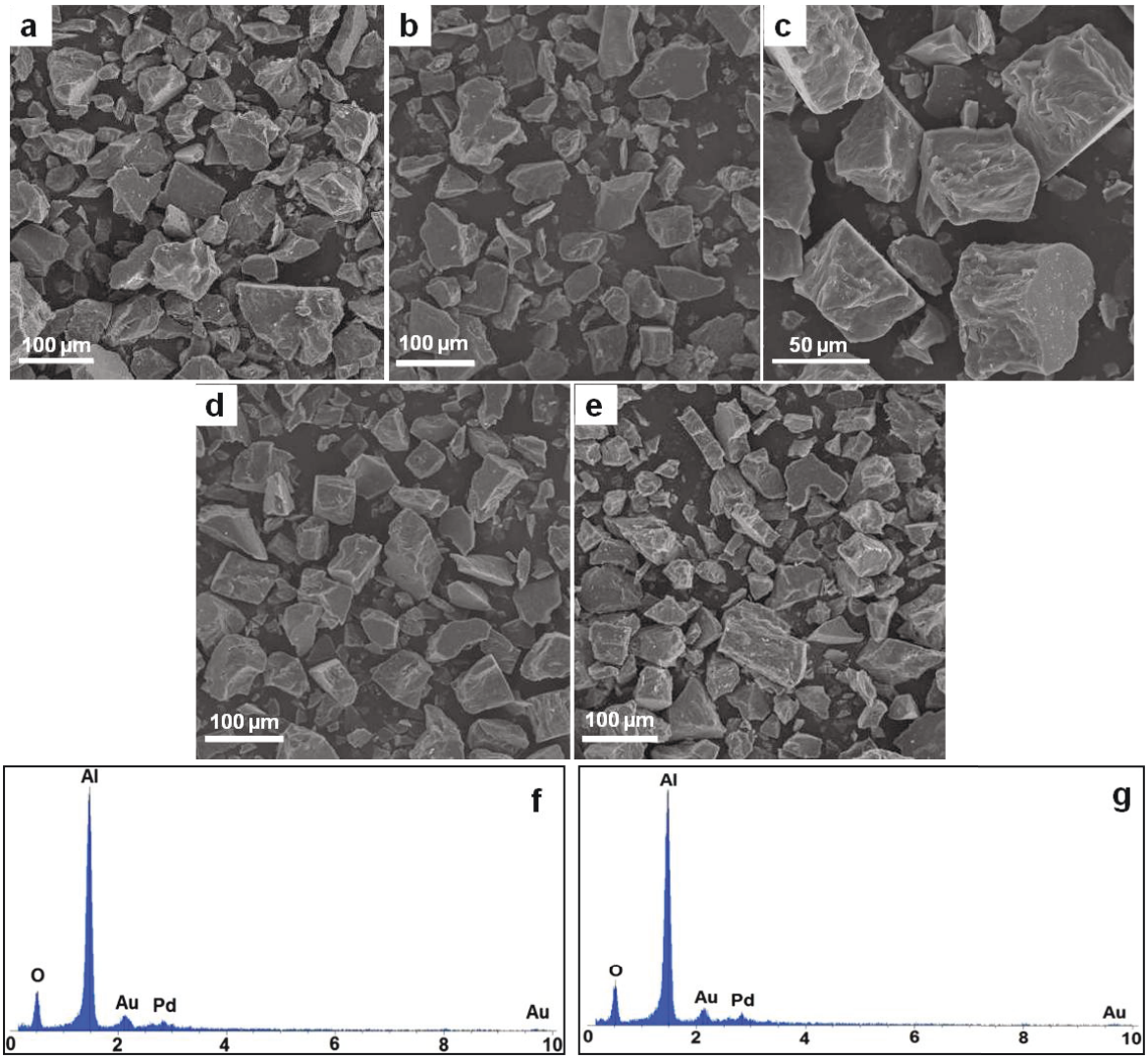

Figure 28. Representative SEM images obtained for OMA microparticles prepared using $Al(OBu^{s})_3$ with different carboxylic acids: (a: Al_2O_3-3) fumaric, (b: Al_2O_3-2) tartaric (c, d: Al_2O_3-4) oxalic and (e: Al_2O_3-1) citric. Energy dispersive X-ray (EDX) spectra of OMA samples obtained using (f: Al_2O_3-4) oxalic and (g: Al_2O_3-3) fumaric acid.

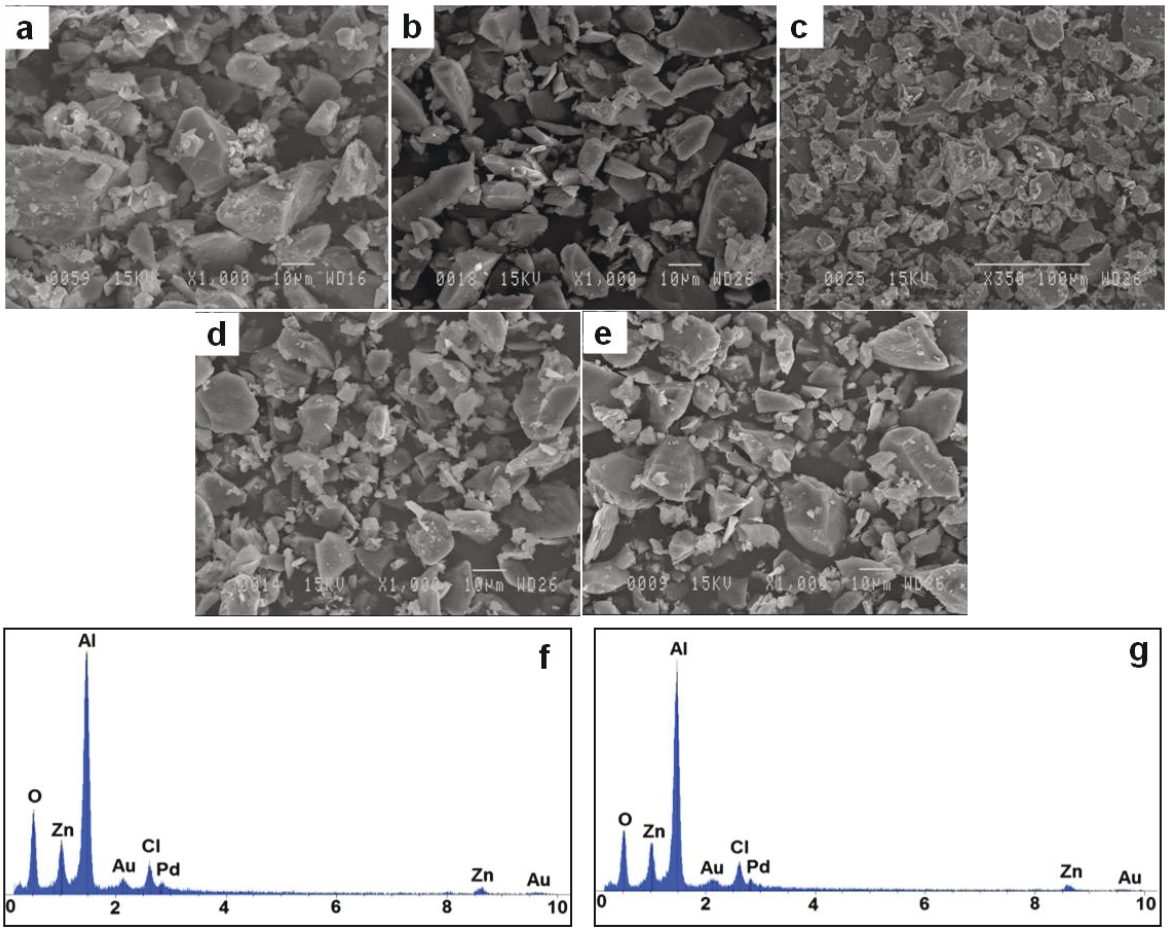

Figure 29. Representative SEM images obtained for $ZnCl_2$-modified OMA supports' microparticles prepared using different carboxylic acids and aluminum precursors: (a: $ZnCl_2$-Al_2O_3-11) tartaric-$Al(OPr^i)_3$, (b: $ZnCl_2$-Al_2O_3-9) tartaric-$Al(OBu^t)_3$, (c: $ZnCl_2$-Al_2O_3-1) citric-$Al(OBu^s)_3$, (d: $ZnCl_2$-Al_2O_3-4) oxalic-$Al(OBu^s)_3$ and (e) oxalic-$Al(NO_3)_3 \cdot 9H_2O$. Energy dispersive X-ray (EDX) spectra of $ZnCl_2$-OMA samples obtained using $Al(OBu^s)_3$ with (f: $ZnCl_2$-Al_2O_3-3) fumaric and (g: $ZnCl_2$-Al_2O_3-1) citric acid.

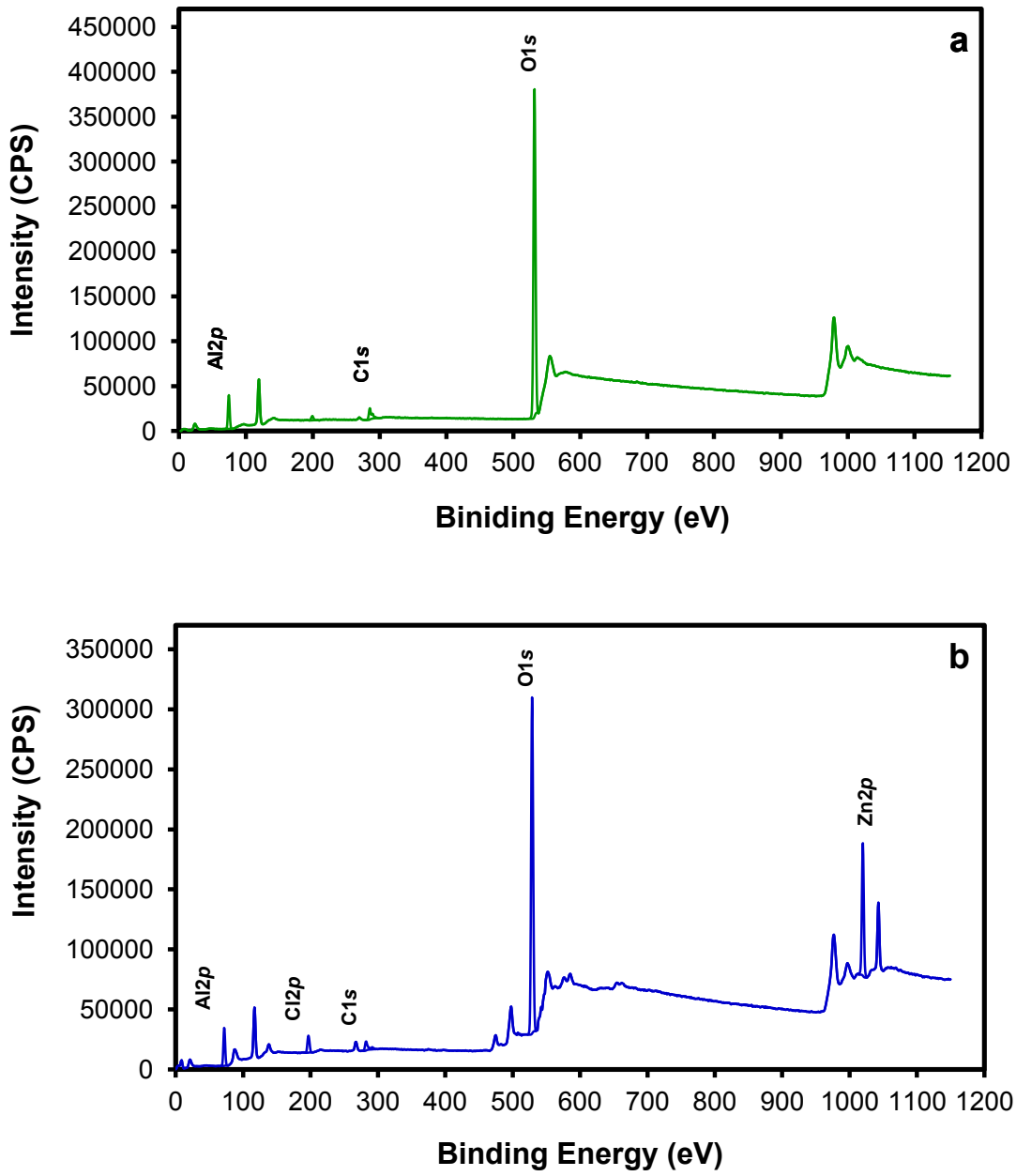

Figure 30. XPS survey spectra of (a) the OMA and (b) the $ZnCl_2$-modified OMA supports samples.

Chapter 5:

One-pot direct synthesis route to self-assembled highly ordered Zn-decorated mesoporous aluminum oxide toward sustainable metathesis heterogeneous catalyst design

Abdelnasser Abidli

Department of Soil Sciences and Agri-Food Engineering, Laval University. G1V 0A6, Quebec City, Quebec, Canada

Published in *RSC Adv.*, **2015**, 5, 92743-92756.

Résumé

Récemment, nous avons préparé l'alumine mésoporeuse organisée dopée avec le chlorure de zinc ($ZnCl_2$-AMO) comme support catalytique, grâce à un processus classique en deux étapes qui englobe la synthèse des AMO, puis une incorporation post-synthèse de $ZnCl_2$. Dans ce travail, nous avons développé une voie de synthèse en une seule étape offrant un accès direct aux supports ($ZnCl_2$-AMO) hexagonaux bien organisés, en employant les mêmes conditions de synthèse que nous avions déjà optimisées pour la synthèse traditionnelle en deux étapes. Nous avons utilisé un processus d'auto-assemblage en phase aqueuse avec le Pluronic F127 comme agent directeur combiné avec une imprégnation *in situ* de $ZnCl_2$. Cette nouvelle approche est compatible avec différents précurseurs d'aluminium communs et différents acides carboxyliques utilisés comme protecteurs d'interface dans le processus d'auto-assemblage. Les matériaux $ZnCl_2$-AMO obtenus ont été caractérisés par différent technique incluant: DRX, adsorption-désorption d'azote, MET, MEB (microscopie électronique à balayage), ADESF, SPX et RMN en état solide (^{1}H et ^{27}Al). Ainsi, ces matériaux ont manifesté des propriétés améliorées par rapport à celles des matériaux synthétisés de façon conventionnelle, en particulier une plus grande surface BET. Les matériaux synthétisés ($ZnCl_2$-AMO) ont ensuite été utilisés comme supports catalytiques pour le méthyltrioxorhénium (MTO), montrant une performance catalytique élevée pour l'auto-métathèse de l'oléate de méthyle, ainsi qu'une meilleure activité et sélectivité envers les produits de métathèse désirés. Ces caractéristiques sont très bénéfiques pour la synthèse à grande échelle grâce à l'introduction rapide, simple, facile et à faible coût de fonctionnalités sur la surface des matériaux mésoporeux sans passer par des procédures en plusieurs étapes.

Abstract

Recently, we have prepared $ZnCl_2$-modifed OMA supports through a conventional two steps process that includes OMA synthesis and then post-synthesis incorporation of $ZnCl_2$. Herein, we developed a direct one-step synthetic route offering access to hexagonally well-organized $ZnCl_2$-OMA materials, employing the same synthesis conditions we have previously optimized for the traditional synthesis. We used an aqueous self-assembly process with Pluronic F127 as a directing agent combined with *in situ* impregnation of $ZnCl_2$. The new approach was found to be compatible with various common aluminum precursors and carboxylic acids used as self-assembly interfacial protectors. The obtained $ZnCl_2$-OMA materials were characterized using XRD, N_2 adsorption-desorption, TEM, SEM, EDX, XPS and ^{1}H and ^{27}Al MAS-NMR techniques. Thus, these materials were found to exhibit improved properties compared to the conventional ones, particularly larger BET surface area. The synthesized $ZnCl_2$-OMA materials were then used as catalytic supports for MTO, showing a high catalytic performance for methyl oleate self-metathesis, demonstrating better activity and selectivity towards desired metathesis reaction products. These features are highly beneficial for large-scale synthesis through fast, simple, easy and low-cost introduction of functionalities on mesoporous materials surface without multi-step procedures.

Keywords: ordered mesoporous alumina; metathesis reaction; catalyst design; one-pot synthesis; *in situ* functionalization

5.1. Introduction

Metal oxide-based supported catalysts are considered as an important class of heterogeneous catalysts [700, 701]. Among these metal oxides, porous systems represent the major share of this family, more particularly mesoporous materials which gathered enormous attention for their wide application spectrum in catalysis [702]. These materials were also advantageously used for other applications including energy conversion and storage, gas sensing as well as adsorption and separation applications [703-706]. Mesoporous aluminum oxide (Al_2O_3) is one of the most commonly used catalyst supports [679]. A variety of active species including organics, metals, organometallics and metal oxides were grafted on alumina surface generating highly robust heterogeneous catalysts [603, 607, 707].

For heterogeneous catalytic conversions, alumina supports are usually modified with other species before incorporation of the active components. These species usually offers better stability to the alumina matrix and the catalyst [708], increase dispersion of active components [709], improve acid-base properties [692, 710, 711], as well as provide enhanced catalytic performance usually through surface synergetic interactions with those species [712]. However, the modification of the catalysts supports is conventionally performed *via* post-synthesis modifications, through a challenging multistep process. These procedures are usually laborious as well as energy and time consuming. Moreover, these features render the synthesis process costly. In addition, the use of several separation and treatment steps increases both the use and generation of possible toxic solvents, compounds and gases. Furthermore, such long processes may hinder the control over the materials synthesis and alter their properties (*e.g.* textural, morphological, chemical, *etc*.) as well as the synthesis yield. These drawbacks present enormous limitations towards large scale synthesis of such modified materials and catalysts, as well as their broad application.

Therefore, the most suitable route for the modification and functionalization of these catalyst supports is to perform an *in situ* incorporation of the desired components, prior to the formation of the host materials. This one-step procedure will highly increase the efficiency of the synthesis process by offering a variety of advantages including faster

synthesis by shortening the process from several days to few hours or minutes. This approach is more cost-effective and leads to higher reaction yields. This renders the introduction of desired functionalities easier and simpler. Moreover, this methodology offers better control over the materials synthesis allowing access to catalytic supports with better properties that are key factor for the enhancement of their catalytic performance.

These hypotheses were fully verified and validated through several experimental studies reported until nowadays. Therefore, this methodology was adopted for the study of metathesis catalysts supported on $ZnCl_2$-modified OMA. Successful synthesis of a highly active metathesis catalysts using MTO supported on functionalized mesoporous alumina was previously reported [430-432]. Through several optimizations, $ZnCl_2$ was shown to be the most suitable metal halide for alumina modification offering the highest metathesis reaction performance among several other metal halides used for the study [430-432]. The MTO supported $ZnCl_2$-modified Al_2O_3 was found to exhibit higher metathesis reaction activity compared to the unmodified alumina [430-432]. This catalysts showed high performance for both methyl oleate and triolein self-metathesis [430-432]. However, this catalyst displayed relatively slow kinetics and unsatisfactory selectivity towards desired metathesis reaction products. Therefore, the traditional alumina support having wormhole-like mesostructure was replaced by a hexagonally ordered mesoporous alumina (OMA), which resulted in an enhanced performance of the MTO-based catalysts for methyl oleate self-metathesis using the $ZnCl_2$-modified OMA supports [657].

These materials were successfully tested for their activity for methyl oleate self-metathesis [657]. Metathesis reaction in one of the most interesting catalytic route providing access to a variety of valuable monomers *via* C=C bond formation [713, 714]. Methyl oleate is chosen as a model molecule having both long carbon chains containing one C=C bond which is subjected to metathesis reaction conditions, and the ester functional group to evaluate the MTO-based catalyst tolerance for functional groups. Also, methyl oleate is a bulky functionalized molecule which is suitable to evaluate the kinetics and molecular diffusion inside the mesoporous network. This renewable substrate originating form vegetable oils represents an interesting feedstock for the synthesis of value-added compounds through metathesis reaction pathway [24, 715].

Therefore, in this study, in order to improve furthermore the MTO-based catalyst, a new direct one-pot aqueous self-assembly strategy for the synthesis of $ZnCl_2$-modified OMA supports was developed. The aim is to improve the synthesis process trough a simpler, faster, easier and cost-effective process. The new synthesis protocol is expected to offer the desired materials with enhanced chemical, morphological, and textural properties which may likely lead to better metathesis reaction performance. In addition, higher synthesis yields are expected to be reached. Detailed characterizations and comparison with alumina-based supports prepared *via* the conventional approach and their catalytic performance are provided.

5.2. Experimental section

5.2.1. One-pot synthesis of $ZnCl_2$-modified ordered mesoporous alumina (OMA)

Well-organized $ZnCl_2$-modified hexagonal mesoporous alumina materials denoted as $ZnCl_2$-OMA were prepared by an easy one-pot synthesis through a combined sol-gel process and *in situ* impregnation method. A detailed description of the chemicals and reagents used can be found in Abidli *et al.* [657]. Various aluminum precursors were used including $Al(OBu^s)_3$, $Al(OPr^i)_3$, $Al(OBu^t)_3$ and $Al(NO_3)_3 \cdot 9H_2O$, with distinct carboxylic acids (citric, tartaric, fumaric, oxalic, malonic, maleic and acetic acid) in order to generalize this methodology and to verify the reproducibility of the newly designed synthesis approach. For a typical synthesis of these modified ordered mesoporous materials; Pluronic F127 (2.17 g) was dissolved in anhydrous ethanol (20 mL) under magnetic stirring at room temperature. Then, the investigated carboxylic acid (2.6 mmol) was added, while the pH of the solution was adjusted below 2 by adding hydrochloric acid (1.0-1.5 mL), giving a clearer solution. Subsequently, the investigated aluminum-precursor (10 mmol) was added under violent magnetic stirring. Simultaneously, $ZnCl_2$ (170 mg, 1.25 mmol) was dissolved in ethanol (10 mL) by applying a 30 s vortex mixing. The dissolved $ZnCl_2$ was then slowly added dropwise to the above Pluronic F127-containing solution under gentle stirring. The resulting mixture was then covered with polyethylene film, and continuously stirred for an additional 5 h at room temperature to homogenize the content. Afterwards, the mixture was transferred for aging into a drying oven at 60 °C, allowing slow and complete evaporation

of solvents within 48h. Finally, the resulting dried solid was annealed at 400 °C with a slow ramping rate (1 °C/min), and calcined for 4 h in air to achieve the final product ($ZnCl_2$-modified OMA supports) with optimized Al:Zn molar ratio of 8:1.

5.2.2. Catalysts preparation and metathesis reaction

The prepared $ZnCl_2$-modified OMA supports were impregnated with 3 wt.% of MTO. Various supports synthesized using different aluminum precursors and carboxylic acids were used, and numerous tests were performed for each catalyst support. Methyl oleate self-metathesis was performed under previously optimized conditions (under atmospheric pressure at 45°C) used for the evaluation of the catalytic performance of conventional MTO-based catalysts [657]. The methyl oleate conversion as well as reaction products identification and quantification were conducted through GC and GC-MS analysis using highly pure commercial standards as described previously [657].

5.2.3. Characterization of the prepared materials and surface properties

Physical properties of calcined samples including the BET specific surface area, total pore volume and BJH pore diameter distribution were measured by nitrogen adsorption-desorption using a volumetric adsorption analyzer (Model Autosorb-1, Quantachrome Instruments). The hexagonal crystalline structure of the calcined $ZnCl_2$-modified alumina samples were characterized by powder X-ray diffraction (XRD). Small-angle X-ray scattering (SAXS) patterns were recorded using Ultima III Rigaku monochromatic diffractometer (Model D/MAX-2200). Transmission electron microscopy (TEM, JEM-1230 electron microscope) was performed in order to examine the structure of the materials' porous network. The samples microstructures and morphologies were observed using a scanning electron microscope (SEM, JEOL model JSM-840A), while the elemental composition and the Al:Zn atomic ratios in the synthesized materials were determined using energy dispersive X-ray spectrometry (EDX, JEOL model JSM-840A). X-ray photoelectron spectroscopy (XPS, AXIS ULTRA from Kratos Analytical) measurements were conducted to identify the materials surface species and their oxidation/coordination states, as well as to confirm the elemental composition and the Al:Zn atomic ratios

analyzed by EDX. Catalyst framework was investigated by proton solid-state NMR spectroscopy (^{1}H MAS NMR), while the form, coordination state and environment of aluminum, as well as the surface and intrinsic Lewis acidic site concentrations were studied by means of aluminum solid-state magic-angle spinning NMR spectroscopy measurements (^{27}Al MAS NMR). See also Abidli *et al.* [657] for more details on characterization experiments and instrumentations.

5.3. Results and discussion

5.3.1. Characterization of the alumina-based materials

5.3.1.1. Nitrogen adsorption-desorption measurements

Figure 31A shows the N_2 adsorption-desorption isotherms of the prepared $ZnCl_2$-modified OMA supports samples synthetized using $Al(OBu^s)_3$ precursor.

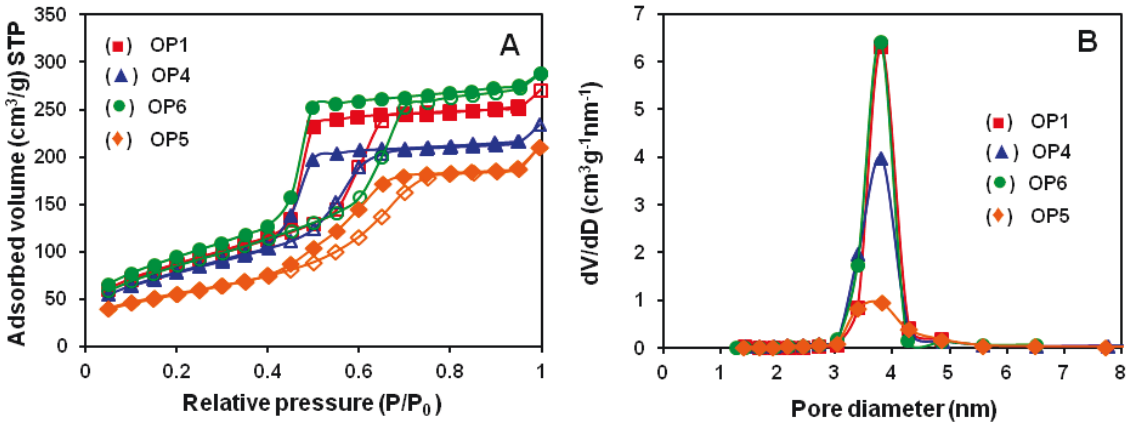

Figure 31. (A) Nitrogen adsorption-desorption isotherms and (B) pore size distributions of the prepared $ZnCl_2$-modified OMA supports samples synthesized using $Al(OBu^s)_3$ with different carboxylic acids: (OP1) $ZnCl_2$-OMA-citric; (OP4) $ZnCl_2$-OMA-oxalic; (OP6) $ZnCl_2$-OMA-malonic and (OP5) $ZnCl_2$-OMA-maleic acid. All samples were calcined at 400 °C.

All obtained isotherms exhibit a typical IV-type curve accompanied with a H1-type hysteresis loop according to IUPAC classification. These results correlate with the capillary condensation of nitrogen inside the confined mesoporous solids, indicating that all samples have organized mesoporous network with uniform and well-defined cylinder-like pore

geometry [676, 716]. Table 10 summarizes the physical properties and porosity parameters of the synthesized $ZnCl_2$-modified OMA supports.

Table 10: Physical properties and porosity parameters obtained for the synthesized $ZnCl_2$-modified OMA supports

$ZnCl_2$-modified OMA supports samples	Acid	Aluminum precursor	Synthesis approach	S_{BET}[a] ($m^2 g^{-1}$)	P_V[b] ($cm^3 g^{-1}$)	d_{BJH}[c] (nm)
$ZnCl_2$-OMA-1 (OP1)	Citric	$Al(OBu^s)_3$	One-pot	307	0.42	3.8
			Two-step[e]	316	0.44	3.8
$ZnCl_2$-OMA-2 (OP2)	Tartaric	$Al(OBu^s)_3$	One-pot	203	0.30	3.8 and 5.6
			Two-step[e]	154	0.26	3.8
$ZnCl_2$-OMA-3 (OP3)	Fumaric	$Al(OBu^s)_3$	One-pot	299	0.41	3.8
			Two-step[e]	214	0.31	3.8
$ZnCl_2$-OMA-4 (OP4)	Oxalic	$Al(OBu^s)_3$	One-pot	282	0.36	3.8
			Two-step[e]	ND	ND	ND
$ZnCl_2$-OMA-5 (OP5)	Maleic	$Al(OBu^s)_3$	One-pot	238	0.27	3.4
			Two-step[e]	ND	ND	ND
$ZnCl_2$-OMA-6 (OP6)	Malonic	$Al(OBu^s)_3$	One-pot	252	0.27	3.4
			Two-step[e]	ND	ND	ND
$ZnCl_2$-OMA-8 (OP8)	Citric	$Al(OBu^t)_3$	One-pot	358	0.67	3.8 and 5.6
			Two-step[e]	239	0.41	4.9
$ZnCl_2$-OMA-9 (OP9)	Tartaric	$Al(OBu^t)_3$	One-pot	307	0.44	3.8
			Two-step[e]	257	0.44	5.6
$ZnCl_2$-OMA-10 (OP10)	Citric	$Al(OPr^i)_3$	One-pot	232	0.47	7.7
			Two-step[e]	241	0.38	3.8 and 4.9
$ZnCl_2$-OMA-11 (OP11)	Tartaric	$Al(OPr^i)_3$	One-pot	219	0.38	3.8 et 4.9
			Two-step[e]	190	0.39	5.7
$ZnCl_2$-OMA-12 (OP12)	Citric	$Al(NO_3)_3 \bullet 9H_2O$	One-pot	201	0.39	3.8 and 4.9
			Two-step[e]	139	0.40	3.8 and 6.5
$ZnCl_2$-OMA-13 (OP13)	Tartaric	$Al(NO_3)_3 \bullet 9H_2O$	One-pot	226	0.41	3.8 et 5.6
			Two-step[e]	222	0.46	3.8
$ZnCl_2$-OMA-14 (OP14)	Malonic	$Al(OBu^t)_3$	One-pot	224	0.41	3.8
			Two-step[e]	ND	ND	ND
$ZnCl_2$-OMA-15 (OP15)	Malonic	$Al(OPr^i)_3$	One-pot	181	0.23	3.4
			Two-step[e]	ND	ND	ND
$ZnCl_2$-OMA-16 (OP16)	Oxalic	$Al(OPr^i)_3$	One-pot	234	0.46	3.8 and 6.5
			Two-step[e]	ND	ND	ND
$ZnCl_2$-OMA-17 (OP17)	Acetic	$Al(OPr^i)_3$	One-pot	199	0.32	3.8 and 4.9
			Two-step[e]	ND	ND	ND
$ZnCl_2$-OMA-18 (OP18)	Maleic	$Al(OPr^i)_3$	One-pot	159	0.34	3.8 and 6.5
			Two-step[e]	ND	ND	ND
$ZnCl_2$-OMA-19 (OP19)	Malonic	$Al(NO_3)_3 \bullet 9H_2O$	One-pot	183	0.33	3.8
			Two-step[e]	ND	ND	ND

[a]BET specific surface area ($m^2 g^{-1}$). [b]BJH pore volume ($cm^3 g^{-1}$) determined at $P/P_0 = 0.997$. [c]BJH average pore diameter (nm). [d]Al:Zn atomic ratio of 8:1 determined by EDX analysis. ND: not determined. [e]BET-BHJ results obtained previously.[657]

Moderate to relatively large BET surface area and pore volume were obtained, up to 358 m^2 g^{-1} and 0.67 cm^3 g^{-1}, respectively. In addition, nearly all the samples displayed uniform narrow pore size distribution with a mean diameter from 3.4 to 6.5 nm. However, some analyzed samples present some secondary porosity (Table 10).

These results suggest that $ZnCl_2$ can be successfully doped inside the mesopores of OMA along with the formation of the desired organized mesostructure. As mentioned above, the one-pot syntheses were performed using distinct aluminum precursors and carboxylic acids in order to generalize the synthesis procedure and verify it's reproducibly. Therefore, we used the same precursors ($Al(OBu^s)_3$, $Al(OPr^i)_3$, $Al(OBu^t)_3$ and $Al(NO_3)_3 \cdot 9H_2O$,) and acids (citric, tartaric, fumaric, oxalic, malonic, maleic and acetic acids) that we previously used for the synthesis of catalytic $ZnCl_2$-modified OMA supports through conventional two-steps process [657]. As depicted in Figure 31 and Table 10, we successfully prepared various $ZnCl_2$-modified OMA supports samples using different carboxylic acids, while no significant differences were observed in their physical properties and their porosity parameters. Furthermore, the targeted organized $ZnCl_2$-modified OMA supports were successfully obtained upon the use of different aluminum precursors with no significant shift as illustrated in Table 10 and Figure 32. This similarity is ascribed to the identical behavior of the investigated precursors and acids, suggesting that the different carboxylic acids tested exhibit similar coordination abilities with the metal centers (Al) *via* monodentate or bridging bidentate modes during the mesophase formation pathway [657, 675]. On the other hand, the investigated aluminum precursors proved also similar chelation abilities of their metallic centers (Al) with both the templating agent (Pluronic F127) fragments and the added carboxylic acids used as organic-inorganic interfacial protectors assisting the ordered self-assembly process. This kind of organized assembly is tailored by means of several interfacial interactions including covalent and hydrogen bonding as well as van der Waals interactions, which play a pivotal role in the mesophase construction [586, 677].

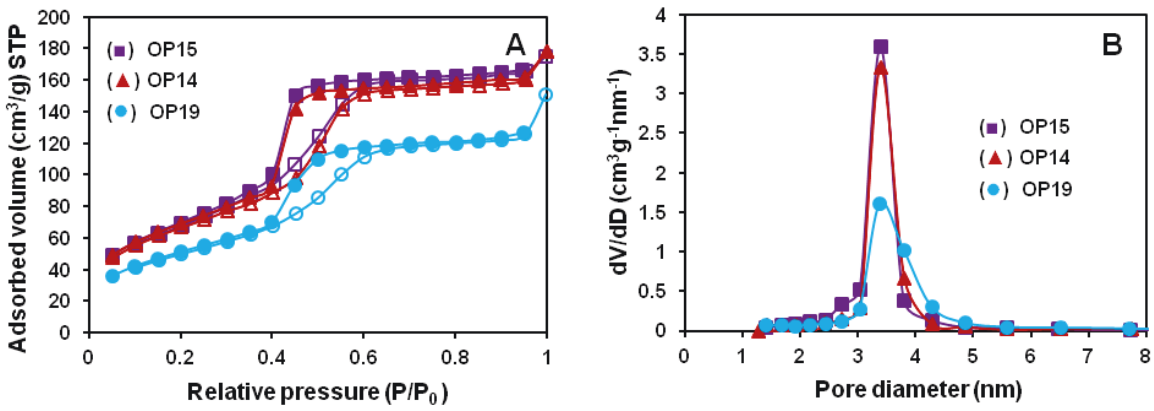

Figure 32. (A) Nitrogen adsorption-desorption isotherms and (B) BJH pore size distributions curves of the prepared one-pot $ZnCl_2$-modified OMA supports samples using malonic acid with different aluminum precursors: (OP15) $ZnCl_2$-OMA-Al(OPr^i)$_3$; (OP14) $ZnCl_2$-OMA-Al(OBu^t)$_3$ and (OP19) $ZnCl_2$-OMA-Al$(NO_3)_3 \cdot 9H_2O$. All samples were calcined at 400 °C.

In comparison with the materials synthesized *via* the conventional two-steps process [657], as depicted in Table 10, almost all the newly prepared $ZnCl_2$-modified OMA supports samples (one-pot) possess larger BET surface area. As we reported previously, we believe that the lower BET surface area obtained through the two-steps synthesis is primarily ascribed to the additional calcination step during the $ZnCl_2$ impregnation, as well as the filling of added $ZnCl_2$ inside the already formed mesopores [657].

These troublesome effects were advantageously avoided using the one-pot synthesis process were *in situ* impregnation of $ZnCl_2$ occurred with no need for subsequent annealing step that may alter the materials surface. Meanwhile, both synthesis procedures led to $ZnCl_2$-modified OMA supports with relatively similar total pore volume and pore size distributions (Table 10), suggesting that independently from the synthesis process, similar porosity features can be obtained using the same aluminum precursors and carboxylic acids having identical ligands and carbon chain length, respectively.

5.3.1.2. X-ray diffraction (XRD) analysis

The prepared one-pot $ZnCl_2$-modified OMA supports calcined at 400 °C were analyzed by powder X-ray diffraction to verify their mesoscopic order. Figure 33 shows the small-angle X-ray scattering (SAXS) patterns of the calcined $ZnCl_2$-modified OMA supports samples.

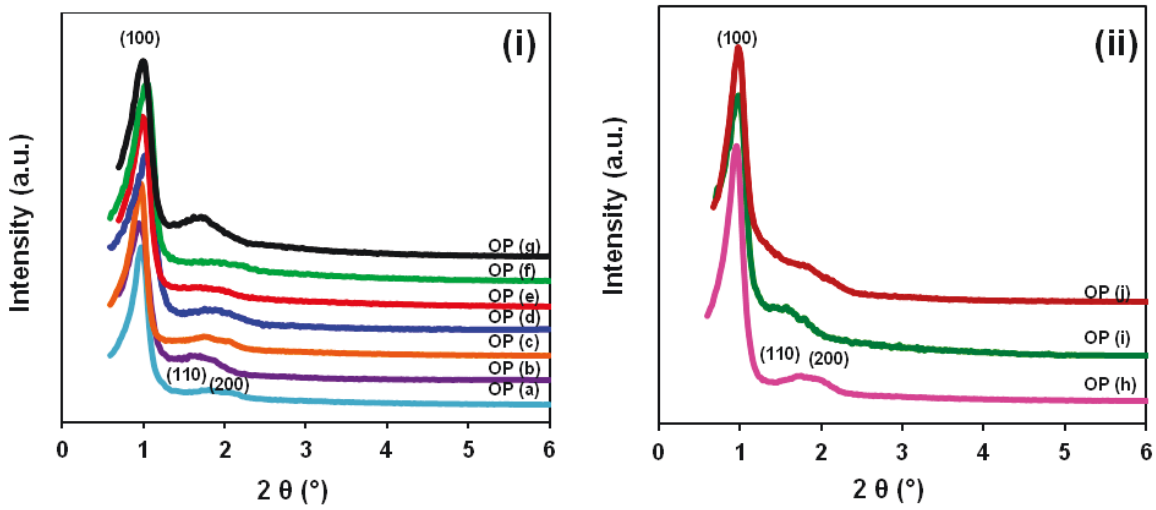

Figure 33. Small-angle X-ray scattering (SAXS) patterns of $ZnCl_2$-modified OMA supports prepared (i) using $Al(OBu^s)_3$ with different carboxylic acids: (a, OP1) $ZnCl_2$-OMA-citric; (b, OP2) $ZnCl_2$-OMA-tartaric; (c, OP5) $ZnCl_2$-OMA-maleic; (d, OP6) $ZnCl_2$-OMA-malonic; (e, OP3) $ZnCl_2$-OMA-fumaric; (f, OP4) $ZnCl_2$-OMA-oxalic and (e, OP7) $ZnCl_2$-OMA-acetic acid; and (ii) using malonic acid with different aluminum precursors: (h, OP15) $ZnCl_2$-OMA-$Al(OPr^i)_3$; (i, OP14) $ZnCl_2$-OMA-$Al(OBu^t)_3$ and (j, OP19) $ZnCl_2$-OMA-$Al(NO_3)_3 \cdot 9H_2O$. All samples were calcined at 400 °C.

The patterns exhibit a major sharp and well-resolved peak at a 2θ value of 1.0 ° indexed as the (100) Bragg reflection of the 2-D hexagonal *p6mm* structure (space group), with two minor peaks observed at 2θ = 1.8 and 2.1 ° those corresponding to the higher order (110) and (200) reflections, respectively [596, 598]. These results suggest the well-ordered mesoporous network of the analyzed $ZnCl_2$-modified OMA supports samples with hexagonal arrays without any lattice shrinkage. As illustrated from the BET results, similarly, the XRD analysis revealed no significant shift in the XRD patterns when using distinct carboxylic acids (Figure 33i) or different aluminum precursors (Figure 33ii). It is worth to note that the obtained XRD analysis results were similar to those obtained for the

$ZnCl_2$-modified OMA supports samples prepared using the conventional two-steps process where the 2-D hexagonal *p6mm* structure was also detected for the prepared samples [657].

5.3.1.3. Morphology and structure of $ZnCl_2$-modified OMA: TEM and SEM analysis

5.3.1.3.1. Transmission electron microscopy (TEM) analysis

After organic molecules (surfactant and carboxylic acid) removal at 400 °C, the samples were also analyzed by transmission electron microscopy (TEM). The observed images are represented in Figure 34 along the 001 and 110 directions for the obtained $ZnCl_2$-modified OMA supports.

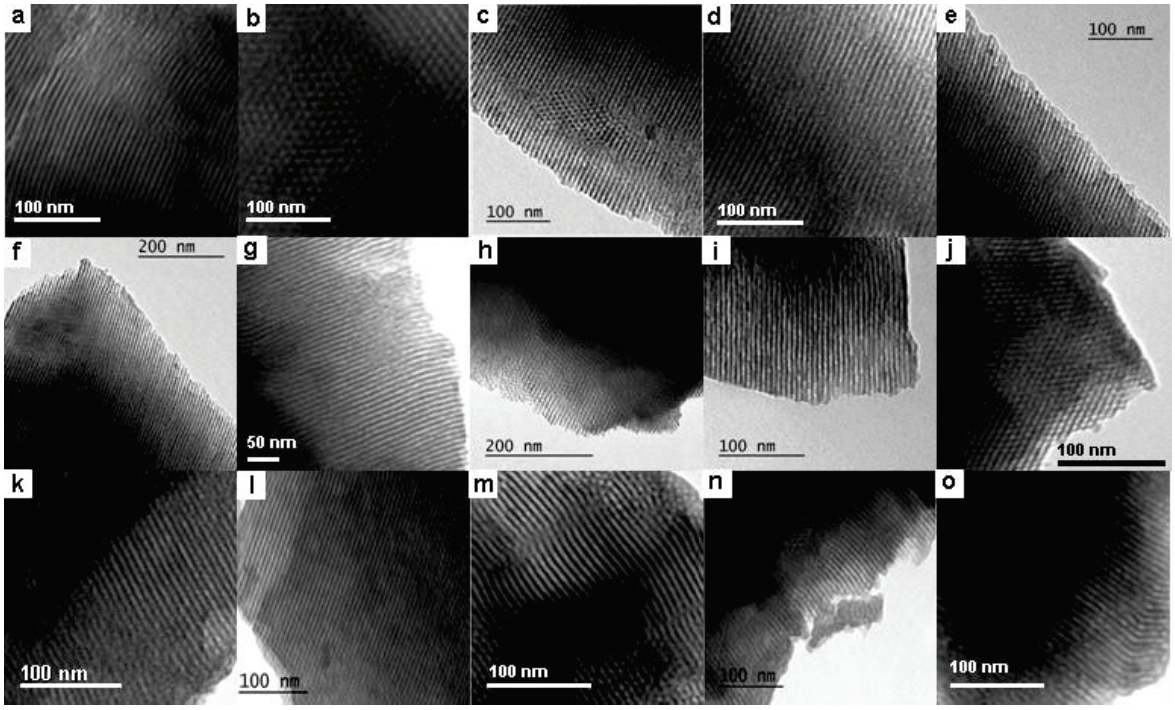

Figure 34. TEM images of the $ZnCl_2$-modified OMA supports synthesized using $Al(OBu^s)_3$ with different carboxylic acids: (a: OP1) citric, (c: OP2) tartaric, (d: OP6) malonic, (e, f: OP5) maleic, (g: OP3) fumaric and (i: OP4) oxalic acid, viewed along the [110] orientation, and (b: OP1) citric, (h: OP3) fumaric and (j: OP7) acetic acid, viewed along the [001] orientation. And using different aluminum precursors; $Al(OPr^i)_3$ for (k) fumaric and (n: OP11) tartaric acid; $Al(NO_3)_3 \cdot 9H_2O$ for (l: OP12) citric and $Al(OBu^t)_3$ for (m: OP8) citric and (o: OP9) tartaric acid, viewed along the [110] orientation. All samples were calcined at 400 °C.

In a good agreement with the results illustrated from the SAXS and N_2 adsorption-desorption analyses (Figures 31-33), the TEM micrographs (Figure 34) confirm the presence of hexagonal ordering in the prepared one-pot mesoporous $ZnCl_2$-modified OMA supports. Furthermore, as evidenced by SAXS and N_2 adsorption-desorption measurements, highly ordered 2-D hexagonal mesostructure was successfully obtained upon the use of different aluminum precursors and diverse carboxylic acids as depicted in Figure 34. The extremely well-ordered hexagonal arrangement of tubular mesopores along the [001] direction, and the alignment of uniform and non-interconnected cylindrical mesopores along the [110] direction are observed in all analyzed $ZnCl_2$-modified OMA supports samples. In addition, the diameter of the cylindrical mesopores as observed from the TEM micrographs was around 5 nm, which is in agreement with the obtained N_2 adsorption-desorption data. The observed organized structure of the materials prepared through one-pot process was similar to that observed for the $ZnCl_2$-modified OMA supports samples prepared using the conventional two-steps process [657]. The TEM data confirm again that the presence of $ZnCl_2$ during the mesophase formation does not alter the organized assembly of the alumina during the templating and the calcination process, and preserves the organized alumina framework.

5.3.1.3.2. Scanning electron microscopy (SEM) observations

To probe into the morphological features of the synthesized $ZnCl_2$-modified OMA supports, the prepared samples were examined by SEM. Figures 35a-d show plane-view SEM images of the $ZnCl_2$-modified OMA supports samples. The mesoporous $ZnCl_2$-modified OMA supports' microparticles exhibit a non-uniform three-dimensional (3D) architecture ranging from cuboid-like to plate-like shaped morphologies resulting from irregular crystal growth *via* assembly-aggregation of several nanocrystals. Thus, the observed microparticles have a non-uniform particle size distribution varying from 20 to 50 μm with gaps between crystals (Figures 35a-d). However, a relatively smooth particle surface is obtained, suggesting the excellent incorporation of $ZnCl_2$. The $ZnCl_2$-modified OMA supports prepared using the conventional two-steps process was previously found to have smaller microparticles with less regular shape and morphology, which was ascribed to the mechano-chemical dislocation effect occurred during the $ZnCl_2$ impregnation step [657].

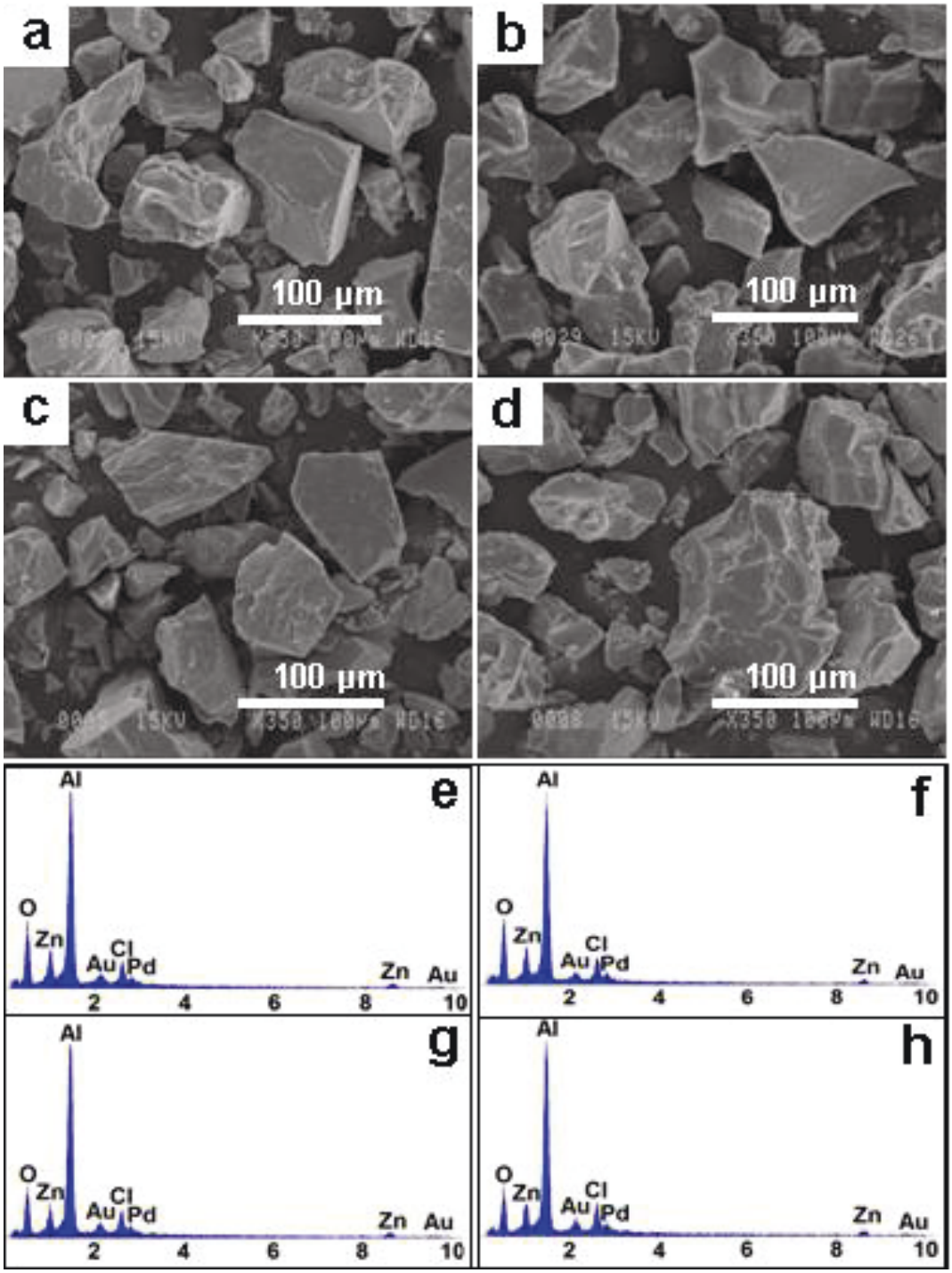

Figure 35. Representative SEM images (a-d) and energy dispersive X-ray (EDX) spectra (e-h) obtained for one-pot $ZnCl_2$-modified OMA supports' microparticles prepared using different aluminum precursors and carboxylic acids: (a, e: OP4) $Al(OBu^s)_3$-oxalic acid; (b, f: OP11) $Al(OPr^i)_3$-tartaric acid; (c, g) $Al(OBu^t)_3$-fumaric acid and (d, h: OP12) $Al(NO_3)_3 \cdot 9H_2O$-citric acid. All samples were calcined at 400 °C.

Unlike the two-steps conventional approach, the newly designed one-pot process led to efficient and homogeneous incorporation of $ZnCl_2$ particles in the OMA matrix. However, we believe that the presence of $ZnCl_2$ in the surfactant micelle before thermal treatment is among the reasons that led to relatively larger particles (compared to two-steps process) where $ZnCl_2$ is entirely embedded in OMA phase. Furthermore, as shown from previous analysis data (XRD, BET and TEM), the use of various carboxylic acids and aluminum precursors did not result in any significant morphology changes (Figures 35a-d).

5.3.1.4. Elemental analysis: energy-dispersive X-ray spectroscopy (EDX)

As depicted in Figures 35e-h displaying the EDX spectra obtained for the prepared one-pot $ZnCl_2$-modified OMA supports samples, O and Al sharp signals were detected along with Zn and Cl signals which belong to Al_2O_3 and $ZnCl_2$ species, respectively. These elements were detected for all the analyzed samples synthesized using various carboxylic acids and aluminum precursors. These results show again the efficiency of the *in situ* incorporation of $ZnCl_2$ into OMA. Additionally, Au, Pd and C signals were detected (Figures 35e-h), which are due to residuals of the Au/Pd and C films used for the specimens preparation for analysis.

5.3.1.5. X-ray photoelectron spectroscopy (XPS) measurements

To precisely determine the elemental composition of the $ZnCl_2$-modified OMA supports as well as the electronic state and environment of the detected elements (Al, O, Zn and Cl) and the bonding configurations of the related species, X-ray photoelectron spectroscopy (XPS) measurements were conducted. The XPS spectra obtained are displayed in Figure 36. The survey spectrum (Figure 36a) possesses four main peaks centered at around 75 eV, 200 eV, 530 eV and 1020 eV, which are assigned to Al, Cl, O and Zn species, respectively. These elements are attributed to $ZnCl_2$ and Al_2O_3 phases. Similar compositions were found in the analyzed samples prepared using different carboxylic acids and aluminum precursors (see Figure 39 in the supporting information), without any significant effect of these experimental conditions. Moreover, in all analyzed samples, the calculated Cl : Zn ratios from the survey spectra obtained were always found to be lower than the nominal 2 : 1 atomic ratio for the incorporated $ZnCl_2$, where higher Zn amounts were detected compared to Cl (Cl/Zn ~ 0.61-0.68). These results suggest that in addition to $ZnCl_2$ and Zn-Cl species,

the samples contain further Zn-containing species like bridging Al-O-Zn-O-Al or $Zn(OH)_2$ species. However, thermal decomposition of $ZnCl_2$ may partially occur at higher annealing temperatures [657]. The decovolution of each element spectrum is then necessary to investigate the exact species formed in the surface and the framework of the prepared one-pot $ZnCl_2$-modified OMA supports.

The Al 2*p* spectrum displayed in Figure 36b revealed the presence of one component, the peak at 74.4 eV corresponds to Al present in the Al_2O_3 phase [680, 717]. Subsequently, the O 1*s* spectrum (Figure 36c) can be deconvoluted into two components. Two peaks with similar intensities are observed at 531.2 eV and 532.5 eV, which are attributed to bulk oxygen present in the Al_2O_3 lattice (Al-O-Al) and higher concentration hydroxyl groups (Al-O-H) present in the Al_2O_3 materials surface, respectively [680, 718-720]. The absence of a third peak at higher Binding Energy (BE) indicates that no molecular H_2O is physisorbed at this temperature [720]. These binding energy values are slightly higher compared to those reported for the pure alumina materials [657]. This could be due to the presence of $ZnCl_2$ and its interactions with the species present in the alumina phase, which leads to a slight change in the electronic environment of these elements. The hydroxyl group peak at 532.5 eV may also correspond to the $Zn(OH)_2$ species that results from $ZnCl_2$ interaction with alumina surface [721]. However, the O 1s XPS data obtained previously for the two-steps prepared $ZnCl_2$-modified OMA supports showed a lower intensity (amount) of Al-O-H peak compared to that of Al-O-Al [657]. On the other hand herein the two peak intensities are quite equal. This could be due to elimination on the second calcination step which helps avoiding further dehydroxylation of alumina surface. The zinc species bonding configurations were also investigated. The Zn $2p_{3/2}$ spectrum (Figure 36d) shows one component with a sharp peak at 1022.1 eV, which could be assigned to distinct Zn^{2+} species including Zn-O, $ZnCl_2$ or $Zn(OH)_2$ [657, 685, 722]. We then studied the Cl^- spectrum (Figure 36e). The spectrum can be deconvoluted into two components; a well-defined peak at 198.9 eV and a smaller peak at 200.5 eV correspond to Zn-Cl $2p_{3/2}$ and Zn-Cl $2p_{1/2}$ species, respectively [657, 684, 722]. In addition to the possible Zn-containing species like bridging Al-O-Zn-O-Al or $Zn(OH)_2$ species, the Zn-Cl species are likely bonded to the alumina surface through interactions with surface hydroxyl groups.

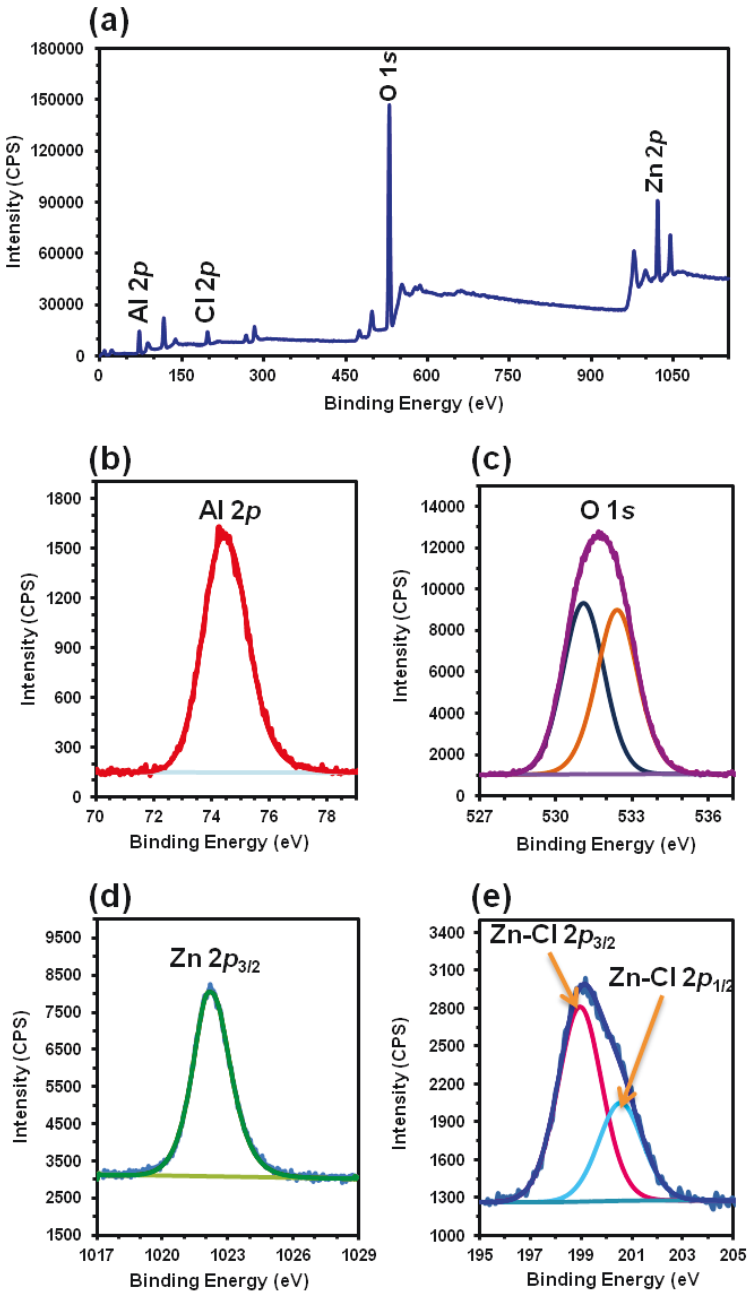

Figure 36. XPS analysis of $ZnCl_2$-modified OMA (OP6) supports sample synthesized using malonic acid with $Al(OBu^s)_3$ aluminum precursor: (a) survey spectrum and (b) Al 2*p*, (c) O 1*s*, (d) Zn $2p_{3/2}$ and (e) Cl $2p_{3/2}$-Cl $2p_{1/2}$ deconvoluted spectra. All shifts for the samples were corrected by normalization of the C 1*s* binding energy to 285.0 eV.

Logically, with the presence of Zn precursors in the reaction mixture before the formation of the alumina phase we suspected the formation of other phases besides the one formed

with alumina only. Zinc aluminate ($ZnAl_2O_4$) and zinc oxide (ZnO) are the most likely phases to be obtained under such conditions. Fortunately, the XPS measurements are clear evidence that no $ZnAl_2O_4$ phase was formed along with the $ZnCl_2$-modified OMA supports phase. If $ZnAl_2O_4$ phase was present, the XPS analysis would show a single O 1*s* component associated with a peak at 531.4 eV, while Zn 2 $p_{3/2}$ and Zn 2 $p_{1/2}$ peaks would appear at 1044.9 eV and 1021.5-1021.9 eV, respectively [682, 723].

Similarly, no evidence of formation of zinc oxide phase (ZnO) was found, which is characterized by Zn 2 $p_{3/2}$ and Zn 2 $p_{1/2}$ peaks at 1021.5 eV and 1044.6 eV [682]. It is worth to mention that even if $ZnCl_2$ thermal decomposition is possible, the resulted Zn is likely converted into the species cited above, while no trace of elemental Zn were found in the analyzed samples which can result in two Zn 2 $p_{3/2}$ and Zn 2 $p_{1/2}$ peaks at lower BE values of 1021.4 eV and 1044.5 eV, respectively [682].

5.3.1.6. Solid-state NMR spectroscopy analysis

5.3.1.6.1. ^1H MAS NMR

After performing several characterizations that evidenced the formation of hexagonally organized mesoporous alumina materials doped with $ZnCl_2$ species, further characterization must be conducted to investigate the nature of interactions and intimate contact occurring on the alumina- $ZnCl_2$ interface. Therefore, we performed ^1H MAS NMR experiments to evaluate the $ZnCl_2$ bonding with alumina surface. Figure 37 shows the ^1H MAS NMR spectra of several $ZnCl_2$-modified OMA supports samples in which three broad resonance peaks were displayed. The first peak at 1.8 ppm is attributed to the protons of the basic terminal hydroxyl groups present on the $ZnCl_2$-modified OMA supports surface [687]. The second peak at 3.9 ppm is assigned to the protons of the acidic bridging hydroxyl groups also present on the $ZnCl_2$-modified OMA supports surface [687]. Both basic and acidic groups present moderate strength [638, 687]. However, unlike the XPS measurement which showed no evidence of the presence of physisorbed water on the $ZnCl_2$-modified OMA supports surface (O 1*s* spectrum, Figure 36c), the ^1H MAS NMR analysis revealed the presence of moisture trace on the analyzed samples. Therefore, the third peak at 4.2 ppm corresponds to the hydrogen-bonded water which is physisorbed on the $ZnCl_2$-modified OMA supports surface [687, 688]. The use of various aluminum precursors and diverse

carboxylic acids for the synthesis of the $ZnCl_2$-modified OMA supports led to no significant effect on the surface composition as confirmed by ^1H MAS NMR analysis (Figure 37, see also Figures 40-42 in the supporting information).

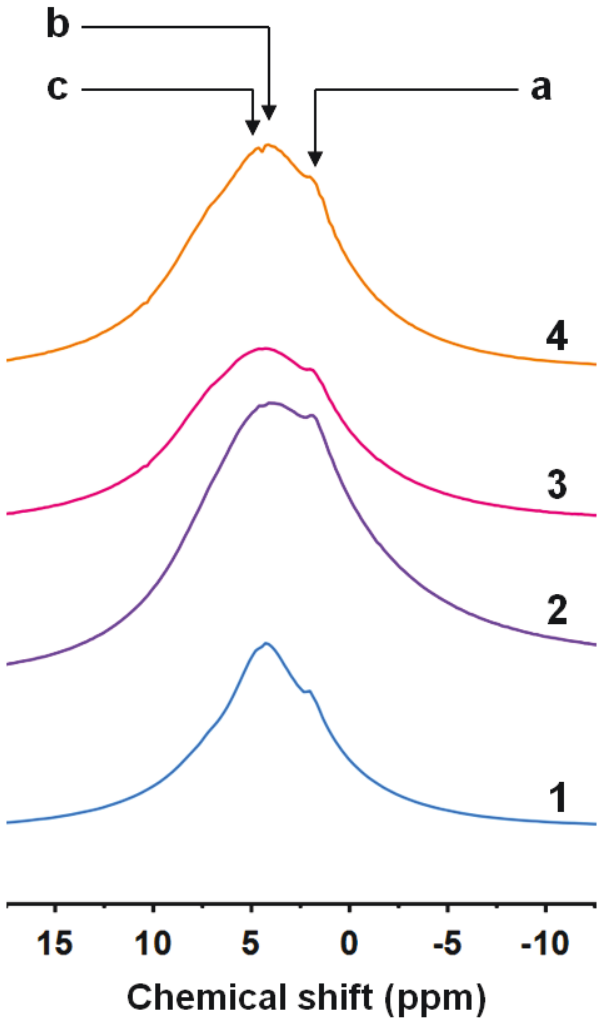

Figure 37. ^1H MAS NMR spectra of $ZnCl_2$-modified OMA supports samples prepared using citric acid with different aluminum precursors: (1: OP8) $Al(OBu^t)_3$, (2: OP1) $Al(OBu^s)_3$, (3: OP12) $Al(NO_3)_3 \bullet 9H_2O$ and (4: OP10) $Al(OPr^i)_3$. Indicating (a) basic terminal hydroxyl groups, (b) acidic bridging hydroxyl groups, and (c) hydrogen bonded water physisorbed on alumina surface. All samples were calcined at 400 °C.

Furthermore, unlike the two-steps impregnation of $ZnCl_2$ that we have recently reported demonstrating a selective interaction of $ZnCl_2$ with basic terminal hydroxyl groups leading

to the formation of various Al-O-Zn-Cl species [657], the *in situ* incorporation of $ZnCl_2$ did not lead to total neutralization of the basic terminal hydroxyl groups (1.8 ppm). These results do not exclude the usual preferential interaction of the $ZnCl_2$ with basic terminal hydroxyl groups, which may lead to a loss in Brønsted acidity [430-432, 634, 657, 688]. However, this may suggest that the elimination of a second calcination step at 400 °C may enhance the concentration of the surface hydroxyl groups, as a result of avoiding further dehydroxylation of alumina surface under such high thermal treatment conditions. On the other hand, the elimination of this second calcination step may be the reason behind the detection of the physisorbed water trace in almost all analyzed samples (Figure 37, see also Figure 40-42).

Ultimately, combination of XPS and ^{1}H MAS NMR data suggests that various Al-O-Zn-Cl/Al-O-Zn-O-Al surface species can be formed through interaction of $ZnCl_2$/Zn-Cl/Zn components with either basic terminal hydroxyl groups, acidic bridging hydroxyl groups or both.

5.3.1.6.2. ^{27}Al MAS NMR

^{27}Al MAS NMR analysis was conducted to investigate the Al environment and the changes related to the *in situ* $ZnCl_2$ incorporation. Figure 38 shows the various coordination detected for Al species in the analyzed as-prepared (uncalcined) and calcined $ZnCl_2$-modified OMA supports samples. A single sharp resonance peak was observed at around 0 ppm for the as-prepared sample (Figure 38a). This suggests that the uncalcined sample mainly contains octahedral Al^{3+} species. This peak can be associated with the presence of the AlOOH boehmite intermediate phase [689, 690], which will be then converted to alumina phase after annealing. Afterwards, the calcined $ZnCl_2$-modified OMA supports samples were analyzed. The ^{27}Al MAS NMR spectra displayed in Figures 38b-e show a change of Al species coordination. We then observed the rise of one sharp and two broad resonance peaks (Figure 38b-e). The major well-defined resonance peak centered at 3 ppm is attributed to the octahedral Al^{3+} species in the alumina phase (AlO_6) [601, 690]. Subsequently, the two broad minor resonance peaks centred at 32 and 63 ppm (Figures 38b-e) correspond to the penta- and tetrahedral Al^{3+} species in the alumina phase (AlO_5, AlO_4), respectively [690]. As reported recently in our work, this conversion of the

octahedral Al^{3+} species upon calcination to pentahedral and tetrahedral Al^{3+} species is attributed to the partial substitution of oxygen ions by hydroxyl groups in octahedral Al centers during the calcination process [657, 691, 692]. All ^{27}Al MAS NMR spectra for the samples prepared using different carboxylic acids and diverse aluminum precursors show approximately the same profile regardless of the experimental conditions (Figure 38, see also Figures 43-45 in the supporting information).

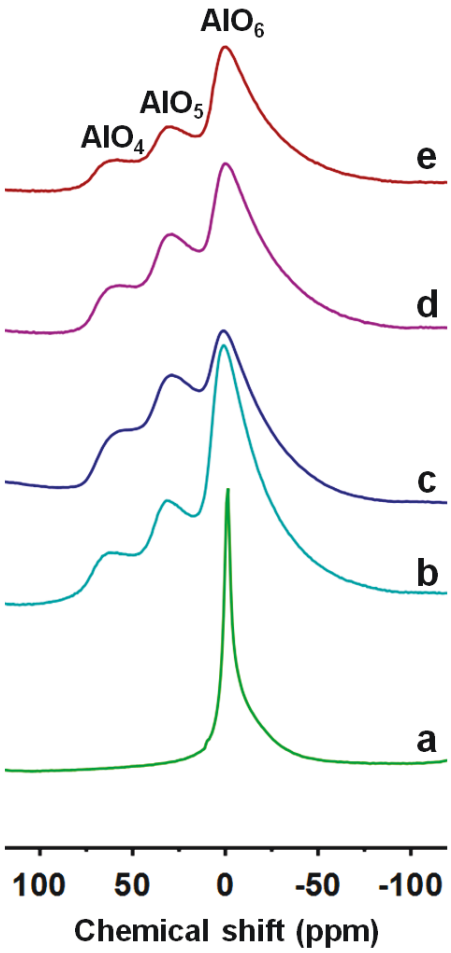

Figure 38. ^{27}Al MAS NMR spectra of (a) as-prepared $ZnCl_2$-modified OMA supports sample synthesized using citric acid and $Al(OBu^s)_3$. And calcined $ZnCl_2$-modified OMA supports samples prepared using citric acid with different aluminum precursors: (b: OP1) $Al(OBu^s)_3$, (c: OP8) $Al(OBu^t)_3$, (d: OP10) $Al(OPr^i)_3$ and (e: OP12) $Al(NO_3)_3 \cdot 9H_2O$. Samples (b) to (e) were calcined at 400 °C.

It is worth to mention that unlike alumina phase, the ^{27}Al MAS NMR spectra of the $ZnAl_2O_4$ spinel obtained under similar thermal conditions (300-500 °C) exhibits a single peak around 0 ppm which is characteristic of Al^{3+} ions occupying AlO_6 sites [724].

In comparison, the $ZnCl_2$-modified OMA supports samples prepared using the two step process resulted in AlO_5 and AlO_6 resonance peaks with relatively similar intensities [657]. Herein, we observe that the AlO_5 resonance peaks have lower intensities compared to those of the AlO_6 resonance peaks (Figure 8, see also Figures 43-45), indicating the lower number of AlO_5 sites.

This suggests that the in the one-pot prepared $ZnCl_2$-modified OMA supports the $ZnCl_2$ was preferably doped on these sites. This suggestion is in a good agreement with the earlier speculation about the distribution of the Al^{3+} species in the alumina matrix; where it has been proposed that AlO_6 sites are found in the bulk of the alumina inorganic framework walls, while the AlO_4 and AlO_5 sites are likely on the surface [601]. A similar phenomenon was recently observed for the Cu-Al_2O_3 system [693].

5.3.2. One-pot formation of the $ZnCl_2$-modified OMA

In our previous work we showed that the organized self-assembly of the alumina mesophase in governed by the complexation effect of the interfacial protectors (carboxylic acids) [657]. Subsequently, and based on the characterizations data, particularly XPS and MAS NMR, herein we propose a similar mechanism for the formation of well-dispersed zinc species within the OMA channels *via* a one-pot process. The HCl is required to adjust the solution pH; however the strong interaction of Cl^- with Al sites can lead the organized assembly to collapse during the sol-gel process. Thus, carboxylic acids play a major role to prevent this phenomenon by interaction of their carboxylate fragments with the Al centers during the self-assembly process though monodentate or bridging bidentate modes. Meanwhile, the added zinc precursor migrates inside the Pluronic F127 surfactant micelles during the evaporation-induced self-assembly process [725, 726]. Therefore, the removal of the organic molecules *via* calcination at high temperatures leads to simultaneous mesoporous channels formation and grafting of zinc species

on formed alumina surface hydroxyl groups, while maintaining the well-ordered internal mesopore architecture. This tentative formation process is illustrated in Scheme 12.

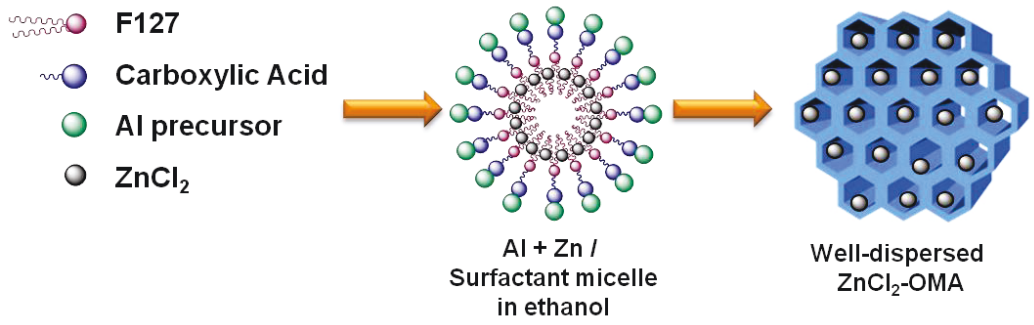

Scheme 12. Schematic representation of the one-pot evaporation induced self-assembly process for the formation of $ZnCl_2$ embedded in well-organized mesoporous alumina (OMA) materials

5.3.3. Catalytic performance of the $ZnCl_2$-modified OMA-based catalysts

The newly synthesized 3 wt.% MTO/$ZnCl_2$-OMA catalysts were evaluated for their metathesis reaction activity. The self-metathesis reaction was carried out as a model reaction, one of the representative Re-catalyzed reactions (Scheme 13).

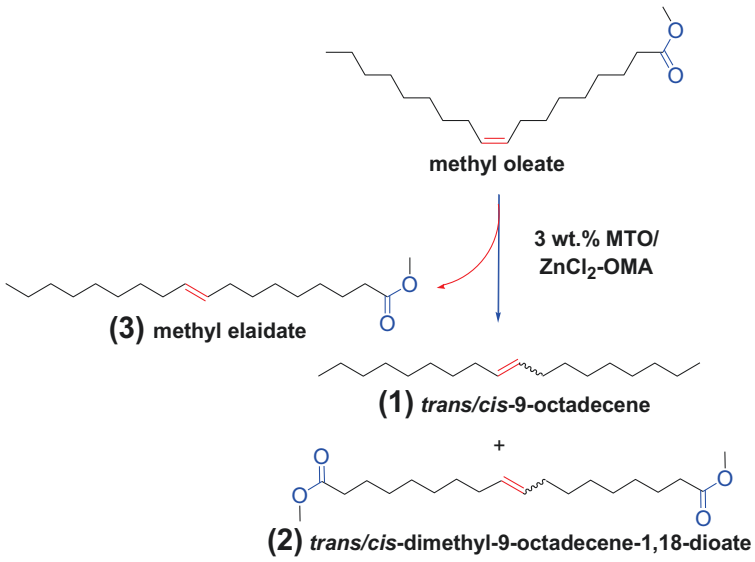

Scheme 13. Methyl oleate self-metathesis observed products

Also, we have chosen methyl oleate as the model substrate to verify both the catalyst tolerance for bulky functionalized molecules (functional groups) as well as the mesoporous network for bulky functionalized molecules diffusion abilities (Scheme 13).

The experiments were carried out under similar conditions of temperature (45 °C) and pressure (atmospheric pressure) during 90 min of reaction time, to those we previously optimized for the same class of catalyst and reaction [430, 431, 657].

In order to highlight the advantage of the newly prepared $ZnCl_2$-modified OMA supports as catalytic supports for MTO, an extended comparison with other alumina-based catalytic support we previously synthesized and used for the design of the MTO-based catalyst is presented (Table 11).

Several one-pot prepared supports were used and numerous experiments were performed for each supports in order to investigate their performance and verify the reproducibility of the process. The data reported in Table 11 (Entry 1, 3, 5 and 7) are average values for several metathesis reaction experiments conducted for similar catalysts supported over $ZnCl_2$-modified OMA supports prepared with the same aluminum precursors and carboxylic acids.

The other alumina supports used for comparison include the $ZnCl_2$-modified (Table 11, Entry 8) and unmodified (Table 11, Entry 9) conventional wormhole-like alumina those we have reported earlier [430-432]; as well as the well-ordered hexagonal $ZnCl_2$-modified OMA supports prepared *via* two steps process those we have also recently reported (Table 11, Entry 2, 4 and 6) [657]. Also the newly one-pot prepared $ZnCl_2$-modified OMA-based heterogeneous metathesis catalyst performance (Table 11, Entry 1, 3, 5 and 7) has been compared to that of the homogeneous commercially available and widely used 2nd generation Grubbs catalyst (Table 11, Entry 10).

Table 11: Catalytic performance for methyl oleate self-metathesis over heterogeneous 3 wt.% MTO/$ZnCl_2$-OMA catalysts supported on organized mesoporous alumina ($ZnCl_2$-modified OMA) prepared *via* two-steps or one-pot process. And comparison with metathesis reaction performance of 3 wt.% / *meso*-Al_2O_3 and homogeneous 2nd generation Grubbs catalyst.

Entry	Catalyst[a]	Conv (%)[b]	Metathesis reaction products (%)[c]					DMP (%)[d]	*S*[e]	Ref.
			(1) *trans*	(1) *cis*	(2) *trans*	(2) *cis*	(3)			
1	3 wt.% MTO/$ZnCl_2$-OMA-1 (op: OP1): $Al(OBu^s)_3$ + Citric	80,2	13,7	12,7	14,9	6,9	32,0	48,2	1.51	This work
2	3 wt.% MTO/$ZnCl_2$-OMA-1 (ts): $Al(OBu^s)_3$ + citric	78.2	15.5	14.3	9.1	4.3	35.0	43.2	1.23	Abidli *et al.* [657]
3	3 wt.% MTO/$ZnCl_2$-OMA-2 (op: OP2): $Al(OBu^s)_3$ + Tartaric	93,6	48,8	17,1	5,4	2,4	19,9	73,7	3.70	This work
4	3 wt.% MTO/$ZnCl_2$-OMA-2 (ts): $Al(OBu^s)_3$ + tartaric	88.2	29.3	8.5	12.9	4.6	32.9	55.3	1.68	Abidli *et al.* [657]
5	3 wt.% MTO/$ZnCl_2$-OMA-11 (op: OP11): $Al(OPr^i)_3$ + Tartaric	86,7	34,8	9,4	9,1	2,5	30,9	55,8	1.81	This work
6	3 wt.% MTO/$ZnCl_2$-OMA-11 (ts): $Al(OPr^i)_3$ + tartaric	87.4	31.8	8.9	14.1	2.4	30.2	57.2	1.89	Abidli *et al.* [657]
7	3 wt.% MTO/$ZnCl_2$-OMA-9 (op: OP9): $Al(OBu^t)_3$ + Tartaric	79,8	14,1	13,2	13,6	6,4	32,5	47,3	1.46	This work
8	3 wt.% MTO/$ZnCl_2$-*meso*-Al_2O_3 (ts): ($Al(OBu^s)_3$)	86.7	24.4	8.3	16.2	3.6	34.3	52.4	1.53	Pillai *et al.* [430-432]
9	3 wt.% MTO/*meso*-Al_2O_3: ($Al(OBu^s)_3$)	2.4	0.2	0.3	0.2	0.3	1.4	1.0	0.71	Pillai *et al.* [430-432]
10	2nd generation Grubbs catalyst	89.6	20,1	3,9	21,0	4,2	40,4	49,2	1.22	Pillai *et al.* [430-432]

[a] *meso*-Al_2O_3 represents the wormhole-like mesoporous alumina.
[b] Conv.: conversion.
[c] The numbers appearing for the metathesis reaction products 1, 2, and 3 (Scheme 13) are expressed in terms of individual product yield ($yield_i$).
[d] DMP: desired metathesis reaction products.
[e] *S:* the selectivity.
op: $ZnCl_2$-modified OMA supports prepared through one-pot process. ts: $ZnCl_2$-modified OMA supports prepared through two-steps process.

Briefly, the addition of $ZnCl_2$ to alumina supports was found to offer a great catalytic promoting effect for the metathesis reaction [430-432]. The unmodified wormhole-like alumina supports showed the weakest metathesis reaction performance among all tested

catalysts, while their promoted counterparts showed much more enhanced catalytic performance (Table 11, Entry 8) [430-432]. Recently, $ZnCl_2$-modified OMA supports were shown to be the most suitable support of MTO-based catalysts showing relatively better methyl oleate conversions [657]. In all cases methyl oleate self-metathesis leads to the formation of both desired metathesis reaction products including 9-octadecene and dimethyl-9-octadecene-1,18-dioate (Scheme 13) as well as undesired product (methyl elaidate, Scheme 13). However, using the ordered alumina supports, improved selectivity was reached towards the desired metathesis reaction products (Table 11, Entry 2, 4 and 6). More interestingly, it was demonstrated that the new catalyst design based on organized mesoporous network has an enormous effect on improving the reaction rate for the conversion of such bulky functionalized molecule (methyl oleate) [657]. This enhancement is attributed to the absence of diffusion limitations of substrates and metathesis reaction products within the ordered cylindrical mesopores of these supports compared to the disordered and interconnected pores of the wormhole-like alumina supports where molecular diffusion limitations and blocking effects may occur. All these features were also provided using similar one-pot synthesized $ZnCl_2$-modified OMA supports, which offered also better activity than the MTO-based catalysts supported over $ZnCl_2$-modified and unmodified wormhole-like alumina (Table 11).

The catalytic performance of the successfully prepared $ZnCl_2$-modified OMA supports *via* a one-pot synthesis process studied in this work was also compared to the performance of the $ZnCl_2$-modified OMA-based catalysts previously prepared through two steps process. Interestingly the one-pot prepared $ZnCl_2$-modified OMA supports were found to be the best catalytic supports for MTO. Metathesis reaction data displayed in Table 11 (Entry 1, 3, 5 and 7) show higher catalytic performance including methyl oleate conversion (up to 93.6%), desired metathesis reaction products yield (up to 73.7 %) and selectivity (up to 3.7), using these catalytic supports. For the structure-activity correlation, we believe that this enhanced performance may arise from various factors. Firstly, the newly one pot-prepared $ZnCl_2$-modified OMA supports exhibit larger BET surface area (Table 10) compared to the two steps-prepared $ZnCl_2$-modified OMA supports. The lower BET surface area of the later is due to the subsequent calcination step and pore filling with $ZnCl_2$ upon modification, which alter their textural properties. The BET specific surface area was

dramatically dropped upon incorporation of $ZnCl_2$ [657]. On the other hand, during the one pot synthesis of $ZnCl_2$-modified OMA supports this additional annealing step was avoided with *in situ* impregnation of $ZnCl_2$. This is in a good agreement with several studies showing that supported catalysts' activity is often proportional to the specific surface area of these catalysts [643, 727-733]. Furthermore, higher BET surface area favors better dispersion of supported MTO species, which improves the concentration and availability of metathesis active species and intermediates allowing more efficient use of exposed supported MTO molecules. Secondly, unlike the two steps synthesis process, avoiding a second calcination step during the one-pot preparation process reduces the dehydroxylation of the alumina surface as illustrated above in XPS and MAS NMR sections. Along with this, we showed that $ZnCl_2$ is incorporated on the alumina *via* interactions with surface hydroxyl groups. As a result, inhibited dehydroxylation may allow better incorporation of Zn active intermediates which are crucial for the MTO metathesis catalytic action, displaying a key synergetic effect. Finally, we believe that the single-step approach allow simultaneous zinc species deposition and mesopores walls formation, releasing more homogeneous and well-dispersed zinc species on the OMA surface. Moreover, this simultaneous process may result in a confinement effect of ordered mesochannels of OMA inhibiting Zn species aggregation and growth. This agglomeration phenomenon may likely occur during the two steps synthesis which restricts Zn species interactions with alumina surface and limits their availability for the catalytic process. It is also worth to mention that the separate wet impregnation method during the two-steps synthesis was found to alter the textural and morphological properties of the OMA (mechano-chemical effect), along with formation of $ZnCl_2$ aggregates, as revealed by SEM images [657].

The results are very exciting showing higher performance, even better than those obtained with the traditional highly active 2nd generation Grubbs catalyst (Table 11, Entry 10), with slightly better methyl oleate conversion (93.6% *vs*. 89.6%), but exhibiting much more selectivity towards desired metathesis reaction products (73.7% *vs*. 49.2%). It is worth to mention that we previously showed that the OMA-supported MTO-based catalysts was found to exhibit fast kinetics [657], comparable to that observed over the Grubbs catalyst [431], with the possibility of recycling and reuse for further metathesis reaction runs.

In addition to the enhanced catalytic activity of the MTO-based catalysts using the newly prepared $ZnCl_2$-modified OMA supports, this one-pot synthesis process presents further advantages. Economically, compared to the two-steps process, this process allowed a reduced use of solvents. Also, it reduces energy consumption through elimination of additional evaporation and calcination steps, while reducing enormously the preparation time. More interestingly, using the one-pot process, higher synthesis yields were reached, obtaining almost 75% higher amounts of $ZnCl_2$-modified OMA supports in weight, than those obtained using the two-steps process. This was mainly attributed to limitation of weight loss during the two subsequent calcination processes.

5.4. Conclusions

A novel straightforward one-pot sol-gel synthesis approach for zinc-doped well-organized mesoporous alumina preparation was developed. *In situ* $ZnCl_2$ incorporation was successfully achieved along with the formation of ordered alumina mesoporous network. Based on XPS data, $ZnCl_2$ was impregnated *via* interaction with surface hydroxyl groups. Furthermore, the XPS measurements confirmed that Al-O-Zn-Cl were the major surface species formed upon $ZnCl_2$ interaction with surface hydroxyl groups. Moreover, in order to establish an efficient low-cost production process, this rapid and sustainable methodology was found to be suitable even when using inexpensive aluminum precursors such as aluminum nitrate nonahydrate. The use of various aluminum precursors and carboxylic acid did not result in any significant difference between the prepared materials due to the similar self-assembly pathway during the sol-gel synthesis. Furthermore, the materials prepared *via* the one-pot route exhibited higher BET surface area compared to the conventionally two steps synthesized materials. Outstanding arrangement of the mesopores was observed by TEM micrographs. Not surprisingly, these materials with such enhanced features exhibited better catalytic performance for methyl oleate self-metathesis when used as support for the MTO-based catalysts. Avoiding the second calcination step, which is usually performed during the conventional synthesis, led to a limited dehydroxylation phenomena. Thus, materials with enhanced hydroxyl group concentration and availability on the alumina surface were obtained, which was a key factor for an effective incorporation of $ZnCl_2$ and MTO species. Therefore, a better catalytic performance was reached. This might promise

further catalytic applications of these well ordered supports. On the other hand, rather than modified-alumina, the successful one-pot strategy could be extended and stimulate further attempts to prepare other functional materials that are conventionally prepared through laborious multistep processes, especially, doped or modified functionalized mesoporous materials that are widely used in catalysis. This successful methodology is a step forward towards an easy and efficient scalability.

Acknowledgements

Financial support from the Natural Sciences and Engineering Research Council of Canada (NSERC) and Canadian Foundation for Innovation (CFI) is greatly appreciated. A. Abidli would like to thank Prof. Khaled Belkacemi for the N_2 adsorption-desorption analysis and for providing his laboratory facility at Laval University where the materials/catalysts synthesis and the metathesis reaction experiments were conducted. A. Abidli acknowledges Alain Adnot, Pierre Audet, Prof. Safia Hamoudi, Ronan Corcuff, André Ferland and Richard Janvier for the XPS, MAS NMR, XRD, GC-MS, SEM and TEM analyses, respectively. A great appreciation is dedicated to Dr K. T. Venkateswara Rao for his valuable suggestions and advices.

Supporting information

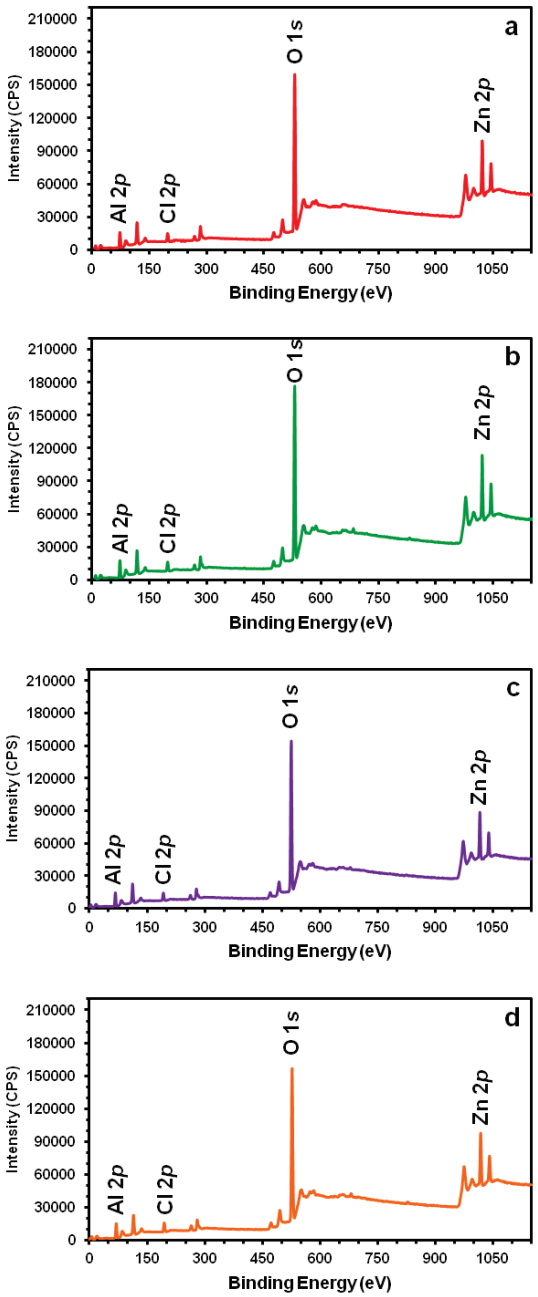

Figure 39. XPS survey spectra of the $ZnCl_2$-modified OMA supports samples synthesized using diverse carboxylic acids and aluminum precursors: (a: OP4) $Al(OBu^s)_3$-oxalic acid; (b: OP11) $Al(OPr^i)_3$-tartaric acid; (c) $Al(OBu^t)_3$-fumaric acid and (d: OP12) $Al(NO_3)_3 \bullet 9H_2O$-citric acid. All samples were calcined at 400 °C. All shifts for the samples were corrected by normalization of the C 1*s* binding energy to 285.0 eV.

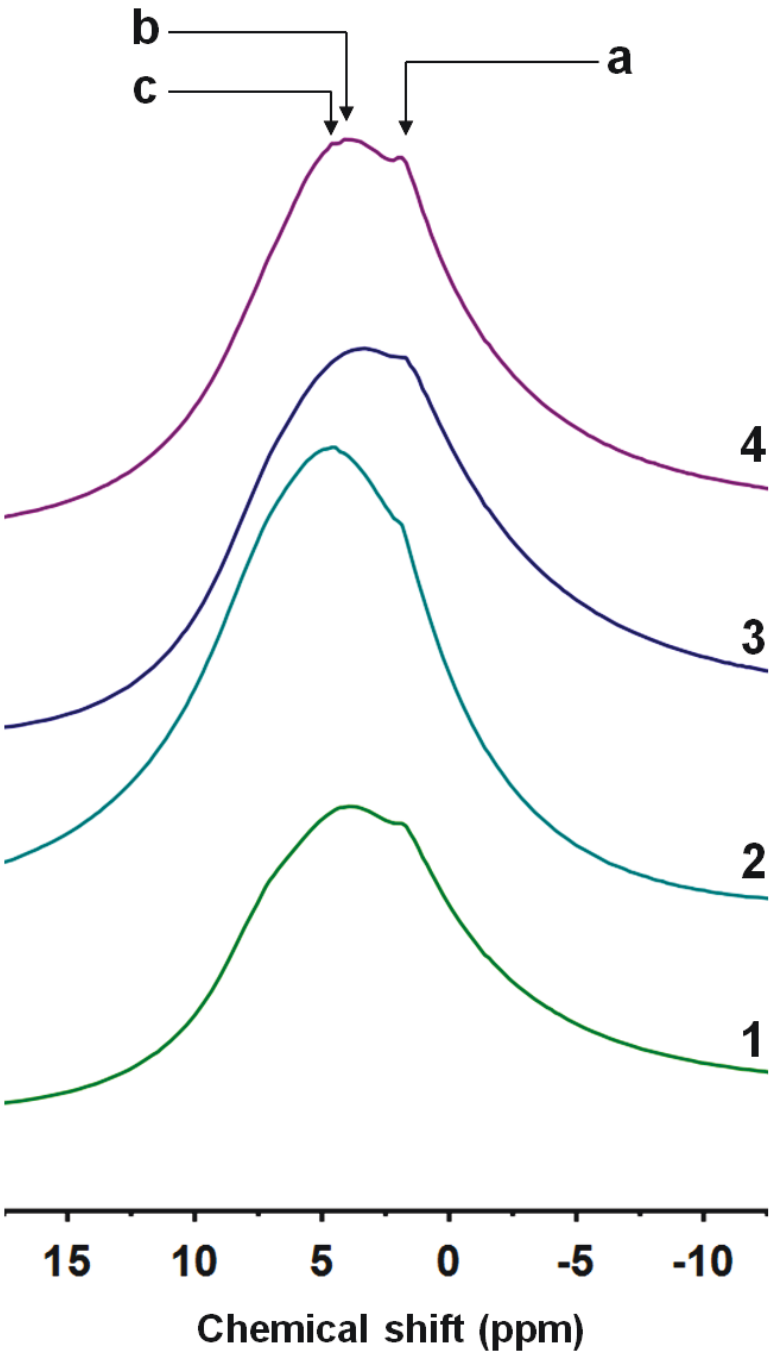

Figure 40. ^{1}H MAS NMR spectra of $ZnCl_2$-modified OMA supports samples prepared using $Al(OBu^{s})_3$ aluminum precursor with different carboxylic acids: (1: OP3) fumaric, (2: OP6) malonic, (3: OP5) maleic, and (4: OP1) citric acid. Indicating (a) basic terminal hydroxyl groups, (b) acidic bridging hydroxyl groups, and (c) hydrogen bonded water physisorbed on alumina surface. All samples were calcined at 400 °C.

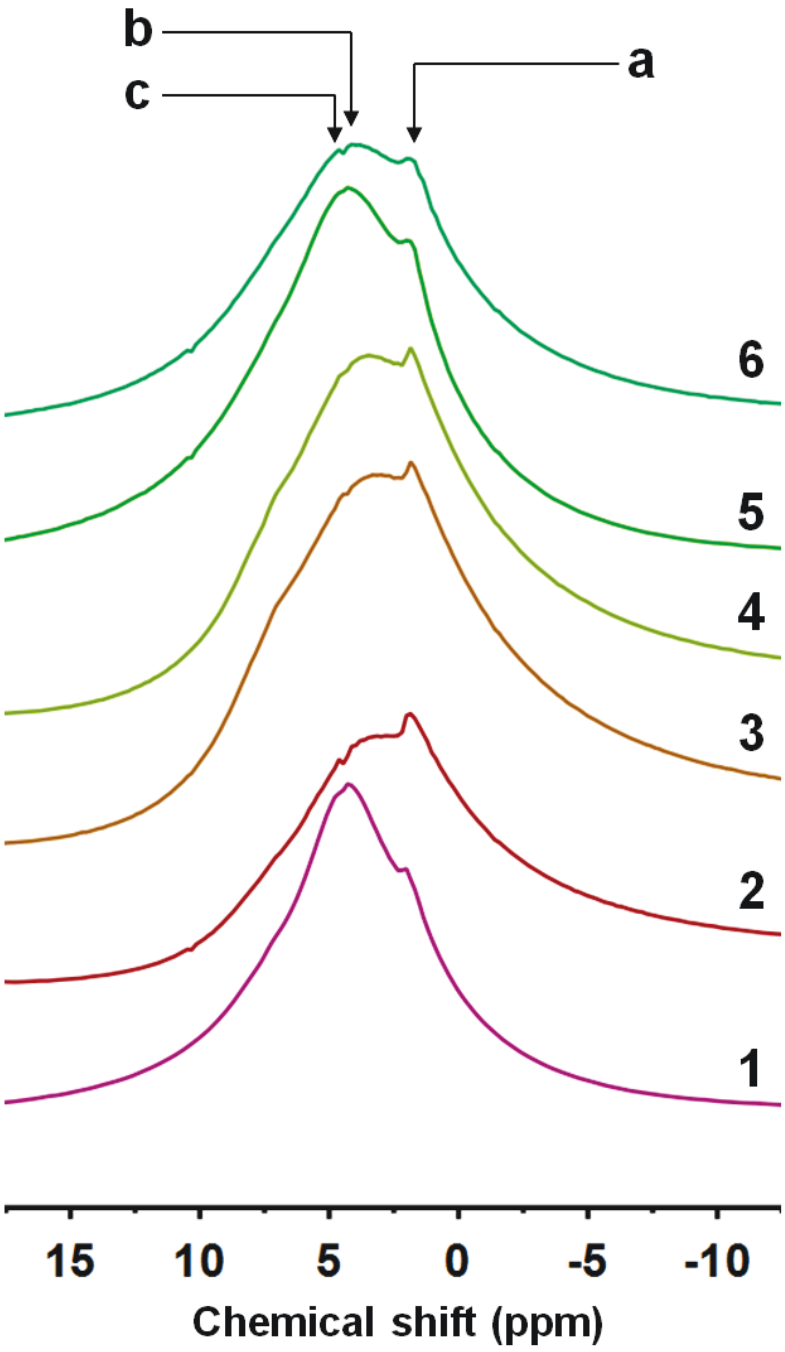

Figure 41. ^{1}H MAS NMR spectra of $ZnCl_2$-modified OMA supports samples prepared using $Al(OBu^t)_3$ aluminum precursor with different carboxylic acids: (1: OP8) citric, (2: OP14) malonic, (3) maleic, (4) fumaric, (5) oxalic, and (6) acetic acid. Indicating (a) basic terminal hydroxyl groups, (b) acidic bridging hydroxyl groups, and (c) hydrogen bonded water physisorbed on alumina surface. All samples were calcined at 400 °C.

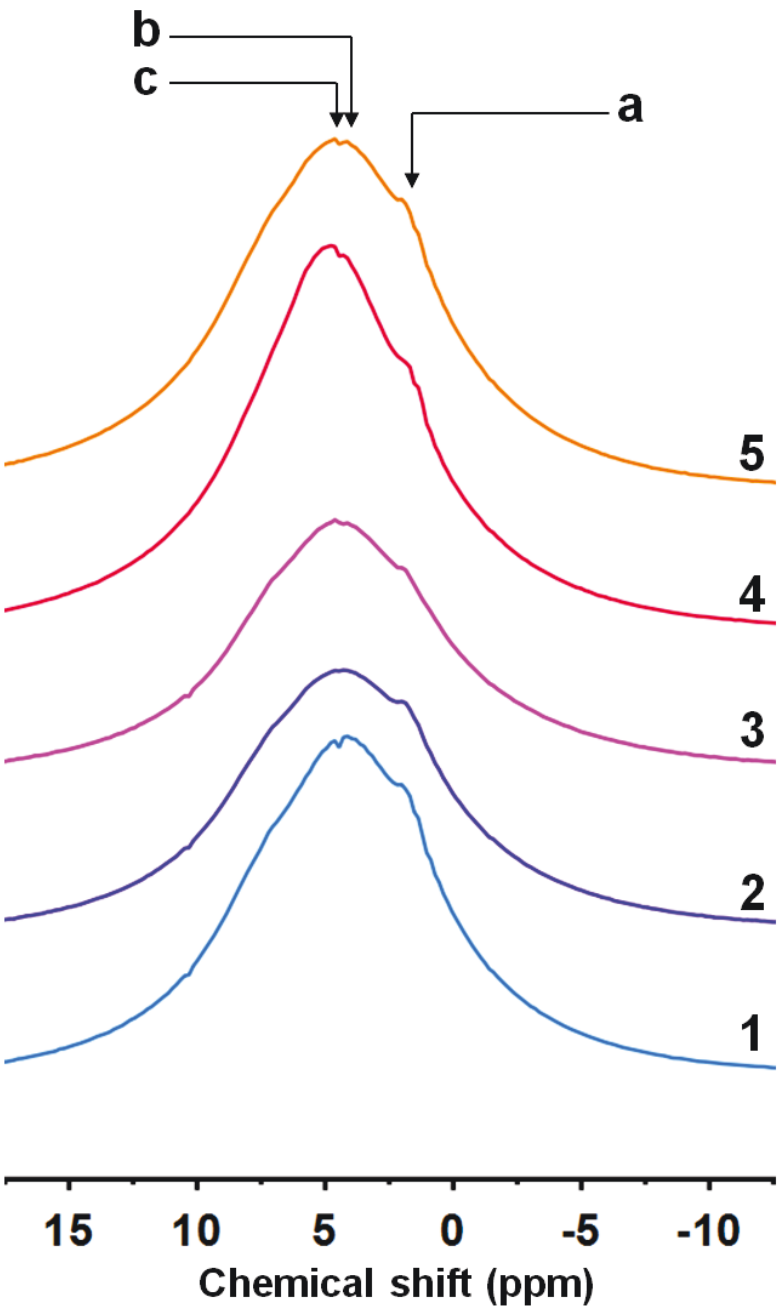

Figure 42. ^{1}H MAS NMR spectra of $ZnCl_2$-modified OMA supports samples prepared using different aluminum precursors: $Al(OPr^{i})_3$ with (1, OP10) citric, (3, OP11) tartaric, and (5, OP17) acetic acid; and $Al(NO_3)_3 \bullet 9H_2O$ with (2, OP12) citric and (4, OP13) tartaric acid. Indicating (a) basic terminal hydroxyl groups, (b) acidic bridging hydroxyl groups, and (c) hydrogen bonded water physisorbed on alumina surface. All samples were calcined at 400 °C.

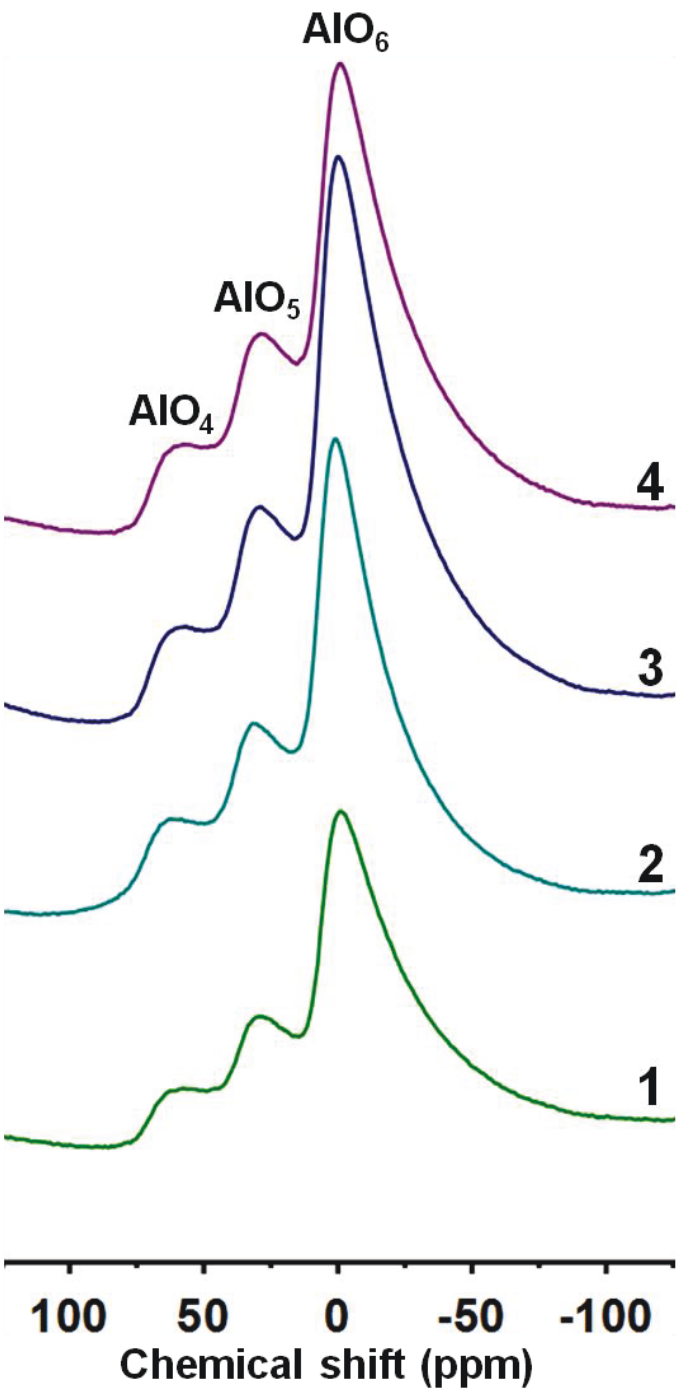

Figure 43. ^{27}Al MAS NMR spectra of $ZnCl_2$-modified OMA supports samples prepared using $Al(OBu^s)_3$ aluminum precursor with different carboxylic acids: (1: OP3) fumaric, (2: OP4) oxalic, (3: OP6) malonic, and (4, OP5) maleic acid. All samples were calcined at 400 °C.

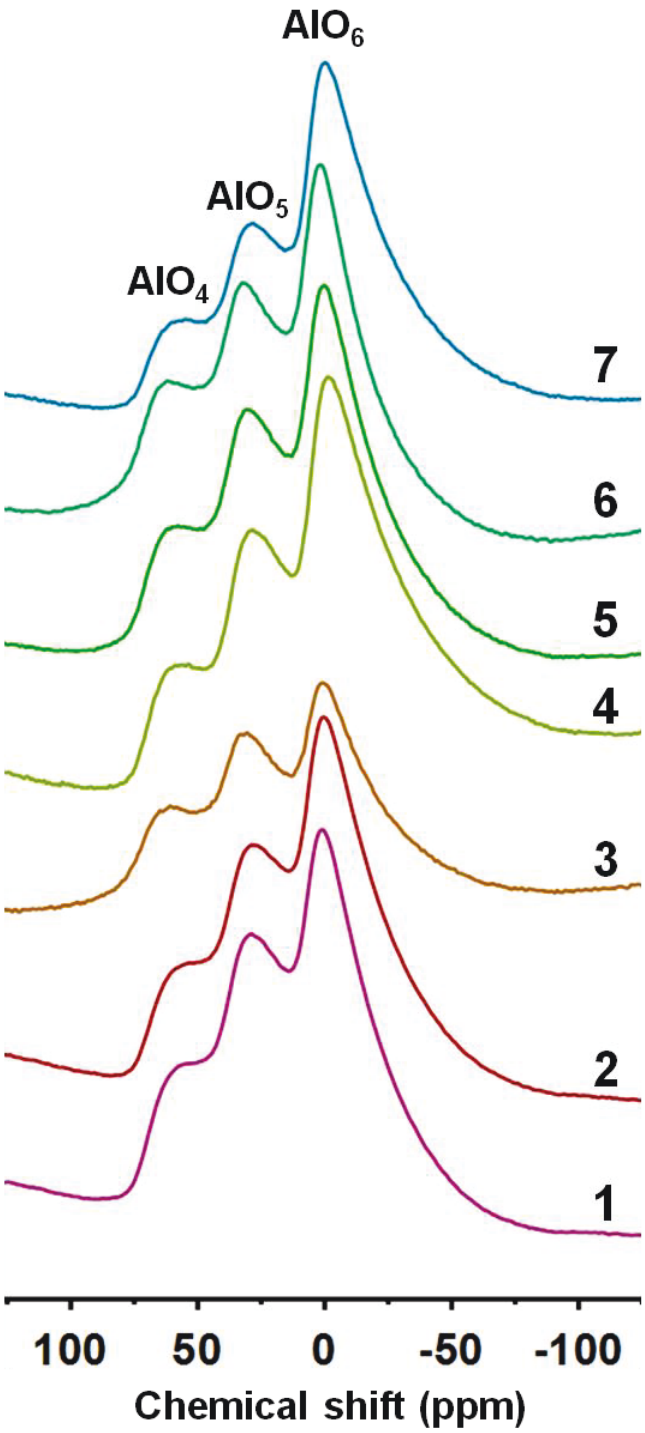

Figure 44. ^{27}Al MAS NMR spectra of $ZnCl_2$-modified OMA supports samples prepared using $Al(OBu^t)_3$ aluminum precursor with different carboxylic acids: (1: OP8) citric, (2: OP9) tartaric, (3: OP14) malonic, (4) maleic, (5) fumaric, (6) oxalic, and (7) acetic acid. All samples were calcined at 400 °C.

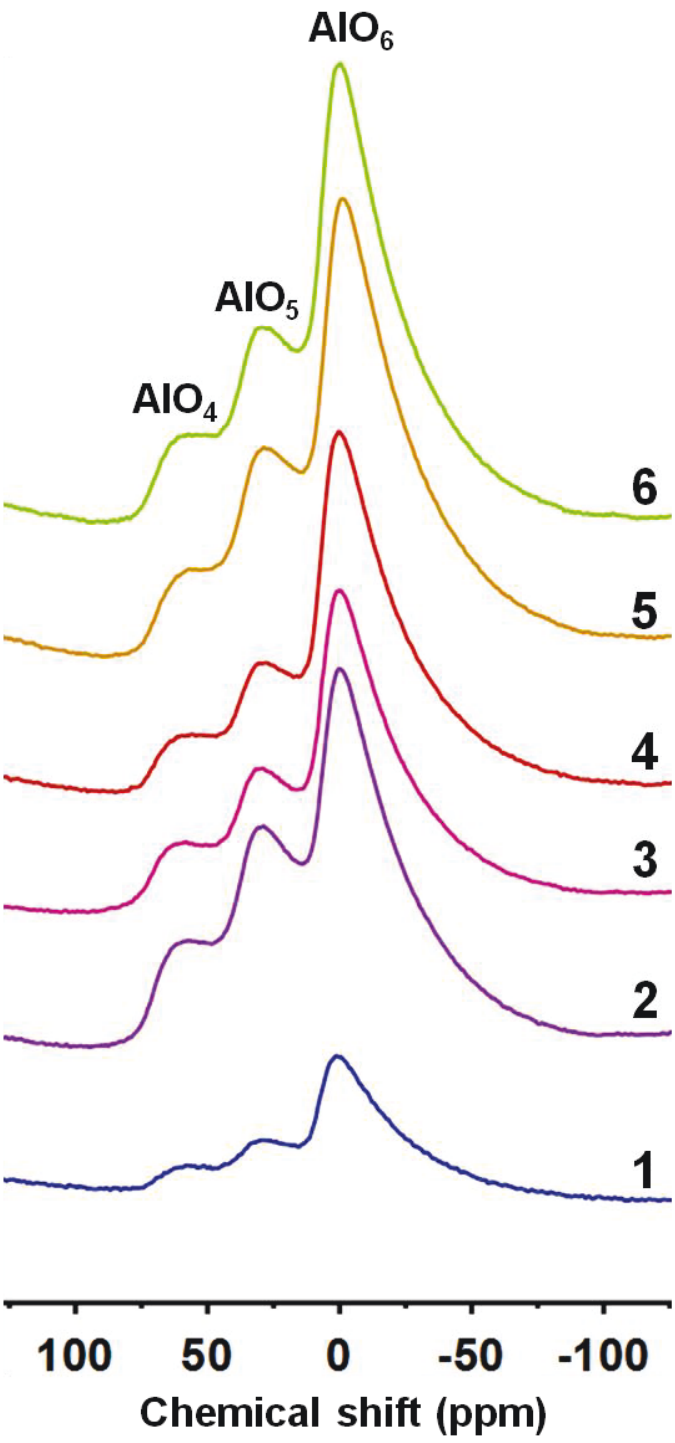

Figure 45. ^{27}Al MAS NMR spectra of $ZnCl_2$-modified OMA supports samples prepared using different aluminum precursors: $Al(NO_3)_3 \bullet 9H_2O$ with (1) acetic, (3, OP12) citric, and (5, OP13) tartaric acid; and $Al(OPr^i)_3$ with (2, OP10) citric, (4, OP11) tartaric, and (6, OP17) acetic acid. All samples were calcined at 400 °C.

Chapter 6:

Well-defined MTO-based catalyst: metathesis activity, surface active sites and mechanistic pathway

Abdelnasser Abidli

Department of Soil Sciences and Agri-Food Engineering, Laval University. G1V 0A6, Quebec City, Quebec, Canada

Résumé

L'alumine mésoporeuse ordonnée (AMO) hexagonale fonctionnalisées avec du $ZnCl_2$ a été préparé en utilisant les deux processus; celle en plusieurs étapes et celle en une seule étape. Puis, le méthyltrioxorhénium (MTO) a été supporté sur ces matériaux mésoporeux. Les catalyseurs MTO/$ZnCl_2$-AMO ont été caractérisés par adsorption-désorption d'azote, DRX, MET, MEB, ADESF, et l' SPX. Les deux supports catalytiques ont permis de générer la même espèce active à base de Re sur la surface pour effectuer la métathèse catalytique. Toutefois, les caractéristiques des supports $ZnCl_2$-AMO synthétisés en une seule étape ont été améliorées, y compris une surface BET supérieure (jusqu'à 358 m^2 g^{-1}), une concentration plus élevée des groupes hydroxyles sur la surface, ainsi que la dispersion uniforme d'espèces de zinc conduisant à une meilleure performance catalytique du MTO. Ces catalyseurs ont atteint une conversion de l'oléate de méthyle plus élevée (jusqu'à 94%) avec une sélectivité améliorée vers les produits de métathèse désirés (jusqu'à 74%). Les structures organisées des catalyseurs manifestent une stabilité remarquable après l'imprégnation du MTO ainsi qu'après la réaction de métathèse. En se basant sur les analyses des sites actifs de surface et des composés du mélange réactionnel, un mécanisme global de la formation de tous les produits de métathèse est proposé. Un cycle catalytique complet pour la génération des espèces actives de Re est aussi proposé.

Abstract

$ZnCl_2$-modified hexagonally ordered mesoporous aluminas have been prepared using two-steps and one-pot processes. Then MTO has been supported on these mesoporous materials. The 3 wt.% MTO/$ZnCl_2$-OMA catalysts were characterized by N_2 adsorption-desorption, XRD, TEM, SEM, EDX, and XPS analysis. It was found that both catalytic supports helped to generate the same metathesis catalytic active surface Re species. However, the improved features of the one-pot synthesized $ZnCl_2$-modified OMA supports including higher BET surface (up to 358 m^2 g^{-1}), higher surface hydroxyl groups' concentration as well as the uniform dispersion of zinc species led to enhanced MTO-based catalysts performance. These catalysts reached higher methyl oleate conversion (up to 94%) with improved selectivity towards desired metathesis reaction products (up to 74%). The catalysts organized structure manifested a remarkable stability after MTO impregnation as well as after metathesis reaction run. Based on the analysis of surface active sites and reaction mixture compounds, a comprehensive mechanism of the formation of all metathesis reaction products and a full catalytic cycle for the Re-species generation are proposed.

Keywords: functionalized ordered mesoporous alumina; supported metathesis catalyst; methyl oleate; one-pot synthesis; MTO

6.1. Introduction

Metathesis reaction is among the most sustainable catalytic transformations with high atom efficiency through the reorganization of the substrates fragments offering access to a variety of valuable molecules *via* formation of C-C double bonds [734]. Metathesis reaction can be conducted within various approaches including self-metathesis, cross-metathesis, ring-closing metathesis, ring-opening metathesis reactions [340], *etc*. The versatility of this synthetic tool is now considered as a key strategy in several fields including organic and polymer chemistry [734, 735], especially, towards highly efficient application in total synthesis of complexe natural products [736]. The early pioneering work of Chauvin, Grubbs and Schrock on olefin metathesis had a great impact on the chemistry science and chemical industry[737]; they were jointly awarded the 2005 Nobel Prize in Chemistry [55-57, 738]. Since the last two decades, impressive progresses have been made in this area, and numerous applications took advantage of this versatile carbon-carbon bond-forming method [739].

Both homogeneous and heterogeneous metathesis catalysts development enjoyed an impressive growth. Several homogeneous catalysts were developed for this purpose using various metallic centers and carbenic ligands. However, the major share of homogeneous catalysts is based on ruthenium, tungsten and molybdenum complexes [740, 741]. Nowadays, various homogeneous catalysts are commercially available [742]. In addition to their solubility is various media including water [743], these homogeneous catalysts are generally highly active and easy to modulate (*e.g.* ligand variation) with deep understanding of their mechanism, activity and molecular behavior [744, 745].

On the other hand, several heterogeneous catalysts were successfully developed for metathesis reaction applications such as supported metal oxides including rhenium oxide (Re_2O_7) [746], tungsten oxide (WO_3) [747] and molybdenum oxide (MoO_3) [748]. Similarly to their homogeneous counterparts, heterogeneous metathesis catalysts also witnessed a remarkable progress in a sustainable fashion, particularly within the emergence of the *so-called* surface organometallic chemistry (SOMC) concept, which bridges the gap between homogeneous and heterogeneous catalysis [360, 424, 429]. This methodology

allows the synthesis and identification of highly active and well-defined supported alkylidene surface species. Several catalytic supports were used including alumina and silica, while various species were grafted on these supports surface such as tungsten [749, 750], molybdenum [751, 752], tantalum [753-755], chromium [347], ruthenium [756, 757], and rhenium-based organometallic complexes [405, 427].

Among the rhenium-based supported heterogeneous catalysts, MTO was found to exhibit excellent metathesis reaction activity with a high stability and functional group tolerance [35, 36, 408, 414]. Among various catalytic supports alumina was found to be the most suitable support for MTO. Recently, a successful preparation of $ZnCl_2$-modified wormhole-like alumina-supported MTO-based catalysts was reported [430-432]. The MTO was proved to be highly active for both methyl oleate and triolein self-metathesis [430-432]. Afterwards, in order to improve the MTO-based catalyst performance, the wormhole-like alumina support was replaced with highly organized mesoporous alumina (OMA) support [657]. Thus, compared to the conventional wormhole-like alumina, higher reaction rate and selectivity towards desired metathesis reaction products were achieved over this newly designed MTO-based catalyst for methyl oleate self-metathesis due to the well-ordered mesoporous network of the OMA supports [657]. More recently, a new one-pot preparation of the $ZnCl_2$-modified OMA supports was designed (Chapter 5) [758]. This new methodology offered better supports with enhanced textural and surface properties, which led to enhanced metathesis reaction performance of the supported MTO-based catalyst for methyl oleate self-metathesis.

Herein, a comparative study of the different synthesized MTO-based catalysts is presented. Full characterization of the catalysts morphology, structure and composition is performed. Also, further investigation on the formation of the surface Re-based active species is conducted. These extensive characterizations allowed us to propose the full mechanistic route to methyl oleate self-metathesis products formation, as well as the catalytic cycle showing both productive and non-productive metathesis reaction pathways and the regeneration of the Re-based surface species.

6.2. Experimental section

6.2.1. Materials and chemicals

Pluronic F127 ($EO_{106}PO_{70}EO_{106}$, MW = 12 600), aluminum isopropoxide $Al(OPr^i)_3$ (≥98.0%), aluminum-tri-*sec*-butoxide $Al(OBu^s)_3$ (97.0%), citric acid (≥99.5%), L-(+)-tartaric acid (≥99.5 %), fumaric acid (≥99.5 %), oxalic acid (>99.0%), maleic acid (≥99.0%), malonic acid (99.0%), acetic acid (≥99.7%), zinc chloride ($ZnCl_2$, 99.9%), methyltrioxorhenium (VII) (MTO, CH_3ReO_3 with Re 71.0-76.0 %), oleic acid (technical grade) and boron trifluoride-methanol solution ($BF_3 \cdot MeOH$, 14% in methanol) were purchased from Sigma-Aldrich Canada (Oakville, ON, Canada). Aluminum tri-*tert*-butoxide $Al(OBu^t)_3$ (97.0%) was purchased from VWR International (Mississauga, ON, Canada). Aluminum nitrate nonahydrate $Al(NO_3)_3 \bullet 9H_2O$ (99.9%), hydrochloric acid (HCl, 36.5-38 wt%) and malonic acid (≥99.0%) were purchased from Acros Organics (Morris Plains, NJ, USA). Cyclohexane (99.9%), hexane (99.0%), and EtOH (99.9%) were purchased from Fisher Scientific (Ottawa, Ontario, Canada). All reagents were used as received without further purification. All gases used were provided by Praxair at a purity of at least 99.995%.

6.2.2. Catalytic supports synthesis

The $ZnCl_2$-modified OMA supports were prepared using two different synthesis processes that we have recently developed including two-steps (ts) and one-pot (op) processes [657, 758]. First, the two-steps (ts) process consists on the synthesis of well-ordered hexagonal mesoporous alumina (OMA), then functionalization *via* post-modification using $ZnCl_2$ (Chapter 4) [657]. For the second synthesis process we have recently developed a rapid one-pot (op) preparation of $ZnCl_2$-modified OMA supports [758]. This methodology consist on a combined sol-gel and *in situ* wet impregnation processes (Chapter 5) [758]. For both synthesis methods, we used Pluronic F127 as templating agent in anhydrous EtOH. Carboxylic acid acids were used as complexation agents, while HCl was used as a solution pH adjustor. Various aluminum precursors were used in addition to $ZnCl_2$. Solvent removal was performed in a drying oven at 60 °C, while calcination temperature was set at 400 °C in air. Furthermore, in order to generalize and verify the reproducibility of both synthesis

methodologies (ts, op) various aluminum precursors including $Al(OBu^s)_3$, $Al(OPr^i)_3$, $Al(OBu^t)_3$ and $Al(NO_3)_3 \cdot 9H_2O$, were screened along with distinct carboxylic acids (citric, tartaric, fumaric, oxalic, malonic, maleic and acetic acids).

6.2.3. Synthesis of well-defined metathesis catalysts: MTO impregnation on well-organized $ZnCl_2$-modified OMA

MTO impregnation was performed according to the procedure recently reported [430-432]. Detailed preparation procedure is described in Chapter 4 (Section 4.2.3).

6.2.4. Catalysts characterization: detailed experiments and instrumentations

Nitrogen adsorption/desorption isotherms, specific surface area, total pore volume and pore size distribution curves of the prepared samples were obtained using a volumetric adsorption analyzer (Model Autosorb-1, Quantachrome Instruments, Boyton Beach, FL) at 77 K. All powder X-ray diffraction (XRD) experiments were conducted on an Ultima III Rigaku monochromatic X-ray diffractometer (Cu Kα). Transmission electron microscopy (TEM) was conducted using a JEOL JEM-1230 field emission electron microscope. The microstructure and surface topography of the designed catalysts were analyzed by scanning electron microscopy (SEM) using JEOL JSM-840A scanning electron microscope. Energy dispersive X-ray analysis was carried out by using an EDS spectrometer attached to the SEM to know the elemental composition of prepared samples. X-ray photoelectron spectroscopy was employed to probe the chemical state of synthesized samples' elements. XPS spectra were collected using a Kratos AXIS ULTRA spectrometer with a standard Al Kα source (1486.6 eV) and a working pressure of less than 10^{-7} Torr. Detailed analysis experiments and parameters are provided in Chapter 4.

6.2.5. Methylation of crude oleic acid

Methyl oleate was chosen as a model molecule for bulky functionalized olefinic substrates for metathesis reaction. Thus, pure samples were prepared *via* methylation of crude oleic acid (technical grade). The samples purity was checked (by GC) before their injection in the metathesis reaction mixture. 200 mg of oleic acid were loaded in a 4 Dr glass vial,

dissolved in 1 mL of hexane, then 1 mL of boron trifluoride-methanol solution (BF_3•CH_3OH, 14%) was added. The mixture was stirred magnetically, and refluxed at 80 °C for 30 min in a water bath. The mixture was then allowed to cool down to RT, and 2 mL of deionized water were subsequently added allowing the aqueous-methanol layer to separate. Afterwards, it was extracted five times with hexane (2 mL). The collected organic layers were dried over anhydrous sodium sulfate (N_2SO_4) column. Finally, the solvent was removed under reduced pressure, affording methyl oleate as a faint yellow viscous liquid. Yield and purity of methyl oleate were determined by GC analysis.

6.2.6. Methyl oleate self-metathesis reaction

The synthesized 3 wt.% MTO/$ZnCl_2$-OMA catalysts performance was then evaluated for methyl oleate self-metathesis as the model reaction test allowing efficient comparison between different catalysts for their metathesis reaction activity with bulky functionalized olefins. In a typical experimental metathesis reaction procedure, the as-prepared MTO-based catalyst was introduced into a nitrogen purged 10 mL flat bottomed batch glass reactor equipped with inserted individual thermocouple. The catalyst was then suspended in 1 mL of hexane, and 750 mg (2.5 mmol) of methyl oleate (in 2 mL of hexane) was added to the catalyst under slow N_2 flow. Afterwards, the reactor was loaded in the reaction chamber in a glove box. The reaction was carried out under controlled dry atmosphere at 45 °C. All experiments were carried out at atmospheric pressure for 5h under stirring speed of 600 rmp to avoid external mass transfer limitations. Finally, the catalyzed metathesis reaction was stopped by addition of acetone enabling desorption of the reactants and products from the catalytic surface sites and the reactor was cooled to RT. The reaction mixture solution was separated from the solid catalyst through syringe filtration using non-sterile 13 mm Nylon ChromspecTM syringe filters with 0.2 μm pore size (Chromspec Inc., Brockville, ON, Canada), then the solvents were removed under reduced pressure. The obtained final reaction mixture was subjected to analysis.

6.2.7. Metathesis reaction products analysis

The metathesis reaction products mixture was analyzed quantitatively and qualitatively by means of gas chromatography (GC) and gas chromatography-mass spectroscopy (GC-MS).

6.2.7.1. Gas chromatography (GC) analysis

Gas chromatographic analysis was carried out in a Hewlett-Packard (Agilent, Wilmington, DE) HP6890 series gas chromatography system with capillary inlet (split-split mode) using a constant split ratio of 50:1. The system was equipped with an automatic liquid sampler and a flame ionization detector (FID) using BPX-70 capillary column (60 m length × 250 μm i.d. × 0.25 μm film thickness). Hydrogen was used as carrier gas with a constant flow rate of 1.2 mL/min set at a linear velocity of 22 cm/s at 100 °C. The injection port and the detector were held at 250 °C and 1 μL sample was injected. The oven temperature profile was set at initial temperature of 60 °C; then ramp at 10 °C/min to 190 °C; held for 15 min; and then to 240 °C at a ramp of 5 °C/min; and held at this temperature for 10 min, for a total run time of 48 min [759]. The metathesis reaction products were identified and quantified using commercially available highly pure external standards.

6.2.7.2. Gas chromatography-mass spectroscopy (GC-MS) analysis

Gas chromatography-mass spectroscopy characterization of metathesis reaction products was carried out using a Hewlett-Packard (Agilent, Wilmington, DE) HP 6890 instrument with a capillary inlet (split-split mode) with a constant split ratio of 50:1. Agilent 5973 network mass selective detector was used in electron ionization mode (70 eV), set to scan from 42 to 500 *m/z* at a rate of 3.19 scans/s. The system was equipped with HP DB-5 capillary column (30 m long × 250 μm i.d. × 0.25 μm film thickness). The column flow rate was 1 mL min^{-1}**,** with hydrogen as carrier gas set at a linear velocity of 22 cm/s at 100 °C. The injector and detector transfer line temperatures were set at 250 °C and 170 °C, respectively, with an injection volume of 1.0 μL**.** The oven temperature profile was: initial temperature 100 °C; held for 1 min; ramp at 10 °C/min to 250 °C; held for 15 min. Product identification was accomplished using the NIST 2005 library. The identification of metathesis reaction products were confirmed from the fragmentation patterns of the mass spectra. The collected data were analyzed using GC Chemstation Agilent software. All the solvents and standards used were GC grade (Aldrich, 99.9 %).

6.3. Results and discussion

6.3.1. Supported catalysts characterization: structure, morphology and composition

Figure 46 shows the nitrogen sorption isotherms (Figure 46i) and the corresponding pore size distribution curves (Figure 46ii) of the synthesized $ZnCl_2$-modified OMA supports. The measurements showed IV-type isotherms with an H1 hysteresis loop following the IUPAC classification, displaying one step capillary condensation in the adsorption branch which indicates the nitrogen filling within the uniform mesopores [676]. These catalytic supports were found to exhibit uniform and narrow pore size distribution (around 4-5 nm, Figure 46ii), with total pore volume around 0.40 cm^3g^{-1}. Both two-steps and one-pot prepared supports analysis revealed similar porous information with no significant difference in the shape of adsorption–desorption isotherms, pore size distribution and total pore volume. However, the one-pot prepared supports showed larger BET surface area (up to 358 $m^2 g^{-1}$) compared to the conventionally (two-steps) prepared supports (up to 239 $m^2 g^{-1}$) [758]. The additional calcination step and pore filling with $ZnCl_2$ during the two-steps synthesis process are suggested to be responsible for this drop in the surface area [657].

Afterwards, MTO was supported on these prepared $ZnCl_2$-modified OMA supports, and their catalytic performance was investigated for methyl oleate self-metathesis reaction. The stability of the supports organized structure was then studied using several techniques including XRD, TEM, SEM and EDX. Therefore, both fresh and spent catalysts were analyzed.

The low-angle XRD patterns obtained for the synthesized catalysts before and after metathesis reaction are displayed in Figure 46iii. The samples showed main reflections at 0.9-1.2°, 1.5-1.8° and 2.1-2.3° (2θ) which could be indexed as (100) and (110) and (200) reflections of *p6mm* two-dimensional hexagonal structure, respectively [596, 598]. These diffraction peaks indicate the existence of long-range ordered mesopores in the analyzed catalysts samples. Interestingly, the structure ordering of the $ZnCl_2$-modified OMA supports was maintained after MTO incorporation as well as after subjecting the catalysts for methyl oleate self- metathesis reaction conditions. However, MTO impregnation as well

as metathesis reaction conditions caused a slight decrease in the XRD intensity of the small (110) and (200) reflections compared to the supports (Chapter 5 and [657]).

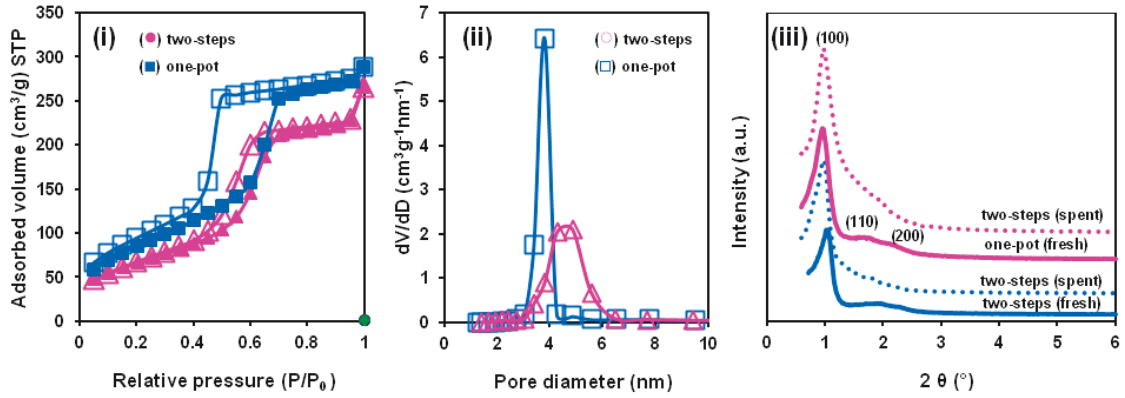

Figure 46. (i) Nitrogen adsorption-desorption isotherms; (ii) pore size distributions of the prepared $ZnCl_2$-modified OMA supports calcined at 400 °C, and (iii) small-angle powder X-ray diffraction patterns of the synthesized MTO-based catalysts samples calcined at 540 °C. All samples were prepared using $Al(OBu^t)_3$ and citric acid *via* both two-steps and one-pot process.

In order to further confirm the presence and stability of ordered mesoporous structure in the 3 wt.% MTO/$ZnCl_2$-OMA catalyst samples, their TEM images were taken. In agreement with nitrogen sorption and XRD data, evidence for the formation and stability of ordered mesostructure is provided by TEM images shown in Figures 47a-f. Highly ordered and non-interconnected cylindrical pores aligned along the [110] orientation and hexagonally arranged along the [001] orientation were observed. The supports porous structure seems to be identical for both catalysts samples supported on either one-pot or conventionally synthesized (two-steps) supports. Furthermore, these TEM characterizations demonstrate that the 2D-hexagonal mesoporous structure was maintained after MTO grafting before and after being subjected to metathesis reaction conditions.

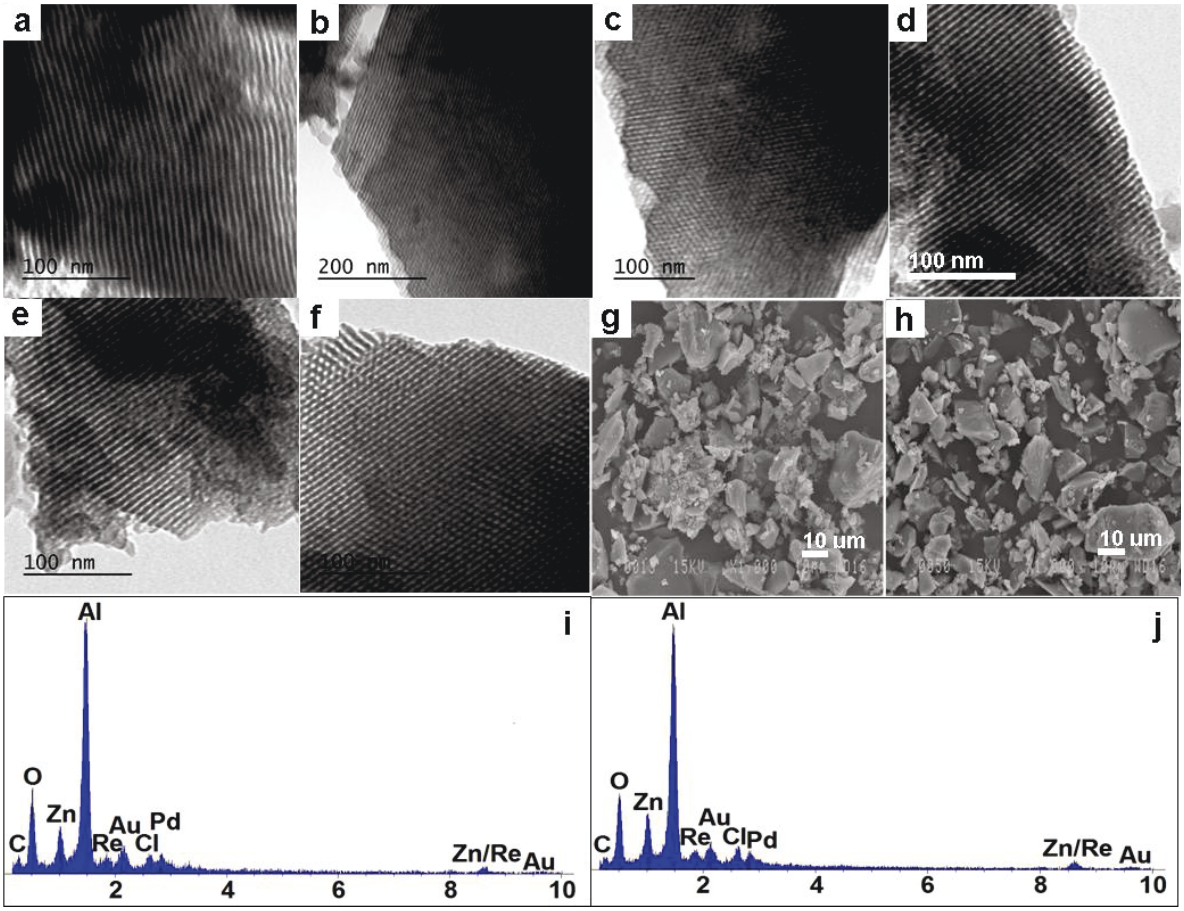

Figure 47. TEM images of the 3 wt.% MTO/$ZnCl_2$-OMA catalysts prepared using catalyst supports synthesized using $Al(OBu^s)_3$ and citric acid *via* two steps [ts] and one-pot [op] processes: (a) cat-$Al(OBu^s)_3$-citric-ts-fresh, (b) cat-$Al(OBu^s)_3$-citric-ts-spent, (d) cat-$Al(OBu^s)_3$-citric-op-fresh and (e) cat-$Al(OBu^s)_3$-citric-op-spent viewed along the [001] orientation, and (c) cat-$Al(OBu^s)_3$-citric-ts and (f) cat-$Al(OBu^s)_3$-citric-op fresh catalysts viewed along the [110] orientation. And representative SEM images (g, h) and energy dispersive X-ray (EDX) spectra (i, j) obtained for the (g, i) cat-$Al(OBu^s)_3$-citric-ts and (h, j) cat-$Al(OBu^s)_3$-citric-op fresh catalysts. All samples were calcined at 450 °C.

TEM images also illustrate the uniform dispersion of the Re species formed on the interface of the inner mesoporous walls of the $ZnCl_2$-modified OMA supports. On the other hand, SEM observation of the fresh bulk catalysts depicted in Figures 47g-h showed an irregular 3D cuboid shape of the catalysts microparticles ranging from 8-30 μm. Smaller particles (< 10 μm) were also observed which could be assigned to alumina particles grounded under

the mechano-chemical effect of the reaction conditions or may corresponds to the agglomeration of few MTO and/or $ZnCl_2$ small crystals.

The SEM images taken from the spent catalysts samples showed similar particle morphology compared to the fresh ones (See Figure 49 of the Supporting information). The catalyst particles then showed less uniform shape compared to those of the supports used for MTO grafting [657].

The EDX measurements were also conducted accompanying with the SEM observations to monitor the chemical elemental compositions of the designed metathesis catalysts. The EDX spectra of the freshly prepared catalysts samples showed in Figures 47i-j revealed the presence of the expected elements in the catalyst structure, namely oxygen, aluminum, zinc, chlorine, as well as carbon and rhenium. The detected elements were found in close stoichiometric ratios to alumina, $ZnCl_2$ and MTO composition. Subsequently, EDX data of the spent catalysts also showed similar composition indicating the maintained catalysts integrity and structure (See Figure 50 of the Supporting information). In addition, palladium and gold were also detected in the EDX spectra; these elements originated from the Au/Pd films used in the samples' preparation to improve the surface conductivity.

6.3.2. Catalysts evaluation for methyl oleate self-metathesis

As mentioned above, the designed 3wt.% MTO/$ZnCl_2$-OMA catalysts were evaluated for their performance in bulky functionalized olefin self-metathesis as a representative reaction using methyl oleate as an ideal substrate. This reaction generates two main important and desired compounds, namely *trans*/*cis*-9-octadecene (**DC-1**) and *trans*/*cis*-dimethyl-9-octadecene-1,18-dioate (**DC-2**), while unfortunately unavoidable production of undesired metathesis reaction product (methyl elaidate, **UC**) also occurs, which results from the non-productive metathesis reaction pathway. All identified methyl oleate self-metathesis reaction products are illustrated in Scheme 14. Analysis of reaction mixture was performed using both GC and GC-MS techniques in order to investigate methyl oleate conversion as well as to distinguish positional and geometrical isomers (*trans* and *cis* coumpounds). For a given double bond the *tran*s isomers nearly always elute before the corresponding *cis* compounds on polar phase like the BPX-70 capillary column used for GC which is highly

polar [760, 761]. On the other hand *cis* isomers elute before the corresponding *trans* compounds in non-polar phase which is the case of DB-5 capillary column used for GC-MS [761]. Thus isomers identifications became easier from the representative GC and GC-MS chromatograms (See Figure 51 of the Supporting information). In addition, highly pure commercial standards were used to verify the reaction mixture composition.

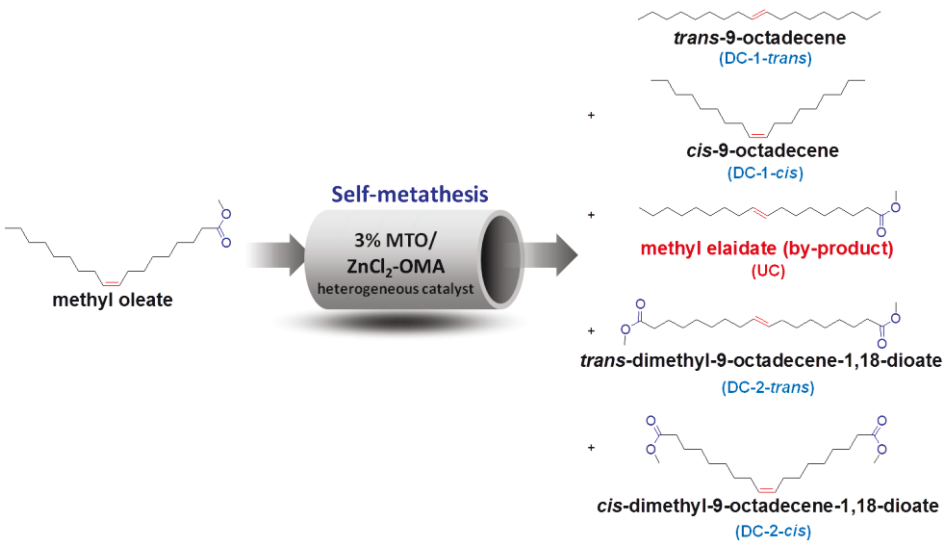

Scheme 14. Methyl oleate self-metathesis reaction products over MTO-based catalyst

As shown previously (See Table 11 in Chapter 5, Section 5.3.3), for the results obtained for methyl oleate self-metathesis reactions over various catalysts, where the newly prepared OMA-based catalysts were compared with wormhole-like alumina-based metathesis catalysts, a shift in the catalysts activity was observed:

First, the $ZnCl_2$-modified OMA supports showed better activity and selectivity owing to the synergetic effect between alumina surface hydroxyl group, $ZnCl_2$ and MTO offering better metathesis active sites surface coverage as was previously demonstrated [430-432]. Furthermore, the MTO-based catalysts supported on OMA exhibited better performance compared to wormhole-like alumina supported catalysts. This was suggested to be due to the enhanced kinetics inside the organized mesoporous network due to more exposed Re active sites and improved molecular diffusion of substrates and products, as well as the inhibited blocking effect that may occur in the interconnected wormhole-like alumina network [657]. In addition, this rate enhancement offered better selectivity by reducing the

side reaction pathway leading to lower methyl elaidate (by-product) formation. Also, the performance of catalysts supported on both one-pot and two-steps synthesized supports were compared. The metathesis reaction results showed an improved methyl oleate conversion (up to 94%) as well as a higher selectivity towards desired metathesis reaction products (up to 74%) using the one-pot synthesized $ZnCl_2$-modified OMA supports [758].

We believe that this enhancement is due to several features including: higher BET surface area, lower dehydroxylation rate and higher surface OH groups concentrations, as well as improved $ZnCl_2$ impregnation through *in situ* process. All these factors are responsible for better synergetic effects between surface sites, as well as enhanced dispersion and availability of active metathesis Re-based carbenic species

6.3.3. Catalysts active sites and intermediates analysis

To better understand the catalytic properties of MTO-based catalysts, surface elemental analysis of the catalyst samples was performed by XPS. Table 12 summarises the composition detected for the $ZnCl_2$-modified OMA supports before and after incorporation of MTO.

In agreement with EDX analysis, the XPS analysis revealed the presence of the expected elements binding energy values in the 3 wt.% MTO/$ZnCl_2$-OMA catalysts samples, namely Al 2*p*, O 1*s*, Zn 2*p* and Cl 2*p* (See also Figure 52 of the Supporting information). In summary, the Al 2*p* binding energy value corresponds to aluminum composition in the alumina framework walls [657]. O 1*s* binding energy values corresponds to the oxygen composition in the alumina matrix (Al-O-Al), alumina surface hydroxyl groups (Al-O-H) and hydrogen-bonded physisorbed water (in the case of two-steps synthesized $ZnCl_2$-modified OMA supports) [657]. Zn 2*p* binding energy values could be assigned to various Zn-containing surface species such as Zn-Cl, $Zn(OH)_2$, Zn-O, but mainly Zn-O-Zn-Cl species [657], while Cl 2*p* binding energy values correspond to Zn-bonded chlorine species [657]. A slight increase in the binding energy values was observed between modified and unmodified OMA samples components. This may be ascribed to the incorporation of $ZnCl_2$ and its bonding to these species inducing an electronic environment change. Similarly, for

both one-pot and two-steps prepared samples a slight shift was observed after MTO incorporation which indicates the bonding of Re-based species to the detected surface sites.

Table 12: XPS data of Al, O, Zn and Cl elements from the 3 wt.% MTO/$ZnCl_2$-OMA catalysts samples prepared using the $ZnCl_2$-modified OMA supports synthesized *via* either the classical two-steps or the one-pot process.

Elements	Two-steps synthesis			One-pot synthesis			
	Support BE (eV) [657]	**Catalyst BE (eV)**	**ΔBE (eV)**	**Support BE (eV)** [758]	**Catalyst BE (eV)**	**ΔBE (eV)**	**Assignment**
Al 2*p* (1)	74.3						[Al] Al_2O_3 phase
Al 2*p* (2)	74.7	75.0	+ 0.3	74.4	74.8	+ 0.4	[Al] Al_2O_3 phase
O 1*s* (1)	530.9						[O] Al_2O_3 phase
	532.1						[O] OH: Al_2O_3 surface
	533.1						[O] H_2O physisorbed
O 1*s* (2)	531.3	332.5	+ 1.2	531.2	331.6	+ 0.4	[O] Al_2O_3 phase
	532.7	333.6	+ 0.9	532.5	333.0	+ 0.5	[O] OH: Al_2O_3 surface
	533.9	334.7	+ 0.8				[O] H_2O physisorbed
Zn $2p_{3/2}$	1022.5	1023.8	+ 1.3	1022.1	1022.9	+ 0.8	Zn^{2+} surface species
Cl $2p_{3/2}$	199.3	200.6	+ 1.3	198.9	199.2	+ 0.3	Cl^-: Zn-Cl
Cl $2p_{1/2}$	200.9	202.2	+ 1.3	200.5	200.8	+ 0.3	Cl^-: Zn-Cl

(1) Alumina only; (2) $ZnCl_2$-modified OMA supports; All shifts for the samples were corrected by normalization of the C 1*s* binding energy to 285.0 eV.

In addition to Al, O, Zn and Cl species, XPS measurements also revealed the presence of Re species which corresponds to the chemisorbed MTO species, as depicted in the survey spectra of the analyzed catalysts samples (Figures 49a, 49c). Two Re-based components can be distinguished (Figures 49b, 49d, see also Figure 53 of the Supporting information) which are detected at different BE values: 44.86 and 47.29 eV, assigned to Re $4f_{7/2}$ components of the MTO-based surface species. These peaks are ascribed to the binding energy of Re^{+6} and Re^{+7} species respectively. In agreement with the present results, previous studies using solid-state NMR techniques showed that the plausible Re species formed on the alumina surface are the major inactive oxo species (Scheme 15i) and the minor active μ-methylene species (Scheme 15ii) after reaction of MTO with Al surface Lewis acid sites [422, 425, 762]. These species correspond to the coordination states of Re^{+6} and Re^{+7}, respectively.

The μ-methylene species are generated through heterolytic splitting of C-H bond on Lewis acidic Al centers, which also generates OH surface groups (Scheme 15ii). However, these μ-methylene species are probably converted into the metathesis active alkylidene surface species (Scheme 15iii) *via* a tautomerization or hydrogen transfer mechanism [422, 425, 762].

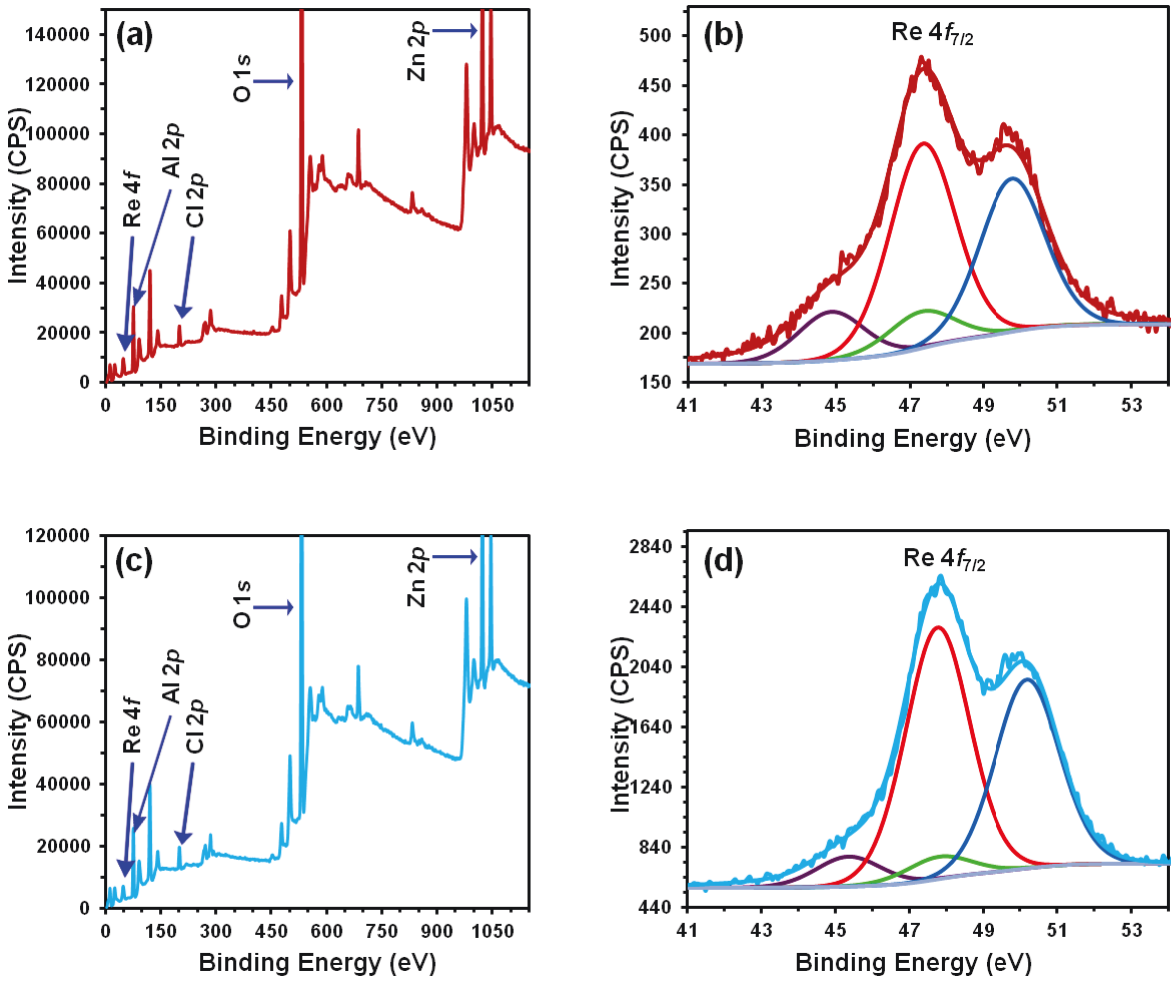

Figure 48. XPS analysis of the 3 wt.% MTO/$ZnCl_2$-OMA catalysts samples prepared using $ZnCl_2$-modified OMA supports synthesized with malonic acid and $Al(OBu^s)_3$ aluminum precursor *via* (a, b) two-steps or (c, d) one-pot process: (a, c) survey spectra and (b, d) Re 4*f* deconvoluted spectra. All shifts for the samples were corrected by normalization of the C 1*s* binding energy to 285.0 eV.

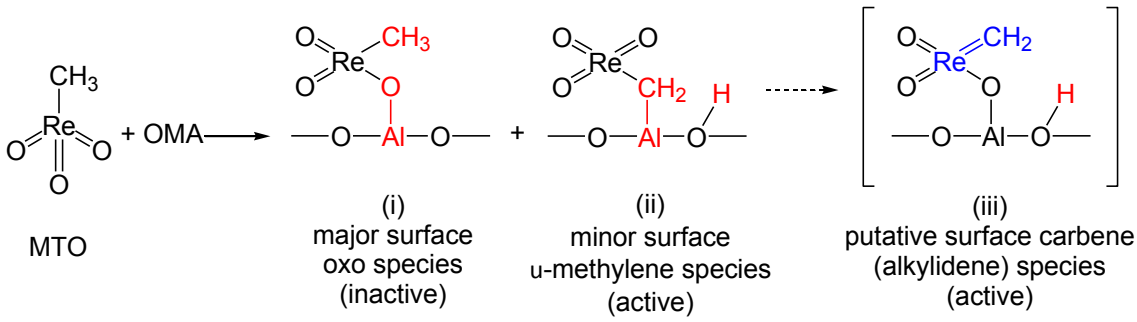

Scheme 15. OMA-supported MTO surface species.

6.3.4. Mechanistic studies for methyl oleate self-metathesis products formation

After identifying the surface active species, the mechanistic pathways for metathesis reaction products formation were studied. Considering methyl oleate as a bulky functionalized molecule, its geometry at the solid-liquid interface with the catalysts is a crucial parameter that controls the metathesis reaction products *cis*/*trans* isomers formation and distribution. On the other hand, the solid catalyst support is considered as a rigid catalyst ligand that applies a steric hindrance, which also is a key factor controlling methyl oleate geometry at the solid-liquid interface. Therefore, simply four interaction approaches of methyl oleate with the catalyst surface could be suggested (Scheme 16).

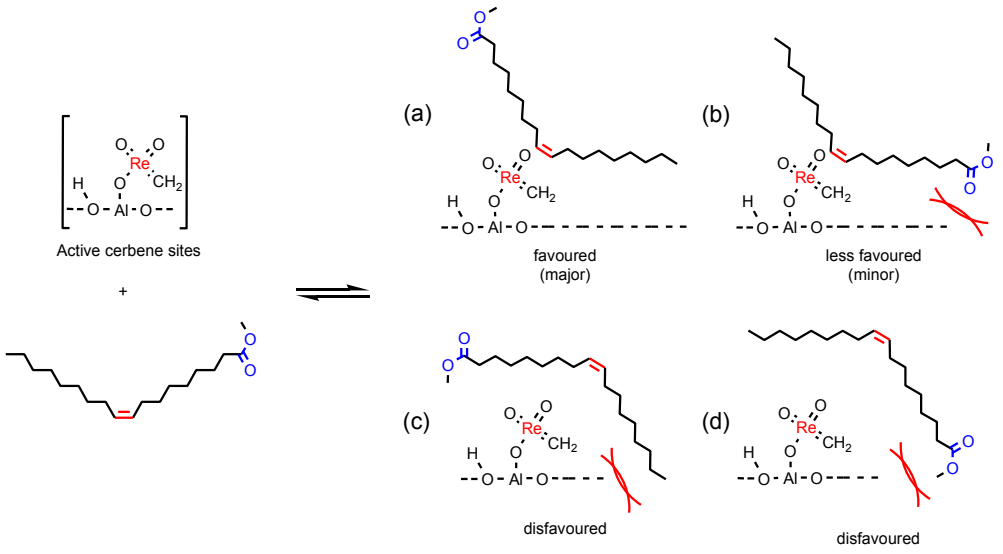

Scheme 16. The four plausible approaches for methyl oleate self-metathesis withdrawn to the surface Re active species.

Reasonably, the favored approaches are those which occur with less steric hindrance controlled mainly by both the *cis* geometry of methyl oleate and the bulkier ester side of the molecule.

Taking into account the majorly favored approaches (Scheme 16a-b), we attempted to propose the full mechanistic pathways that lead to the formation of each metathesis reaction products with the precise isomers selectivity. Conventionally, the olefin metathesis reaction process involves two main steps; the catalyst imitation forming the propagating active species followed by the catalyst propagation leading to the metathesis reaction products formation [340]. First, the interaction of methyl oleate molecules with the surface active carbenic species (Re=C) leads to the formation of the *so-called* metathesis propagating active species (PAS, Scheme 17a-b). These species represent the new carbenic species that consist of one of the two fragments of the olefinic chain [413, 763]. In this study, these species are denoted as PAS1 (Scheme 17a) and PAS2 (Scheme 17b), holding the ester side and the alkyl chain fragments, respectively.

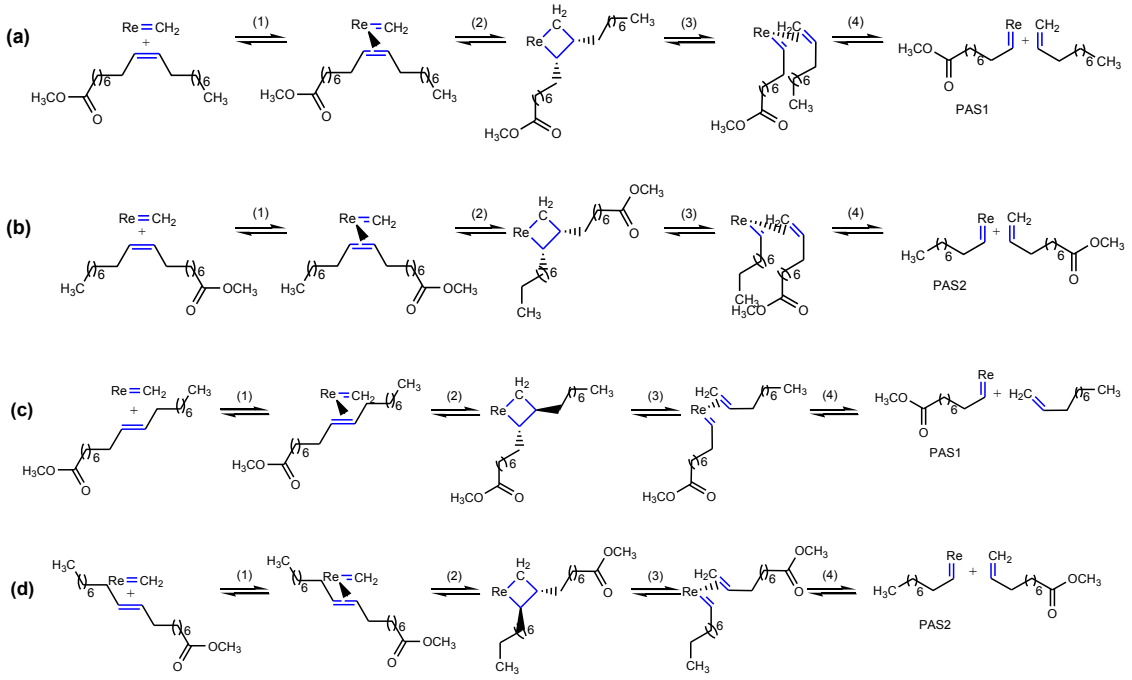

Scheme 17. The mechanistic pathway for the formation of the metathesis propagating active species (PAS1 and PAS2) from methyl oleate including four steps: (1) coordination; (2) [2+2] cycloaddition; (3) cyclorversion and (4) decoordination.

Methyl elaidate also is among metathesis reaction products present in the reaction mixture. It is worth to mention that, either methyl oleate or methyl elaidate are similarly withdrawn to the MTO active species on the surface to regenerate the same propagating active species (PAS1 and PAS2, see Scheme 17c-d).

Afterwards, the methyl oleate substrates interact with the interfacial generated PAS1 and PAS2. As displayed in Scheme 18a-d both *trans* and *cis* metathesis reaction products isomers are formed upon interaction of PAS1 with methyl oleate.

Also, the mechanistic pathways illustrate clearly the regeneration of the propagating active species. Similarly to PAS1, *trans* and *cis* metathesis reaction products are also obtained upon interaction of methyl oleate with PAS2 (Scheme 18e-h). However, the different withdrawing approaches are controlling parameters for *cis*/*trans* isomers formation when methyl oleate/elaidate is withdrawn again to the generated propagating active species (PAS1 and PAS2). These mechanistic pathways illustrate clearly the unavoidable route to methyl oleate, the starting materials, through the *so-called* non-productive regenerating pathway (Scheme 18d), which prevent achieving quantitative conversion (100 %). Also methyl elaidate formation is inevitable *via* the *so-called* non-productive isomerization pathway as illustrated in Scheme 18b.

According to Scheme 18, all the *anti* approaches correspond to the *trans* metathesis reaction products formation, while all the *syn* approaches lead to the formation of *cis* metathesis reaction products. Therefore, considering the less steric hindrance, the *anti* approaches seem to be the majorly favoured approach. Interestingly, this hypothesis is found to be in agreement with the experimental results where higher methyl oleate self-metathesis *trans* products yields were obtained compared to the *cis* products.

As pointed out above, methyl elaidate is one of the methyl oleate self-metathesis products. However, it is never excluded that this later can also undergo metathetic transformations. Interestingly, the self-metathesis of methyl elaidate also leads to the formation of the same metathesis reaction products, similarly to those observed for methyl oleate self-metathesis (Scheme 19).

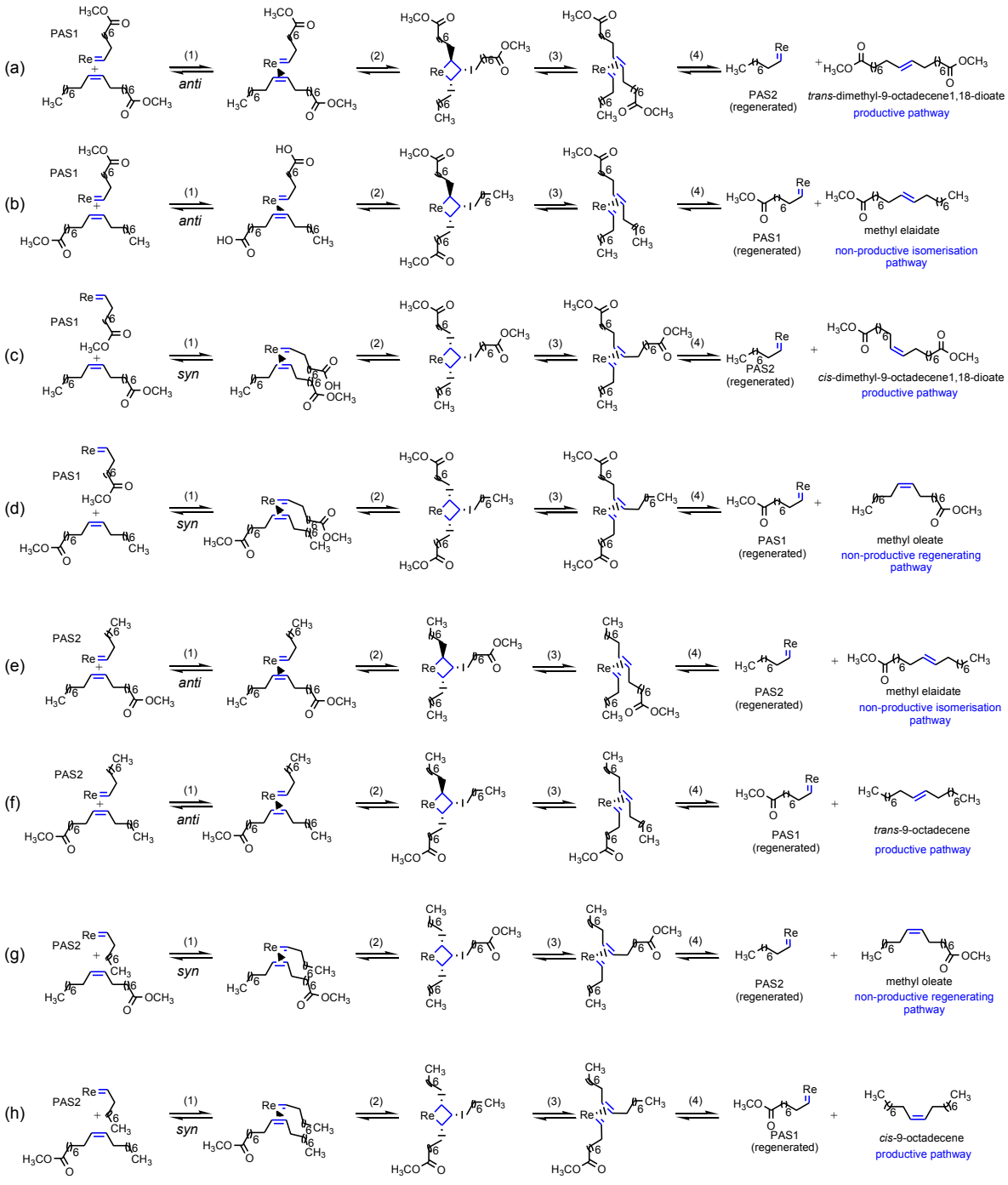

Scheme 18. The mechanistic pathway for the formation of the metathesis reaction products (*trans* and *cis*) from the propagating active species (a-d) PAS1 and (e-h) PAS2 with methyl oleate including four steps: (1) coordination; (2) [2+2] cycloaddition; (3) cyclorversion and (4) decoordination.

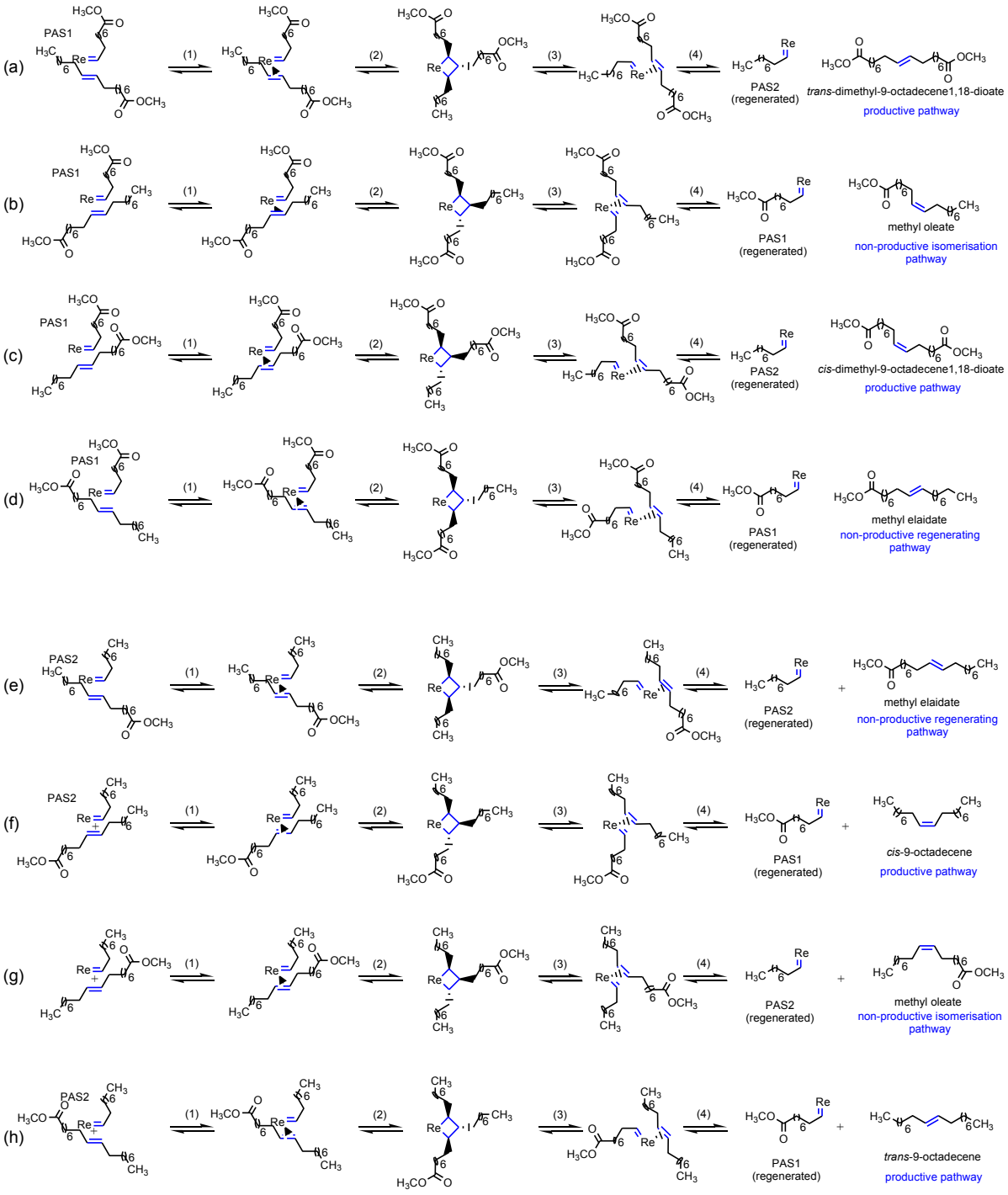

Scheme 19. The mechanistic pathway for the formation of the metathesis reaction products (*trans* and *cis*) from the propagating active species (a-d) PAS1 and (e-h) PAS2 with methyl elaidate including four steps: (1) coordination; (2) [2+2] cycloaddition; (3) cyclorversion and (4) decoordination.

Finally, these insights guided us to propose a comprehensive catalytic cycle for methyl oleate self-metathesis process illustrating the generation of the propagating active species starting from Re=CH_2 (chemisorbed MTO), methyl oleate self-metathesis products formation, as well as the Re=CH_2 regeneration pathways (Scheme 20).

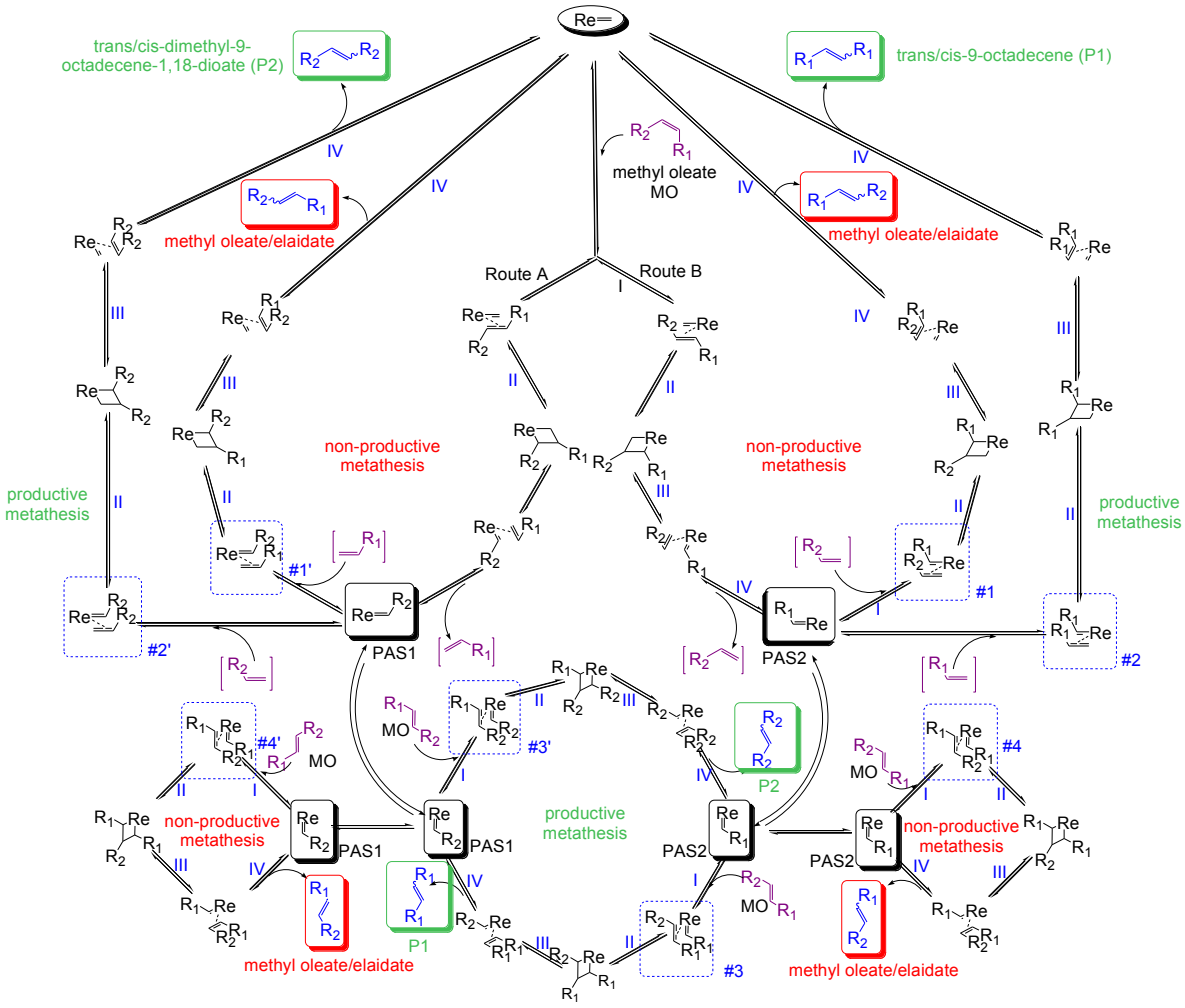

Scheme 20. The proposed catalytic cycle for methyl oleate self-metathesis reaction and active species regeneration. Each cycle include four steps: (I) coordination; (II) [2+2] cycloaddition; (III) cyclorversion and (IV) decoordination. R_1 = alkyl chain fragment; R_2 = ester side fragment. All transition states #1, 1', 2, 2', 3, 3', 4 and 4' could be eitheir *anti* or *syn* leading to eitheir *trans* or *cis* isomers, respectiviely.

6.4. Conclusions

In the study, supported mesostructured 3 wt.% MTO/$ZnCl_2$-OMA catalysts with high surface area and narrow mesopore size distributions have been successfully prepared using modified organized mesoporous alumina supports. The synthesized catalysts were found to be highly active for methyl oleate self-metathesis reaction using 3 wt.% MTO with a great organized structure stability. The catalysts supported on $ZnCl_2$-modified OMA supports prepared *via* an improved evaporation-induced self-assembly (EISA) method through one-step process exhibits superior catalytic activity compared to those supported on $ZnCl_2$-modified OMA supports prepared *via* traditional two-steps process. The catalysts characterization revealed a synergetic effect between Zn and Re species responsible for metathesis reaction activity. The highly dispersed Zn species, high surface area and low surface dehydroxylation were responsible for the improved catalytic activity and selectivity. The catalytically active sites are suggested to be the surface Re-based carbenic compounds. Furthermore, the methyl oleate and support surface were found to display steric hindrance to metathesis intermediate active species which is considered as the governing factor controlling the products formation pathways and selectivity.

Acknowledgements

This work was financially supported by the Natural Sciences and Engineering Research Council of Canada (NSERC) and Canadian Foundation for Innovation (CFI). A. Abidli also thanks Prof. Khaled Belkacemi for the N_2 adsorption-desorption analysis and for providing his laboratory facility at Laval University where the materials/catalysts synthesis and the metathesis reaction experiments were conducted. Alain Adnot, Prof. Safia Hamoudi, Ronan Corcuff, André Ferland and Richard Janvier are gratefully acknowledged for the XPS, XRD, GC-MS, SEM and TEM measurements, respectively.

Supporting information

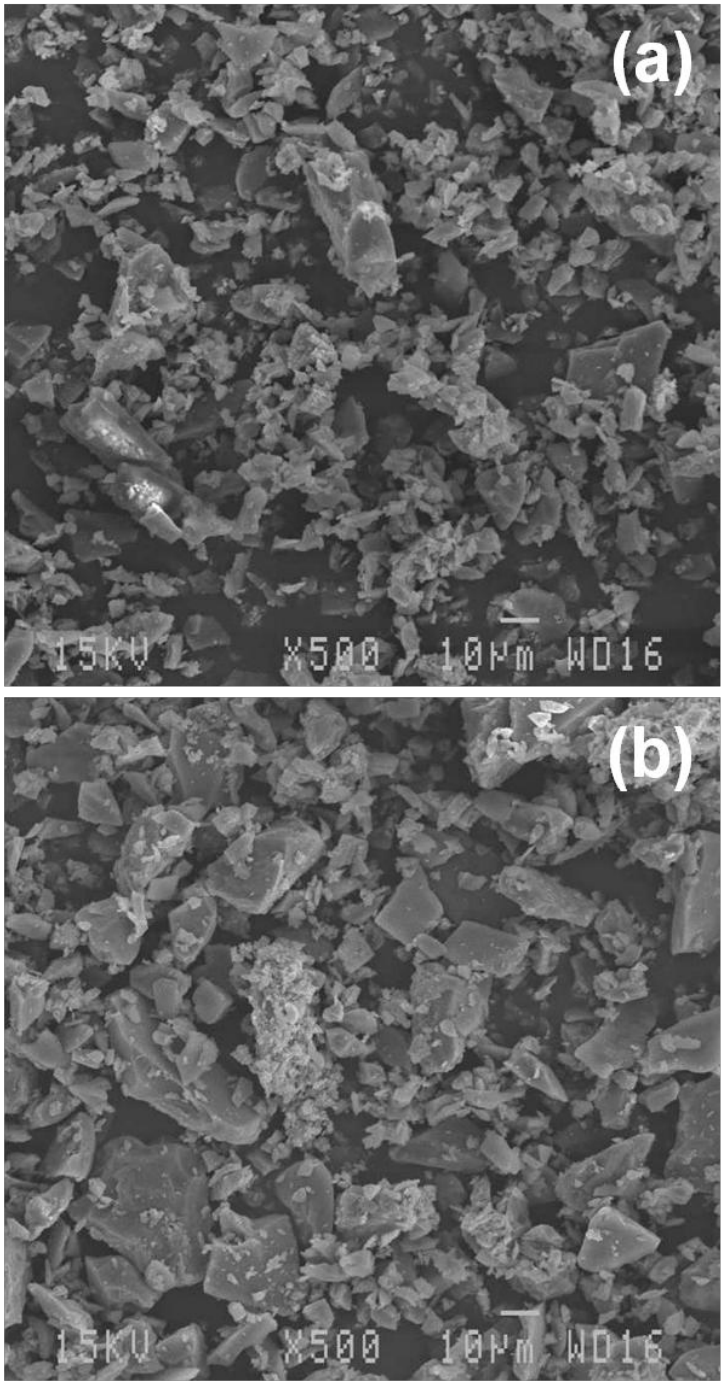

Figure 49. Representative SEM images obtained for the spent catalysts: (a) cat-Al(OBu^s)$_3$-citric-ts and (b) cat-Al(OBu^s)$_3$-citric-op catalysts. All samples were calcined at 450 °C.

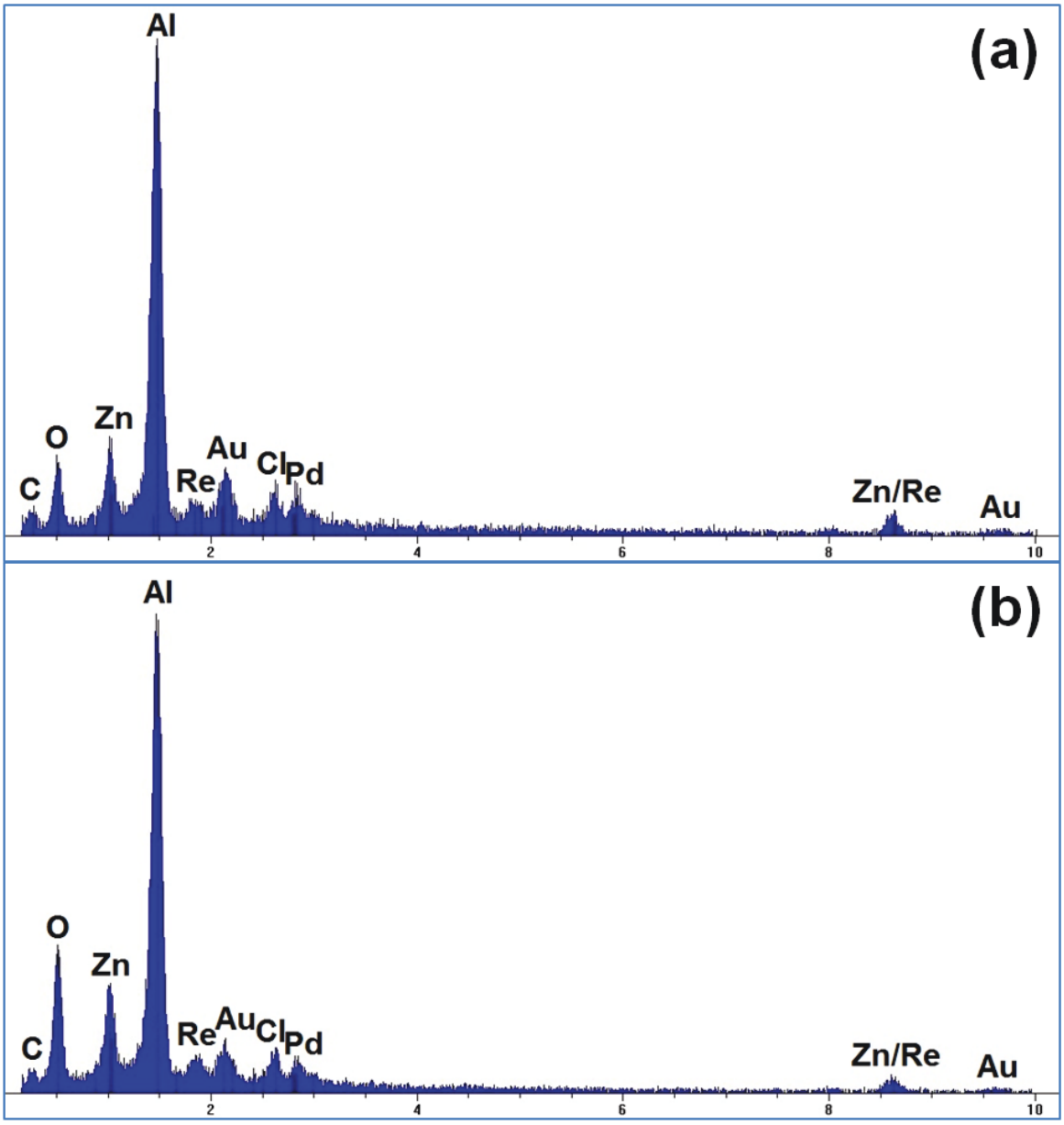

Figure 50. Representative energy dispersive X-ray (EDX) spectra obtained for the spent catalysts: (a) cat-Al(OBu^s)$_3$-citric-ts and (b) cat-Al(OBu^s)$_3$-citric-op catalysts. All samples were calcined at 450 °C.

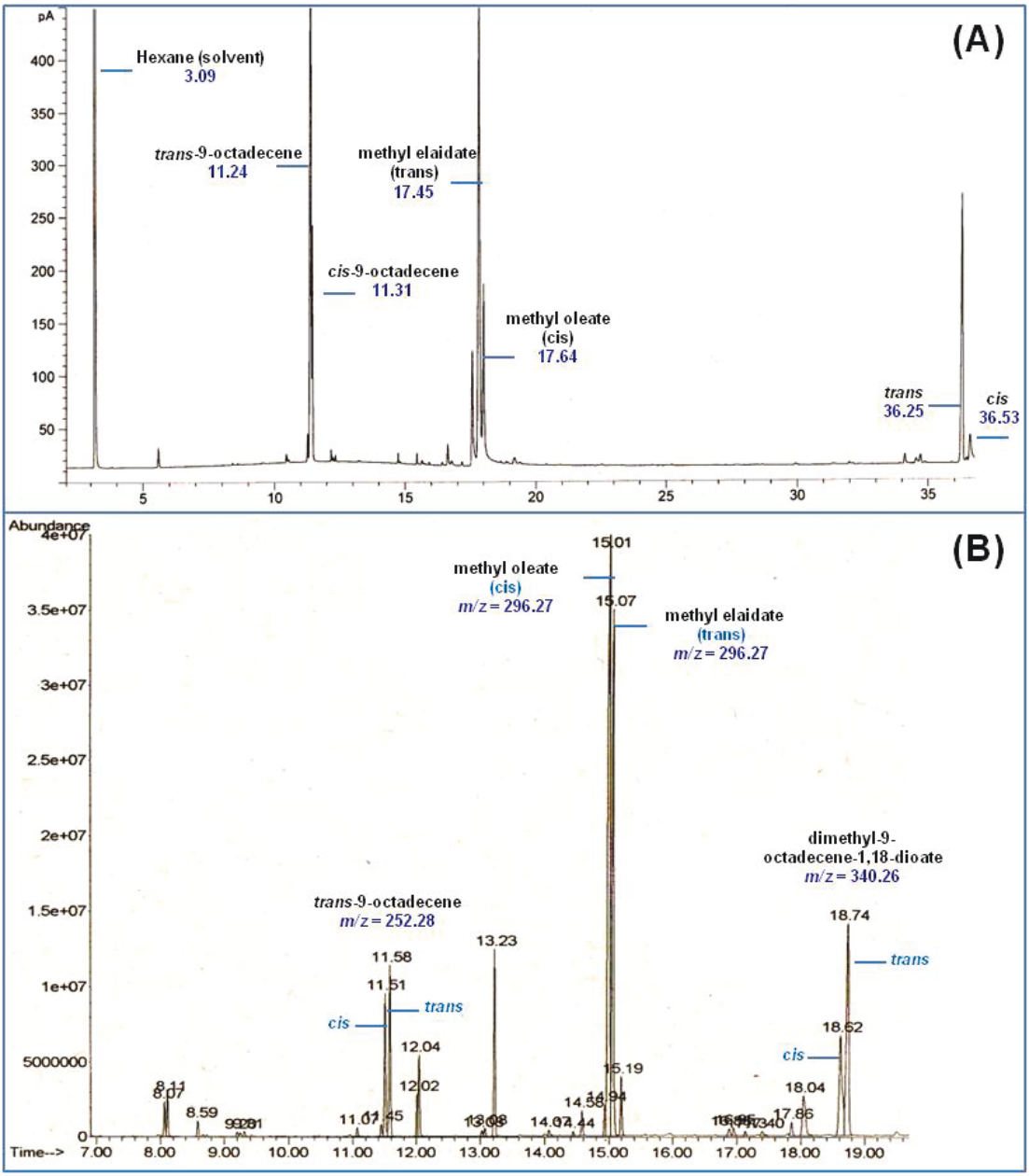

Figure 51. GC (A) and GC-MS (B) chromatograms showing metathesis reaction products in the final reaction mixture of methyl oleate self-metathesis over MTO-based catalysts

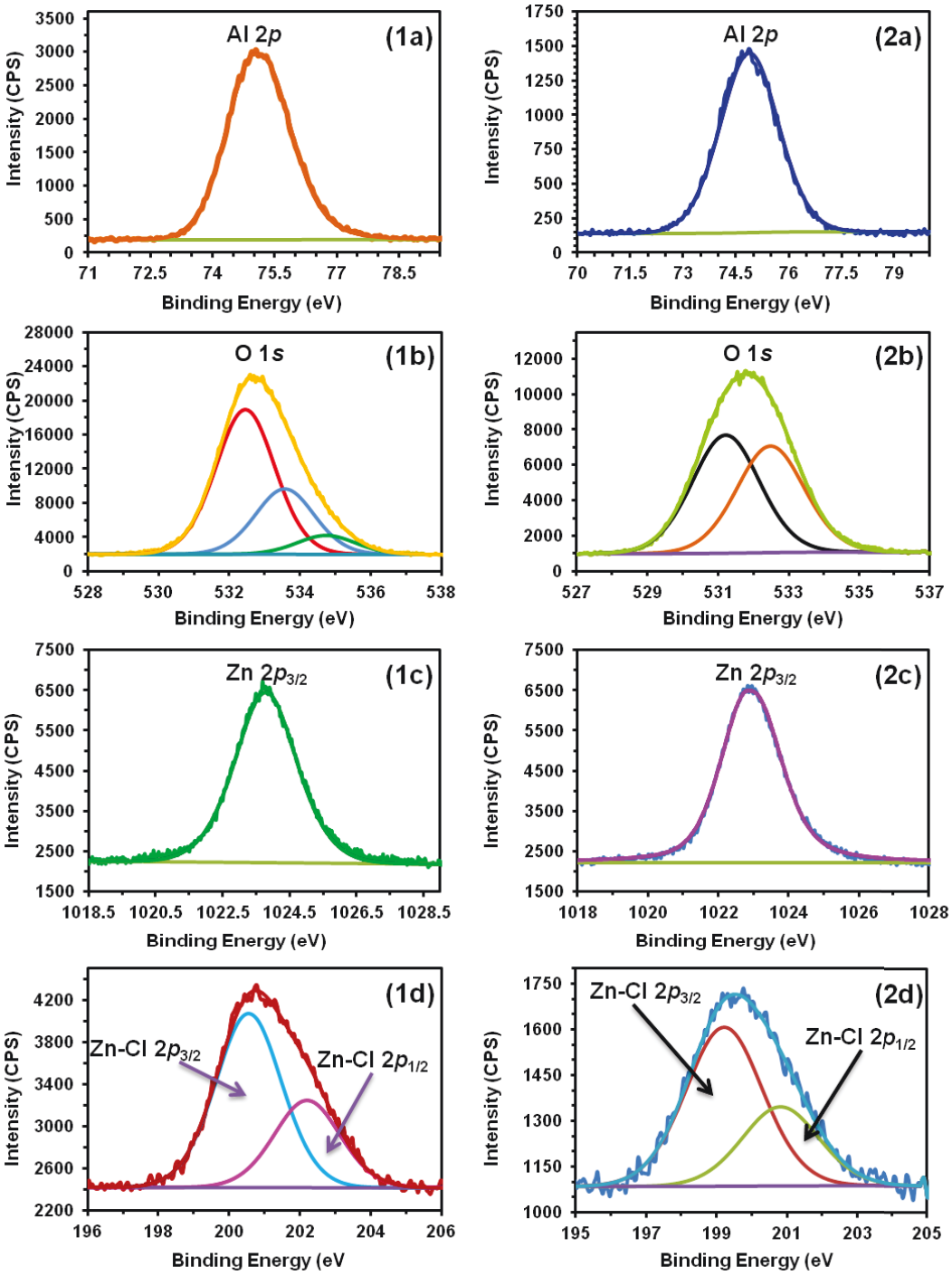

Figure 52. XPS analysis of 3 wt.% MTO/$ZnCl_2$-OMA samples prepared using $ZnCl_2$-modified OMA supports synthesized with malonic acid and $Al(OBu^s)_3$ aluminum precursor *via* (1) two-steps or (2) one-pot process: (a) Al 2*p*, (b) O 1s, (c) Zn $2p_{3/2}$ and (d) Cl $2p_{3/2}$-Cl $2p_{1/2}$ deconvoluted spectra. All shifts for the samples were corrected by normalization of the C 1*s* binding energy to 285.0 eV.

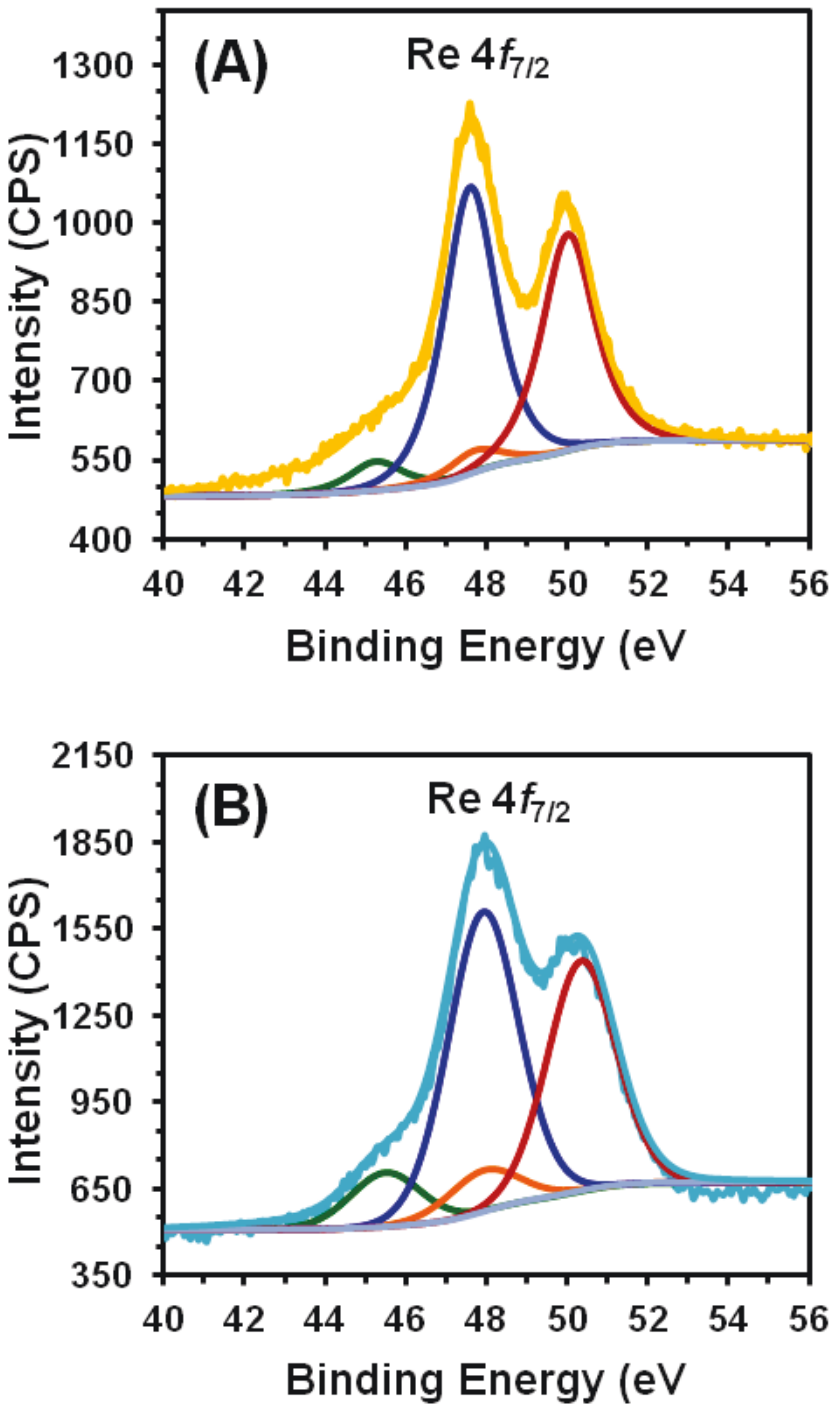

Figure 53. Re 4*f* deconvoluted XPS spectra of the 3 wt.% MTO/$ZnCl_2$-OMA catalysts samples prepared using $ZnCl_2$-modified OMA supports synthesized with tartaric acid and $Al(OPr^i)_3$ aluminum precursor *via* (A) two-steps or (B) one-pot process. All shifts for the samples were corrected by normalization of the C 1*s* binding energy to 285.0 eV.

Chapter 7: Conclusions and future outlook

Herein in this chapter, we recap the principal contributions and concluding remarks, as well as the main findings and progress achieved in this research project. In addition, we present future research opportunities.

7.1. General conclusions

The main targeted objective of this research project is to design an efficient, highly active and well-defined metathesis catalyst, aiming to improve the MTO-based catalyst performance towards bulky functionalized olefin metathesis (*e.g.* methyl oleate self-metathesis). Thus, overcoming the selectivity issues and expecting to enhance the metathesis reaction rate. The new catalyst design is based on using $ZnCl_2$ impregnated on hexagonal well-organized mesoporous alumina ($ZnCl_2$-modified OMA) as a suitable support for the MTO-based catalysts, especially when used for the conversion of bulky functionalized substrates. The present work is divided into two main parts depending on the strategy adopted for the preparation of the catalytic supports used in this study. First, a two-step process was performed for the synthesis of the alumina-based catalyst carrier, through preparation of OMA support *via* a sol-gel process and then its modification with $ZnCl_2$ *via* a wet impregnation method. The second approach consists on preparing the $ZnCl_2$-modified OMA supports *via* one-pot process through a combined sol-gel/*in situ* impregnation method. The explored strategies led to an enhancement of the MTO-based catalysts performance including the metathesis reaction rate, conversion and selectivity.

In the two-steps approach, the most challenging tasks in this first part are to prepare mesoporous alumina with highly ordered hexagonal structure and to manage the preservation of this organized structure after $ZnCl_2$ incorporation. Thus, we successful synthesized hexagonal well-ordered mesoporous alumina and $ZnCl_2$-modified alumina in a simple, versatile, and reproducible process carried out by a bottom-up approach through an sol-gel evaporation-induced self-assembly (EISA) method. The synthesis was performed using Pluronic F127 template and different carboxylic acids and aluminum precursors which are found to be controlling parameters in this sol-gel synthesis. The spectroscopic investigations on the materials growth and formation mechanism revealed that the complexation abilities of carboxylic acids with Al centers are the key factor, leading to successful well-ordered assembly process. However, the overall results and characterization showed no significant effect of the acids and precursors variation on the synthesis pathways or the obtained materials properties. The synthesis allowed the formation of well-organized mesoporous alumina materials with large specific surface area and total pore volumes, as

well as a regular narrow average pore size distribution. Interestingly, uniform mesoporous network with well-arranged cylindrical pores was observed for the newly prepared materials as shown by TEM micrographs, while the organized structure was well maintained after $ZnCl_2$ incorporation. $ZnCl_2$ greatly enhanced Lewis acidity of the supports, and Al-O-Zn-Cl species were mainly formed on the surface as illustrated with XPS and MAS NMR analysis. These acidity enhancement and surface species are believed to be the responsible for MTO grafting and performance.

The prepared organized mesoporous materials *via* two-steps approach were then evaluated as supports for the MTO-based catalysts for methyl oleate self-metathesis. High methyl oleate conversion was obtained under optimized conditions. Also, higher selectivity was achieved using the OMA supports compared to both wormhole-like alumina-based heterogeneous catalyst and the commercially available Grubbs 2nd generation homogeneous metathesis catalyst. This enhanced selectivity could be mainly due to the uniform well-structured and non-interconnected porous network. It is worth to mention that we also achieved three times higher metathesis reaction rate using the OMA-based supports compared to the wormhole-like alumina support. This is due to the enhanced mass transfer features through the hexagonal mesoporous network, and the observed improved kinetic profile was comparable to that obtained using the Grubbs 2nd generation catalyst. Furthermore, this enhanced reaction rate could be one of the reasons behind the improved selectivity, reducing the residence time inside the porous network, then not giving enough time for the side reaction to occur (methyl elaidate formation). The mechanistic investigations revealed that it is impossible to achieve quantitative methyl oleate conversion and desired metathesis reaction products selectivity, which are due to the unpreventable regeneration pathway of methyl oleate and the inescapable methyl elaidate formation route (non-productive metathesis reaction), respectively. The enhancements reported in this study using the newly designed catalyst are considered very satisfactory results.

For the second approach, the new one-pot methodology that we have developed is this project for the synthesis of the $ZnCl_2$-modified OMA supports is highly efficient, through a combined OMA synthesis and in situ $ZnCl_2$ incorporation with a single annealing step. This

synthesis strategy is rapid simple and cost-effective, and offers access to $ZnCl_2$-modified OMA supports with better features and higher synthesis yields compared to the two-steps approach. These enhanced properties including textural (*e.g.* larger surface area) and highly dispersed active surface sites (e.g. due to lower dehydroxylation rate) led to improved methyl oleate self-metathesis performance (conversion and selectivity) of the MTO-based catalysts. Therefore, the activity of the MTO-based catalysts supported on one-pot prepared supports outperformed the MTO-based catalysts supported on conventionally two-steps synthesized supports. These results are very promising towards opening up future opportunities for robust heterogeneous catalysts design as well as towards large-scale applications. However, both conventionally and one-pot synthesized supports led to the generation of similar Re-based carbenic surface species.

In summary, herein we demonstrated in this study that the catalytic supports, particularly for porous systems, evidently play the key role in the catalytic activity of supported catalyst and their robustness. Therefore, several parameters can control the reaction rate and selectivity including the uniformity of pore channels, pores structure and interconnectivity of porous network. However, the total pore volume, pore cavity/diameter and size enabling an efficient grafting of active species and diffusion of bulky functionalized substrates avoiding pore blocking phenomena are also important factors to be considered in the design of efficient heterogeneous catalytic systems. In addition to the improved substrates (methyl oleate) accessibility to active surface sites, optimization of these sites availability and efficiency is another key factor towards improving the catalysts performance. Herein, we showed that larger specific surface area allowed better activity via increasing the MTO loading, leading to higher active sites concentration. Also, the enhanced surface species of $ZnCl_2$-modified OMA supports including efficient Zn-based species grafting as well as lower dehydroxylation rate (one-pot synthesis) allowed better impregnation of MTO and enhanced synergetic effect. However, the highly organized structure of the $ZnCl_2$-modified OMA supports is the main factor contributing to enhanced MTO-based active surface sites population. Unlike tortuous channels of wormhole-like alumina support, the straight OMA channels allowed more exposed active MTO surface sites which enhance the reaction rate and the efficiency of the loaded MTO molecules, particularly when used for the conversion of such bulky functionalized substrates like methyl oleate.

7.2. Future outlook

Looking ahead, many challenges in the development of robust (metathesis) catalysts remain. Herein, we propose some interesting recommendations and research opportunities which can be further pursued and explored in the future:

(i) The catalysts developed in this project exhibit a high performance for metathesis reaction of bulky functionalized molecules. The obtained methyl oleate self-metathesis products are interesting symmetrical monomers for the synthesis of ecofriendly bio-based polymers (*e.g.* bioplastics, biosurfactants, *etc.*). Thus, it is worth to evaluate the developed catalysts for other metathesis reaction applications using various bulky functionalized substrates towards the synthesis of diverse symmetrical building polymer blocks *via* self-metathesis strategy. Also, interesting asymmetrical blocks can be accessed *via* bulky functionalized substrates cross-metathesis approach with small simple or other bulky functionalized molecules.

(ii) Further comparison of catalytic performance of the prepared organized mesoporous alumina with that of commercial alumina should be investigated for this catalyst as well as other catalysts and catalytic applications. Moreover, the successful synthesis approaches developed herein are key points to elaborate a promising strategy for the synthesis and functionalization of various novel metal-doped well-organized supports. Moreover, they can pave the way to explore opportunities for the large-scale production of a wide range of these interesting organized modified-mesoporous materials as catalytic supports or adsorbents. Theses ordered materials are potential candidates as catalysts supports not only of bulky functionalized molecules metathesis reaction, but it can also be adopted for other heterogeneous catalytic reactions (*e.g.* dehydrogenation, catalytic polymerization, *etc.*), particularly when shape-selectivity is critical. Furthermore, these promising catalytic supports can be used for the development of other supported metathesis catalysts using other metathesis active species than MTO, such as metal carbides (*e.g.* tungsten, molybdenum carbides, *etc.*) or even for the heterogenization of homogeneous catalysts (*e.g.* Grubbs', Hoveyda-Grubbs catalysts, *etc.*) *via* covalent bonding to the OMA supports.

(iii) As suggested above, these supports can be used for the conversion and the synthesis of bulkier molecules than methyl oleate through various catalytic applications. However, with increased molecular size of substrates, intermediates, active species and products, these mesoporous channels may be blocked which hinder the mass transfer phenomena and the reaction kinetics. Thus, the addition of swelling agent (organic auxiliaries: fluorocarbons, trimethylbenzene (TMB) dodecylamine, *n*-heptane, *etc.*) for the synthesis of organized mesoporous materials could be an excellent alternative to obtain desired larger total pore volume and wider pore opening/diameter, but the maintenance of the organized structure will be definitely a great challenge in the presence of swelling agents.

(iv) There are still further opportunities to develop a greener metathesis reaction approach. For instance using the same catalyst and substrate, performing metathesis reaction under microwave and/or ionic liquids conditions is highly recommended and worth to study. The high cost of MTO is a limitation of the developed catalysts, thus studying the catalysts recycling and reuse is one of the tasks that should be addressed in the future. Especially, in a continuous flow system, this will be a step forward towards industrial applications of these catalysts which could be of great interest and a great achievement in this area.

(v) The newly designed MTO-based catalysts exhibited remarkable performance for methyl oleate self-metathesis. Therefore, this reaction offered access to highly important monomers, namely 9-octadecene and functionalized dimethyl-9-octadecene-1,18-dioate. These long chain unsaturated monomers are suitable starting materials for the synthesis of potential partially or fully biosourced (co)polymers. Also, these molecules are easy to handle during polymerization processes, for instance using chain limiter in order to obtain controlled average number molecular weights, which is often challenging in polymer chemistry. Interestingly, these bio-based polymers could have a wide application spectrum (*e.g.* coating, packaging, automotive, medical sectors, *etc.*), using a biodegradable matrix due to their environmental benefits, thus offering the possibility to create a sustainable industry and reduce CO_2 emissions. Unlike synthetic polymers which feedstock can be derived from petrochemicals or chemical processes. However, efforts should be made to resolve related issues such as material structures and processing, and lack the desired mechanical properties and aqueous stability. More importantly, catalytic process such as

metathesis reaction renders the production of such polymers efficient and cost-effective, particularly when using crude used vegetable oil as renewable and low-cost starting materials.

Notes and references

[1] N.K. Sidda, B. Espejo-Garcia, F.J. Lopez-Pellicer, M.Á. Latre, F.J. Zarazaga-Soria, Role of Decision Support System for Renewable Energy Outreach, Environ. Sci. Technol., 48 (2014) 15-16.

[2] T. Abbasi, S.A. Abbasi, Is the Use of Renewable Energy Sources an Answer to the Problems of Global Warming and Pollution?, Critical Reviews in Environmental Science and Technology, 42 (2011) 99-154.

[3] H. Wöhrnschimmel, M. MacLeod, K. Hungerbuhler, Emissions, Fate and Transport of Persistent Organic Pollutants to the Arctic in a Changing Global Climate, Environ. Sci. Technol., 47 (2013) 2323-2330.

[4] P. Rogers, Climate change and global warming: A new role for science in decision making, Environ. Sci. Technol., 24 (1990) 428-430.

[5] M. Asif, T. Muneer, Energy supply, its demand and security issues for developed and emerging economies, Renewable and Sustainable Energy Reviews, 11 (2007) 1388-1413.

[6] A. Chel, G. Kaushik, Renewable energy for sustainable agriculture, Agronomy Sust. Developm., 31 (2011) 91-118.

[7] Y. Hou, R. Vidu, P. Stroeve, Solar Energy Storage Methods, Ind. Eng. Chem. Res., 50 (2011) 8954-8964.

[8] J. Bozell Joseph, Chemicals and Materials from Renewable Resources, Chemicals and Materials from Renewable Resources, American Chemical Society2001, pp. 1-9.

[9] R. Narayan, Biomass (Renewable) Resources for Production of Materials, Chemicals, and Fuels, Emerging Technologies for Materials and Chemicals from Biomass, American Chemical Society1992, pp. 1-10.

[10] M. Besson, P. Gallezot, C. Pinel, Conversion of Biomass into Chemicals over Metal Catalysts, Chem. Rev., 114 (2014) 1827-1870.

[11] P.J. Deuss, K. Barta, J.G. de Vries, Homogeneous catalysis for the conversion of biomass and biomass-derived platform chemicals, Catal. Sci. Technol., 4 (2014) 1174-1196.

[12] D.M. Alonso, S.G. Wettstein, J.A. Dumesic, Bimetallic catalysts for upgrading of biomass to fuels and chemicals, Chem. Soc. Rev., 41 (2012) 8075-8098.

[13] G.W. Huber, S. Iborra, A. Corma, Synthesis of Transportation Fuels from Biomass: Chemistry, Catalysts, and Engineering, Chem. Rev., 106 (2006) 4044-4098.

[14] D. Liu, E.Y.X. Chen, Organocatalysis in biorefining for biomass conversion and upgrading, Green Chem., 16 (2014) 964-981.

[15] P.S. Shuttleworth, M. De bruyn, H.L. Parker, A.J. Hunt, V.L. Budarin, A.S. Matharu, J.H. Clark, Applications of nanoparticles in biomass conversion to chemicals and fuels, Green Chem., 16 (2014) 573-584.

[16] R.A. Sheldon, Green and sustainable manufacture of chemicals from biomass: state of the art, Green Chem., 16 (2014) 950-963.

[17] K.-i. Shimizu, A. Satsuma, Toward a rational control of solid acid catalysis for green synthesis and biomass conversion, Energy Environ. Sci., 4 (2011) 3140-3153.

[18] M. Sankar, N. Dimitratos, P.J. Miedziak, P.P. Wells, C.J. Kiely, G.J. Hutchings, Designing bimetallic catalysts for a green and sustainable future, Chem. Soc. Rev., 41 (2012) 8099-8139.

[19] C. Chatterjee, F. Pong, A. Sen, Chemical conversion pathways for carbohydrates, Green Chem., 17 (2015) 40-71.

[20] R.W. Gosselink, S.A.W. Hollak, S.-W. Chang, J. van Haveren, K.P. de Jong, J.H. Bitter, D.S. van Es, Reaction Pathways for the Deoxygenation of Vegetable Oils and Related Model Compounds, ChemSusChem, 6 (2013) 1576-1594.

[21] S. De, B. Saha, R. Luque, Hydrodeoxygenation processes: Advances on catalytic transformations of biomass-derived platform chemicals into hydrocarbon fuels, Bioresour. Technol., 178 (2015) 108-118.

[22] S.R. Collinson, W. Thielemans, The catalytic oxidation of biomass to new materials focusing on starch, cellulose and lignin, Coord. Chem. Rev., 254 (2010) 1854-1870.

[23] M.J. Climent, A. Corma, S. Iborra, Conversion of biomass platform molecules into fuel additives and liquid hydrocarbon fuels, Green Chem., 16 (2014) 516-547.

[24] S. Chikkali, S. Mecking, Refining of Plant Oils to Chemicals by Olefin Metathesis, Angew. Chem. Int. Ed., 51 (2012) 5802-5808.
[25] A. Behr, A. Westfechtel, J. Pérez Gomes, Catalytic Processes for the Technical Use of Natural Fats and Oils, Chemical Engineering & Technology, 31 (2008) 700-714.
[26] N. Popoff, E. Mazoyer, J. Pelletier, R.M. Gauvin, M. Taoufik, Expanding the scope of metathesis: a survey of polyfunctional, single-site supported tungsten systems for hydrocarbon valorization, Chem. Soc. Rev., 42 (2013) 9035-9054.
[27] K.V.S. Ranganath, S. Onitsuka, A.K. Kumar, J. Inanaga, Recent progress of N-heterocyclic carbenes in heterogeneous catalysis, Catal. Sci. Technol., 3 (2013) 2161-2181.
[28] R. Rinaldi, F. Schuth, Design of solid catalysts for the conversion of biomass, Energy Environ. Sci., 2 (2009) 610-626.
[29] L. Wang, F.-S. Xiao, Nanoporous catalysts for biomass conversion, Green Chem., 17 (2015) 24-39.
[30] H. Balcar, J. Čejka, Mesoporous molecular sieves as advanced supports for olefin metathesis catalysts, Coord. Chem. Rev., 257 (2013) 3107-3124.
[31] S. Lwin, I.E. Wachs, Olefin Metathesis by Supported Metal Oxide Catalysts, ACS Catal., 4 (2014) 2505-2520.
[32] N. Rendón, F. Blanc, C. Copéret, Well-defined silica supported metallocarbenes: Formation and reactivity, Coord. Chem. Rev., 253 (2009) 2015-2020.
[33] K.R. Jain, F.E. Kühn, Immobilization of organorhenium(VII) oxides, J. Organomet. Chem., 692 (2007) 5532-5540.
[34] F.E. Kühn, A. Scherbaum, W.A. Herrmann, Methyltrioxorhenium and its applications in olefin oxidation, metathesis and aldehyde olefination, J. Organomet. Chem., 689 (2004) 4149-4164.
[35] B. Schmidt, Methyltrioxorhenium – from oxidation and cyclopropanation to metathesis, J. Prakt. Chem./Chem.-Ztg., 339 (1997) 493-496.
[36] W.A. Herrmann, W. Wagner, U.N. Flessner, U. Volkhardt, H. Komber, Methyltrioxorhenium as Catalyst for Olefin Metathesis, Angew. Chem., Int. Ed. Engl., 30 (1991) 1636-1638.
[37] B.E. Leach, CHAPTER 1 - Industrial Catalysis: Chemistry Applied to Your Life-Style and Environment, in: B.E. Leach (Ed.) Applied Industrial Catalysis, Academic Press1983, pp. 1-30.
[38] L. Lloyd, The First Catalysts, Handbook of Industrial Catalysts, Springer US2011, pp. 23-71.
[39] C.A. Busacca, D.R. Fandrick, J.J. Song, C.H. Senanayake, The Growing Impact of Catalysis in the Pharmaceutical Industry, Adv. Synth. Catal., 353 (2011) 1825-1864.
[40] P. Howard, G. Morris, G. Sunley, Chapter 1 Introduction: Catalysis in the Chemical Industry, Metal-catalysis in Industrial Organic Processes, The Royal Society of Chemistry2006, pp. 1-22.
[41] J.G. de Vries, S.D. Jackson, Homogeneous and heterogeneous catalysis in industry, Catal. Sci. Technol., 2 (2012) 2009-2009.
[42] L.E. Manzer, Toward catalysis in the 21st century chemical industry, Catal. Today, 18 (1993) 199-207.
[43] S. Bhaduri, D. Mukesh, Chemical Industry and Homogeneous Catalysis, Homogeneous Catalysis: Mechanisms and Industrial Applications, John Wiley & Sons, Inc.2002, pp. 1-12.
[44] I. Chorkendorff, J.W. Niemantsverdriet, Introduction to Catalysis, Concepts of Modern Catalysis and Kinetics, Wiley-VCH Verlag GmbH & Co. KGaA2005, pp. 1-21.
[45] W.A. Nugent, T.V. RajanBabu, M.J. Burk, Beyond Nature's Chiral Pool: Enantioselective Catalysis in Industry, Science, 259 (1993) 479-483.
[46] H.-U. Blaser, B. Pugin, F. Spindler, Progress in enantioselective catalysis assessed from an industrial point of view, J. Mol. Catal. A: Chem., 231 (2005) 1-20.
[47] B. Cornils, W.A. Herrmann, Concepts in homogeneous catalysis: the industrial view, J. Catal., 216 (2003) 23-31.
[48] F.N. Guerzoni, J. Abbot, Cracking of an industrial feedstock over combinations of H-ZSM-5 and HY: The influence of H-ZSM-5 pretreatment, Appl. Catal., A, 120 (1994) 55-69.
[49] V. Adeeva, W.M.H. Sachtler, Mechanism of butane isomerization over industrial isomerization catalysts, Appl. Catal., A, 163 (1997) 237-243.

[50] N. Martín, M. Viniegra, R. Zarate, G. Espinosa, N. Batina, Coke characterization for an industrial Pt–Sn/γ-Al2O3 reforming catalyst, Catal. Today, 107–108 (2005) 719-725.
[51] R. Noyori, Asymmetric Catalysis: Science and Opportunities (Nobel Lecture), Angew. Chem. Int. Ed., 41 (2002) 2008-2022.
[52] W.S. Knowles, Asymmetric Hydrogenations (Nobel Lecture), Angew. Chem. Int. Ed., 41 (2002) 1998-2007.
[53] K.B. Sharpless, Searching for New Reactivity (Nobel Lecture), Angew. Chem. Int. Ed., 41 (2002) 2024-2032.
[54] A. Ault, The Nobel Prize in Chemistry for 2001, J. Chem. Educ., 79 (2002) 572.
[55] R.H. Grubbs, Olefin-Metathesis Catalysts for the Preparation of Molecules and Materials (Nobel Lecture), Angew. Chem. Int. Ed., 45 (2006) 3760-3765.
[56] R.R. Schrock, Multiple Metal–Carbon Bonds for Catalytic Metathesis Reactions (Nobel Lecture), Angew. Chem. Int. Ed., 45 (2006) 3748-3759.
[57] Y. Chauvin, Olefin Metathesis: The Early Days (Nobel Lecture), Angew. Chem. Int. Ed., 45 (2006) 3740-3747.
[58] A.M. Echavarren, Nobel Prize Awarded for Catalysis, ChemCatChem, 2 (2010) 1331-1332.
[59] A. Suzuki, Cross-Coupling Reactions Of Organoboranes: An Easy Way To Construct C□C Bonds (Nobel Lecture), Angew. Chem. Int. Ed., 50 (2011) 6722-6737.
[60] E.-i. Negishi, Magical Power of Transition Metals: Past, Present, and Future (Nobel Lecture), Angew. Chem. Int. Ed., 50 (2011) 6738-6764.
[61] Climate Change 2007: Synthesis Report: Contribution of Working Groups I, II and III to the Fourth Assessment Report of the Intergovernmental Panel on Climate Change, Cambridge University Press, Cambridge, United Kingdom and New York, NY, USA.
[62] P.T. Anastas, J.C. Warner, Green Chemistry: Theory And Practice, Oxford University Press, USA1998.
[63] P.T. Anastas, L.B. Bartlett, M.M. Kirchhoff, T.C. Williamson, The role of catalysis in the design, development, and implementation of green chemistry, Catal. Today, 55 (2000) 11-22.
[64] J.M. DeSimone, Practical Approaches to Green Solvents, Science, 297 (2002) 799-803.
[65] J.-Q. Wang, F. Cai, E. Wang, L.-N. He, Supercritical carbon dioxide and poly(ethylene glycol): an environmentally benign biphasic solvent system for aerobic oxidation of styrene, Green Chem., 9 (2007) 882-887.
[66] P.G. Jessop, Searching for green solvents, Green Chem., 13 (2011) 1391-1398.
[67] N. Yan, C. Xiao, Y. Kou, Transition metal nanoparticle catalysis in green solvents, Coord. Chem. Rev., 254 (2010) 1179-1218.
[68] L. Álvarez de Cienfuegos, R. Robles, D. Miguel, J. Justicia, J.M. Cuerva, Reduction Reactions in Green Solvents: Water, Supercritical Carbon Dioxide, and Ionic Liquids, ChemSusChem, 4 (2011) 1035-1048.
[69] I.T. Horvath, H. Mehdi, V. Fabos, L. Boda, L.T. Mika, [gamma]-Valerolactone-a sustainable liquid for energy and carbon-based chemicals, Green Chem., 10 (2008) 238-242.
[70] W. Leitner, Supercritical Carbon Dioxide as a Green Reaction Medium for Catalysis, Acc. Chem. Res., 35 (2002) 746-756.
[71] G. Centi, S. Perathoner, Catalysis and sustainable (green) chemistry, Catal. Today, 77 (2003) 287-297.
[72] M. Cvjetko Bubalo, S. Vidović, I. Radojčić Redovniković, S. Jokić, Green solvents for green technologies, J. Chem. Technol. Biotechnol., (2015) n/a-n/a.
[73] A.K. Rathi, M.B. Gawande, R. Zboril, R.S. Varma, Microwave-assisted synthesis – Catalytic applications in aqueous media, Coord. Chem. Rev., 291 (2015) 68-94.
[74] K. Sivula, F. Le Formal, M. Grätzel, Solar Water Splitting: Progress Using Hematite (α-Fe2O3) Photoelectrodes, ChemSusChem, 4 (2011) 432-449.
[75] R.A. Sheldon, I. Arends, U. Hanefeld, Green Chemistry and Catalysis, Wiley2007.
[76] J.M. Thomas, Heterogeneous Catalysis and the Challenges of Powering the Planet, Securing Chemicals for Civilised Life, and Clean Efficient Utilization of Renewable Feedstocks, ChemSusChem, 7 (2014) 1801-1832.

[77] X. Guo, Y.N. Yan, Y.H. Zhang, Y. Tang, Heterogeneously Catalytic Transformation of Biomass-Derived Sugars, Prog. Chem., 25 (2013) 1915-1927.
[78] W. Deng, Q. Zhang, Y. Wang, Catalytic transformations of cellulose and its derived carbohydrates into 5-hydroxymethylfurfural, levulinic acid, and lactic acid, Sci. China Chem., 58 (2015) 29-46.
[79] E. Lam, J.H.T. Luong, Carbon Materials as Catalyst Supports and Catalysts in the Transformation of Biomass to Fuels and Chemicals, ACS Catal., 4 (2014) 3393-3410.
[80] L. Hu, G. Zhao, W. Hao, X. Tang, Y. Sun, L. Lin, S. Liu, Catalytic conversion of biomass-derived carbohydrates into fuels and chemicals via furanic aldehydes, RSC Adv., 2 (2012) 11184-11206.
[81] Y. Nakagawa, S. Liu, M. Tamura, K. Tomishige, Catalytic Total Hydrodeoxygenation of Biomass-Derived Polyfunctionalized Substrates to Alkanes, ChemSusChem, 8 (2015) 1114-1132.
[82] Y. Nakagawa, M. Tamura, K. Tomishige, Catalytic Reduction of Biomass-Derived Furanic Compounds with Hydrogen, ACS Catal., 3 (2013) 2655-2668.
[83] T.N. Pham, T. Sooknoi, S.P. Crossley, D.E. Resasco, Ketonization of Carboxylic Acids: Mechanisms, Catalysts, and Implications for Biomass Conversion, ACS Catal., 3 (2013) 2456-2473.
[84] H. Wang, J. Male, Y. Wang, Recent Advances in Hydrotreating of Pyrolysis Bio-Oil and Its Oxygen-Containing Model Compounds, ACS Catal., 3 (2013) 1047-1070.
[85] U. Biermann, W. Friedt, S. Lang, W. Lühs, G. Machmüller, J.O. Metzger, M. Rüsch gen. Klaas, H.J. Schäfer, M.P. Schneider, New Syntheses with Oils and Fats as Renewable Raw Materials for the Chemical Industry, Angew. Chem. Int. Ed., 39 (2000) 2206-2224.
[86] U. Biermann, W. Friedt, S. Lang, W. Lühs, G. Machmüller, U.O. Metzger, M.R. Gen. Klaas, H.J. Schäfer, M.P. Schneider, New Syntheses with Oils and Fats as Renewable Raw Materials for the Chemical Industry, Biorefineries-Industrial Processes and Products, Wiley-VCH Verlag GmbH2008, pp. 253-289.
[87] C. Hu, D. Creaser, S. Siahrostami, H. Gronbeck, H. Ojagh, M. Skoglundh, Catalytic hydrogenation of C[double bond, length as m-dash]C and C[double bond, length as m-dash]O in unsaturated fatty acid methyl esters, Catal. Sci. Technol., 4 (2014) 2427-2444.
[88] C. Aouf, E. Durand, J. Lecomte, M.-C. Figueroa-Espinoza, E. Dubreucq, H. Fulcrand, P. Villeneuve, The use of lipases as biocatalysts for the epoxidation of fatty acids and phenolic compounds, Green Chem., 16 (2014) 1740-1754.
[89] Q. Bu, H. Lei, A.H. Zacher, L. Wang, S. Ren, J. Liang, Y. Wei, Y. Liu, J. Tang, Q. Zhang, R. Ruan, A review of catalytic hydrodeoxygenation of lignin-derived phenols from biomass pyrolysis, Bioresour. Technol., 124 (2012) 470-477.
[90] Y.-C. Lin, Catalytic valorization of glycerol to hydrogen and syngas, Int. J. Hydrogen Energy, 38 (2013) 2678-2700.
[91] N.H. Tran, G.S.K. Kannangara, Conversion of glycerol to hydrogen rich gas, Chem. Soc. Rev., 42 (2013) 9454-9479.
[92] Y. Kwon, M.T.M. Koper, Electrocatalytic Hydrogenation and Deoxygenation of Glucose on Solid Metal Electrodes, ChemSusChem, 6 (2013) 455-462.
[93] J. Zhang, S. Wu, Y. Liu, B. Li, Hydrogenation of glucose over reduced Ni/Cu/Al hydrotalcite precursors, Catal. Commun., 35 (2013) 23-26.
[94] V.V. Ordomsky, V.L. Sushkevich, J.C. Schouten, J. van der Schaaf, T.A. Nijhuis, Glucose dehydration to 5-hydroxymethylfurfural over phosphate catalysts, J. Catal., 300 (2013) 37-46.
[95] J. He, Y. Zhang, E.Y.X. Chen, Chromium(0) Nanoparticles as Effective Catalyst for the Conversion of Glucose into 5-Hydroxymethylfurfural, ChemSusChem, 6 (2013) 61-64.
[96] S. Despax, B. Estrine, N. Hoffmann, J. Le Bras, S. Marinkovic, J. Muzart, Isomerization of d-glucose into d-fructose with a heterogeneous catalyst in organic solvents, Catal. Commun., 39 (2013) 35-38.
[97] F. Wang, H.-Z. Wu, C.-L. Liu, R.-Z. Yang, W.-S. Dong, Catalytic dehydration of fructose to 5-hydroxymethylfurfural over Nb2O5 catalyst in organic solvent, Carbohydr. Res., 368 (2013) 78-83.
[98] E. Smolentseva, B.T. Kusema, S. Beloshapkin, M. Estrada, E. Vargas, D.Y. Murzin, F. Castillon, S. Fuentes, A. Simakov, Selective oxidation of arabinose to arabinonic acid over Pd–Au catalysts supported on alumina and ceria, Appl. Catal., A, 392 (2011) 69-79.

[99] B.T. Kusema, B.C. Campo, O.A. Simakova, A.-R. Leino, K. Kordás, P. Mäki-Arvela, T. Salmi, D.Y. Murzin, Selective Oxidation of D-Galactose over Gold Catalysts, ChemCatChem, 3 (2011) 1789-1798.
[100] S. Malik, A. Ghosh, K. Mukherjee, B. Saha, Combination of Best Promoter and Micellar Catalyst for Cr(VI) Oxidation of Lactose to Lactobionic Acid in Aqueous Medium at Room Temperature, Tenside Surfactants Detergents, 51 (2014) 325-332.
[101] N. Meyer, M. Devillers, S. Hermans, Boron nitride supported Pd catalysts for the hydrogenation of lactose, Catal. Today, 241, Part B (2015) 200-207.
[102] C. Aouf, D. Harakat, J. Muzart, B. Estrine, S. Marinkovic, C. Ernenwein, J. Le Bras, Low Catalyst Loadings for the Production of Carboxylic Acids from Polysaccharides and Hydrogen Peroxide, ChemSusChem, 3 (2010) 1200-1203.
[103] Y. Sugano, M.d.C. Vestergaard, M. Saito, E. Tamiya, A carbon nanotube structured biomimetic catalyst for polysaccharide degradation, Chem. Commun., 47 (2011) 7176-7178.
[104] K.-i. Shimizu, H. Furukawa, N. Kobayashi, Y. Itaya, A. Satsuma, Effects of Bronsted and Lewis acidities on activity and selectivity of heteropolyacid-based catalysts for hydrolysis of cellobiose and cellulose, Green Chem., 11 (2009) 1627-1632.
[105] L. Hu, L. Lin, Z. Wu, S. Zhou, S. Liu, Chemocatalytic hydrolysis of cellulose into glucose over solid acid catalysts, Appl. Catal., B, 174–175 (2015) 225-243.
[106] W. Deng, M. Liu, X. Tan, Q. Zhang, Y. Wang, Conversion of cellobiose into sorbitol in neutral water medium over carbon nanotube-supported ruthenium catalysts, J. Catal., 271 (2010) 22-32.
[107] M. Liu, W. Deng, Q. Zhang, Y. Wang, Y. Wang, Polyoxometalate-supported ruthenium nanoparticles as bifunctional heterogeneous catalysts for the conversions of cellobiose and cellulose into sorbitol under mild conditions, Chem. Commun., 47 (2011) 9717-9719.
[108] X. Tan, W. Deng, M. Liu, Q. Zhang, Y. Wang, Carbon nanotube-supported gold nanoparticles as efficient catalysts for selective oxidation of cellobiose into gluconic acid in aqueous medium, Chem. Commun., (2009) 7179-7181.
[109] J. Zhang, X. Liu, M.N. Hedhili, Y. Zhu, Y. Han, Highly Selective and Complete Conversion of Cellobiose to Gluconic Acid over Au/Cs2HPW12O40 Nanocomposite Catalyst, ChemCatChem, 3 (2011) 1294-1298.
[110] Y. Nakagawa, K. Tomishige, Total hydrogenation of furan derivatives over silica-supported Ni–Pd alloy catalyst, Catal. Commun., 12 (2010) 154-156.
[111] N.-T. Le, P. Lakshmanan, K. Cho, Y. Han, H. Kim, Selective oxidation of 5-hydroxymethyl-2-furfural into 2,5-diformylfuran over VO2+ and Cu2+ ions immobilized on sulfonated carbon catalysts, Appl. Catal., A, 464–465 (2013) 305-312.
[112] B. Karimi, H.M. Mirzaei, E. Farhangi, Fe3O4@SiO2–TEMPO as a Magnetically Recyclable Catalyst for Highly Selective Aerobic Oxidation of 5-Hydroxymethylfurfural into 2,5-Diformylfuran under Metal- and Halogen-Free Conditions, ChemCatChem, 6 (2014) 758-762.
[113] A. Jain, S.C. Jonnalagadda, K.V. Ramanujachary, A. Mugweru, Selective oxidation of 5-hydroxymethyl-2-furfural to furan-2,5-dicarboxylic acid over spinel mixed metal oxide catalyst, Catal. Commun., 58 (2015) 179-182.
[114] K. Xiong, W.-S. Lee, A. Bhan, J.G. Chen, Molybdenum Carbide as a Highly Selective Deoxygenation Catalyst for Converting Furfural to 2-Methylfuran, ChemSusChem, 7 (2014) 2146-2149.
[115] Y. Yang, Z. Du, Y. Huang, F. Lu, F. Wang, J. Gao, J. Xu, Conversion of furfural into cyclopentanone over Ni-Cu bimetallic catalysts, Green Chem., 15 (2013) 1932-1940.
[116] X.-L. Li, J. Deng, J. Shi, T. Pan, C.-G. Yu, H.-J. Xu, Y. Fu, Selective conversion of furfural to cyclopentanone or cyclopentanol using different preparation methods of Cu-Co catalysts, Green Chem., 17 (2015) 1038-1046.
[117] S. Liu, Y. Amada, M. Tamura, Y. Nakagawa, K. Tomishige, One-pot selective conversion of furfural into 1,5-pentanediol over a Pd-added Ir-ReOx/SiO2 bifunctional catalyst, Green Chem., 16 (2014) 617-626.
[118] M.M. Villaverde, N.M. Bertero, T.F. Garetto, A.J. Marchi, Selective liquid-phase hydrogenation of furfural to furfuryl alcohol over Cu-based catalysts, Catal. Today, 213 (2013) 87-92.

[119] M. Signoretto, F. Menegazzo, L. Contessotto, F. Pinna, M. Manzoli, F. Boccuzzi, Au/ZrO2: an efficient and reusable catalyst for the oxidative esterification of renewable furfural, Appl. Catal., B, 129 (2013) 287-293.
[120] J. Le Nôtre, J. van Haveren, D.S. van Es, Synthesis of Isoidide through Epimerization of Isosorbide using Ruthenium on Carbon, ChemSusChem, 6 (2013) 693-700.
[121] A. Lerchner, S. Achatz, C. Rausch, T. Haas, A. Skerra, Coupled Enzymatic Alcohol-to-Amine Conversion of Isosorbide using Engineered Transaminases and Dehydrogenases, ChemCatChem, 5 (2013) 3374-3383.
[122] J. Holladay, T. Werpy, D. Muzatko, Catalytic hydrogenation of glutamic acid, Appl. Biochem. Biotechnol., 115 (2004) 857-869.
[123] J. Le Nôtre, S.C.M. Witte-van Dijk, J. van Haveren, E.L. Scott, J.P.M. Sanders, Synthesis of Bio-Based Methacrylic Acid by Decarboxylation of Itaconic Acid and Citric Acid Catalyzed by Solid Transition-Metal Catalysts, ChemSusChem, 7 (2014) 2712-2720.
[124] L. Li, S. Liu, J. Xu, S. Yu, F. Liu, C. Xie, X. Ge, J. Ren, Esterification of itaconic acid using Ln∼SO42−/TiO2–SiO2 (Ln = La3+, Ce4+, Sm3+) as catalysts, J. Mol. Catal. A: Chem., 368–369 (2013) 24-30.
[125] I. Volovych, M. Schwarze, T. Hamerla, J. Blum, R. Schomäcker, Enantioselective hydrogenation of itaconic acid and its derivates with sol–gel immobilized Rh/BPPM catalysts, J. Mol. Catal. A: Chem., 366 (2013) 359-367.
[126] C. Tang, J. Peng, X. Li, Z. Zhai, W. Bai, N. Jiang, H. Gao, Y. Liao, Efficient and selective conversion of lactic acid into acetaldehyde using a mesoporous aluminum phosphate catalyst, Green Chem., 17 (2015) 1159-1166.
[127] Y. Takeda, T. Shoji, H. Watanabe, M. Tamura, Y. Nakagawa, K. Okumura, K. Tomishige, Selective Hydrogenation of Lactic Acid to 1,2-Propanediol over Highly Active Ruthenium–Molybdenum Oxide Catalysts, ChemSusChem, (2014) n/a-n/a.
[128] J. Zhang, Y. Zhao, X. Feng, M. Pan, J. Zhao, W. Ji, C.-T. Au, Na2HPO4-modified NaY nanocrystallites: efficient catalyst for acrylic acid production through lactic acid dehydration, Catal. Sci. Technol., 4 (2014) 1376-1385.
[129] K.-T. Li, C.-K. Wang, Esterification of lactic acid over TiO2–Al2O3 catalysts, Appl. Catal., A, 433–434 (2012) 275-279.
[130] A.M. Ruppert, J. Grams, M. Jędrzejczyk , J. Matras-Michalska, N. Keller, K. Ostojska, P. Sautet, Titania-Supported Catalysts for Levulinic Acid Hydrogenation: Influence of Support and its Impact on γ-Valerolactone Yield, ChemSusChem, (2015) n/a-n/a.
[131] P.P. Upare , J.-M. Lee, Y.K. Hwang , D.W. Hwang, J.-H. Lee, S.B. Halligudi, J.-S. Hwang, J.-S. Chang Direct Hydrocyclization of Biomass-Derived Levulinic Acid to 2-Methyltetrahydrofuran over Nanocomposite Copper/Silica Catalysts, ChemSusChem, 4 (2011) 1749-1752.
[132] Y. Kuwahara, W. Kaburagi, K. Nemoto, T. Fujitani, Esterification of levulinic acid with ethanol over sulfated Si-doped ZrO2 solid acid catalyst: Study of the structure–activity relationships, Appl. Catal., A, 476 (2014) 186-196.
[133] C. Delhomme, S.L.M. Goh, F.E. Kühn, D. Weuster-Botz, Esterification of bio-based succinic acid in biphasic systems: Comparison of chemical and biological catalysts, J. Mol. Catal. B: Enzym., 80 (2012) 39-47.
[134] U.G. Hong, J.K. Kim, J. Lee, J.K. Lee, J.H. Song, J. Yi, I.K. Song, Hydrogenation of succinic acid to tetrahydrofuran over ruthenium-carbon composite catalysts: Effect of HCl concentration in the preparation of the catalysts, J. Ind. Eng. Chem., 20 (2014) 3834-3840.
[135] K.H. Kang, U.G. Hong, Y. Bang, J.H. Choi, J.K. Kim, J.K. Lee, S.J. Han, I.K. Song, Hydrogenation of succinic acid to 1,4-butanediol over Re–Ru bimetallic catalysts supported on mesoporous carbon, Appl. Catal., A, 490 (2015) 153-162.
[136] U.G. Hong, H.W. Park, J. Lee, S. Hwang, I.K. Song, Hydrogenation of succinic acid to γ-butyrolactone (GBL) over ruthenium catalyst supported on surfactant-templated mesoporous carbon, J. Ind. Eng. Chem., 18 (2012) 462-468.

[137] S. Yang, M. Besson, C. Descorme, Catalytic wet air oxidation of succinic acid over Ru and Pt catalysts supported on CexZr1 − xO2 mixed oxides, Appl. Catal., B, 165 (2015) 1-9.
[138] W.-C. Wang, C.-J. Bai, N. Thapaliya, The production of renewable transportation fuel through fed-batch and continuous deoxygenation of vegetable oil derived fatty acids over Pd/C catalyst, Int. J. Energy Res., (2015) DOI: 10.1002/er.3309.
[139] S. Verma, M. Aila, S. Kaul, S.L. Jain, Immobilized oxo-vanadium Schiff base on graphene oxide as an efficient and recyclable catalyst for the epoxidation of fatty acids and esters, RSC Adv., 4 (2014) 30598-30604.
[140] T. Khlebnikova, Z. Pai, L. Fedoseeva, Y. Mattsat, Catalytic oxidation of fatty acids. II. Epoxidation and oxidative cleavage of unsaturated fatty acid esters containing additional functional groups, React. Kinet. Catal. Lett., 98 (2009) 9-17.
[141] H. Bonin, A. Keraani, J.-L. Dubois, M. Brandhorst, C. Fischmeister, C. Bruneau, Cross-metathesis of fatty acid methyl esters with acrolein: An entry to a variety of bifunctional compounds, Eur. J. Lipid Sci. Technol., 117 (2015) 209-216.
[142] E.M. Santos, A.P.d.C. Teixeira, F.G. da Silva, T.E. Cibaka, M.H. Araújo, W.X.C. Oliveira, F. Medeiros, A.N. Brasil, L.S. de Oliveira, R.M. Lago, New heterogeneous catalyst for the esterification of fatty acid produced by surface aromatization/sulfonation of oilseed cake, Fuel, 150 (2015) 408-414.
[143] V. Udayakumar, A. Pandurangan, Catalytic activity of mesoporous V/SBA-15 in the transesterification and esterification of fatty acids, J. Porous Mater., 21 (2014) 921-931.
[144] N. Weber, P. Weitkamp, K.D. Mukherjee, Fatty Acid Steryl, Stanyl, and Steroid Esters by Esterification and Transesterification in Vacuo Using Candida rugosa Lipase as Catalyst, J. Agric. Food. Chem., 49 (2001) 67-71.
[145] K. Kon, W. Onodera, S. Takakusagi, K.-i. Shimizu, Hydrodeoxygenation of fatty acids and triglycerides by Pt-loaded Nb2O5 catalysts, Catal. Sci. Technol., 4 (2014) 3705-3712.
[146] N. Mo, P.E. Savage, Hydrothermal Catalytic Cracking of Fatty Acids with HZSM-5, ACS Sustainable Chem. Eng., 2 (2014) 88-94.
[147] H. Iida, D. Itoh, S. Minowa, A. Yanagisawa, A. Igarashi, Hydrogenation of soybean oil over various platinum catalysts: Effects of support materials on trans fatty acid levels, Catal. Commun., 62 (2015) 1-5.
[148] L. He, H. Cheng, G. Liang, Y. Yu, F. Zhao, Effect of structure of CuO/ZnO/Al2O3 composites on catalytic performance for hydrogenation of fatty acid ester, Appl. Catal., A, 452 (2013) 88-93.
[149] N.T. Fairweather, M.S. Gibson, H. Guan, Homogeneous Hydrogenation of Fatty Acid Methyl Esters and Natural Oils under Neat Conditions, Organometallics, 34 (2015) 335-339.
[150] G. Onyestyák, S. Harnos, D. Kalló, Indium, as an efficient co-catalyst of Cu/Al2O3 in the selective hydrogenation of biomass derived fatty acids to alcohols, Catal. Commun., 26 (2012) 19-24.
[151] D.J. Ostgard, R. Olindo, M. Berweiler, S. Röder, T. Tacke, The chemoselective hydrogenation of tallow nitriles to unsaturated 1° fatty amines with carbon modified Ni catalysts, Catal. Today, 121 (2007) 106-114.
[152] S.C.C. Wiedemann, J.A. Stewart, F. Soulimani, T. van Bergen-Brenkman, S. Langelaar, B. Wels, P. de Peinder, P.C.A. Bruijnincx, B.M. Weckhuysen, Skeletal isomerisation of oleic acid over ferrierite in the presence and absence of triphenylphosphine: Pore mouth catalysis and related deactivation mechanisms, J. Catal., 316 (2014) 24-35.
[153] K. Komura, Y. Nakano, M. Koketsu, Mesoporous silica MCM-41 as a highly active, recoverable and reusable catalyst for direct amidation of fatty acids and long-chain amines, Green Chem., 13 (2011) 828-831.
[154] N. Laosiripojana, W. Kiatkittipong, S. Charojrochkul, S. Assabumrungrat, Effects of support and co-fed elements on steam reforming of palm fatty acid distillate (PFAD) over Rh-based catalysts, Appl. Catal., A, 383 (2010) 50-57.
[155] A. Acevedo, S. Fomine, S. Gutiérrez, M.A. Tlenkopatchev, Metathesis of terpenes using the second generation Grubbs Ru–alkylidene catalysts: Computational modeling, J. Organomet. Chem., 765 (2014) 17-22.

[156] S. Fomine, M.A. Tlenkopatchev, Metathesis transformations of terpenes. Computational modeling of (−)-α-pinene ring opening by ruthenium and tungsten carbene catalysts, J. Organomet. Chem., 701 (2012) 68-74.
[157] S. Liu, L. Zhou, S. Yu, C. Xie, F. Liu, Z. Song, Polymerization of α-pinene using Lewis acidic ionic liquid as catalyst for production of terpene resin, Biomass Bioenergy, 57 (2013) 238-242.
[158] P.A. Robles-Dutenhefner, K.A. da Silva Rocha, E.M.B. Sousa, E.V. Gusevskaya, Cobalt-catalyzed oxidation of terpenes: Co-MCM-41 as an efficient shape-selective heterogeneous catalyst for aerobic oxidation of isolongifolene under solvent-free conditions, J. Catal., 265 (2009) 72-79.
[159] M.L. Casella, G.F. Santori, A. Moglioni, V. Vetere, J.F. Ruggera, G.M. Iglesias, O.A. Ferretti, Stereoselective hydrogenation of terpenes using platinum-based catalysts, Appl. Catal., A, 318 (2007) 1-8.
[160] F. Zaccheria, N. Ravasio, A. Fusi, M. Rodondi, R. Psaro, Tuning Selectivity in Terpene Chemistry: Selective Hydrogenation versus Cascade Reactions over Copper Catalysts, Adv. Synth. Catal., 347 (2005) 1267-1272.
[161] A. Celik, S.L. Flitsch, N.J. Turner, Efficient terpene hydroxylation catalysts based upon P450 enzymes derived from Actinomycetes, Org. Biomol. Chem., 3 (2005) 2930-2934.
[162] V. Maraval, J.-E. Ancel, B. Meunier, Manganese(III) Porphyrin Catalysts for the Oxidation of Terpene Derivatives: A Comparative Study, J. Catal., 206 (2002) 349-357.
[163] M. Guidotti, L. Conti, A. Fusi, N. Ravasio, R. Psaro, Diastereoselective epoxidation of hydroxy-containing unsaturated terpenes on heterogeneous titanium-catalyst, J. Mol. Catal. A: Chem., 182–183 (2002) 151-156.
[164] P. Lesage, J.-P. Candy, C. Hirigoyen, F. Humblot, M. Leconte, J.-M. Basset, An example of the valorization of terpenes: The selective isomerization of 3-carene to 2-carene in the presence of silica supported nickel catalysts modified by tetrabutyl tin, J. Mol. Catal. A: Chem., 112 (1996) 303-309.
[165] L. Kollár, J. Bakos, B. Heil, P. Sándor, G. Szalontai, Hydroformylation of chiral terpenes with PtCl(SnCl3)-(bis-phosphine) as catalyst, J. Organomet. Chem., 385 (1990) 147-152.
[166] M.-Y. Chen, Y.-B. Huang, H. Pang, X.-X. Liu, Y. Fu, Hydrodeoxygenation of lignin-derived phenols into alkanes over carbon nanotube supported Ru catalysts in biphasic systems, Green Chem., 17 (2015) 1710-1717.
[167] C. Zhang, J. Xing, L. Song, H. Xin, S. Lin, L. Xing, X. Li, Aqueous-phase hydrodeoxygenation of lignin monomer eugenol: Influence of Si/Al ratio of HZSM-5 on catalytic performances, Catal. Today, 234 (2014) 145-152.
[168] B. Sedai, C. Díaz-Urrutia, R.T. Baker, R. Wu, L.A.P. Silks, S.K. Hanson, Aerobic Oxidation of β-1 Lignin Model Compounds with Copper and Oxovanadium Catalysts, ACS Catal., 3 (2013) 3111-3122.
[169] A.J.R. Hensley, Y. Wang, J.-S. McEwen, Phenol Deoxygenation Mechanisms on Fe(110) and Pd(111), ACS Catal., 5 (2015) 523-536.
[170] R. Trane-Restrup, A.D. Jensen, Steam reforming of cyclic model compounds of bio-oil over Ni-based catalysts: Product distribution and carbon formation, Appl. Catal., B, 165 (2015) 117-127.
[171] H.A. Meylemans, T.J. Groshens, B.G. Harvey, Synthesis of Renewable Bisphenols from Creosol, ChemSusChem, 5 (2012) 206-210.
[172] X. Gao, S. Zhu, Y. Li, Graphene oxide as a facile solid acid catalyst for the production of bioadditives from glycerol esterification, Catal. Commun., 62 (2015) 48-51.
[173] M. Popova, A. Szegedi, A. Ristic, N.N. Tusar, Glycerol acetylation on mesoporous KIL-2 supported sulphated zirconia catalysts, Catal. Sci. Technol., 4 (2014) 3993-4000.
[174] S. Sandesh, A.B. Halgeri, G.V. Shanbhag, Utilization of renewable resources: Condensation of glycerol with acetone at room temperature catalyzed by organic–inorganic hybrid catalyst, J. Mol. Catal. A: Chem., 401 (2015) 73-80.
[175] M. Dalil, D. Carnevali, J.-L. Dubois, G.S. Patience, Transient acrolein selectivity and carbon deposition study of glycerol dehydration over WO3/TiO2 catalyst, Chem. Eng. J., 270 (2015) 557-563.

[176] A. Ciftci, D.A.J.M. Ligthart, E.J.M. Hensen, Influence of Pt particle size and Re addition by catalytic reduction on aqueous phase reforming of glycerol for carbon-supported Pt(Re) catalysts, Appl. Catal., B, 174–175 (2015) 126-135.
[177] L. Liu, B. Wang, Y. Du, Z. Zhong, A. Borgna, Bifunctional Mo3VOx/H4SiW12O40/Al2O3 catalysts for one-step conversion of glycerol to acrylic acid: Catalyst structural evolution and reaction pathways, Appl. Catal., B, 174–175 (2015) 1-12.
[178] F. Mauriello, H. Ariga, M.G. Musolino, R. Pietropaolo, S. Takakusagi, K. Asakura, Exploring the catalytic properties of supported palladium catalysts in the transfer hydrogenolysis of glycerol, Appl. Catal., B, 166–167 (2015) 121-131.
[179] C. Xu, Y. Du, C. Li, J. Yang, G. Yang, Insight into effect of acid/base nature of supports on selectivity of glycerol oxidation over supported Au-Pt bimetallic catalysts, Appl. Catal., B, 164 (2015) 334-343.
[180] S.E. Kondawar, A.S. Potdar, C.V. Rode, Solvent-free carbonylation of glycerol with urea using metal loaded MCM-41 catalysts, RSC Adv., 5 (2015) 16452-16460.
[181] L.P. Ozorio, R. Pianzolli, L. da Cruz Machado, J.L. Miranda, C.C. Turci, A.C.O. Guerra, E.F. Souza-Aguiar, C.J.A. Mota, Metal-impregnated zeolite Y as efficient catalyst for the direct carbonation of glycerol with CO2, Appl. Catal., A, In Press (2014) doi:10.1016/j.apcata.2014.1012.1010.
[182] A. Ibhadon, P. Fitzpatrick, Heterogeneous Photocatalysis: Recent Advances and Applications, Catalysts, 3 (2013) 189-218.
[183] G. Palmisano, V. Augugliaro, M. Pagliaro, L. Palmisano, Photocatalysis: a promising route for 21st century organic chemistry, Chem. Commun., (2007) 3425-3437.
[184] G. Palmisano, E. Garcia-Lopez, G. Marci, V. Loddo, S. Yurdakal, V. Augugliaro, L. Palmisano, Advances in selective conversions by heterogeneous photocatalysis, Chem. Commun., 46 (2010) 7074-7089.
[185] Z. Liu, Y. Jin, F. Teng, X. Hua, M. Chen, An efficient Ce-doped MoO3 catalyst and its photo-thermal catalytic synergetic degradation performance for dye pollutant, Catal. Commun., 66 (2015) 42-45.
[186] R. Sugrañez, J. Balbuena, M. Cruz-Yusta, F. Martín, J. Morales, L. Sánchez, Efficient behaviour of hematite towards the photocatalytic degradation of NOx gases, Appl. Catal., B, 165 (2015) 529-536.
[187] X. Auvray, L. Olsson, Stability and activity of Pd-, Pt- and Pd–Pt catalysts supported on alumina for NO oxidation, Appl. Catal., B, 168–169 (2015) 342-352.
[188] G. Dong, W. Ho, L. Zhang, Photocatalytic NO removal on BiOI surface: The change from nonselective oxidation to selective oxidation, Appl. Catal., B, 168–169 (2015) 490-496.
[189] L. Liao, S. Heylen, B. Vallaey, M. Keulemans, S. Lenaerts, M.B.J. Roeffaers, J.A. Martens, Photocatalytic carbon oxidation with nitric oxide, Appl. Catal., B, 166–167 (2015) 374-380.
[190] J. Quiroz Torres, S. Royer, J.-P. Bellat, J.-M. Giraudon, J.-F. Lamonier, Formaldehyde: Catalytic Oxidation as a Promising Soft Way of Elimination, ChemSusChem, 6 (2013) 578-592.
[191] S. Jiang, E.S. Handberg, F. Liu, Y. Liao, H. Wang, Z. Li, S. Song, Effect of doping the nitrogen into carbon nanotubes on the activity of NiO catalysts for the oxidation removal of toluene, Appl. Catal., B, 160–161 (2014) 716-721.
[192] S. Li, H. Wang, W. Li, X. Wu, W. Tang, Y. Chen, Effect of Cu substitution on promoted benzene oxidation over porous CuCo-based catalysts derived from layered double hydroxide with resistance of water vapor, Appl. Catal., B, 166–167 (2015) 260-269.
[193] S.S. Acharyya, S. Ghosh, R. Bal, Fabrication of three dimensional (3D) hierarchical Ag/WO3 flower-like catalyst materials for the selective oxidation of m-xylene to isophthalic acid, Chem. Commun., 51 (2015) 5998-6001.
[194] N. Zabat, M. Abbessi, Elimination of the methyl blue from wastewater by advanced oxidation process in the presence of an heteropolyanion of Dawson type as a catalyst, Res. Chem. Intermed., 41 (2015) 1691-1702.
[195] M. Jiménez, M. Ignacio Maldonado, E.M. Rodríguez, A. Hernández-Ramírez, E. Saggioro, I. Carra, J.A. Sánchez Pérez, Supported TiO2 solar photocatalysis at semi-pilot scale: degradation of pesticides found in citrus processing industry wastewater, reactivity and influence of photogenerated species, J. Chem. Technol. Biotechnol., 90 (2015) 149-157.

[196] H. Lv, H. Zhao, T. Cao, L. Qian, Y. Wang, G. Zhao, Efficient degradation of high concentration azo-dye wastewater by heterogeneous Fenton process with iron-based metal-organic framework, J. Mol. Catal. A: Chem., 400 (2015) 81-89.
[197] W.-J. Liu, T.-T. Qian, H. Jiang, Bimetallic Fe nanoparticles: Recent advances in synthesis and application in catalytic elimination of environmental pollutants, Chem. Eng. J., 236 (2014) 448-463.
[198] Y. Yuan, H. Tao, J. Fan, L. Ma, Degradation of p-chloroaniline by persulfate activated with ferrous sulfide ore particles, Chem. Eng. J., 268 (2015) 38-46.
[199] E.I. Seck, J.M. Doña-Rodríguez, C. Fernández-Rodríguez, O.M. González-Díaz, J. Araña, J. Pérez-Peña, Photocatalytic removal of 2,4-dichlorophenoxyacetic acid by using sol–gel synthesized nanocrystalline and commercial TiO2: Operational parameters optimization and toxicity studies, Appl. Catal., B, 125 (2012) 28-34.
[200] K. Hanna, C. de Brauer, P. Germain, J.M. Chovelon, C. Ferronato, Degradation of pentachlorophenol in cyclodextrin extraction effluent using a photocatalytic process, Sci. Total Environ., 332 (2004) 51-60.
[201] M.M.R. Feijen-Jeurissen, J.J. Jorna, B.E. Nieuwenhuys, G. Sinquin, C. Petit, J.-P. Hindermann, Mechanism of catalytic destruction of 1,2-dichloroethane and trichloroethylene over γ-Al2O3 and γ-Al2O3 supported chromium and palladium catalysts, Catal. Today, 54 (1999) 65-79.
[202] X. Ma, X. Feng, J. Guo, H. Cao, X. Suo, H. Sun, M. Zheng, Catalytic oxidation of 1,2-dichlorobenzene over Ca-doped FeOx hollow microspheres, Appl. Catal., B, 147 (2014) 666-676.
[203] S. Kundu, A. Chanda, J.V.K. Thompson, G. Diabes, S.K. Khetan, A.D. Ryabov, T.J. Collins, Rapid degradation of oxidation resistant nitrophenols by TAML activator and H2O2, Catal. Sci. Technol., 5 (2015) 1775-1782.
[204] S. Guo, G. Zhang, J.C. Yu, Enhanced photo-Fenton degradation of rhodamine B using graphene oxide–amorphous FePO4 as effective and stable heterogeneous catalyst, J. Colloid Interface Sci., 448 (2015) 460-466.
[205] S.Y. Wong, R.W. Hartel, Crystallization in Lactose Refining—A Review, J. Food Sci., 79 (2014) R257-R272.
[206] C. Giang, A. Osatiashtiani, V. dos Santos, A. Lee, D. Wilson, K. Waldron, K. Wilson, Valorisation of Vietnamese Rice Straw Waste: Catalytic Aqueous Phase Reforming of Hydrolysate from Steam Explosion to Platform Chemicals, Catalysts, 4 (2014) 414-426.
[207] R. Madrid, F. Margarido, C.A. Nogueira, Valorisation of rice husk by chemical and thermal treatments, Mater. Sci. Forum, 2013, pp. 659-664.
[208] A.S. Burange, M.B. Gawande, F.L.Y. Lam, R.V. Jayaram, R. Luque, Heterogeneously catalyzed strategies for the deconstruction of high density polyethylene: plastic waste valorisation to fuels, Green Chem., 17 (2015) 146-156.
[209] S. Awad, M. Paraschiv, E.G. Varuvel, M. Tazerout, Optimization of biodiesel production from animal fat residue in wastewater using response surface methodology, Bioresour. Technol., 129 (2013) 315-320.
[210] M.S. Duyar, M.A.A. Treviño, R.J. Farrauto, Dual function materials for CO2 capture and conversion using renewable H2, Appl. Catal., B, 168–169 (2015) 370-376.
[211] Y. Xu, X. Yin, Y. Huang, P. Du, B. Zhang, Hydrogen Production on a Hybrid Photocatalytic System Composed of Ultrathin CdS Nanosheets and a Molecular Nickel Complex, Chem. - Eur. J., 21 (2015) 4571-4575.
[212] C.G. Morales-Guio, L.-A. Stern, X. Hu, Nanostructured hydrotreating catalysts for electrochemical hydrogen evolution, Chem. Soc. Rev., 43 (2014) 6555-6569.
[213] K.J.P. Schouten, F. Calle-Vallejo, M.T.M. Koper, A Step Closer to the Electrochemical Production of Liquid Fuels, Angew. Chem. Int. Ed., 53 (2014) 10858-10860.
[214] O.B. Ayodele, H.U. Farouk, J. Mohammed, Y. Uemura, W.M.A.W. Daud, Effect of precursor acidity on zeolite supported Pd catalyst properties and hydrodeoxygenation activity for the production of biofuel, J. Mol. Catal. A: Chem., 400 (2015) 179-186.
[215] K. Stawicka, M. Trejda, M. Ziolek, The production of biofuels additives on sulphonated MCF materials modified with Nb and Ta—Towards efficient solid catalysts of esterification, Appl. Catal., A, 467 (2013) 325-334.

[216] N. Degirmenbasi, N. Boz, D.M. Kalyon, Biofuel production via transesterification using sepiolite-supported alkaline catalysts, Appl. Catal., B, 150–151 (2014) 147-156.
[217] K. Yan, A. Chen, Selective hydrogenation of furfural and levulinic acid to biofuels on the ecofriendly Cu–Fe catalyst, Fuel, 115 (2014) 101-108.
[218] K. Koh, J.E. Seo, J.H. Lee, A. Goswami, C.W. Yoon, T. Asefa, Ultrasmall palladium nanoparticles supported on amine-functionalized SBA-15 efficiently catalyze hydrogen evolution from formic acid, J. Mater. Chem. A, 2 (2014) 20444-20449.
[219] R.B. Getman, Y.-S. Bae, C.E. Wilmer, R.Q. Snurr, Review and Analysis of Molecular Simulations of Methane, Hydrogen, and Acetylene Storage in Metal–Organic Frameworks, Chem. Rev., 112 (2012) 703-723.
[220] A. Débart, A.J. Paterson, J. Bao, P.G. Bruce, α-MnO2 Nanowires: A Catalyst for the O2 Electrode in Rechargeable Lithium Batteries, Angew. Chem. Int. Ed., 47 (2008) 4521-4524.
[221] D. Bhuyan, M. Saikia, L. Saikia, Magnetically recoverable Fe3O4@SBA-15: An improved catalyst for three component coupling reaction of aldehyde, amine and alkyne, Catal. Commun., 58 (2015) 158-163.
[222] J. Mondal, T. Sen, A. Bhaumik, Fe3O4@mesoporous SBA-15: a robust and magnetically recoverable catalyst for one-pot synthesis of 3,4-dihydropyrimidin-2(1H)-ones via the Biginelli reaction, Dalton Trans., 41 (2012) 6173-6181.
[223] R. Hudson, Y. Feng, R.S. Varma, A. Moores, Bare magnetic nanoparticles: sustainable synthesis and applications in catalytic organic transformations, Green Chem., 16 (2014) 4493-4505.
[224] L.M. Rossi, N.J.S. Costa, F.P. Silva, R. Wojcieszak, Magnetic nanomaterials in catalysis: advanced catalysts for magnetic separation and beyond, Green Chem., 16 (2014) 2906-2933.
[225] R.B. Nasir Baig, M.N. Nadagouda, R.S. Varma, Magnetically retrievable catalysts for asymmetric synthesis, Coord. Chem. Rev., 287 (2015) 137-156.
[226] V. Polshettiwar, R. Luque, A. Fihri, H. Zhu, M. Bouhrara, J.-M. Basset, Magnetically Recoverable Nanocatalysts, Chem. Rev., 111 (2011) 3036-3075.
[227] A. Hu, G.T. Yee, W. Lin, Magnetically Recoverable Chiral Catalysts Immobilized on Magnetite Nanoparticles for Asymmetric Hydrogenation of Aromatic Ketones, J. Am. Chem. Soc., 127 (2005) 12486-12487.
[228] T. Cheng, D. Zhang, H. Li, G. Liu, Magnetically recoverable nanoparticles as efficient catalysts for organic transformations in aqueous medium, Green Chem., 16 (2014) 3401-3427.
[229] V. Polshettiwar, J.-M. Basset, D. Astruc, Editorial: Nanoscience Makes Catalysis Greener, ChemSusChem, 5 (2012) 6-8.
[230] A. Dhakshinamoorthy, S. Navalon, M. Alvaro, H. Garcia, Metal Nanoparticles as Heterogeneous Fenton Catalysts, ChemSusChem, 5 (2012) 46-64.
[231] N. Bion, D. Duprez, F. Epron, Design of Nanocatalysts for Green Hydrogen Production from Bioethanol, ChemSusChem, 5 (2012) 76-84.
[232] S.B. Kalidindi, B.R. Jagirdar, Nanocatalysis and Prospects of Green Chemistry, ChemSusChem, 5 (2012) 65-75.
[233] C. Mateo, J.M. Palomo, G. Fernandez-Lorente, J.M. Guisan, R. Fernandez-Lafuente, Improvement of enzyme activity, stability and selectivity via immobilization techniques, Enzyme Microb. Technol., 40 (2007) 1451-1463.
[234] P. Jochems, Y. Satyawali, L. Diels, W. Dejonghe, Enzyme immobilization on/in polymeric membranes: status, challenges and perspectives in biocatalytic membrane reactors (BMRs), Green Chem., 13 (2011) 1609-1623.
[235] E. Magner, Immobilisation of enzymes on mesoporous silicate materials, Chem. Soc. Rev., 42 (2013) 6213-6222.
[236] M. Hartmann, X. Kostrov, Immobilization of enzymes on porous silicas - benefits and challenges, Chem. Soc. Rev., 42 (2013) 6277-6289.
[237] H.R. Luckarift, J.C. Spain, R.R. Naik, M.O. Stone, Enzyme immobilization in a biomimetic silica support, Nat Biotech, 22 (2004) 211-213.

[238] R.C. Rodrigues, C. Ortiz, A. Berenguer-Murcia, R. Torres, R. Fernandez-Lafuente, Modifying enzyme activity and selectivity by immobilization, Chem. Soc. Rev., 42 (2013) 6290-6307.
[239] M.C.R. Franssen, P. Steunenberg, E.L. Scott, H. Zuilhof, J.P.M. Sanders, Immobilised enzymes in biorenewables production, Chem. Soc. Rev., 42 (2013) 6491-6533.
[240] S. Dutta, K.C.W. Wu, Enzymatic breakdown of biomass: enzyme active sites, immobilization, and biofuel production, Green Chem., 16 (2014) 4615-4626.
[241] M.B. Ansorge-Schumacher, O. Thum, Immobilised lipases in the cosmetics industry, Chem. Soc. Rev., 42 (2013) 6475-6490.
[242] R. DiCosimo, J. McAuliffe, A.J. Poulose, G. Bohlmann, Industrial use of immobilized enzymes, Chem. Soc. Rev., 42 (2013) 6437-6474.
[243] S. Cantone, V. Ferrario, L. Corici, C. Ebert, D. Fattor, P. Spizzo, L. Gardossi, Efficient immobilisation of industrial biocatalysts: criteria and constraints for the selection of organic polymeric carriers and immobilisation methods, Chem. Soc. Rev., 42 (2013) 6262-6276.
[244] A. Liese, L. Hilterhaus, Evaluation of immobilized enzymes for industrial applications, Chem. Soc. Rev., 42 (2013) 6236-6249.
[245] S. Horikoshi, N. Serpone, Role of microwaves in heterogeneous catalytic systems, Catal. Sci. Technol., 4 (2014) 1197-1210.
[246] S. Bigdeli, S. Fatemi, Fast carbon nanofiber growth on the surface of activated carbon by microwave irradiation: A modified nano-adsorbent for deep desulfurization of liquid fuels, Chem. Eng. J., 269 (2015) 306-315.
[247] S. Joseph, B. Mathew, Microwave assisted facile green synthesis of silver and gold nanocatalysts using the leaf extract of Aerva lanata, Spectrochim. Acta, Part A, 136, Part C (2015) 1371-1379.
[248] P. Dou, F. Tan, W. Wang, A. Sarreshteh, X. Qiao, X. Qiu, J. Chen, One-step microwave-assisted synthesis of Ag/ZnO/graphene nanocomposites with enhanced photocatalytic activity, J. Photochem. Photobiol., A, 302 (2015) 17-22.
[249] M. Baghbanzadeh, L. Carbone, P.D. Cozzoli, C.O. Kappe, Microwave-Assisted Synthesis of Colloidal Inorganic Nanocrystals, Angew. Chem. Int. Ed., 50 (2011) 11312-11359.
[250] H. El-Deeb, M. Bron, Microwave-assisted polyol synthesis of PtCu/carbon nanotube catalysts for electrocatalytic oxygen reduction, J. Power Sources, 275 (2015) 893-900.
[251] B. Subramanya, D.K. Bhat, Novel one-pot green synthesis of graphene in aqueous medium under microwave irradiation using a regenerative catalyst and the study of its electrochemical properties, New J. Chem., 39 (2015) 420-430.
[252] J. Ren, M. Ren, D. Wang, J. Lin, Z. Li, Mechanism of microwave-induced carbothermic reduction and catalytic performance of Cu/activated carbon catalysts in the oxidative carbonylation of methanol, J. Therm. Anal. Calorim., (2015) 1-11.
[253] S. Mintova, S. Mo, T. Bein, Nanosized AlPO4-5 Molecular Sieves and Ultrathin Films Prepared by Microwave Synthesis, Chem. Mater., 10 (1998) 4030-4036.
[254] W. Cao, L. Chen, Z. Qi, Microwave-assisted synthesis of Ag/Ag2SO4/ZnO nanostructures for efficient visible-light-driven photocatalysis, J. Mol. Catal. A: Chem., 401 (2015) 81-89.
[255] A. Bhattacharjee, M. Ahmaruzzaman, A green and novel approach for the synthesis of SnO2 nanoparticles and its exploitation as a catalyst in the degradation of methylene blue under solar radiation, Mater. Lett., 145 (2015) 74-78.
[256] T. Alvaro-Munoz, E. Sastre, C. Marquez-Alvarez, Microwave-assisted synthesis of plate-like SAPO-34 nanocrystals with increased catalyst lifetime in the methanol-to-olefin reaction, Catal. Sci. Technol., 4 (2014) 4330-4339.
[257] M. Gharibeh, G.A. Tompsett, W.C. Conner, Microwave Reaction Enhancement: The Rapid Synthesis of SAPO-11 Molecular Sieves, Top. Catal., 49 (2008) 157-166.
[258] S.H. Jhung, J.-S. Chang, J.S. Hwang, S.-E. Park, Selective formation of SAPO-5 and SAPO-34 molecular sieves with microwave irradiation and hydrothermal heating, Microporous Mesoporous Mater., 64 (2003) 33-39.

[259] S.C. Laha, G. Kamalakar, R. Gläser, Microwave-assisted synthesis of [Cr]APO-5, Microporous Mesoporous Mater., 90 (2006) 45-52.
[260] S. Chen, Y. Zhao, B. Sun, Z. Ao, X. Xie, Y. Wei, G. Wang, Microwave-assisted Synthesis of Mesoporous Co3O4 Nanoflakes for Applications in Lithium Ion Batteries and Oxygen Evolution Reactions, ACS Appl. Mater. Interfaces, 7 (2015) 3306-3313.
[261] A.C. Cole, J.L. Jensen, I. Ntai, K.L.T. Tran, K.J. Weaver, D.C. Forbes, J.H. Davis, Novel Brønsted Acidic Ionic Liquids and Their Use as Dual Solvent−Catalysts, J. Am. Chem. Soc., 124 (2002) 5962-5963.
[262] N. Audic, H. Clavier, M. Mauduit, J.-C. Guillemin, An Ionic Liquid-Supported Ruthenium Carbene Complex: A Robust and Recyclable Catalyst for Ring-Closing Olefin Metathesis in Ionic Liquids, J. Am. Chem. Soc., 125 (2003) 9248-9249.
[263] H.-P. Zhu, F. Yang, J. Tang, M.-Y. He, Bronsted acidic ionic liquid 1-methylimidazolium tetrafluoroborate: a green catalyst and recyclable medium for esterification, Green Chem., 5 (2003) 38-39.
[264] G. Zhao, T. Jiang, H. Gao, B. Han, J. Huang, D. Sun, Mannich reaction using acidic ionic liquids as catalysts and solvents, Green Chem., 6 (2004) 75-77.
[265] X. Chen, Y. Guan, A.A. Abdeltawab, S.S. Al-Deyab, X. Yuan, C. Wang, G. Yu, Using functional acidic ionic liquids as both extractant and catalyst in oxidative desulfurization of diesel fuel: An investigation of real feedstock, Fuel, 146 (2015) 6-12.
[266] A.M. da Costa Lopes, R. Bogel-Łukasik, Acidic Ionic Liquids as Sustainable Approach of Cellulose and Lignocellulosic Biomass Conversion without Additional Catalysts, ChemSusChem, 8 (2015) 947-965.
[267] J. Dupont, G.S. Fonseca, A.P. Umpierre, P.F.P. Fichtner, S.R. Teixeira, Transition-Metal Nanoparticles in Imidazolium Ionic Liquids: Recycable Catalysts for Biphasic Hydrogenation Reactions, J. Am. Chem. Soc., 124 (2002) 4228-4229.
[268] Q. Yao, M. Sheets, An ionic liquid-tagged second generation Hoveyda–Grubbs ruthenium carbene complex as highly reactive and recyclable catalyst for ring-closing metathesis of di-, tri- and tetrasubstituted dienes, J. Organomet. Chem., 690 (2005) 3577-3584.
[269] P. Nehra, B. Khungar, K. Pericherla, S.C. Sivasubramanian, A. Kumar, Imidazolium ionic liquid-tagged palladium complex: an efficient catalyst for the Heck and Suzuki reactions in aqueous media, Green Chem., 16 (2014) 4266-4271.
[270] M. Dewan, A. De, S. Mozumdar, Efficient and reusable ionic liquid stabilized magnetic cobalt nanoparticles as catalysts for aza- and thia-Michael reactions, Inorg. Chem. Commun., 53 (2015) 92-96.
[271] L. Jing, M. Wang, X. Li, R. Xiao, Y. Zhao, Y. Zhang, Y.-M. Yan, Q. Wu, K. Sun, Covalently functionalized TiO2 with ionic liquid: A high-performance catalyst for photoelectrochemical water oxidation, Appl. Catal., B, 166–167 (2015) 270-276.
[272] S. Doherty, J.G. Knight, M.A. Carroll, J.R. Ellison, S.J. Hobson, S. Stevens, C. Hardacre, P. Goodrich, Efficient and selective hydrogen peroxide-mediated oxidation of sulfides in batch and segmented and continuous flow using a peroxometalate-based polymer immobilised ionic liquid phase catalyst, Green Chem., 17 (2015) 1559-1571.
[273] P. Sharma, M. Gupta, Silica functionalized sulphonic acid coated with ionic liquid: an efficient and recyclable heterogeneous catalyst for the one-pot synthesis of 1,4-dihydropyridines under solvent-free conditions, Green Chem., 17 (2015) 1100-1106.
[274] N. Azgomi, M. Mokhtary, Nano-Fe3O4@SiO2 supported ionic liquid as an efficient catalyst for the synthesis of 1,3-thiazolidin-4-ones under solvent-free conditions, J. Mol. Catal. A: Chem., 398 (2015) 58-64.
[275] W. Liu, D. Wang, Y. Duan, Y. Zhang, F. Bian, Palladium supported on poly (ionic liquid) entrapped magnetic nanoparticles as a highly efficient and reusable catalyst for the solvent-free Heck reaction, Tetrahedron Lett., 56 (2015) 1784-1789.
[276] M.R. Nabid, Y. Bide, Z. Habibi, Synthesis of a yolk/shell Fe3O4@poly(ionic liquid)s-derived nitrogen doped graphitic porous carbon materials and its application as support for nickel catalysts, RSC Adv., 5 (2015) 2258-2265.

[277] H. Wan, Z. Wu, W. Chen, G. Guan, Y. Cai, C. Chen, Z. Li, X. Liu, Heterogenization of ionic liquid based on mesoporous material as magnetically recyclable catalyst for biodiesel production, J. Mol. Catal. A: Chem., 398 (2015) 127-132.
[278] L. Zhou, A. Zhao, Z. Wang, Z. Chen, J. Ren, X. Qu, Ionic Liquid-Assisted Synthesis of Multicolor Luminescent Silica Nanodots and Their Use as Anticounterfeiting Ink, ACS Appl. Mater. Interfaces, 7 (2015) 2905-2911.
[279] I. Do, L.T. Drzal, Ionic Liquid-Assisted Synthesis of Pt Nanoparticles onto Exfoliated Graphite Nanoplatelets for Fuel Cells, ACS Appl. Mater. Interfaces, 6 (2014) 12126-12136.
[280] A.I. Saugar, A. Mayoral, J. Pérez-Pariente, Solvothermal synthesis of disordered mesoporous materials based on a Si–N framework in ionic liquids, Microporous Mesoporous Mater., 186 (2014) 146-154.
[281] Z. Du, E. Li, G. Li, F. Cheng, G. Wang, One-step strategy for synthesis of yolk–shell silica spheres using trisiloxane-tailed ionic liquids as a template, J. Mater. Sci., 49 (2014) 4919-4926.
[282] Y.L. Verma, R.K. Singh, I.-K. Oh, S. Chandra, Ionic liquid template assisted synthesis of porous nano-silica nails, RSC Adv., 4 (2014) 39978-39983.
[283] X. Liu, R. Liu, S. Chen, B. Liang, Hydrothermal synthesis of CdSe hierarchical dendrites using ionic liquid as template, Mater. Lett., 66 (2012) 264-266.
[284] D. Mao, X. Lü, Z. Jiang, J. Xie, X. Lu, W. Wei, A.M. Showkot Hossain, Ionic liquid-assisted hydrothermal synthesis of square BiOBr nanoplates with highly efficient photocatalytic activity, Mater. Lett., 118 (2014) 154-157.
[285] R. Gobel, Z.-L. Xie, M. Neumann, C. Gunter, R. Lobbicke, S. Kubo, M.-M. Titirici, C. Giordano, A. Taubert, Synthesis of mesoporous carbon/iron carbide hybrids with unusually high surface areas from the ionic liquid precursor [Bmim][FeCl4], CrystEngComm, 14 (2012) 4946-4951.
[286] R. Li, Y. Luan, H. Zou, J. Du, T. Mu, Z. Li, Synthesis and gas-sensing properties of ZnO particles from an ionic liquid precursor, RSC Adv., 2 (2012) 3049-3056.
[287] X.S. Zhao, X.Y. Bao, W. Guo, F.Y. Lee, Immobilizing catalysts on porous materials, Mater. Today, 9 (2006) 32-39.
[288] P. McMorn, G.J. Hutchings, Heterogeneous enantioselective catalysts: strategies for the immobilisation of homogeneous catalysts, Chem. Soc. Rev., 33 (2004) 108-122.
[289] A.F. Trindade, P.M.P. Gois, C.A.M. Afonso, Recyclable Stereoselective Catalysts, Chem. Rev., 109 (2009) 418-514.
[290] C. Copéret, J.M. Basset, Strategies to Immobilize Well-Defined Olefin Metathesis Catalysts: Supported Homogeneous Catalysis vs. Surface Organometallic Chemistry, Adv. Synth. Catal., 349 (2007) 78-92.
[291] P.D. Raytchev, L. Roussi, J.-P. Dutasta, A. Martinez, V. Dufaud, Homogeneous and silica-supported azidoproazaphosphatranes as efficient catalysts for the synthesis of substituted coumarins, Catal. Commun., 28 (2012) 1-4.
[292] C. Saluzzo, M. Lemaire, Homogeneous-Supported Catalysts for Enantioselective Hydrogenation and Hydrogen Transfer Reduction, Adv. Synth. Catal., 344 (2002) 915-928.
[293] S. Kumar, O.P. Khatri, S. Cordier, R. Boukherroub, S.L. Jain, Graphene Oxide Supported Molybdenum Cluster: First Heterogenized Homogeneous Catalyst for the Synthesis of Dimethylcarbonate from CO2 and Methanol, Chem. - Eur. J., 21 (2015) 3488-3494.
[294] J. Nakazawa, A. Yata, T. Hori, T.D.P. Stack, Y. Naruta, S. Hikichi, Catalytic Alkane Oxidation by Homogeneous and Silica-supported Cobalt(II) Complex Catalysts with a Triazolyl Group-containing Tetradentate Ligand, Chem. Lett., 42 (2013) 1197-1199.
[295] C. Liu, M. Lin, K. Fang, Y. Meng, Y. Sun, Preparation of nanostructured molybdenum carbides for CO hydrogenation, RSC Adv., 4 (2014) 20948-20954.
[296] C. Avendano, A. Briceno, F.J. Mendez, J.L. Brito, G. Gonzalez, E. Canizales, R. Atencio, P. Dieudonne, Novel MoO2/carbon hierarchical nano/microcomposites: synthesis, characterization, solid state transformations and thiophene HDS activity, Dalton Trans., 42 (2013) 2822-2830.
[297] Y. Shen, P. Zhao, Q. Shao, Porous silica and carbon derived materials from rice husk pyrolysis char, Microporous Mesoporous Mater., 188 (2014) 46-76.

[298] S. Zhang, M. Zeng, J. Li, J. Li, J. Xu, X. Wang, Porous magnetic carbon sheets from biomass as an adsorbent for the fast removal of organic pollutants from aqueous solution, J. Mater. Chem. A, 2 (2014) 4391-4397.
[299] S.E. Elaigwu, G.M. Greenway, Biomass derived mesoporous carbon monoliths via an evaporation-induced self-assembly, Mater. Lett., 115 (2014) 117-120.
[300] S. Kubo, I. Tan, R.J. White, M. Antonietti, M.-M. Titirici, Template Synthesis of Carbonaceous Tubular Nanostructures with Tunable Surface Properties, Chem. Mater., 22 (2010) 6590-6597.
[301] K.H. Adolfsson, S. Hassanzadeh, M. Hakkarainen, Valorization of cellulose and waste paper to graphene oxide quantum dots, RSC Adv., 5 (2015) 26550-26558.
[302] H. Awala, J.-P. Gilson, R. Retoux, P. Boullay, J.-M. Goupil, V. Valtchev, S. Mintova, Template-free nanosized faujasite-type zeolites, Nat Mater, 14 (2015) 447-451.
[303] J.-Y. Park, X.G. Zhao, H.-B. Gu, Synthesis and characterization of SnO2 nanostructure using Bombyx mori (L.) silkworm cocoon as biomass template for photocatalytic reaction, Mater. Lett., 141 (2015) 187-190.
[304] S. Lunge, S. Singh, A. Sinha, Magnetic iron oxide (Fe3O4) nanoparticles from tea waste for arsenic removal, J. Magn. Magn. Mater., 356 (2014) 21-31.
[305] K.-J. Hwang, D. Kang, S. Lee, C.-H. Hwang, C. Kim, N. Kim, S. Jin, I.-H. Lee, J.-Y. Park, Synthesis and characterization of hollow TiO2 fibers using Ceiba pentandra (L.) Gaertn. (kapok) as a natural template, Mater. Lett., 115 (2014) 265-267.
[306] H. Liu, G. Lu, Y. Guo, Y. Wang, Y. Guo, Synthesis of mesoporous Pt/Al2O3 catalysts with high catalytic performance for hydrogenation of acetophenone, Catal. Commun., 10 (2009) 1324-1329.
[307] X. Zhang, W. He, Y. Yue, R. Wang, J. Shen, S. Liu, J. Ma, M. Li, F. Xu, Bio-synthesis participated mechanism of mesoporous LiFePO4/C nanocomposite microspheres for lithium ion battery, J. Mater. Chem., 22 (2012) 19948-19956.
[308] J. Zhu, J. Jia, F.-l. Kwong, D.H.L. Ng, Synthesis of 6H-SiC nanowires on bamboo leaves by carbothermal method, Diamond Relat. Mater., 33 (2013) 5-11.
[309] Y. Huo, Z. Chang, W. Li, S. Liu, B. Dong, Reuse and Valorization of Vanadium and Tungsten from Waste V2O5–WO3/TiO2 SCR Catalyst, Waste Biomass Valor, 6 (2015) 159-165.
[310] L. Guo, D.G. Morris, X. Liu, C. Vaslet, R.H. Hurt, A.B. Kane, Iron Bioavailability and Redox Activity in Diverse Carbon Nanotube Samples, Chem. Mater., 19 (2007) 3472-3478.
[311] C. Buzea, I. Pacheco, K. Robbie, Nanomaterials and nanoparticles: Sources and toxicity, Biointerphases, 2 (2007) MR17-MR71.
[312] S. Sharifi, S. Behzadi, S. Laurent, M. Laird Forrest, P. Stroeve, M. Mahmoudi, Toxicity of nanomaterials, Chem. Soc. Rev., 41 (2012) 2323-2343.
[313] P.C. Ray, H. Yu, P.P. Fu, Toxicity and Environmental Risks of Nanomaterials: Challenges and Future Needs, Journal of environmental science and health. Part C, Environmental carcinogenesis & ecotoxicology reviews, 27 (2009) 1-35.
[314] A. Paul, H. Al Kindi, R. Medhi, V. Manoharan, S. Prakash, D. Sum-Tim, Chapter 18 - Nanomaterials and Cardiovascular Toxicity, in: M. Ramachandran (Ed.) Heart and Toxins, Academic Press, Boston, 2015, pp. 547-570.
[315] K. Vasilev, H. Chen, P. Murray, The Potential of Nanomaterials for Drug Delivery, Cell Tracking, and Regenerative Medicine 2013, J. Nanomater., 2014 (2014) 2.
[316] C.S.S.R. Kumar, F. Mohammad, Magnetic nanomaterials for hyperthermia-based therapy and controlled drug delivery, Adv. Drug Delivery Rev., 63 (2011) 789-808.
[317] J.A. Hubbell, A. Chilkoti, Nanomaterials for Drug Delivery, Science, 337 (2012) 303-305.
[318] H.A. Khan, R. Shanker, Toxicity of Nanomaterials, BioMed Research International, 2015 (2015) 2.
[319] R. Guadagnini, B. Halamoda Kenzaoui, L. Walker, G. Pojana, Z. Magdolenova, D. Bilanicova, M. Saunders, L. Juillerat-Jeanneret, A. Marcomini, A. Huk, M. Dusinska, L.M. Fjellsbø, F. Marano, S. Boland, Toxicity screenings of nanomaterials: challenges due to interference with assay processes and components of classic in vitro tests, Nanotoxicology, 9 (2015) 13-24.

[320] L. Zhang, T. Ying, H.Y. Yang, Z.X. Chang, D.L. Li, Toxic leaching of heavy metals in copper catalyst residue, Asian J. Chem., 25 (2013) 1651-1653.
[321] I. Gaballah, M. Djona, J.C. Mugica, R. Solozobal, Recycling of Materials in Industry Valuable metals recovery from spent catalysts by selective chlorination, Resources, Conservation and Recycling, 10 (1994) 87-96.
[322] X. Liu, L. Guo, D. Morris, A.B. Kane, R.H. Hurt, Targeted removal of bioavailable metal as a detoxification strategy for carbon nanotubes, Carbon, 46 (2008) 489-500.
[323] D. Sun, L. Chang, J. Tay, J. Navratil, C. Easton, Recovery and Marine Clay Stabilization of Heavy Metals Present in Spent Hydrotreating Catalysts, Journal of Environmental Engineering, 127 (2001) 916-921.
[324] K.M. Nampoothiri, N.R. Nair, R.R. John, Technol. Biores., 101 (2010) 8493.
[325] D. Szegda, J. Song, M.K. Warby, J.R. Whiteman, Computational modelling of a thermoforming process for thermoplastic starch, AIP Conf. Proc., 908 (2007) 35-48.
[326] D.P. Serrano, J. Aguado, J.M. Escola, Developing Advanced Catalysts for the Conversion of Polyolefinic Waste Plastics into Fuels and Chemicals, ACS Catal., 2 (2012) 1924-1941.
[327] F. Gironi, V. Piemonte, Life cycle assessment of polylactic acid and polyethylene terephthalate bottles for drinking water, Environ. Prog. Sustainable Energy, 30 (2011) 459-468.
[328] T. Iwata, Biodegradable and Bio-Based Polymers: Future Prospects of Eco-Friendly Plastics, Angew. Chem. Int. Ed., 54 (2015) 3210-3215.
[329] T.G. Volova, M.I. Golyshev, M.Y. Trusova, N.O. Zhila, M.V. Kartushinskaya, Degradation of bioplastic in environment, Dokl. Akad. Nauk, 397 (2004) 708-710.
[330] J. Sarasa, J.M. Gracia, C. Javierre, Study of the biodisintegration of a bioplastic material waste, Bioresour. Technol., 100 (2009) 3764-3768.
[331] S.Y. Lee, Deciphering bioplastic production, Nat. Biotechnol., 24 (2006) 1227-1229.
[332] N. Gangurde, R. Sayyed, S. Kiran, A. Gulati, Development of eco-friendly bioplastic like PHB by distillery effluent microorganisms, Environ Sci Pollut Res, 20 (2013) 488-497.
[333] Y. Jiang, L. Marang, J. Tamis, M.C.M. van Loosdrecht, H. Dijkman, R. Kleerebezem, Waste to resource: Converting paper mill wastewater to bioplastic, Water Res., 46 (2012) 5517-5530.
[334] M. Ben, T. Mato, A. Lopez, M. Vila, C. Kennes, M.C. Veiga, Bioplastic production using wood mill effluents as feedstock, Water Sci. Technol., 63 (2011) 1196-1202.
[335] B. Brehmer, R.M. Boom, J. Sanders, Maximum fossil fuel feedstock replacement potential of petrochemicals via biorefineries, Chem. Eng. Res. Des., 87 (2009) 1103-1119.
[336] A.J.J.E. Eerhart, A.P.C. Faaij, M.K. Patel, Replacing fossil based PET with biobased PEF; process analysis, energy and GHG balance, Energy Environ. Sci., 5 (2012) 6407-6422.
[337] Y. Matsuda, Y. Ichihara, K. Yoshida, T. Tochioka, Development of bioplastic for automobile parts, Rev. Automot. Eng., 30 (2009) 95-97.
[338] J. Miyamoto, S. Aoki, K. Hirosawa, Cell phones using bioplastic, NTT Tech. Rev., 5 (2007) 36-42.
[339] S. Papong, P. Malakul, R. Trungkavashirakun, P. Wenunun, T. Chom-in, M. Nithitanakul, E. Sarobol, Comparative assessment of the environmental profile of PLA and PET drinking water bottles from a life cycle perspective, J. Cleaner Prod., 65 (2014) 539-550.
[340] A.H. Hoveyda, A.R. Zhugralin, The remarkable metal-catalysed olefin metathesis reaction, Nature, 450 (2007) 243-251.
[341] A.W. Anderson, N.G. Merckling, Polymeric bicyclo-(2,2,1)-2-heptene, U.S. Patent, 2721189 (A) (1955) October 18.
[342] R.L. Banks, G.C. Bailey, Olefin Disproportionation. A New Catalytic Process, I&EC Prod. Res. Dev., 3 (1964) 170-173.
[343] P. Jean-Louis Hérisson, Y. Chauvin, Catalyse de transformation des oléfines par les complexes du tungstène. II. Télomérisation des oléfines cycliques en présence d'oléfines acycliques, Die Makromol. Chem., 141 (1971) 161-176.
[344] U.H.F. Bunz, L. Kloppenburg, Alkyne Metathesis as a New Synthetic Tool: Ring-Closing, Ring-Opening, and Acyclic, Angew. Chem. Int. Ed., 38 (1999) 478-481.
[345] A. Furstner, P.W. Davies, Alkyne metathesis, Chem. Commun., (2005) 2307-2320.

[346] W. Zhang, J.S. Moore, Alkyne Metathesis: Catalysts and Synthetic Applications, Adv. Synth. Catal., 349 (2007) 93-120.
[347] V. Vidal, A. Théolier, J. Thivolle-Cazat, J.-M. Basset, Metathesis of Alkanes Catalyzed by Silica-Supported Transition Metal Hydrides, Science, 276 (1997) 99-102.
[348] J.-M. Basset, C. Copéret, D. Soulivong, M. Taoufik, J. Thivolle-Cazat, From Olefin to Alkane Metathesis: A Historical Point of View, Angew. Chem. Int. Ed., 45 (2006) 6082-6085.
[349] A.S. Goldman, A.H. Roy, Z. Huang, R. Ahuja, W. Schinski, M. Brookhart, Catalytic Alkane Metathesis by Tandem Alkane Dehydrogenation-Olefin Metathesis, Science, 312 (2006) 257-261.
[350] A.M. Rouhi, OLEFIN METATHESIS: BIG-DEAL REACTION, Chem. Eng. News,, 80 (2002) 29-38.
[351] D. Bicchielli, Y. Borguet, L. Delaude, A. Demonceau, I. Dragutan, V. Dragutan, C. Jossifov, R. Kalinova, F. Nicks, X. Sauvage, Recent Applications of Alkene Metathesis in Fine Chemical Synthesis, in: V. Dragutan, A. Demonceau, I. Dragutan, E. Finkelshtein (Eds.) Green Metathesis Chemistry, Springer Netherlands2010, pp. 207-274.
[352] R.L. Banks, D.S. Banaslak, P.S. Hudson, J.R. Norell, Specialty chemicals via olefin metathesis, J. Mol. Catal., 15 (1982) 21-33.
[353] M. Sherwood, Shell Higher Olefins Process (SHOP) using MoO3/Al2O3, Chem. Ind. (London), (1982) 994-995.
[354] G.C. Bond, Catalytic properties of 0.3% Pt/Al2O3 (EUROPT-3) and of 0.3% Pt−0.3% Re/Al2O3 (EUROPT-4), Journal of Molecular Catalysis, 81 (1993) 99-118.
[355] M. Behrens, F. Studt, I. Kasatkin, S. Kühl, M. Hävecker, F. Abild-Pedersen, S. Zander, F. Girgsdies, P. Kurr, B.-L. Kniep, M. Tovar, R.W. Fischer, J.K. Nørskov, R. Schlögl, The Active Site of Methanol Synthesis over Cu/ZnO/Al2O3 Industrial Catalysts, Science, 336 (2012) 893-897.
[356] M.M. Hossain, L. Atanda, N. Al-Yassir, S. Al-Khattaf, Kinetics modeling of ethylbenzene dehydrogenation to styrene over a mesoporous alumina supported iron catalyst, Chem. Eng. J., 207–208 (2012) 308-321.
[357] H.S. Taylor, A Theory of the Catalytic Surface, Proc. R. Soc. London, Ser. A, 108 (1925) 105-111.
[358] R.H. Crabtree, Deactivation in Homogeneous Transition Metal Catalysis: Causes, Avoidance, and Cure, Chem. Rev., 115 (2015) 127-150.
[359] M. Argyle, C. Bartholomew, Heterogeneous Catalyst Deactivation and Regeneration: A Review, Catalysts, 5 (2015) 145-269.
[360] C. Copéret, M. Chabanas, R. Petroff Saint-Arroman, J.-M. Basset, Homogeneous and Heterogeneous Catalysis: Bridging the Gap through Surface Organometallic Chemistry, Angew. Chem. Int. Ed., 42 (2003) 156-181.
[361] J.M. Thomas, R. Raja, D.W. Lewis, Single-Site Heterogeneous Catalysts, Angew. Chem. Int. Ed., 44 (2005) 6456-6482.
[362] E. Gross, J.H.C. Liu, F.D. Toste, G.A. Somorjai, Control of selectivity in heterogeneous catalysis by tuning nanoparticle properties and reactor residence time, Nat. Chem., 4 (2012) 947-952.
[363] M.P. de Almeida, S.A.C. Carabineiro, The Best of Two Worlds from the Gold Catalysis Universe: Making Homogeneous Heterogeneous, ChemCatChem, 4 (2012) 18-29.
[364] C.M. Friesen, C.D. Montgomery, S.A.J.U. Temple, The first fluorous biphase hydrogenation catalyst incorporating a perfluoropolyalkylether: [RhCl(PPh2(C6H4C(O)OCH2CF(CF3)(OCF2CF(CF3))nF))3] with n = 4–9, J. Fluorine Chem., 144 (2012) 24-32.
[365] Y. Wang, J. Zhou, K. Liu, L. Dai, Bi-SO3H-functionalized room temperature ionic liquids based on bipyridinium: highly efficient and recyclable catalysts for the synthesis of naphthalene-condensed oxazinone derivatives, RSC Adv., 3 (2013) 9965-9972.
[366] H. Rajaei, A. Amin, A. Golchehre, F. Esmaeilzadeh, Investigation on the effect of different supercritical fluid extraction process on the activation of the R-134 catalyst, J. Supercrit. Fluids, 67 (2012) 1-6.
[367] S.N. Gaydamaka, V.V. Timofeev, D.A. Lemenovskii, S.V. Kardashev, O.O. Parenago, V.N. Bagratashvili, S.A. Sergienko, G.P. Brusova, V.V. Lunin, The possibility of supercritical fluid regeneration for Pt-Re/γ-Al2O3 industrial reforming catalyst in O3/CO2 mixtures, Catal. Ind., 5 (2013) 216-222.
[368] M. Xiao, C. Zhao, H. Chen, B. Yang, J. Wang, “Ship-in-a-Bottle” Growth of Noble Metal Nanostructures, Adv. Funct. Mater., 22 (2012) 4526-4532.

[369] Z.J. Zhao, Z.Y.J. Zhan, Development of new ruthenium catalysts for metathesis reactions, Chim. Oggi-Chem. Today, 24 (2006) 8-9.
[370] M.B. Herbert, R.H. Grubbs, Z-Selective Cross Metathesis with Ruthenium Catalysts: Synthetic Applications and Mechanistic Implications, Angew. Chem. Int. Ed., 54 (2015) 5018-5024.
[371] E.O. Fischer, S. Vigoureux, Über Aromatenkomplexe von Metallen, XVI. Cyclopentadienyl-vanadin-oxy-dichlorid, Chem. Ber., 91 (1958) 1342-1344.
[372] M. Cousins, M.L.H. Green, 164. Allyl, alkyl, and olefin complexes of molybdenum, J. Chem. Soc., (1963) 889-894.
[373] W.A. Herrmann, Essays on organometallic chemistry, VII. Laboratory curiosities of yesterday, catalysts of tomorrow: organometallic oxides, J. Organomet. Chem., 500 (1995) 149-173.
[374] H.W. Roesky, I. Haiduc, N.S. Hosmane, Organometallic Oxides of Main Group and Transition Elements Downsizing Inorganic Solids to Small Molecular Fragments, Chem. Rev., 103 (2003) 2579-2596.
[375] B.S. Lane, K. Burgess, Metal-Catalyzed Epoxidations of Alkenes with Hydrogen Peroxide, Chem. Rev., 103 (2003) 2457-2474.
[376] C.C. Romão, F.E. Kühn, W.A. Herrmann, Rhenium(VII) Oxo and Imido Complexes: Synthesis, Structures, and Applications, Chem. Rev., 97 (1997) 3197-3246.
[377] H. Balcar, D. Mishra, E. Marceau, X. Carrier, N. Žilková, Z. Bastl, Molybdenum oxide catalysts for metathesis of higher 1-alkenes via supporting MoO2(acetylacetonate)2 and MoO2(glycolate)2 on SBA-15 mesoporous molecular sieves, Appl. Catal., A, 359 (2009) 129-135.
[378] T.I. Bhuiyan, P. Arudra, M.M. Hossain, M.N. Akhtar, A.M. Aitani, R.H. Abudawoud, S.S. Al-Khattaf, Kinetics modelling of 2-butene metathesis over tungsten oxide containing mesoporous silica catalyst, Can. J. Chem. Eng., (2014) n/a-n/a.
[379] Y.-Y. Lai, M. Bornand, P. Chen, Homogeneous Model Complexes for Supported Rhenia Metathesis Catalysts, Organometallics, 31 (2012) 7558-7565.
[380] E. Verkuijlen, F. Kapteijn, J.C. Mol, C. Boelhouwer, Heterogeneous metathesis of unsaturated fatty acid esters, J. Chem. Soc., Chem. Commun., (1977) 198-199.
[381] A. Ellison, A.K. Coverdale, P.F. Dearing, The metathesis of unsaturated esters over Re207/Al203 catalysts, J. Mol. Catal., 28 (1985) 141-167.
[382] A. Ellison, A. Bickerstaffe, G. Diakun, P. Worthington, Characterisation of rhenium oxide-alumina metathesis catalysts, J. Mol. Catal., 36 (1986) 67-77.
[383] X. Xiaoding, J.C. Mol, Re2O7/SiO2[middle dot]Al2O3-SnR4 or -PbR4, a highly active catalyst for the metathesis of functionalized alkenes, J. Chem. Soc., Chem. Commun., (1985) 631-633.
[384] X. Xiaoding, C. Boelhouwer, J.I. Benecke, D. Vonk, J.C. Mol, Re2O7/Al2O3[middle dot]B2O3 metathesis catalysts, J. Chem. Soc., Faraday Trans. 1, 82 (1986) 1945-1953.
[385] X. Xiaoding, J.C. Mol, C. Boelhouwer, Surface acidity of some Re2O7-containing metathesis catalysts. An in situ Fourier transform infrared study using pyridine adsorption, J. Chem. Soc., Faraday Trans. 1, 82 (1986) 2707-2718.
[386] R. Spronk, A. Andreini, J.C. Mol, Deactivation of rhenium-based catalysts for the metathesis of propene, J. Mol. Catal., 65 (1991) 219-235.
[387] M. Sibeijn, R. Spronk, J.A.R. Veen, J.C. Mol, IR studies of Re2O7 metathesis catalysts supported on alumina and phosphated alumina, Catal. Lett., 8 (1991) 201-208.
[388] R. Spronk, J.C. Mol, Regeneration of rhenium-based catalysts for the metathesis of propene, Appl. Catal., 76 (1991) 143-152.
[389] R.H.A. Bosma, G.C.N. Van Den Aardweg, J.C. Mol, Heterogeneous metathesis of unsaturated esters using a rhenium-based catalyst, J. Organomet. Chem., 255 (1983) 159-171.
[390] X. Xiaoding, P. Imhoff, G.C.N. van den Aardweg, J.C. Mol, Mixed-oxide catalysts for the metathesis of functionalized alkenes, J. Chem. Soc., Chem. Commun., (1985) 273-275.
[391] D. Mandelli, M.D.M. Jannini, R. Buffon, U. Schuchardt, Ethenolysis of esters of vegetable oils: Effect of B2O3 addition to Re2O7/SiO2.Al2O3-SnBu4 and CH3ReO3/SiO2.Al2O3 metathesis catalysts, Journal of the American Oil Chemists' Society, 73 (1996) 229-232.

[392] R. Buffon, I.J. Marochio, C.B. Rodella, J.C. Mol, Germanium and silicon compounds as promoters for Re2O7/SiO2-Al2O3 metathesis catalysts, J. Mol. Catal. A: Chem., 190 (2002) 171-176.
[393] M. Selva, S. Guidi, A. Perosa, M. Signoretto, P. Licence, T. Maschmeyer, Continuous-flow alkene metathesis: the model reaction of 1-octene catalyzed by Re2O7/[gamma]-Al2O3 with supercritical CO2 as a carrier, Green Chem., 14 (2012) 2727-2737.
[394] D. Commereuc, New homogeneous rhenium-based metathesis catalysts as models of the rhenium on alumina heterogeneous catalyst, J. Chem. Soc., Chem. Commun., (1995) 791-792.
[395] W.S. Greenlee, M.F. Farona, Olefin metathesis by rhenium carbonyl halide-alkylaluminum halide catalysts. Direct evidence for a coordinated carbene initiated process, Inorg. Chem., 15 (1976) 2129-2134.
[396] J.C. Mol, Application of olefin metathesis in oleochemistry: an example of green chemistry, Green Chem., 4 (2002) 5-13.
[397] M. Högerl, F.E. Kühn, (Cyclopentadienyl)trioxorhenium(VII) – no Match for Methyltrioxorhenium (MTO), Z. Anorg. Allg. Chem., 634 (2008) 1444-1447.
[398] I.R. Beattie, P.J. Jones, Methyltrioxorhenium. An air-stable compound containing a carbon-rhenium bond, Inorg. Chem., 18 (1979) 2318-2319.
[399] W.A. Herrmann, J.G. Kuchler, J.K. Felixberger, E. Herdtweck, W. Wagner, Methylrhenium Oxides: Synthesis from R2O7 and Catalytic Activity in Olefin Metathesis, Angew. Chem., Int. Ed. Engl., 27 (1988) 394-396.
[400] W.A. Herrmann, F.E. Kuehn, R.W. Fischer, W.R. Thiel, C.C. Romao, Multiple bonds between main-group elements and transition metals. 113. Simple and efficient synthesis of methyltrioxorhenium(VII): a general method, Inorg. Chem., 31 (1992) 4431-4432.
[401] Z. Zhu, J.H. Espenson, Organic Reactions Catalyzed by Methylrhenium Trioxide: Dehydration, Amination, and Disproportionation of Alcohols, J. Org. Chem., 61 (1996) 324-328.
[402] W.A. Herrmann, J.G. Kuchler, G. Weischselbaumer, E. Herdtweck, P. Kiprof, Mehrfachbindungen zwischen Hauptgruppenelementen und Übergangsmettalen: LXIV. Methyl(trioxo)rhenium: Basenaddukte und Basenreaktionen. Kristallstruktur von [Natrium(benzo-15-krone-5)]-perrhenat, J. Organomet. Chem., 372 (1989) 351-370.
[403] F.E. Kuehn, W.A. Herrmann, R. Hahn, M. Elison, J. Bluemel, E. Herdtweck, Multiple Bonds between Main-Group Elements and Transition Metals. 130. (Cyclopentadienyl)trioxorhenium(VII): Synthesis, Derivatives, and Properties, Organometallics, 13 (1994) 1601-1606.
[404] W.A. Herrmann, C.C. Romao, R.W. Fischer, P. Kiprof, C. de Méric de Bellefon, Alkyl- and Arylrhenium Trioxides, Angew. Chem., Int. Ed. Engl., 30 (1991) 185-187.
[405] M. Chabanas, A. Baudouin, C. Copéret, J.-M. Basset, A Highly Active Well-Defined Rhenium Heterogeneous Catalyst for Olefin Metathesis Prepared via Surface Organometallic Chemistry, J. Am. Chem. Soc., 123 (2001) 2062-2063.
[406] K.P.J. Williams, K. Harrison, Raman spectroscopic studies of the effects of tin promotion on a rhenium/alumina dismutation catalyst, J. Chem. Soc., Faraday Trans., 86 (1990) 1603-1606.
[407] F.D. Hardcastle, I.E. Wachs, J.A. Horsley, G.H. Via, The structure of surface rhenium oxide on alumina from laser raman spectroscopy and x-ray absorption near-edge spectroscopy, J. Mol. Catal., 46 (1988) 15-36.
[408] R. Buffon, A. Auroux, F. Lefebvre, M. Leconte, A. Choplin, J.M. Basset, W.A. Herrmann, A surface organometallic approach to the synthesis of rhenium-based catalysts for the metathesis of olefins: CH3ReO3/Nb2O5, J. Mol. Catal., 76 (1992) 287-295.
[409] T.M. Mathew, J.A.K. du Plessis, J.J. Prinsloo, Methyltrioxorhenium on silica–alumina as metathesis catalyst of 1-octene, J. Mol. Catal. A: Chem., 148 (1999) 157-164.
[410] A.M.J. Rost, H. Schneider, J.P. Zoller, W.A. Herrmann, F.E. Kühn, Methyltrioxorhenium heterogenized on commercially available supporting materials as cyclooctene metathesis catalyst, J. Organomet. Chem., 690 (2005) 4712-4718.
[411] T. Bein, C. Huber, K. Moller, C.-G. Wu, L. Xu, Methyltrioxorhenium Encapsulated in Zeolite Y: Tunable Olefin Metathesis Catalyst, Chem. Mater., 9 (1997) 2252-2254.

[412] R. Buffon, A. Choplin, M. Leconte, J.M. Basset, R. Touroude, W.A. Herrmann, Surface organometallic chemistry of rhenium: Attempts to characterize a surface carbene in metathesis of olefins with the catalyst CH3ReO3/Nb2O5, J. Mol. Catal., 72 (1992) L7-L10.
[413] A. Salameh, A. Baudouin, D. Soulivong, V. Boehm, M. Roeper, J.-M. Basset, C. Copéret, CH3-ReO3 on γ-Al2O3: Activity, selectivity, active site and deactivation in olefin metathesis, J. Catal., 253 (2008) 180-190.
[414] A. Salameh, A. Baudouin, J.-M. Basset, C. Copéret, Tuning the Selectivity of Alumina-Supported (CH3)ReO3 by Modifying the Surface Properties of the Support, Angew. Chem. Int. Ed., 47 (2008) 2117-2120.
[415] A. Salameh, A. Baudouin, J.-M. Basset, C. Copéret, Tuning the Selectivity of Alumina-Supported (CH3)ReO3 by Modifying the Surface Properties of the Support, Angewandte Chemie, 120 (2008) 2147-2150.
[416] A. Salameh, J. Joubert, A. Baudouin, W. Lukens, F. Delbecq, P. Sautet, J.M. Basset, C. Copéret, CH3ReO3 on γ-Al2O3: Understanding Its Structure, Initiation, and Reactivity in Olefin Metathesis, Angew. Chem. Int. Ed., 46 (2007) 3870-3873.
[417] A. Salameh, J. Joubert, A. Baudouin, W. Lukens, F. Delbecq, P. Sautet, J.M. Basset, C. Copéret, CH3ReO3 on γ-Al2O3: Understanding Its Structure, Initiation, and Reactivity in Olefin Metathesis, Angewandte Chemie, 119 (2007) 3944-3947.
[418] L.J. Morris, A.J. Downs, T.M. Greene, G.S. McGrady, W.A. Herrmann, P. Sirsch, O. Gropen, W. Scherer, Photo-induced tautomerisation of methyltrioxorhenium(): the intermediate in olefin metathesis?, Chem. Commun., (2000) 67-68.
[419] L.J. Morris, A.J. Downs, J.C. Green, T.M. Greene, S.J. Teat, S. Parsons, Structural studies and matrix photochemistry of tetramethyloxorhenium(vi), (CH3)4ReO, and related compounds, J. Chem. Soc., Dalton Trans., (2002) 3142-3152.
[420] A.J. Downs, G. Dierker, J.C. Green, T.M. Greene, G. Sean McGrady, L.J. Morris, W. Scherer, P. Sirsch, Vibrational properties and matrix photochemistry of trimethyldioxorhenium(vii), (CH3)3ReO2, J. Chem. Soc., Dalton Trans., (2002) 3349-3360.
[421] L.J. Morris, A.J. Downs, T.M. Greene, G.S. McGrady, W.A. Herrmann, P. Sirsch, W. Scherer, O. Gropen, Matrix Photochemistry of Methyltrioxorhenium(VII), CH3ReO3: Formation of the Methylidene Tautomer H2CRe(O)2OH and Its Potential Relevance to Olefin Metathesis, Organometallics, 20 (2001) 2344-2352.
[422] R. Wischert, C. Copéret, F. Delbecq, P. Sautet, Revisiting the Structure of Methyltrioxorhenium Chemisorbed on Alumina, ChemCatChem, 2 (2010) 812-815.
[423] J. Joubert, A. Salameh, V. Krakoviack, F. Delbecq, P. Sautet, C. Copéret, J.M. Basset, Heterolytic Splitting of H2 and CH4 on γ-Alumina as a Structural Probe for Defect Sites, J. Phys. Chem. B, 110 (2006) 23944-23950.
[424] C. Coperet, Design and understanding of heterogeneous alkene metathesis catalysts, Dalton Trans., (2007) 5498-5504.
[425] A.W. Moses, C. Raab, R.C. Nelson, H.D. Leifeste, N.A. Ramsahye, S. Chattopadhyay, J. Eckert, B.F. Chmelka, S.L. Scott, Spectroscopically Distinct Sites Present in Methyltrioxorhenium Grafted onto Silica−Alumina, and Their Abilities to Initiate Olefin Metathesis, J. Am. Chem. Soc., 129 (2007) 8912-8920.
[426] A. Poater, X. Solans-Monfort, E. Clot, C. Copéret, O. Eisenstein, Understanding d0-Olefin Metathesis Catalysts: Which Metal, Which Ligands?, J. Am. Chem. Soc., 129 (2007) 8207-8216.
[427] X. Solans-Monfort, E. Clot, C. Copéret, O. Eisenstein, d0 Re-Based Olefin Metathesis Catalysts, Re(:CR)(CHR)(X)(Y): The Key Role of X and Y Ligands for Efficient Active Sites, J. Am. Chem. Soc., 127 (2005) 14015-14025.
[428] J.L. Bilhou, J.M. Basset, R. Mutin, W.F. Graydon, A stereochemical study of metathesis and cis-trans isomerization of 2-pentenes, J. Am. Chem. Soc., 99 (1977) 4083-4090.
[429] C. Coperet, Molecular design of heterogeneous catalysts: the case of olefin metathesis, New J. Chem., 28 (2004) 1-10.

[430] S.K. Pillai, S. Hamoudi, K. Belkacemi, Metathesis of methyloleate over methyltrioxorhenium supported on ZnCl2-promoted mesoporous alumina, Applied Catalysis A: General, 455 (2013) 155-163.
[431] S.K. Pillai, S. Hamoudi, K. Belkacemi, Functionalized value-added products via metathesis of methyloleate over methyltrioxorhenium supported on ZnCl2-promoted mesoporous alumina, Fuel, 110 (2013) 32-39.
[432] S.K. Pillai, A. Abidli, K. Belkacemi, Triacylglycerol self-metathesis over highly chemoselective methyltrioxorhenium supported on ZnCl2-promoted mesoporous alumina, Appl. Catal., A, 479 (2014) 121-133.
[433] M. Rouhi, OLEFIN METATHESIS GETS NOBEL NOD, Chem. Eng. News,, 83 (2005) 8.
[434] P.T. Anastas, J.C. Warner, Green Chemistry: Theory and Practice, Oxford University Press: New York, (1998) 30.
[435] R. Gedye, F. Smith, K. Westaway, H. Ali, L. Baldisera, L. Laberge, J. Rousell, The use of microwave ovens for rapid organic synthesis, Tetrahedron Lett., 27 (1986) 279-282.
[436] R.J. Giguere, T.L. Bray, S.M. Duncan, G. Majetich, Application of commercial microwave ovens to organic synthesis, Tetrahedron Lett., 27 (1986) 4945-4948.
[437] F. Nicks, Y. Borguet, X. Sauvage, D. Bicchielli, S. Delfosse, L. Delaude, A. Demonceau, Microwave-Assisted Olefin Metathesis, in: V. Dragutan, A. Demonceau, I. Dragutan, E. Finkelshtein (Eds.) Green Metathesis Chemistry, Springer Netherlands2010, pp. 327-358.
[438] Y. Coquerel, J. Rodriguez, Microwave-Assisted Olefin Metathesis, Eur. J. Org. Chem., 2008 (2008) 1125-1132.
[439] J. Tomasek, J. Schatz, Olefin metathesis in aqueous media, Green Chem., 15 (2013) 2317-2338.
[440] P. Sledz, M. Mauduit, K. Grela, Olefin metathesis in ionic liquids, Chem. Soc. Rev., 37 (2008) 2433-2442.
[441] M. Freemantle, ALKENE METATHESIS IN IONIC LIQUIDS, Chem. Eng. News,, 80 (2002) 38-39.
[442] N. Jain, A. Kumar, S. Chauhan, S.M.S. Chauhan, Chemical and biochemical transformations in ionic liquids, Tetrahedron, 61 (2005) 1015-1060.
[443] J. Hoffmann, M. Nuchter, B. Ondruschka, P. Wasserscheid, Ionic liquids and their heating behaviour during microwave irradiation - a state of the art report and challenge to assessment, Green Chem., 5 (2003) 296-299.
[444] L. Liao, L. Liu, C. Zhang, S. Gong, Microwave-Assisted Ring-Opening Polymerization of ε-Caprolactone in the Presence of Ionic Liquid, Macromol. Rapid Commun., 27 (2006) 2060-2064.
[445] K. Chanda, B. Maiti, C.-C. Tseng, C.-M. Sun, Microwave-Assisted Linear Approach Toward Highly Substituted Benzo[d]oxazol-5-yl-1H-benzo[d]imidazole on Ionic Liquid Support, ACS Comb. Sci., 14 (2012) 115-123.
[446] S. Mallakpour, Z. Rafiee, New developments in polymer science and technology using combination of ionic liquids and microwave irradiation, Prog. Polym. Sci., 36 (2011) 1754-1765.
[447] S. Mallakpour, Z. Rafiee, Use of ionic liquid and microwave irradiation as a convenient, rapid and eco-friendly method for synthesis of novel optically active and thermally stable aromatic polyamides containing N-phthaloyl-l-alanine pendent group, Polym. Degrad. Stab., 93 (2008) 753-759.
[448] E.M. Omar, M.B.A. Rahman, E. Abdulmalek, B.A. Tejo, B. Ni, A.D. Headley, Optimization of Microwave-Assisted Michael Addition Reaction Catalyzed by L-Proline in Ionic Liquid Medium Using Response Surface Methodology, Synth. Commun., 44 (2013) 381-398.
[449] S.S. Shamekhi, F. Nourmohammadian, Microwave-assisted synthesis of diketopyrrolopyrrole pigments in ionic liquid, Pigm. Resin Technol., 42 (2013) 215-222.
[450] X. Lang, M. Shi, Y. Chu, W. Liu, Z. Chen, C. Ma, Microwave-assisted synthesis of Pt-WC/TiO2 in ionic liquid and its application for methanol oxidation, J. Solid State Electrochem., 17 (2013) 2401-2408.
[451] C. Wang, J. Liu, W. Leng, Y. Gao, Rapid and Efficient Functionalized Ionic Liquid-Catalyzed Aldol Condensation Reactions Associated with Microwave Irradiation, Int. J. Mol. Sci., 15 (2014) 1284-1299.
[452] A.V. Vasnev, A.A. Greish, L.M. Kustov, Metathesis of hex-1-ene in ionic liquids, Mendeleev Commun., 14 (2004) 59-60.

[453] A.A. Greish, L.M. Kustov, A.V. Vasnev, Co-metathesis of ethylene and olefinic compounds in ionic liquids, Mendeleev Commun., 21 (2011) 329-330.
[454] C.P. Ferraz, B. Autenrieth, W. Frey, M.R. Buchmeiser, Ionic Grubbs–Hoveyda Complexes for Biphasic Ring-Opening Metathesis Polymerization in Ionic Liquids: Access to Low Metal Content Polymers, ChemCatChem, 6 (2014) 191-198.
[455] C. Simocko, Y. Yang, T.M. Swager, K.B. Wagener, Metathesis Step-Growth Polymerizations in Ionic Liquid, ACS Macro Lett., 2 (2013) 1061-1064.
[456] R.C. Buijsman, E. van Vuuren, J.G. Sterrenburg, Ruthenium-Catalyzed Olefin Metathesis in Ionic Liquids, Org. Lett., 3 (2001) 3785-3787.
[457] D.B.G. Williams, M. Ajam, A. Ranwell, Highly Selective Metathesis of 1-Octene in Ionic Liquids, Organometallics, 25 (2006) 3088-3090.
[458] H. Clavier, N. Audic, J.-C. Guillemin, M. Mauduit, Olefin metathesis in room temperature ionic liquids using imidazolium-tagged ruthenium complexes, J. Organomet. Chem., 690 (2005) 3585-3599.
[459] S.-W. Chen, J.H. Kim, K.Y. Ryu, W.-W. Lee, J. Hong, S.-g. Lee, Novel imidazolium ion-tagged Ru-carbene complexes: synthesis and applications for olefin metathesis in ionic liquid, Tetrahedron, 65 (2009) 3397-3403.
[460] A. Keraani, M. Rabiller-Baudry, C. Fischmeister, C. Bruneau, Immobilisation of an ionically tagged Hoveyda catalyst on a supported ionic liquid membrane: An innovative approach for metathesis reactions in a catalytic membrane reactor, Catal. Today, 156 (2010) 268-275.
[461] G. Liu, H. He, J. Wang, Ferrocene Redox Controlled Reversible Immobilization of Ruthenium Carbene in Ionic Liquid: A Versatile Catalyst for Ring-Closing Metathesis, Adv. Synth. Catal., 351 (2009) 1610-1620.
[462] C.S. Consorti, G.L.P. Aydos, G. Ebeling, J. Dupont, On the Immobilization of Ruthenium Metathesis Catalysts in Imidazolium Ionic Liquids, Organometallics, 28 (2009) 4527-4533.
[463] C. Thurier, C. Fischmeister, C. Bruneau, H. Olivier-Bourbigou, P.H. Dixneuf, Ethenolysis of Methyl Oleate in Room-Temperature Ionic Liquids, ChemSusChem, 1 (2008) 118-122.
[464] P. Gallezot, Process options for converting renewable feedstocks to bioproducts, Green Chem., 9 (2007) 295-302.
[465] M.A.R. Meier, J.O. Metzger, U.S. Schubert, Plant oil renewable resources as green alternatives in polymer science, Chem. Soc. Rev., 36 (2007) 1788-1802.
[466] Y. Xia, R.C. Larock, Vegetable oil-based polymeric materials: synthesis, properties, and applications, Green Chem., 12 (2010) 1893-1909.
[467] J.O. Metzger, U. Bornscheuer, Lipids as renewable resources: current state of chemical and biotechnological conversion and diversification, Appl. Microbiol. Biotechnol., 71 (2006) 13-22.
[468] F.D. Gunstone, Fatty acids and glycerides, Nat. Prod. Rep., 1 (1984) 483-497.
[469] F.D. Gunstone, Fatty acids and glycerides, Nat. Prod. Rep., 4 (1987) 95-112.
[470] F.D. Gunstone, Fatty acids and glycerides, in: F.D. Gunstone (Ed.) Aliphatic and Related Natural Product Chemistry: Volume 2, The Royal Society of Chemistry1981, pp. 194-223.
[471] F.D. Gunstone, Fatty acids and glycerides, in: F.D. Gunstone (Ed.) Aliphatic and Related Natural Product Chemistry: Volume 3, The Royal Society of Chemistry1983, pp. 209-249.
[472] M.S.F.L.K. Jie, Fatty acids and glycerides, Nat. Prod. Rep., 6 (1989) 231-261.
[473] A. Corma, S. Iborra, A. Velty, Chemical Routes for the Transformation of Biomass into Chemicals, Chem. Rev., 107 (2007) 2411-2502.
[474] J. Fernández-Martínez, M. Mancha, J. Osorio, R. Garcés, Sunflower mutant containing high levels of palmitic acid in high oleic background, Euphytica, 97 (1997) 113-116.
[475] H.B. White, Jr., F.W. Quackenbush, A.H. Probst, Occurrence and inheritance of linolenic and linoleic acids in soybean seeds, J. Am. Oil Chem. Soc., 38 (1961) 113-117.
[476] R.E. Beal, V.E. Sohns, R.A. Eisenhauer, E.L. Griffin, Jr., Production of linolenic acid from linseed oil, J. Am. Oil Chem. Soc., 38 (1961) 524-527.
[477] Z. Yun, R. Qian, R. Shao, M. Yang, M. Shi, Separation of erucic acid from rape-seed oil using supercritical carbon dioxide with entrainer, Chin. J. Chem. Eng., 10 (2002) 673-676.

[478] G. Piazza, H. Farrell, Jr., Generation of ricinoleic acid from castor oil using the lipase from ground oat (Avena sativa L.) seeds as a catalyst, Biotechnol. Lett, 13 (1991) 179-184.
[479] S.-W. Kim, M.-K. Park, K.-S. Bae, M.-S. Rhee, J.-R. Liu, Production of petroselinic acid from cell suspension cultures of Coriandrum sativum, Phytochemistry, 42 (1996) 1581-1582.
[480] L. Crombie, S.J. Holloway, Origins of conjugated triene fatty acids. The biosynthesis of calendic acid by Calendula officinalis, J. Chem. Soc., Chem. Commun., (1984) 953-955.
[481] R.T. O'Connor, D.C. Heinzelman, A.F. Freeman, F.C. Pack, Spectrophotometric Determination of Alpha-Eleostearic Acid in Freshly Extracted Tung Oil Determination of Extinction Coefficients in Oil Solvents, Ind. Eng. Chem., Anal. Ed., 17 (1945) 467-470.
[482] M.F. Lie Ken Jie, M. Pasha, F. Ahmad, Ultrasound-assisted synthesis of santalbic acid and a study of triacylglycerol species inSantalum album (Linn.) seed oil, Lipids, 31 (1996) 1083-1089.
[483] A.E. Thompson, D.A. Dierig, R. Kleiman, Variation in Vernonia galamensis flowering characteristics, seed oil and vernolic acid contents, Ind. Crops Prod., 3 (1994) 175-183.
[484] L. Montero de Espinosa, M.A.R. Meier, Plant oils: The perfect renewable resource for polymer science?!, Eur. Polym. J., 47 (2011) 837-852.
[485] L. Maisonneuve, T. Lebarbe, E. Grau, H. Cramail, Structure-properties relationship of fatty acid-based thermoplastics as synthetic polymer mimics, Polym. Chem., 4 (2013) 5472-5517.
[486] M.R.L. Furst, R.L. Goff, D. Quinzler, S. Mecking, C.H. Botting, D.J. Cole-Hamilton, Polymer precursors from catalytic reactions of natural oils, Green Chem., 14 (2012) 472-477.
[487] J.F. Heidrich, Oleochemicals: Feedstock or auxiliary, J. Am. Oil Chem. Soc., 61 (1984) 271-275.
[488] A.S. More, B. Gadenne, C. Alfos, H. Cramail, AB type polyaddition route to thermoplastic polyurethanes from fatty acid derivatives, Polym. Chem., 3 (2012) 1594-1605.
[489] M.R.L. Furst, T. Seidensticker, D.J. Cole-Hamilton, Polymerisable di- and triesters from Tall Oil Fatty Acids and related compounds, Green Chem., 15 (2013) 1218-1225.
[490] A. Jones, A. Mandal, S. Sharma, Protein-based bioplastics and their antibacterial potential, J. Appl. Polym. Sci., 132 (2015) n/a-n/a.
[491] M.B. Agustin, B. Ahmmad, S.M.M. Alonzo, F.M. Patriana, Bioplastic based on starch and cellulose nanocrystals from rice straw, J. Reinf. Plast. Compos., 33 (2014) 2205-2213.
[492] M. Venkateswar Reddy, K. Amulya, M.V. Rohit, P.N. Sarma, S. Venkata Mohan, Valorization of fatty acid waste for bioplastics production using Bacillus tequilensis: Integration with dark-fermentative hydrogen production process, Int. J. Hydrogen Energy, 39 (2014) 7616-7626.
[493] M. Zhang, A. Sun, Y. Meng, L. Wang, H. Jiang, G. Li, High activity ordered mesoporous carbon-based solid acid catalyst for the esterification of free fatty acids, Microporous Mesoporous Mater., 204 (2015) 210-217.
[494] L. Ha, J. Mao, J. Zhou, Z.C. Zhang, S. Zhang, Skeletal isomerization of unsaturated fatty acids on Beta zeolites: Effects of calcination temperature and additives, Appl. Catal., A, 356 (2009) 52-56.
[495] R. Malacea, P. Dixneuf, Alkene Metathesis and Renewable Materials: Selective Transformations of Plant Oils, in: V. Dragutan, A. Demonceau, I. Dragutan, E. Finkelshtein (Eds.) Green Metathesis Chemistry, Springer Netherlands2010, pp. 185-206.
[496] J.C. Mol, Metathesis of functionalized acyclic olefins, J. Mol. Catal., 65 (1991) 145-162.
[497] J.C. Mol, Metathesis of functionalized olefins, J. Mol. Catal., 15 (1982) 35-45.
[498] C. Boelhouwer, Functionalised olefin metathesis, J. Mol. Catal., 46 (1988) 297-303.
[499] J.C. Mol, Metathesis of unsaturated fatty acid esters and fatty oils, J. Mol. Catal., 90 (1994) 185-199.
[500] P.B. Van Dam, M.C. Mittelmeijer, C. Boelhouwer, Metathesis of unsaturated fatty acid esters by a homogeneous tungsten hexachloride-tetramethyltin catalyst, J. Chem. Soc., Chem. Commun., (1972) 1221-1222.
[501] P.B. Dam, M.C. Mittelmeijer, C. Boelhouwer, Homogeneous catalytic metathesis of unsaturated fatty esters: New synthetic method for preparation of unsaturated mono-and dicarboxylic acids, J Am Oil Chem Soc, 51 (1974) 389-392.
[502] C. Boelhouwer, J.C. Mol, Metathesis of fatty acid esters, Journal of the American Oil Chemists' Society, 61 (1984) 425-430.

[503] E. Verkuijlen, C. Boelhouwer, Metathesis of Unsaturated Fatty Esters, Fette, Seifen, Anstrichm., 78 (1976) 444-447.
[504] F.B.H. Ahmad, M.A. Yarmo, A. Alimuniar, Co-metathesis reaction of methyl linoleate with ethene over WCl6 catalyst, J. Mol. Catal., 89 (1994) 357-364.
[505] D.S. Banasiak, Insect pheromones from olefin metathesis, J. Mol. Catal., 28 (1985) 107-115.
[506] F. Quignard, M. Leconte, J.-M. Basset, Synthesis and catalytic properties of W(OAr)2Cl2(CHCMe3)(OR2) and W(OAr)2Cl(CHCMe3)(CH2CMe3)(OR2)(Ar = 2,6-disubstituted phenyl; R = Et or Pri), new uni-component catalysts for metathesis of acyclic and cyclic olefins, with or without functional groups, J. Chem. Soc., Chem. Commun., (1985) 1816-1817.
[507] F. Quignard, M. Leconte, J.M. Basset, Aryloxide ligands in metathesis of olefins and olefinic esters: catalytic behaviour of W(OAr)2Cl4 complexes associated with alkyl-tin or alkyl-lead cocatalysts; alkylation of W(OAr)2Cl4 by SnMe4, Sn(n-Bu)4, Pb(n-Bu)4, MgNp2: synthesis of W(OAr)2Cl2(CHCMe3)(OR2) and W(OAr)2Cl(CHCMe3)(CH2CMe3)(OR2), J. Mol. Catal., 36 (1986) 13-29.
[508] C.J. Schaverien, J.C. Dewan, R.R. Schrock, Multiple metal-carbon bonds. 43. Well-characterized, highly active, Lewis acid free olefin metathesis catalysts, J. Am. Chem. Soc., 108 (1986) 2771-2773.
[509] G.B. Djigoué, M.A.R. Meier, Improving the selectivity for the synthesis of two renewable platform chemicals via olefin metathesis, Appl. Catal., A, 368 (2009) 158-162.
[510] T.T.T. Ho, T. Jacobs, M.A.R. Meier, A Design-of-Experiments Approach for the Optimization and Understanding of the Cross-Metathesis Reaction of Methyl Ricinoleate with Methyl Acrylate, ChemSusChem, 2 (2009) 749-754.
[511] R. Holser, K. Doll, S. Erhan, Metathesis of methyl soyate with ruthenium catalysts, Fuel, 85 (2006) 393-395.
[512] H. Ngo, T. Foglia, Synthesis of Long Chain Unsaturated-α,ω-Dicarboxylic Acids from Renewable Materials via Olefin Metathesis, J. Am. Oil Chem. Soc., 84 (2007) 777-784.
[513] F.B.H. Ahmad, S. Hamdan, M.A. Yarmo, A. Alimunir, Co-metathesis reaction of crude palm oil and ethene, Journal of the American Oil Chemists' Society, 72 (1995) 757-758.
[514] B.B. Marvey, J.A.K. du Plessis, H.C.M. Vosloo, J.C. Mol, Metathesis of unsaturated fatty acid esters derived from South African sunflower oil in the presence of a 3 wt.% Re2O7/SiO2–Al2O3/SnBu4 catalyst, Journal of Molecular Catalysis A: Chemical, 201 (2003) 297-308.
[515] Y. Vyshnavi, R.B.N. Prasad, M.S.L. Karuna, Metathesis of tobacco fatty acid methyl esters: Generation of industrially important platform chemicals, Ind. Crops Prod., 50 (2013) 701-706.
[516] M.A. Yarmo, A. Alimuniar, R. Abd Ghani, A.R. Sulaiman, M. Ghani, H. Omar, A. Malek, Transesterification products from the metathesis reaction of palm oil, J. Mol. Catal., 76 (1992) 373-379.
[517] N.A.M. Nordin, B.M. Yamin, M.A. Yarmo, K. Pardan, A.B. Alimuniar, Metathesis of palm oil, J. Mol. Catal., 65 (1991) 163-172.
[518] C. Boelhouwer, J.C. Mol, Metathesis reactions of fatty acid esters, Prog. Lipid Res., 24 (1985) 243-267.
[519] B. Marciniec, L. Rzejak, J. Gulinski, Z. Foltynowicz, W. Urbaniak, Ruthenium and rhodium complex catalysts for metathesis of silicon olefins, J. Mol. Catal., 46 (1988) 329-340.
[520] B. Marciniec, H. Maciejewski, J. Guliński, L. Rzejak, Metathesis of silicon containing olefins: II. Synthesis of 1,2-bis(silyl)ethenes by metathesis of vinylsilanes, J. Organomet. Chem., 362 (1989) 273-279.
[521] Z. Foltynowicz, B. Marciniec, Metathesis of silicon-containing olefins: IV. Synthesis of 1-triethoxysilyl-1-alkenes by cross-metathesis of vinyltriethoxysilane with 1-alkenes, J. Organomet. Chem., 376 (1989) 15-20.
[522] E. Benetskiy, S. Lühr, M. Vilches-Herrera, D. Selent, H. Jiao, L. Domke, K. Dyballa, R. Franke, A. Börner, Rhodium-Catalyzed Nonisomerizing Hydroformylation of Methyl Oleate Applying Lactame-Based Phosphoramidite Ligands, ACS Catal., 4 (2014) 2130-2136.
[523] P. Spannring, I. Prat, M. Costas, M. Lutz, P.C.A. Bruijnincx, B.M. Weckhuysen, R.J.M. Klein Gebbink, Fe(6-Me-PyTACN)-catalyzed, one-pot oxidative cleavage of methyl oleate and oleic acid into carboxylic acids with H2O2 and NaIO4, Catal. Sci. Technol., 4 (2014) 708-716.

[524] J.T. Christl, P. Roesle, F. Stempfle, P. Wucher, I. Göttker-Schnetmann, G. Müller, S. Mecking, Catalyst Activity and Selectivity in the Isomerising Alkoxycarbonylation of Methyl Oleate, Chem. - Eur. J., 19 (2013) 17131-17140.
[525] Y. Schrodi, T. Ung, A. Vargas, G. Mkrtumyan, C.W. Lee, T.M. Champagne, R.L. Pederson, S.H. Hong, Ruthenium Olefin Metathesis Catalysts for the Ethenolysis of Renewable Feedstocks, CLEAN – Soil, Air, Water, 36 (2008) 669-673.
[526] K.M. Doll, Increased functionality of methyl oleate using alkene metathesis, Int. J. Sust. Eng., (2013) 1-8.
[527] K.A. Burdett, L.D. Harris, P. Margl, B.R. Maughon, T. Mokhtar-Zadeh, P.C. Saucier, E.P. Wasserman, Renewable Monomer Feedstocks via Olefin Metathesis: Fundamental Mechanistic Studies of Methyl Oleate Ethenolysis with the First-Generation Grubbs Catalyst, Organometallics, 23 (2004) 2027-2047.
[528] M.B. Dinger, J.C. Mol, High Turnover Numbers with Ruthenium-Based Metathesis Catalysts, Adv. Synth. Catal., 344 (2002) 671-677.
[529] A. Nickel, T. Ung, G. Mkrtumyan, J. Uy, C. Lee, D. Stoianova, J. Papazian, W.-H. Wei, A. Mallari, Y. Schrodi, R. Pederson, A Highly Efficient Olefin Metathesis Process for the Synthesis of Terminal Alkenes from Fatty Acid Esters, Top. Catal., 55 (2012) 518-523.
[530] P.A. Thomas, B.B. Marvey, C18:1 methyl ester metathesis in [bmim][X] type ionic liquids, Int. J. Mol. Sci., 10 (2009) 5020-5030.
[531] R. Kadyrov, C. Azap, S. Weidlich, D. Wolf, Robust and Selective Metathesis Catalysts for Oleochemical Applications, Top. Catal., 55 (2012) 538-542.
[532] J. Zhang, S. Song, X. Wang, J. Jiao, M. Shi, Ruthenium-catalyzed olefin metathesis accelerated by the steric effect of the backbone substituent in cyclic (alkyl)(amino) carbenes, Chem. Commun., 49 (2013) 9491-9493.
[533] P.A. Thomas, B.B. Marvey, E.E. Ebenso, Metathesis of fatty acid ester derivatives in 1,1-dialkyl and 1,2,3-trialkyl imidazolium type ionic liquids, Int. J. Mol. Sci., 12 (2011) 3989-3997.
[534] J. Patel, S. Mujcinovic, W.R. Jackson, A.J. Robinson, A.K. Serelis, C. Such, High conversion and productive catalyst turnovers in cross-metathesis reactions of natural oils with 2-butene, Green Chem., 8 (2006) 450-454.
[535] B.B. Marvey, C.K. Segakweng, M.H.C. Vosloo, Ruthenium carbene mediated metathesis of oleate-type fatty compounds, Int. J. Mol. Sci., 9 (2008) 615-625.
[536] J.-M. Brégeault, B. El Ali, J. Martin, C. Martin, F. Derdar, G. Bugli, M. Delamar, Novel rhenium catalysts (chlorides and/or alkoxides dispersed on inorganic supports) for metathesis: A comparison with ammonium perrhenate precursors, J. Mol. Catal., 46 (1988) 37-60.
[537] A. Kajetanowicz, A. Sytniczuk, K. Grela, Metathesis of renewable raw materials-influence of ligands in the indenylidene type catalysts on self-metathesis of methyl oleate and cross-metathesis of methyl oleate with (Z)-2-butene-1,4-diol diacetate, Green Chem., 16 (2014) 1579-1585.
[538] C.B. Rodella, J.A.M. Cavalcante, R. Buffon, Metathesis of methyl oleate over rhenium oxide-based catalysts supported on borated silica–alumina: catalyst recycling, Appl. Catal., A, 274 (2004) 213-217.
[539] M. Sibeijn, J.C. Mol, Activity of supported Re2O7 catalysts for the metathesis of methyl oleate, Appl. Catal., 67 (1990) 279-295.
[540] J. Zelin, A.F. Trasarti, C.R. Apesteguía, Self-metathesis of methyl oleate on silica-supported Hoveyda–Grubbs catalysts, Catal. Commun., 42 (2013) 84-88.
[541] H. Kohashi, T. Foglia, Metathesis of methyl oleate with a homogeneous and a heterogeneous catalyst, J. Am. Oil Chem. Soc., 62 (1985) 549-554.
[542] J. Tsuji, S. Hashiguchi, Metathesis reactions of unsaturated esters catalyzed by homogenous tungsten complexes. Syntheses of civetone and macrolides, J. Organomet. Chem., 218 (1981) 69-80.
[543] C.B. Rodella, R. Buffon, Characterization and catalytic performance of rhenium oxide-based catalysts supported on borated silica-alumina, Appl. Catal., A, 263 (2004) 203-211.
[544] J.C. Mol, Activity and stability of laser-photoreduced supported molybdenum oxide metathesis catalysts, Catal. Lett., 23 (1994) 113-118.

[545] G.S. Forman, R.M. Bellabarba, R.P. Tooze, A.M.Z. Slawin, R. Karch, R. Winde, Metathesis of renewable unsaturated fatty acid esters catalysed by a phoban-indenylidene ruthenium catalyst, J. Organomet. Chem., 691 (2006) 5513-5516.
[546] P.O. Nubel, C.L. Hunt, A convenient catalyst system employing RuCl3 or RuBr3 for metathesis of acyclic olefins, J. Mol. Catal. A: Chem., 145 (1999) 323-327.
[547] M. Chabanas, C. Copéret, J.-M. Basset, Re-Based Heterogeneous Catalysts for Olefin Metathesis Prepared by Surface Organometallic Chemistry: Reactivity and Selectivity, Chem. - Eur. J., 9 (2003) 971-975.
[548] J. Cabrera, R. Padilla, M. Bru, R. Lindner, T. Kageyama, K. Wilckens, S.L. Balof, H.-J. Schanz, R. Dehn, J.H. Teles, S. Deuerlein, K. Müller, F. Rominger, M. Limbach, Linker-Free, Silica-Bound Olefin-Metathesis Catalysts: Applications in Heterogeneous Catalysis, Chem. - Eur. J., 18 (2012) 14717-14724.
[549] Z. Yinghuai, L. Kuijin, N. Huimin, L. Chuanzhao, L.P. Stubbs, C.F. Siong, T. Muihua, S.C. Peng, Magnetic Nanoparticle Supported Second Generation Hoveyda–Grubbs Catalyst for Metathesis of Unsaturated Fatty Acid Esters, Adv. Synth. Catal., 351 (2009) 2650-2656.
[550] B. Autenrieth, F. Willig, D. Pursley, S. Naumann, M.R. Buchmeiser, Ionically Tagged Ru–Alkylidenes for Metathesis Reactions under Biphasic Liquid–Liquid Conditions, ChemCatChem, 5 (2013) 3033-3040.
[551] B. Autenrieth, W. Frey, M.R. Buchmeiser, A Dicationic Ruthenium Alkylidene Complex for Continuous Biphasic Metathesis Using Monolith-Supported Ionic Liquids, Chem. - Eur. J., 18 (2012) 14069-14078.
[552] R. Duque, E. Ochsner, H. Clavier, F. Caijo, S.P. Nolan, M. Mauduit, D.J. Cole-Hamilton, Continuous flow homogeneous alkene metathesis with built-in catalyst separation, Green Chem., 13 (2011) 1187-1195.
[553] D. Bek, H. Balcar, N.z.d. Zilkova, A.t. Zukal, M. Horacek, J.i. Cejka, Grubbs Catalysts Immobilized on Mesoporous Molecular Sieves via Phosphine and Pyridine Linkers, ACS Catal., 1 (2011) 709-718.
[554] H. Balcar, T. Shinde, N. Žilková, Z. Bastl, Hoveyda-Grubbs type metathesis catalyst immobilized on mesoporous molecular sieves MCM-41 and SBA-15, Beilstein J. Org. Chem., 7 (2011) 22-28.
[555] M. Abbas, C. Slugovc, Optimized reaction conditions for the cross-metathesis of methyl oleate and oleylamine with ethyl acrylate, Monatshefte für Chemie - Chemical Monthly, 143 (2012) 669-673.
[556] A. Behr, J.P. Gomes, The cross-metathesis of methyl oleate with c/s-2-butene-1,4-diyl diacetate and the influence of protecting groups, Beilstein J. Org. Chem., 7 (2011) 1-8.
[557] M. Sibeijn, J.C. Mol, Ethenolysis of methyl oleate over supported Re-based catalysts, J. Mol. Catal., 76 (1992) 345-358.
[558] X. Miao, C. Fischmeister, C. Bruneau, P.H. Dixneuf, Dimethyl Carbonate: An Eco-Friendly Solvent in Ruthenium-Catalyzed Olefin Metathesis Transformations, ChemSusChem, 1 (2008) 813-816.
[559] R.M. Thomas, B.K. Keitz, T.M. Champagne, R.H. Grubbs, Highly Selective Ruthenium Metathesis Catalysts for Ethenolysis, J. Am. Chem. Soc., 133 (2011) 7490-7496.
[560] D.R. Anderson, T. Ung, G. Mkrtumyan, G. Bertrand, R.H. Grubbs, Y. Schrodi, Kinetic Selectivity of Olefin Metathesis Catalysts Bearing Cyclic (Alkyl)(Amino)Carbenes, Organometallics, 27 (2008) 563-566.
[561] S.C. Marinescu, R.R. Schrock, P. Müller, A.H. Hoveyda, Ethenolysis Reactions Catalyzed by Imido Alkylidene Monoaryloxide Monopyrrolide (MAP) Complexes of Molybdenum, J. Am. Chem. Soc., 131 (2009) 10840-10841.
[562] C.P. Park, M.M. Van Wingerden, S.-Y. Han, D.-P. Kim, R.H. Grubbs, Low Pressure Ethenolysis of Renewable Methyl Oleate in a Microchemical System, Org. Lett., 13 (2011) 2398-2401.
[563] A. Rybak, M.A.R. Meier, Cross-metathesis of fatty acid derivatives with methyl acrylate: renewable raw materials for the chemical industry, Green Chem., 9 (2007) 1356-1361.
[564] K.M. Doll, Increased functionality of methyl oleate using alkene metathesis, Int. J. Sust. Eng., 7 (2013) 322-329.
[565] G.L.P. Aydos, B.C. Leal, O.W. Perez-Lopez, J. Dupont, Ionic-tagged catalytic systems applied to the ethenolysis of methyl oleate, Catal. Commun., 53 (2014) 57-61.
[566] A. Chhetri, K. Watts, M. Islam, Waste Cooking Oil as an Alternate Feedstock for Biodiesel Production, Energies, 1 (2008) 3-18.

[567] E. González, A. Hernández-Matamoros, J.F. Tejeda, Two by-products of the olive oil extraction industry as oleic acid supplement source for Iberian pigs: effect on the meat's chemical composition and induced lipoperoxidation, J. Sci. Food Agric., 92 (2012) 2543-2551.
[568] A. Salvador, A. Cavaleiro, D. Sousa, M.M. Alves, M.A. Pereira, Endurance of methanogenic archaea in anaerobic bioreactors treating oleate-based wastewater, Appl. Microbiol. Biotechnol., 97 (2013) 2211-2218.
[569] A.J. Cavaleiro, A.F. Salvador, J.I. Alves, M. Alves, Continuous High Rate Anaerobic Treatment of Oleic Acid Based Wastewater is Possible after a Step Feeding Start-Up, Environ. Sci. Technol., 43 (2009) 2931-2936.
[570] C. Márquez-Alvarez, N. Žilková, J. Pérez-Pariente, J. Čejka, Synthesis, Characterization and Catalytic Applications of Organized Mesoporous Aluminas, Catal. Rev., 50 (2008) 222-286.
[571] X. Jiang, N. Suzuki, B.P. Bastakoti, K.C.W. Wu, Y. Yamauchi, Synthesis of Continuous Mesoporous Alumina Films with Large-Sized Cage-Type Mesopores by Using Diblock Copolymers, Chem. Asian J., 7 (2012) 1713-1718.
[572] B.P. Bastakoti, S. Ishihara, S.-Y. Leo, K. Ariga, K.C.W. Wu, Y. Yamauchi, Polymeric Micelle Assembly for Preparation of Large-Sized Mesoporous Metal Oxides with Various Compositions, Langmuir, 30 (2014) 651-659.
[573] X. Jiang, H. Oveisi, Y. Nemoto, N. Suzuki, K.C.W. Wu, Y. Yamauchi, Synthesis of highly ordered mesoporous alumina thin films and their framework crystallization to [gamma]-alumina phase, Dalton Trans., 40 (2011) 10851-10856.
[574] A. Taguchi, F. Schüth, Ordered mesoporous materials in catalysis, Microporous Mesoporous Mater., 77 (2005) 1-45.
[575] W. Li, Q. Yue, Y. Deng, D. Zhao, Ordered Mesoporous Materials Based on Interfacial Assembly and Engineering, Adv. Mater., 25 (2013) 5129-5152.
[576] D. Zhao, Y. Wan, W. Zhou, Synthesis Approach of Mesoporous Molecular Sieves, Ordered Mesoporous Materials, Wiley-VCH Verlag GmbH & Co. KGaA2013, pp. 5-54.
[577] L. Calvillo, V. Celorrio, R. Moliner, P.L. Cabot, I. Esparbé, M.J. Lázaro, Control of textural properties of ordered mesoporous materials, Microporous Mesoporous Mater., 116 (2008) 292-298.
[578] C.T. Kresge, M.E. Leonowicz, W.J. Roth, J.C. Vartuli, J.S. Beck, Ordered mesoporous molecular sieves synthesized by a liquid-crystal template mechanism, Nature, 359 (1992) 710-712.
[579] J.S. Beck, J.C. Vartuli, W.J. Roth, M.E. Leonowicz, C.T. Kresge, K.D. Schmitt, C.T.W. Chu, D.H. Olson, E.W. Sheppard, A new family of mesoporous molecular sieves prepared with liquid crystal templates, J. Am. Chem. Soc., 114 (1992) 10834-10843.
[580] D. Zhao, J. Feng, Q. Huo, N. Melosh, G.H. Fredrickson, B.F. Chmelka, G.D. Stucky, Triblock Copolymer Syntheses of Mesoporous Silica with Periodic 50 to 300 Angstrom Pores, Science, 279 (1998) 548-552.
[581] R. Schmidt, M. Stöcker, O. Henrik Ellestad, Characterisation of a cubic mesoporous MCM-48 compared to a hexagonal MCM-41, in: B. Laurent, K. Serge (Eds.) Stud. Surf. Sci. Catal., Elsevier1995, pp. 149-156.
[582] F. Kleitz, S. Hei Choi, R. Ryoo, Cubic Ia3d large mesoporous silica: synthesis and replication to platinum nanowires, carbon nanorods and carbon nanotubes, Chem. Commun., (2003) 2136-2137.
[583] R. Ryoo, S.H. Joo, M. Kruk, M. Jaroniec, Ordered Mesoporous Carbons, Adv. Mater., 13 (2001) 677-681.
[584] S. Jun, S.H. Joo, R. Ryoo, M. Kruk, M. Jaroniec, Z. Liu, T. Ohsuna, O. Terasaki, Synthesis of New, Nanoporous Carbon with Hexagonally Ordered Mesostructure, J. Am. Chem. Soc., 122 (2000) 10712-10713.
[585] P. Yang, T. Deng, D. Zhao, P. Feng, D. Pine, B.F. Chmelka, G.M. Whitesides, G.D. Stucky, Hierarchically Ordered Oxides, Science, 282 (1998) 2244-2246.
[586] P. Yang, D. Zhao, D.I. Margolese, B.F. Chmelka, G.D. Stucky, Generalized syntheses of large-pore mesoporous metal oxides with semicrystalline frameworks, Nature, 396 (1998) 152-155.

[587] Y. Noda, B. Lee, K. Domen, J.N. Kondo, Synthesis of Crystallized Mesoporous Tantalum Oxide and Its Photocatalytic Activity for Overall Water Splitting under Ultraviolet Light Irradiation, Chem. Mater., 20 (2008) 5361-5367.
[588] G.J.d.A.A. Soler-Illia, C. Sanchez, B. Lebeau, J. Patarin, Chemical Strategies To Design Textured Materials: from Microporous and Mesoporous Oxides to Nanonetworks and Hierarchical Structures, Chem. Rev., 102 (2002) 4093-4138.
[589] S. Inagaki, S. Guan, T. Ohsuna, O. Terasaki, An ordered mesoporous organosilica hybrid material with a crystal-like wall structure, Nature, 416 (2002) 304-307.
[590] H. Balcar, J. Čejka, Mesoporous Molecular Sieves Based Catalysts for Olefin Metathesis and Metathesis Polymerization, in: V. Dragutan, A. Demonceau, I. Dragutan, E. Finkelshtein (Eds.) Green Metathesis Chemistry, Springer Netherlands2010, pp. 101-114.
[591] R. Hamtil, N. Žilková, H. Balcar, J. Čejka, Rhenium oxide supported on organized mesoporous alumina — A highly active and versatile catalyst for alkene, diene, and cycloalkene metathesis, Appl. Catal., A, 302 (2006) 193-200.
[592] H. Balcar, R. Hamtil, N. Žilková, J. Čejka, Rhenium Oxide Supported on Mesoporous Organised Alumina as a Catalyst for Metathesis of 1-Alkenes, Catal. Lett., 97 (2004) 25-29.
[593] J. Aguado, J.M. Escola, M.C. Castro, B. Paredes, Metathesis of 1-hexene over rhenium oxide supported on ordered mesoporous aluminas: comparison with Re2O7/γ-Al2O3, Appl. Catal., A, 284 (2005) 47-57.
[594] Y. Yamauchi, N. Suzuki, T. Kimura, Formation of mesoporous oxide fibers in polycarbonate confined spaces, Chem. Commun., (2009) 5689-5691.
[595] H. Oveisi, X. Jiang, M. Imura, Y. Nemoto, Y. Sakamoto, Y. Yamauchi, A Mesoporous γ-Alumina Film with Vertical Mesoporosity: The Unusual Conversion from a Im${\bar 3}$m Mesostructure to Vertically Oriented γ-Alumina Nanowires, Angew. Chem. Int. Ed., 50 (2011) 7410-7413.
[596] K. Niesz, P. Yang, G.A. Somorjai, Sol-gel synthesis of ordered mesoporous alumina, Chem. Commun., (2005) 1986-1987.
[597] Q. Liu, A. Wang, J. Xu, Y. Zhang, X. Wang, T. Zhang, Preparation of ordered mesoporous crystalline alumina replicated by mesoporous carbon, Microporous Mesoporous Mater., 116 (2008) 461-468.
[598] Q. Yuan, A.-X. Yin, C. Luo, L.-D. Sun, Y.-W. Zhang, W.-T. Duan, H.-C. Liu, C.-H. Yan, Facile Synthesis for Ordered Mesoporous γ-Aluminas with High Thermal Stability, J. Am. Chem. Soc., 130 (2008) 3465-3472.
[599] Q. Wu, F. Zhang, J. Yang, Q. Li, B. Tu, D. Zhao, Synthesis of ordered mesoporous alumina with large pore sizes and hierarchical structure, Microporous Mesoporous Mater., 143 (2011) 406-412.
[600] F. Huang, Y. Zheng, G. Cai, Y. Zheng, Y. Xiao, K. Wei, A new synthetic procedure for ordered mesoporous γ-alumina with a large surface area, Scripta Mater., 63 (2010) 339-342.
[601] F. Vaudry, S. Khodabandeh, M.E. Davis, Synthesis of Pure Alumina Mesoporous Materials, Chem. Mater., 8 (1996) 1451-1464.
[602] J. Cejka, P.J. Kooyman, L. Vesela, J. Rathousky, A. Zukal, High-temperature transformations of organised mesoporous alumina, Phys. Chem. Chem. Phys., 4 (2002) 4823-4829.
[603] W. Cai, J. Yu, C. Anand, A. Vinu, M. Jaroniec, Facile Synthesis of Ordered Mesoporous Alumina and Alumina-Supported Metal Oxides with Tailored Adsorption and Framework Properties, Chem. Mater., 23 (2011) 1147-1157.
[604] J.-P. Dacquin, J. Dhainaut, D. Duprez, S. Royer, A.F. Lee, K. Wilson, An Efficient Route to Highly Organized, Tunable Macroporous−Mesoporous Alumina, J. Am. Chem. Soc., 131 (2009) 12896-12897.
[605] S.M. Grant, A. Vinu, S. Pikus, M. Jaroniec, Adsorption and structural properties of ordered mesoporous alumina synthesized in the presence of F127 block copolymer, Colloids Surf., A, 385 (2011) 121-125.
[606] X. Wang, D. Pan, M. Guo, M. He, P. Niu, R. Li, Facile synthesis of highly ordered mesoporous alumina with high thermal and hydrothermal stability using zirconia as promoter, Mater. Lett., 97 (2013) 27-30.
[607] S.M. Morris, P.F. Fulvio, M. Jaroniec, Ordered Mesoporous Alumina-Supported Metal Oxides, J. Am. Chem. Soc., 130 (2008) 15210-15216.

[608] L.-L. Li, W.-T. Duan, Q. Yuan, Z.-X. Li, H.-H. Duan, C.-H. Yan, Hierarchical [gamma]-Al2O3 monoliths with highly ordered 2D hexagonal mesopores in macroporous walls, Chem. Commun., (2009) 6174-6176.
[609] J. Cejka, N. Zilkova, J. Rathousky, A. Zukal, Nitrogen adsorption study of organised mesoporous alumina, Phys. Chem. Chem. Phys., 3 (2001) 5076-5081.
[610] X. Yuan, S. Xu, J. Lü, X. Yan, L. Hu, Q. Xue, Facile synthesis of ordered mesoporous γ-alumina monoliths via polymerization-based gel-casting, Microporous Mesoporous Mater., 138 (2011) 40-44.
[611] M. Jaroniec, P. Fulvio, Standard nitrogen adsorption data for α-alumina and their use for characterization of mesoporous alumina-based materials, Adsorption, 19 (2013) 475-481.
[612] Z. Wu, Q. Li, D. Feng, P.A. Webley, D. Zhao, Ordered Mesoporous Crystalline γ-Al2O3 with Variable Architecture and Porosity from a Single Hard Template, J. Am. Chem. Soc., 132 (2010) 12042-12050.
[613] Q. Liu, A. Wang, X. Wang, T. Zhang, Ordered Crystalline Alumina Molecular Sieves Synthesized via a Nanocasting Route, Chem. Mater., 18 (2006) 5153-5155.
[614] F. Huang, Y. Zheng, Y. Xiao, Y. Zheng, G. Cai, K. Wei, A new synthetic procedure for ordered mesoporous γ-alumina using phthalic acid as an interfacial protector, Mater. Lett., 65 (2011) 244-246.
[615] Q. Sun, Y. Zheng, Z. Li, Y. Zheng, Y. Xiao, G. Cai, Synthesis of ordered mesoporous γ-alumina influenced by the interfacial protector, Mater. Lett., 84 (2012) 44-47.
[616] X.-L. Zheng, Q.-P. Sun, F. Liu, Y. Zheng, J.-B. Weng, Effect of p-aminobenzoic acid on synthesizing ordered mesoporous alumina via the sol–gel method, J. Porous Mater., 21 (2014) 819-825.
[617] Z. Ramli, R. Saleh, The Effect of Synthesis Routes on the Development of Ordered Mesoporous Alumina by Precipitation Method, AIP Conf. Proc., 1136 (2009) 26-30.
[618] S.M. Grant, M. Jaroniec, Effect of cosolvent organic molecules on the adsorption and structural properties of soft-templated ordered mesoporous alumina, J. Colloid Interface Sci., 367 (2012) 129-134.
[619] S.M. Grant, M. Jaroniec, Effect of acid concentration on pore size in polymer-templated mesoporous alumina, J. Mater. Chem., 22 (2012) 86-92.
[620] X. Zhao, Y. Zheng, Y. Zheng, Y. Zhan, X. Zheng, Preparation and pore structure stability at high temperature of silicon-doped ordered mesoporous alumina, RSC Adv., 4 (2014) 12497-12505.
[621] Q. Sun, Y. Zheng, Z. Li, Y. Zheng, Y. Xiao, G. Cai, K. Wei, Studies on the improved thermal stability for doped ordered mesoporous [gamma]-alumina, Phys. Chem. Chem. Phys., 15 (2013) 5670-5676.
[622] F. Huang, Y. Zheng, Z. Li, Y. Xiao, Y. Zheng, G. Cai, K. Wei, Synthesis of highly dispersed ceria-zirconia supported on ordered mesoporous alumina, Chem. Commun., 47 (2011) 5247-5249.
[623] E. Moretti, M. Lenarda, L. Storaro, A. Talon, R. Frattini, S. Polizzi, E. Rodríguez-Castellón, A. Jiménez-López, Catalytic purification of hydrogen streams by PROX on Cu supported on an organized mesoporous ceria-modified alumina, Appl. Catal., B, 72 (2007) 149-156.
[624] Q. Sun, Y. Zheng, Y. Zheng, Y. Xiao, G. Cai, K. Wei, Synthesis of highly thermally stable lanthanum-doped ordered mesoporous alumina, Scripta Mater., 65 (2011) 1026-1029.
[625] Z.-X. Li, F.-B. Shi, L.-L. Li, T. Zhang, C.-H. Yan, A facile route to ordered mesoporous-alumina-supported catalysts, and their catalytic activities for CO oxidation, Phys. Chem. Chem. Phys., 13 (2011) 2488-2491.
[626] H. Oveisi, A. Beitollahi, M. Imura, C.-W. Wu, Y. Yamauchi, Synthesis and characterization of highly ordered titania-alumina mixed oxide mesoporous films with high alumina content, Microporous Mesoporous Mater., 134 (2010) 150-156.
[627] L. Xu, H. Zhao, H. Song, L. Chou, Ordered mesoporous alumina supported nickel based catalysts for carbon dioxide reforming of methane, Int. J. Hydrogen Energy, 37 (2012) 7497-7511.
[628] Y. Bang, S.J. Han, J.G. Seo, M.H. Youn, J.H. Song, I.K. Song, Hydrogen production by steam reforming of liquefied natural gas (LNG) over ordered mesoporous nickel–alumina catalyst, Int. J. Hydrogen Energy, 37 (2012) 17967-17977.
[629] L. Kaluža, M. Zdražil, N. Žilková, J. Čejka, High activity of highly loaded MoS2 hydrodesulfurization catalysts supported on organised mesoporous alumina, Catal. Commun., 3 (2002) 151-157.
[630] T. Xiu, J. Wang, Q. Liu, Ordered bimodal mesoporous boria–alumina composite: One-step synthesis, structural characterization, active catalysis for methanol dehydration, Microporous Mesoporous Mater., 143 (2011) 362-367.

[631] T. Oikawa, Y. Masui, T. Tanaka, Y. Chujo, M. Onaka, Lewis acid-modified mesoporous alumina: A new catalyst carrier for methyltrioxorhenium in metathesis of olefins bearing functional groups, J. Organomet. Chem., 692 (2007) 554-561.
[632] M. Zamora, A. Cordoba, A study of surface hydroxyl groups on .gamma.-alumina, J. Phys. Chem., 82 (1978) 584-588.
[633] J.B. Peri, Infrared and Gravimetric Study of the Surface Hydration of γ-Alumina, J. Phys. Chem., 69 (1965) 211-219.
[634] T. Tovar, S.M. Stewart, S. Scott, Origin of the ZnCl2 Effect on CH3ReO3/γ-Al2O3 in Olefin Metathesis, Top Catal, 55 (2012) 530-537.
[635] J.A. Biscardi, G.D. Meitzner, E. Iglesia, Structure and Density of Active Zn Species in Zn/H-ZSM5 Propane Aromatization Catalysts, J. Catal., 179 (1998) 192-202.
[636] J. Penzien, A. Abraham, J.A. van Bokhoven, A. Jentys, T.E. Müller, C. Sievers, J.A. Lercher, Generation and Characterization of Well-Defined Zn2+ Lewis Acid Sites in Ion Exchanged Zeolite BEA, J. Phys. Chem. B, 108 (2004) 4116-4126.
[637] S.A. Schmidt, N. Kumar, A. Shchukarev, K. Eränen, J.-P. Mikkola, D.Y. Murzin, T. Salmi, Preparation and characterization of neat and ZnCl2 modified zeolites and alumina for methyl chloride synthesis, Appl. Catal., A, 468 (2013) 120-134.
[638] H. Knözinger, P. Ratnasamy, Catalytic Aluminas: Surface Models and Characterization of Surface Sites, Catal. Rev., 17 (1978) 31-70.
[639] Y. Luo, K. Wang, Y. Xu, X. Wang, Q. Qian, Q. Chen, The role of Cu species in electrospun CuO-CeO2 nanofibers for total benzene oxidation, New J. Chem., 39 (2015) 1001-1005.
[640] F. Amano, K. Nogami, M. Tanaka, B. Ohtani, Correlation between Surface Area and Photocatalytic Activity for Acetaldehyde Decomposition over Bismuth Tungstate Particles with a Hierarchical Structure, Langmuir, 26 (2010) 7174-7180.
[641] N. Mizuno, T. Watanabe, H. Mori, M. Misono, Surface-type and bulk-type (II) catalysis in catalytic oxidations over 12-molybdophosphoric acid and its alkali salts, J. Catal., 123 (1990) 157-163.
[642] J.M. Thomas, W.J. Thomas, Principles and Practice of Heterogeneous Catalysis, 2nd Edition, Wiley-VCH Verlag GmbH & Co. KGaA2015.
[643] D.J.C. Yates, W.F. Taylor, J.H. Sinfelt, Catalysis over Supported Metals. I. Kinetics of Ethane Hydrogenolysis over Nickel Surfaces of Known Area, J. Am. Chem. Soc., 86 (1964) 2996-3001.
[644] X. Zhang, J. Liu, Y. Jing, Y. Xie, Support effects on the catalytic behavior of NiO/Al2O3 for oxidative dehydrogenation of ethane to ethylene, Appl. Catal., A, 240 (2003) 143-150.
[645] R.C. Cioc, E. Ruijter, R.V.A. Orru, Multicomponent reactions: advanced tools for sustainable organic synthesis, Green Chem., 16 (2014) 2958-2975.
[646] M.B.J. Atkinson, S. Oyola-Reynoso, R.E. Luna, D.K. Bwambok, M.M. Thuo, Pot-in-pot reactions: a simple and green approach to efficient organic synthesis, RSC Adv., 5 (2015) 597-607.
[647] Y. Gu, Multicomponent reactions in unconventional solvents: state of the art, Green Chem., 14 (2012) 2091-2128.
[648] B. Jiang, T. Rajale, W. Wever, S.-J. Tu, G. Li, Multicomponent Reactions for the Synthesis of Heterocycles, Chem. Asian J., 5 (2010) 2318-2335.
[649] I. Pastoriza-Santos, D.S. Koktysh, A.A. Mamedov, M. Giersig, N.A. Kotov, L.M. Liz-Marzán, One-Pot Synthesis of Ag@TiO2 Core−Shell Nanoparticles and Their Layer-by-Layer Assembly, Langmuir, 16 (2000) 2731-2735.
[650] A. Cao, Z. Liu, S. Chu, M. Wu, Z. Ye, Z. Cai, Y. Chang, S. Wang, Q. Gong, Y. Liu, A Facile One-step Method to Produce Graphene–CdS Quantum Dot Nanocomposites as Promising Optoelectronic Materials, Adv. Mater., 22 (2010) 103-106.
[651] H. Cheng, B. Huang, Y. Dai, X. Qin, X. Zhang, One-Step Synthesis of the Nanostructured AgI/BiOI Composites with Highly Enhanced Visible-Light Photocatalytic Performances, Langmuir, 26 (2010) 6618-6624.
[652] Y. Weng, L. Zhang, W. Zhu, Y. Lv, One-step facile synthesis of coral-like Zn-doped SnO2 and its cataluminescence sensing of 2-butanone, J. Mater. Chem. A, 3 (2015) 7132-7138.

[653] R.T. Tom, A.S. Nair, N. Singh, M. Aslam, C.L. Nagendra, R. Philip, K. Vijayamohanan, T. Pradeep, Freely Dispersible Au@TiO2, Au@ZrO2, Ag@TiO2, and Ag@ZrO2 Core−Shell Nanoparticles: One-Step Synthesis, Characterization, Spectroscopy, and Optical Limiting Properties, Langmuir, 19 (2003) 3439-3445.
[654] W. Li, Z. Ma, G. Bai, J. Hu, X. Guo, B. Dai, X. Jia, Dopamine-assisted one-step fabrication of Ag@AgCl nanophotocatalyst with tunable morphology, composition and improved photocatalytic performance, Appl. Catal., B, 174–175 (2015) 43-48.
[655] Z.L. Zhao, L.Y. Zhang, S.J. Bao, C.M. Li, One-pot synthesis of small and uniform Au@PtCu core–alloy shell nanoparticles as an efficient electrocatalyst for direct methanol fuel cells, Appl. Catal., B, 174–175 (2015) 361-366.
[656] S. Bouhadoun, C. Guillard, F. Dapozze, S. Singh, D. Amans, J. Bouclé, N. Herlin-Boime, One step synthesis of N-doped and Au-loaded TiO2 nanoparticles by laser pyrolysis: Application in photocatalysis, Appl. Catal., B, 174–175 (2015) 367-375.
[657] A. Abidli, S. Hamoudi, K. Belkacemi, Synthesis, characterization and insights into stable and well organized hexagonal mesoporous zinc-doped alumina as promising metathesis catalysts carrier, Dalton Trans., 44 (2015) 9823-9838.
[658] A. Abidli, S.K. Pillai, S. Hamoudi, K. Belkacemi, Methyltrioxorhenium supported on mesoporous Al2O3 promoted with ZnCl2 as a green heterogeneous catalyst for methyl oleate self-metathesis: reaction kinetics, XXI International Conference on Chemical Reactors (CHEMREACTOR-21) September 22-25, Delft, The Netherlands. ISBN 978-5-906376-06-0, (2014) 184-185.
[659] S.A. Schmidt, M. Peurla, N. Kumar, K. Eränen, D.Y. Murzin, T. Salmi, Preparation of selective ZnCl2/alumina catalysts for methyl chloride synthesis: Influence of pH, precursor and zinc loading, Appl. Catal., A, 490 (2015) 117-127.
[660] N.I. Shuikin, A.B. Kuchkarev, N.A. Pozdnyak, Contact catalytic alkylation of benzene in presence of alumina-supported zinc chloride under conditions of high pressure, Russ. Chem. Bull., 3 (1954) 783-788.
[661] A. Orlović, D. Janaćković, D. Skala, Alumina/silica aerogel with zinc chloride alkylation catalyst: Influence of supercritical drying conditions and aerogel structure on alkylation catalytic activity, Catal. Commun., 3 (2002) 119-123.
[662] B.C. Ranu, M. Saha, A Simple, Efficient, and Selective Method for Tetrahydropyranylation of Alcohols on a Solid Phase of Alumina Impregnated with Zinc Chloride, J. Org. Chem., 59 (1994) 8269-8270.
[663] A.M. Orlovic, D.T. Janackovic, S. Drmanic, Z. Marinkovic, D.U. Skala, Alumina/silica aerogel with zinc chloride as an alkylation catalyst, J. Serb. Chem. Soc., 66 (2001) 685-695.
[664] J. Xu, F. Wu, Q. Jiang, J.-K. Shang, Y.-X. Li, Metal halides supported on mesoporous carbon nitride as efficient heterogeneous catalysts for the cycloaddition of CO2, J. Mol. Catal. A: Chem., 403 (2015) 77-83.
[665] J. Xu, K.-Z. Long, Y. Wang, B. Xue, Y.-X. Li, Fast and facile preparation of metal-doped g-C3N4 composites for catalytic synthesis of dimethyl carbonate, Appl. Catal., A, 496 (2015) 1-8.
[666] E.P. Barrett, L.G. Joyner, P.P. Halenda, The Determination of Pore Volume and Area Distributions in Porous Substances. I. Computations from Nitrogen Isotherms, J. Am. Chem. Soc., 73 (1951) 373-380.
[667] R.B. Anderson, Pore distributions from desorption isotherms, J. Catal., 3 (1964) 50-56.
[668] B.C. Lippens, J.H. de Boer, Studies on pore systems in catalysts: V. The t method, J. Catal., 4 (1965) 319-323.
[669] J.T. Kloprogge, L.V. Duong, B.J. Wood, R.L. Frost, XPS study of the major minerals in bauxite: Gibbsite, bayerite and (pseudo-)boehmite, J. Colloid Interface Sci., 296 (2006) 572-576.
[670] J.F. Moulder, W.F. Stickle, P.E. Sobol, K.D. Bomben, Handbook of X-ray Photoelectron Spectroscopy: A Reference Book of Standard Spectra for Identification and Interpretation of XPS Data, Physical Electronics, Perkin-Elmer Corp1992.
[671] D. Briggs, P. Seah, Practical Surface Analysis: Auger and X-ray photoelectron spectroscopy, John Wiley & Sonsfirst edition 1983, second edition 1990.
[672] D.A. Shirley, High-Resolution X-Ray Photoemission Spectrum of the Valence Bands of Gold, Phys. Rev. B: Condens. Matter Mater. Phys., 5 (1972) 4709-4714.

[673] D. Fenzke, D. Freude, T. Fröhlich, J. Haase, NMR intensity measurements of half-integer quadrupole nuclei, Chem. Phys. Lett., 111 (1984) 171-175.
[674] S. Hayashi, K. Hayamizu, Shift References in High-Resolution Solid-State NMR, Bull. Chem. Soc. Jpn., 62 (1989) 2429-2430.
[675] R.J. Motekaitis, A.E. Martell, Complexes of aluminum(III) with hydroxy carboxylic acids, Inorg. Chem., 23 (1984) 18-23.
[676] M. Kruk, M. Jaroniec, Gas Adsorption Characterization of Ordered Organic−Inorganic Nanocomposite Materials, Chem. Mater., 13 (2001) 3169-3183.
[677] G.J.d.A.A. Soler-Illia, C. Sanchez, Interactions between poly(ethylene oxide)-based surfactants and transition metal alkoxides: their role in the templated construction of mesostructured hybrid organic-inorganic composites, New J. Chem., 24 (2000) 493-499.
[678] Q. Huo, D.I. Margolese, U. Ciesla, P. Feng, T.E. Gier, P. Sieger, R. Leon, P.M. Petroff, F. Schuth, G.D. Stucky, Generalized synthesis of periodic surfactant/inorganic composite materials, Nature, 368 (1994) 317-321.
[679] T. Seki, M. Onaka, Mesoporous Alumina: Synthesis, Characterization, and Catalysis, Advanced Nanomaterials, Wiley-VCH Verlag GmbH & Co. KGaA2010, pp. 481-521.
[680] J. van den Brand, P.C. Snijders, W.G. Sloof, H. Terryn, J.H.W. de Wit, Acid−Base Characterization of Aluminum Oxide Surfaces with XPS, J. Phys. Chem. B, 108 (2004) 6017-6024.
[681] R. Lizárraga, E. Holmström, S.C. Parker, C. Arrouvel, Structural characterization of amorphous alumina and its polymorphs from first-principles XPS and NMR calculations, Phys. Rev. B: Condens. Matter Mater. Phys., 83 (2011) 094201.
[682] B.R. Strohmeier, D.M. Hercules, Surface spectroscopic characterization of the interaction between zinc ions and γ-alumina, J. Catal., 86 (1984) 266-279.
[683] S.W. Gaarenstroom, N. Winograd, Initial and final state effects in the ESCA spectra of cadmium and silver oxides, J. Chem. Phys., 67 (1977) 3500-3506.
[684] R.D. Seals, R. Alexander, L.T. Taylor, J.G. Dillard, Core electron binding energy study of group IIb-VIIa compounds, Inorg. Chem., 12 (1973) 2485-2487.
[685] L.S. Dake, D.R. Baer, J.M. Zachara, Auger parameter measurements of zinc compounds relevant to zinc transport in the environment, Surf. Interface Anal., 14 (1989) 71-75.
[686] G.E. Muilenbenger, Handbook of X-Ray Photoelectron Spectroscopy: Perkin-Elmer Corporation Minnesota, (1979).
[687] E.C. Decanio, J.C. Edwards, J.W. Bruno, Solid-State 1H MAS NMR Characterization of γ-Alumina and Modified γ-Aluminas, J. Catal., 148 (1994) 76-83.
[688] C.E. Bronnimann, I.S. Chuang, B.L. Hawkins, G.E. Maciel, Dehydration of silica-aluminas monitored by high-resolution solid-state proton NMR, J. Am. Chem. Soc., 109 (1987) 1562-1564.
[689] C. Boissière, L. Nicole, C. Gervais, F. Babonneau, M. Antonietti, H. Amenitsch, C. Sanchez, D. Grosso, Nanocrystalline Mesoporous γ-Alumina Powders “UPMC1 Material” Gathers Thermal and Chemical Stability with High Surface Area, Chem. Mater., 18 (2006) 5238-5243.
[690] J.F. Stebbins, Nuclear magnetic resonance spectroscopy of silicates and oxides ingeochemistry and geophysics, Handbook of Physical Constants, V. 2; Ahrens, T. J., Ed.; American Geophysical Union: Washington DC, (1995).
[691] J.A. Wang, X. Bokhimi, A. Morales, O. Novaro, T. López, R. Gómez, Aluminum Local Environment and Defects in the Crystalline Structure of Sol−Gel Alumina Catalyst, J. Phys. Chem. B, 103 (1998) 299-303.
[692] J. Čejka, Organized mesoporous alumina: synthesis, structure and potential in catalysis, Appl. Catal., A, 254 (2003) 327-338.
[693] L. Fu, X. Li, M. Liu, H. Yang, Insights into the nature of Cu doping in amorphous mesoporous alumina, J. Mater. Chem. A, 1 (2013) 14592-14605.
[694] H.J. Kim, H.C. Lee, J.S. Lee, 27Al Triple-Quantum Magic-Angle Spinning Nuclear Magnetic Resonance Characterization of Nanostructured Alumina Materials, J. Phys. Chem. C, 111 (2007) 1579-1583.
[695] M. Liu, H. Yang, Facile synthesis and characterization of macro–mesoporous γ-Al2O3, Colloids Surf., A, 371 (2010) 126-130.

[696] J.-L. Blin, A. Léonard, Z.-Y. Yuan, L. Gigot, A. Vantomme, A.K. Cheetham, B.-L. Su, Hierarchically Mesoporous/Macroporous Metal Oxides Templated from Polyethylene Oxide Surfactant Assemblies, Angew. Chem. Int. Ed., 42 (2003) 2872-2875.
[697] P.C. Hidber, T.J. Graule, L.J. Gauckler, Citric Acid—A Dispersant for Aqueous Alumina Suspensions, J. Am. Ceram. Soc., 79 (1996) 1857-1867.
[698] D.A. Thornton, Infrared spectra of metal β-ketoenolates and related complexes, Coord. Chem. Rev., 104 (1990) 173-249.
[699] T.R. Pauly, Y. Liu, T.J. Pinnavaia, S.J.L. Billinge, T.P. Rieker, Textural Mesoporosity and the Catalytic Activity of Mesoporous Molecular Sieves with Wormhole Framework Structures, J. Am. Chem. Soc., 121 (1999) 8835-8842.
[700] A.K. Santra, D.W. Goodman, Oxide-supported metal clusters: models for heterogeneous catalysts, J. Phys.: Condens. Matter, 15 (2003) R31.
[701] D.W. Lee, B.R. Yoo, Advanced metal oxide (supported) catalysts: Synthesis and applications, J. Ind. Eng. Chem., 20 (2014) 3947-3959.
[702] Y. Rao, D.M. Antonelli, Mesoporous transition metal oxides: characterization and applications in heterogeneous catalysis, J. Mater. Chem., 19 (2009) 1937-1944.
[703] G.A. Seisenbaeva, G. Daniel, V.G. Kessler, J.-M. Nedelec, General Facile Approach to Transition-Metal Oxides with Highly Uniform Mesoporosity and Their Application as Adsorbents for Heavy-Metal-Ion Sequestration, Chem. - Eur. J., 20 (2014) 10732-10736.
[704] Y. Ren, Z. Ma, P.G. Bruce, Ordered mesoporous metal oxides: synthesis and applications, Chem. Soc. Rev., 41 (2012) 4909-4927.
[705] M. Tiemann, Porous Metal Oxides as Gas Sensors, Chem. - Eur. J., 13 (2007) 8376-8388.
[706] T. Waitz, T. Wagner, C.-D. Kohl, M. Tiemann, New mesoporous metal oxides as gas sensors, in: P.M. Antoine Gédéon, B. Florence (Eds.) Stud. Surf. Sci. Catal., Elsevier2008, pp. 401-404.
[707] G. Guerrero, P.H. Mutin, A. Vioux, Organically modified aluminas by grafting and sol-gel processes involving phosphonate derivatives, J. Mater. Chem., 11 (2001) 3161-3165.
[708] X. Chen, Y. Liu, G. Niu, Z. Yang, M. Bian, A. He, High temperature thermal stabilization of alumina modified by lanthanum species, Appl. Catal., A, 205 (2001) 159-172.
[709] L.-f. Yang, C.-k. Shi, X.-e. He, J.-x. Cai, Catalytic combustion of methane over PdO supported on Mg-modified alumina, Appl. Catal., B, 38 (2002) 117-125.
[710] P. Berteau, S. Ceckiewicz, B. Delmon, Role of the acid-base properties of aluminas, modified γ-alumina, and silica-alumina in 1-butanol dehydration, Appl. Catal., 31 (1987) 361-383.
[711] P. Berteau, B. Delmon, Modified Aluminas : Relationship between activity in 1-butanol dehydration and acidity measured by NH3 TPD, Catal. Today, 5 (1989) 121-137.
[712] B. Jongsomjit, J. Panpranot, J.G. Goodwin Jr, Effect of zirconia-modified alumina on the properties of Co/γ-Al2O3 catalysts, J. Catal., 215 (2003) 66-77.
[713] S.J. Connon, S. Blechert, Recent Developments in Olefin Cross-Metathesis, Angew. Chem. Int. Ed., 42 (2003) 1900-1923.
[714] R.H. Grubbs, S. Chang, Recent advances in olefin metathesis and its application in organic synthesis, Tetrahedron, 54 (1998) 4413-4450.
[715] M.A.R. Meier, Metathesis with Oleochemicals: New Approaches for the Utilization of Plant Oils as Renewable Resources in Polymer Science, Macromol. Chem. Phys., 210 (2009) 1073-1079.
[716] J. Rouquerol, F. Rouquerol, K.S.W. Sing, Adsorption by Powders and Porous Solids: Principles, Methodology and Applications, Elsevier Science1998.
[717] A. Hess, E. Kemnitz, A. Lippitz, W.E.S. Unger, D.H. Menz, ESCA, XRD, and IR Characterization of Aluminum Oxide, Hydroxyfluoride, and Fluoride Surfaces in Correlation with Their Catalytic Activity in Heterogeneous Halogen Exchange Reactions, J. Catal., 148 (1994) 270-280.
[718] F. Rueda, J. Mendialdua, A. Rodriguez, R.Casanova, Y. Barbaux, L. Gengembre, L. Jalowiecki, Characterization of Venezuelan laterites by X-ray photoelectron spectroscopy, J. Electron. Spectrosc. Relat. Phenom., 82 (1996) 135-143.

[719] A.F. Carley, M.W. Roberts, An X-Ray Photoelectron Spectroscopic Study of the Interaction of Oxygen and Nitric Oxide with Aluminium, 1978.
[720] V. Coustet, J. Jupille, Hydroxyl groups on oxide surfaces, Nouv Cim D, 19 (1997) 1657-1664.
[721] W. Eisele, A. Ennaoui, P. Schubert-Bischoff, M. Giersig, C. Pettenkofer, J. Krauser, M. Lux-Steiner, S. Zweigart, F. Karg, XPS, TEM and NRA investigations of Zn(Se,OH)/Zn(OH)2 films on Cu(In,Ga)(S,Se)2 substrates for highly efficient solar cells, Sol. Energy Mater. Sol. Cells, 75 (2003) 17-26.
[722] J.C. Klein, D.M. Hercules, Surface characterization of model Urushibara catalysts, J. Catal., 82 (1983) 424-441.
[723] B.R. Strohmeier, Zinc Aluminate (ZnAl2O4) by XPS, Surf. Sci. Spectra, 3 (1994) 128-134.
[724] A. Da Silva, A. de Souza Gonçalves, M. Davolos, Characterization of nanosized ZnAl2O4 spinel synthesized by the sol–gel method, J. Sol-Gel Sci. Technol., 49 (2009) 101-105.
[725] Z.-X. Li, F.-B. Shi, L.-L. Li, T. Zhang, C.-H. Yan, Scheme 1 Phys. Chem. Chem. Phys., 13 (2011) 2488-2491.
[726] N. Wang, Z. Xu, J. Deng, K. Shen, X. Yu, W. Qian, W. Chu, F. Wei, One-pot Synthesis of Ordered Mesoporous NiCeAl Oxide Catalysts and a Study of Their Performance in Methane Dry Reforming, ChemCatChem, 6 (2014) 1470-1480.
[727] M. Ramos, G. Berhault, D.A. Ferrer, B. Torres, R.R. Chianelli, HRTEM and molecular modeling of the MoS2-Co9S8 interface: understanding the promotion effect in bulk HDS catalysts, Catal. Sci. Technol., 2 (2012) 164-178.
[728] I. Ud Din, M.S. Shaharun, D. Subbarao, A. Naeem, Synthesis, characterization and activity pattern of carbon nanofibers based copper/zirconia catalysts for carbon dioxide hydrogenation to methanol: Influence of calcination temperature, J. Power Sources, 274 (2015) 619-628.
[729] D.-J. Chen, Q.-L. Zhang, J.-X. Feng, K.-J. Ju, A.-J. Wang, J. Wei, J.-J. Feng, One-pot wet-chemical co-reduction synthesis of bimetallic gold–platinum nanochains supported on reduced graphene oxide with enhanced electrocatalytic activity, J. Power Sources, 287 (2015) 363-369.
[730] S.Y. Choung, M. Ferrandon, T. Krause, Pt-Re bimetallic supported on CeO2-ZrO2 mixed oxides as water–gas shift catalysts, Catal. Today, 99 (2005) 257-262.
[731] B.W. Hoffer, E. Crezee, P.R.M. Mooijman, A.D. van Langeveld, F. Kapteijn, J.A. Moulijn, Carbon supported Ru catalysts as promising alternative for Raney-type Ni in the selective hydrogenation of d-glucose, Catal. Today, 79–80 (2003) 35-41.
[732] G.S. Sewell, C.T. O'Connor, E. van Steen, Effect of Activation Procedure and Support on the Reductive Amination of Ethanol Using Supported Cobalt Catalysts, J. Catal., 167 (1997) 513-521.
[733] M. Inoue, T. Miyake, Y. Takegami, T. Inui, Direct alcohol synthesis from syngas on Ru-Mo-Na/Al2O3 catalysts: Effects of physical properties of alumina supports, Appl. Catal., 29 (1987) 285-294.
[734] R.H. Grubbs, Olefin metathesis, Tetrahedron, 60 (2004) 7117-7140.
[735] M. Schuster, S. Blechert, Olefin Metathesis in Organic Chemistry, Angew. Chem., Int. Ed. Engl., 36 (1997) 2036-2056.
[736] K.C. Nicolaou, P.G. Bulger, D. Sarlah, Metathesis Reactions in Total Synthesis, Angew. Chem. Int. Ed., 44 (2005) 4490-4527.
[737] J.C. Mol, Industrial applications of olefin metathesis, J. Mol. Catal. A: Chem., 213 (2004) 39-45.
[738] J.-M. Basset, Yves Chauvin (1930-2015), Nature, 519 (2015) 159-159.
[739] T.M. Trnka, R.H. Grubbs, The Development of L2X2RuCHR Olefin Metathesis Catalysts: An Organometallic Success Story, Acc. Chem. Res., 34 (2001) 18-29.
[740] R.R. Schrock, Olefin metathesis by molybdenum imido alkylidene catalysts, Tetrahedron, 55 (1999) 8141-8153.
[741] M. Scholl, S. Ding, C.W. Lee, R.H. Grubbs, Synthesis and Activity of a New Generation of Ruthenium-Based Olefin Metathesis Catalysts Coordinated with 1,3-Dimesityl-4,5-dihydroimidazol-2-ylidene Ligands, Org. Lett., 1 (1999) 953-956.
[742] F. Caijo, F. Tripoteau, A. Bellec, C. Crevisy, O. Basle, M. Mauduit, O. Briel, Screening of a selection of commercially available homogeneous Ru-catalysts in valuable olefin metathesis transformations, Catal. Sci. Technol., 3 (2013) 429-435.

[743] K. Skowerski, G. Szczepaniak, C. Wierzbicka, L. Gulajski, M. Bieniek, K. Grela, Highly active catalysts for olefin metathesis in water, Catal. Sci. Technol., 2 (2012) 2424-2427.
[744] M.S. Sanford, J.A. Love, R.H. Grubbs, Mechanism and Activity of Ruthenium Olefin Metathesis Catalysts, J. Am. Chem. Soc., 123 (2001) 6543-6554.
[745] C. Lujan, S.P. Nolan, E/Z selectivity in ruthenium-mediated cross metathesis, Catal. Sci. Technol., 2 (2012) 1027-1032.
[746] J.C. Mol, Olefin metathesis over supported rhenium oxide catalysts, Catal. Today, 51 (1999) 289-299.
[747] Y. Wang, Q. Chen, W. Yang, Z. Xie, W. Xu, D. Huang, Effect of support nature on WO3/SiO2 structure and butene-1 metathesis, Appl. Catal., A, 250 (2003) 25-37.
[748] P. Topka, H. Balcar, J. Rathouský, N. Žilková, F. Verpoort, J. Čejka, Metathesis of 1-octene over MoO3 supported on mesoporous molecular sieves: The influence of the support architecture, Microporous Mesoporous Mater., 96 (2006) 44-54.
[749] E. Le Roux, M. Taoufik, M. Chabanas, D. Alcor, A. Baudouin, C. Copéret, J. Thivolle-Cazat, J.-M. Basset, A. Lesage, S. Hediger, L. Emsley, Well-Defined Surface Tungstenocarbyne Complexes through the Reaction of [W(≡CtBu)(CH2tBu)3] with Silica, Organometallics, 24 (2005) 4274-4279.
[750] N. Riache, E. Callens, J. Espinas, A. Dery, M.K. Samantaray, R. Dey, J.M. Basset, Striking difference between alkane and olefin metathesis using the well-defined precursor [[triple bond, length as m-dash]Si-O-WMe5]: indirect evidence in favour of a bifunctional catalyst W alkylidene-hydride, Catal. Sci. Technol., 5 (2015) 280-285.
[751] F. Blanc, C. Copéret, J. Thivolle-Cazat, J.-M. Basset, A. Lesage, L. Emsley, A. Sinha, R.R. Schrock, Surface versus Molecular Siloxy Ligands in Well-Defined Olefin Metathesis Catalysts: [{(RO)3SiO}Mo(NAr)(CHtBu)(CH2tBu)], Angew. Chem. Int. Ed., 45 (2006) 1216-1220.
[752] R.P. Saint-Arroman, M. Chabanas, A. Baudouin, C. Copéret, J.-M. Basset, A. Lesage, L. Emsley, Characterization of Surface Organometallic Complexes Using High Resolution 2D Solid-State NMR Spectroscopy. Application to the Full Characterization of a Silica Supported Metal Carbyne: ≡SiO−Mo(≡C−Bu-t)(CH2−Bu-t)2, J. Am. Chem. Soc., 123 (2001) 3820-3821.
[753] E. Le Roux, M. Chabanas, A. Baudouin, A. de Mallmann, C. Copéret, E.A. Quadrelli, J. Thivolle-Cazat, J.-M. Basset, W. Lukens, A. Lesage, L. Emsley, G.J. Sunley, Detailed Structural Investigation of the Grafting of [Ta(CHtBu)(CH2tBu)3] and [Cp*TaMe4] on Silica Partially Dehydroxylated at 700 °C and the Activity of the Grafted Complexes toward Alkane Metathesis, J. Am. Chem. Soc., 126 (2004) 13391-13399.
[754] S. Schinzel, H. Chermette, C. Copéret, J.-M. Basset, Evaluation of the Carbene Hydride Mechanism in the Carbon−Carbon Bond Formation Process of Alkane Metathesis through a DFT Study, J. Am. Chem. Soc., 130 (2008) 7984-7987.
[755] Y. Chen, E. Abou-hamad, A. Hamieh, B. Hamzaoui, L. Emsley, J.-M. Basset, Alkane Metathesis with the Tantalum Methylidene [(≡SiO)Ta(═CH2)Me2]/[(≡SiO)2Ta(═CH2)Me] Generated from Well-Defined Surface Organometallic Complex [(≡SiO)TaVMe4], J. Am. Chem. Soc., 137 (2015) 588-591.
[756] I. Karamé, M. Boualleg, J.-M. Camus, T.K. Maishal, J. Alauzun, J.-M. Basset, C. Copéret, R.J.P. Corriu, E. Jeanneau, A. Mehdi, C. Reyé, L. Veyre, C. Thieuleux, Tailored Ru-NHC Heterogeneous Catalysts for Alkene Metathesis, Chem. - Eur. J., 15 (2009) 11820-11823.
[757] M.K. Samantaray, J. Alauzun, D. Gajan, S. Kavitake, A. Mehdi, L. Veyre, M. Lelli, A. Lesage, L. Emsley, C. Copéret, C. Thieuleux, Evidence for Metal–Surface Interactions and Their Role in Stabilizing Well-Defined Immobilized Ru–NHC Alkene Metathesis Catalysts, J. Am. Chem. Soc., 135 (2013) 3193-3199.
[758] A. Abidli, One-pot direct synthesis route to self-assembled highly ordered Zn-decorated mesoporous aluminium oxide toward efficient and sustainable metathesis heterogeneous catalyst design, RSC Adv., 5 (2015) 92743-92756.
[759] H. Ngo, K. Jones, T. Foglia, Metathesis of unsaturated fatty acids: Synthesis of long-chain unsaturated-α,ω-dicarboxylic acids, J Amer Oil Chem Soc, 83 (2006) 629-634.
[760] C. Chatgilialoglu, C. Ferreri, M. Melchiorre, A. Sansone, A. Torreggiani, Lipid Geometrical Isomerism: From Chemistry to Biology and Diagnostics, Chem. Rev., 114 (2014) 255-284.

[761] W.W. Christie, Gas chromatography analysis od fatty acid derivatives, Gas chromatography and lipids: a practical guide, The Oily Press Ltd1989, pp. 48-74.
[762] M. Valla, M.P. Conley, C. Coperet, MeReO3/Al2O3 and Me4Sn-activated Re2O7/Al2O3 alkene metathesis catalysts have similar active sites, Catal. Sci. Technol., 5 (2015) 1438-1442.
[763] C. Copéret, Stereoselectivity of supported alkene metathesis catalysts: a goal and a tool to characterize active sites, Beilstein J. Org. Chem., 7 (2011) 13-21.